

# **Complement-mediated neuronal loss by sialic acid glycoalyx alterations**

Dissertation

zur

Erlangung des Doktorgrades (Dr. rer. nat.)

der

Mathematisch-Naturwissenschaftlichen Fakultät

der

Rheinischen Friedrich-Wilhelms-Universität Bonn

vorgelegt von

**Christine Klaus**

(geb. Schuy)

aus

Hadamar

Bonn, Oktober 2017



Angefertigt mit Genehmigung der Mathematisch-Naturwissenschaftlichen Fakultät der  
Rheinischen Friedrich-Wilhelms-Universität Bonn

**1. Gutachter:** Prof. Dr. Harald Neumann

**2. Gutachter:** Prof. Dr. Walter Witke

**Tag der Promotion:** 08.03.2018

**Erscheinungsjahr:** 2018



## **Eidesstaatliche Erklärung**

Ich, Christine Klaus, geb. Schuy, versichere hiermit, dass ich die vorliegende Arbeit mit dem Thema „Complement-mediated neuronal loss by sialic acid glycoalyx alterations“ selbständig verfasst und keine anderen Hilfsmittel als die angegebenen benutzt habe. Die Stellen, die anderen Werken dem Wortlaut oder dem Sinne nach entnommen sind, habe ich in jedem einzelnen Falle durch Angaben der Quelle, auch der benutzten Sekundärliteratur, als Entlehnung kenntlich gemacht.

Bonn, den 30. Oktober 2017

Christine Klaus, geb. Schuy



# Index

<b>I.</b>	<b>Zusammenfassung .....</b>	<b>3</b>
<b>II.</b>	<b>Abstract .....</b>	<b>4</b>
<b>III.</b>	<b>List of Figures .....</b>	<b>5</b>
<b>IV.</b>	<b>List of Tables.....</b>	<b>6</b>
<b>V.</b>	<b>List of Abbreviations .....</b>	<b>7</b>
<b>1</b>	<b>Introduction .....</b>	<b>11</b>
<b>1.1</b>	<b>The neuronal glycoalyx .....</b>	<b>11</b>
1.1.1	The structure and function of the neuronal glycoalyx .....	11
1.1.2	The biosynthesis of sialic acids .....	13
1.1.3	Sialoglycoconjugates and their regulation .....	15
1.1.4	The functions of sialic acids .....	17
<b>1.2</b>	<b>The innate immune system as sensor of the glycoalyx .....</b>	<b>18</b>
1.2.1	Microglia – the brain macrophages .....	18
1.2.2	The complement system.....	24
<b>1.3</b>	<b>Modelling alterations in the glycoalyx.....</b>	<b>28</b>
<b>1.4</b>	<b>Aims of this project .....</b>	<b>28</b>
<b>2</b>	<b>Materials and Methods .....</b>	<b>31</b>
<b>2.1</b>	<b>Materials .....</b>	<b>31</b>
2.1.1	Chemicals and Reagents.....	31
2.1.2	Consumables .....	32
2.1.3	Technical equipment .....	32
2.1.4	Buffers and solutions.....	33
2.1.5	Mice.....	34
2.1.6	Primers .....	34
2.1.7	Antibodies .....	36
2.1.8	Kits and markers.....	36
2.1.9	Software .....	37
<b>2.2</b>	<b>Methods.....</b>	<b>38</b>
2.2.1	Mice.....	38
2.2.2	Analysis of gene transcription.....	40
2.2.3	RNA sequencing .....	42
2.2.4	Flow cytometry analysis of GNE <sup>+/-</sup> mice .....	44

2.2.5	Immunohistochemistry of murine brains.....	44
2.2.6	Statistical analysis.....	47
<b>3</b>	<b>Results .....</b>	<b>48</b>
<b>3.1</b>	<b>Characterization of the GNE<sup>+/-</sup> mice.....</b>	<b>48</b>
3.1.1	General observations .....	48
3.1.2	Sialic acid biosynthesis and sialylation status in the brain .....	50
3.1.3	Neurodegeneration in the brain .....	53
3.1.4	RNA sequencing of the brain .....	61
3.1.5	Inflammation analysis on transcript level.....	64
3.1.6	Inflammation analysis on protein level.....	71
<b>3.2</b>	<b>Rescue of the GNE<sup>+/-</sup>-specific phenotype .....</b>	<b>75</b>
3.2.1	RNA sequencing.....	76
3.2.2	Inflammation analysis on transcript level.....	80
3.2.3	Neuronal loss in the brain .....	83
<b>4</b>	<b>Discussion.....</b>	<b>87</b>
<b>4.1</b>	<b>Characterization of the GNE<sup>+/-</sup> mice.....</b>	<b>88</b>
4.1.1	Evaluation of the sialylation status .....	89
4.1.2	Evaluation of the transcriptional and morphological changes in the brain.....	91
4.1.3	Reactivation of developmental synaptic pruning .....	103
<b>4.2</b>	<b>Transgenic mice for modeling an altered glycolyx .....</b>	<b>105</b>
4.2.1	GNE <sup>+/-</sup> mice as model for an altered glycolyx .....	105
4.2.2	Other transgenic mouse models with glycolyx alterations.....	107
4.2.3	Further implications for GNE <sup>+/-</sup> mice .....	108
<b>4.3</b>	<b>Clinical relevance of GNE mutations and mouse models .....</b>	<b>110</b>
4.3.1	GNE myopathy .....	110
4.3.2	Sialuria.....	113
<b>4.4</b>	<b>Summary and further prospects .....</b>	<b>114</b>
<b>5</b>	<b>References .....</b>	<b>116</b>
<b>6</b>	<b>Appendix.....</b>	<b>140</b>
<b>6.1</b>	<b>Lists of differentially expressed genes (DEGs).....</b>	<b>140</b>
<b>7</b>	<b>Acknowledgements.....</b>	<b>143</b>



## I. Zusammenfassung

Im Alter nimmt die Häufigkeit an neurodegenerativen Erkrankungen zu, die mit einem generellen oder zelltypspezifischen Abbau von Nervenzellen einhergehen. Mikroglia, die Gehirnmakrophagen, stehen im ständigen Kontakt mit Nervenzellen, um kleinste Veränderungen wahrnehmen zu können. Dies geschieht über die zelluläre Glykokalyx, ein Geflecht aus verschiedenen Zuckern mit Sialinsäuren als terminaler Zucker.

In der vorliegenden Studie wurde der Einfluss einer veränderten Glykokalyx im Gehirn *in vivo* untersucht. *In vitro*-Experimente zeigten bereits, dass die Entfernung der Sialinsäuren von der neuronalen Glykokalyx zur Komplementrezeptor 3-vermittelten Phagozytose der Nervenzellen durch Mikroglia/Makrophagen führt. Dieser Mechanismus wurde nun erfolgreich in ein Mausmodell übertragen. Als Modell wurde eine Maus verwendet, die heterozygot für das bifunktionelle Enzym UDP-N-Acetylglucosamin-2-Epimerase/N-Acetylmannosaminase ( $GNE^{+/-}$ -Maus) ist und dadurch eine niedrigere Sialylierung aufweist. Diese Mäuse zeigten einen Verlust von Nervenzellen in verschiedenen Gehirnregionen, der sich mit dem Alter weiter verstärkte. Parallel dazu wurde gezeigt, dass vor allem die langkettigen Polysialinsäuren reduziert waren. Trotz kontinuierlichem Nervenzellabbau konnten keine Entzündungsreaktionen im Gehirn festgestellt werden. Sowohl eine Transkriptom-Analyse, als auch eine Astrozyten- und Mikrogliaanalyse im Gehirn zeigten keine großen Auffälligkeiten. Lediglich die stärkere Expressierung eines Mikroglia-/Makrophagenmarkers deutete auf eine erhöhte Mikroglia-Aktivität hin und lässt auf eine homöostatische Phagozytose schließen. Wichtige Erkenntnisse brachte die Kreuzung der  $GNE^{+/-}$ -Maus mit einer Komplementfaktor C3-defizienten Maus. Durch die vollständige Inhibierung des Komplementsystems konnte der Nervenzellabbau selbst bei alten  $GNE^{+/-}$ -Mäusen verhindert und dadurch die Involvierung des Komplementsystems auch *in vivo* nachgewiesen werden.

Somit zeigt die vorliegende Arbeit, dass Sialinsäuren auch im komplexen Organismus eine zentrale Funktion in der Mikroglia-Nervenzell-Kommunikation einnehmen. Eine reduzierte Sialylierung führt zu einer Komplement-vermittelten Phagozytose der Nervenzellen durch Mikroglia. Das untersuchte Mausmodell, sowie die daraus gewonnenen Erkenntnisse bilden eine sehr gute Grundlage um den altersabhängigen Nervenzellverlust weiter zu untersuchen und geeignete Therapieansätze zur Vermeidung von neurodegenerativen Erkrankungen zu entwickeln.

## II. Abstract

Every neuronal cell is covered with a dense structure of glycoconjugates, the glycocalyx. Sialic acids form the terminal ends of the glycocalyx and thus, are more accessible for the cellular environment. Microglia, the brain macrophages constantly survey the brain parenchyma and can sense small alterations in the glycocalyx. Recently, it was demonstrated in murine and human neuron-microglia/macrophage co-cultures that healthy neurons with reduced surface-bound sialic acids were removed by microglia/macrophages in a complement-dependent manner. Although microglial phagocytosis is considered as beneficial, the role of microglia in recognizing sialic acids in neurodegenerative and neuroinflammatory processes is still not fully understood.

In this study, the situation of a desialylated glycocalyx *in vivo* was mimicked by using a mouse heterozygous for the bifunctional enzyme glucosamine-2-epimerase/N-acetylmannosamine kinase (GNE; GNE<sup>+/-</sup> mice). It was shown that *gne* transcription was reduced in the brain of young and old GNE<sup>+/-</sup> mice and a reduced sialylation status was confirmed. In accordance with the *in vitro* data, an increased age-dependent neuronal loss was found in different brain regions of GNE<sup>+/-</sup> mice compared to their wildtype littermates. Histological staining indicated morphological changes in microglia but not in astrocytes. Furthermore, only very minor inflammatory changes were observed in the transcriptome data of the brain pointing towards a homeostatic removal of neurons in GNE<sup>+/-</sup> mice by microglia. Based on the *in vitro* studies, the GNE<sup>+/-</sup> mice were crossbred with mice deficient for the complement component 3 (C3), the central player of the complement cascade, to confirm the involvement of the complement system. The C3-deficiency was able to rescue the neuronal loss in the GNE<sup>+/-</sup> mice. Thus, this study successfully showed that the complement system is involved in microglial removal of neurons *in vivo*.

The *in vivo* data demonstrate the importance of microglial sensing of small alterations in the glycocalyx. Sialic acids seem to play an essential role in maintaining brain homeostasis and might also be involved in synaptic plasticity. However, oxidative stress or aging can lead to a decrease of sialic acids that then might lead to unwanted reactivation of developmental synaptic pruning and consequently to the loss of neurons in the brain. Thus, targeting the neuronal glycocalyx could be a beneficial therapy in age-dependent neuronal loss and neurodegenerative diseases.

### III. List of Figures

<b>Figure 1:</b> Glycosylation pattern of the neuronal glycocalyx.....	12
<b>Figure 2:</b> The two major forms of sialic acids.....	13
<b>Figure 3:</b> Overview of the sialic acid biosynthesis.....	14
<b>Figure 4:</b> Biosynthesis of the major brain gangliosides.....	16
<b>Figure 5:</b> Different microglial phenotypes during development and adulthood of the brain.....	19
<b>Figure 6:</b> A schematic overview of several microglial receptors..	23
<b>Figure 7:</b> Overview of the three complement signaling pathways. ....	26
<b>Figure 8:</b> Proposed model of glycocalyx alteration. ....	30
<b>Figure 9:</b> GNE genotyping example. ....	40
<b>Figure 10:</b> Weight development of GNE mice during aging.....	49
<b>Figure 11:</b> Transcription analysis of <i>gne</i> mRNA levels. ....	51
<b>Figure 12:</b> Detection of different sialic acid lengths in the brain. ....	52
<b>Figure 13:</b> Increasing neurodegeneration in the substantia nigra of GNE <sup>+/-</sup> mice with age.....	55
<b>Figure 14:</b> Increasing neurodegeneration in the CA3 region of the hippocampus of GNE <sup>+/-</sup> mice with age.....	58
<b>Figure 15:</b> No genotype-dependent differences in the width of the dentate gyrus (DG) and the CA3 region during aging. ....	59
<b>Figure 16:</b> RNA sequencing results of 9 months old GNE <sup>+/-</sup> mice compared to wildtype littermates .....	63
<b>Figure 17:</b> Transcriptional profiles of the proinflammatory cytokines Il1b and Tnfa..	66
<b>Figure 18:</b> Transcriptional profiles of components of the complement system.....	68
<b>Figure 19:</b> Transcriptional profiles of microglial markers.....	70
<b>Figure 20:</b> No genotype-dependent differences in the microglia morphology of 9 months old mice..	73
<b>Figure 21:</b> No genotype-dependent differences in astrocytes in the SN pr. ....	75
<b>Figure 22:</b> RNA sequencing results of 9 months old GNE <sup>+/-</sup> C3 <sup>-/-</sup> mice compared to wildtype controls. ....	77
<b>Figure 23:</b> Transcriptional profiles of 9 months old GNE mice in comparison with C3-deficient background. ..	82
<b>Figure 24:</b> Neuronal loss in the substantia nigra of GNE <sup>+/-</sup> C3 <sup>+/+</sup> mice was rescued in GNE <sup>+/-</sup> C3 <sup>-/-</sup> mice.....	84
<b>Figure 25:</b> Neuronal loss in the CA3 region of the hippocampus of GNE <sup>+/-</sup> C3 <sup>+/+</sup> mice was rescued in GNE <sup>+/-</sup> C3 <sup>-/-</sup> mice .....	85
<b>Figure 26:</b> Minor changes in the width of the dentate gyrus (DG) and of the CA3 region in C3-deficient mice.	86

## IV. List of Tables

<b>Table 1:</b> Genotyping primer mix.....	<b>38</b>
<b>Table 2:</b> Genotyping PCR reaction mix .....	<b>39</b>
<b>Table 3:</b> Genotyping programs for thermocycler .....	<b>39</b>
<b>Table 4:</b> Number of measured mice for weight analysis.....	<b>49</b>
<b>Table 5:</b> List of the six shared genes of the GNE vs. LPS-induced neuroinflammation dataset .....	<b>62</b>
<b>Table 6:</b> List of the ten DEGs unique for GNE <sup>+/-</sup> C3 <sup>+/+</sup> .....	<b>78</b>
<b>Table 7:</b> List of the 3 DEGs common in GNE <sup>+/-</sup> C3 <sup>+/+</sup> and GNE <sup>+/-</sup> C3 <sup>-/-</sup> .....	<b>79</b>
<b>Table 8:</b> List of all 45 DEGs in GNE <sup>+/-</sup> vs. wildtype.....	<b>140</b>
<b>Table 9:</b> List of the 50 most differently expressed genes of all 1334 DEGs in GNE <sup>+/+</sup> C3 <sup>-/-</sup> vs. wildtype.....	<b>141</b>
<b>Table 10:</b> List of the 50 most differently expressed genes of all 987 DEGs in GNE <sup>+/-</sup> C3 <sup>-/-</sup> vs. wildtype .....	<b>142</b>

## V. List of Abbreviations

4-HNE	4-hydroxynonenal	Cd68	CD68 antigen
<b>A</b>		CDG	congenital disorders of glycosylation
AD	Alzheimer's disease	Cer	ceramide
adj p	adjusted <i>p</i> -value	Clock	clock circadian regulator
ADP	adenosine diphosphate	CMAH	cytidine monophospho-N-acetylneuraminic acid hydroxylase
Aif1	allograft inflammatory factor 1	CMAS	CMP-Sialic acid synthetase
ALS	amyotrophic lateral sclerosis	CMP	cytidine monophosphate
AMD	age-related macular degeneration	CNS	central nervous system
APOE	apolipoprotein E	CR1	complement receptor 1
Arl4d	ADP-ribosylation factor-like protein 4D	Creb1	cAMP responsive element binding protein 1
ASD	autism spectrum disorders	Crem	cAMP responsive element modulator
Asn	Asparagine	CT	cycle threshold
ATP	adenosine triphosphate	CTP	cytidine triphosphate
<b>B</b>		CX3CL1	fractalkine ligand
BDNF	brain-derived neurotrophic factor	CX3CR1	fractalkine receptor
BSA	bovine serum albumin	Cxcl12	C-X-C Motif Chemokine Ligand 12
Btg2	B cell translocation gene 2	Cxcr4	C-X-C Motif Chemokine Receptor 4
<b>C</b>		Cy3	Cyanine 3
C1qa/b	complement component 1 with q subcomponent, alpha/beta polypeptide	<b>D</b>	
C1qc	complement component 1 with q subcomponent, c chain	DABCO	1,4-diazabicyclo[2.2.2]octane
C3	complement component 3	DAF	decay-accelerating factor
C3 <sup>-/-</sup>	mice deficient for C3	DAMPs	damage-associated molecular patterns
C3b	complement component 3b	DAPI	4',6-diamidino-2-phenylindole
C4b	complement component 4b		
CA	Cornus Ammonis		
CCR7	C-C chemokine receptor type 7		

ddH <sub>2</sub> O	double-distilled water	GNE <sup>+/-</sup>	GNE-heterozygous-deficient mice
Ddit4	DNA-damage-inducible transcript 4	<b>H</b>	
DEGs	differentially expressed genes	HIBM	hereditary inclusion body myopathy
DG	dentate gyrus	<b>I</b>	
Dio2	deiodinase, iodothyronine, type II	Iba1	ionized calcium binding adaptor molecule 1
DMRV	distal myopathy with rimmed vacuoles	IL1b	interleukin 1 beta
<b>E</b>		IPA	Ingenuity Pathway Analysis®
E	embryonic day	ITAM	immunoreceptor tyrosine-based activation motif
EDTA	ethylenediaminetetraacetate	itgam	integrin alpha M
ER	endoplasmic reticulum	ITIM	immunoreceptor tyrosine-based inhibition motif
<b>F</b>		<b>K</b>	
FACS	fluorescence-activated cell sorter	KO	knockout
FC	fold change	<b>L</b>	
FDR	false discovery rate	LPS	lipopolysaccharides
FPKM	fragments per kilobase of transcripts per million mapped genes	<b>M</b>	
<b>G</b>		MAC	membrane-attack complex
GABA	gamma-aminobutyric acid	ManNAc	N-acetylmannosamine
GalNAc	N-acetylgalactosamine	MAPK	mitogen-activated protein kinase
GAPDH	glyceraldehyde-3-phosphate dehydrogenase	MASP	MBL-associated serine proteases
Gfap	glial fibrillary acidic protein	MBL	mannose-binding lectins
GlcNAc	N-acetylglucosamine	MDA	malondialdehyde
GNE	glucosamine (UDP-N-acetyl)-2-epimerase/N-acetylmannosamine kinase	MPTP	1-Methyl-4-phenyl-1,2,3,6-tetrahydropyridin
GNE/C3	GNE <sup>+/-</sup> mice crossed with C3 <sup>-/-</sup> mice	MS	multiple sclerosis
		mTORC1	mammalian target of rapamycin complex-1

<b>N</b>		PFA	paraformaldehyde
NaCl	sodium chloride	P <sub>i</sub> (or PP <sub>i</sub> )	activated phosphate(s)
NADPH	nicotinamide adenine dinucleotide phosphate	PKA	protein kinase A
NANP	N-acetylneuraminic acid phosphatase	PolySTs	polysialyltransferases
NANS	N-acetylneuraminic acid synthase	Ppp1r3g	protein phosphatase 1 regulatory subunit 3G
NaOH	sodium hydroxide	PRRs	pattern recognition receptors
NCAM	neural cell adhesion molecule	PSA-	Polysialylated neural cell
neo	neomycin	NCAM	adhesion molecule
Neu	neuraminidase	<b>R</b>	
Neu5Ac	N-acetylneuraminic acid	REDD1	protein regulated in development and DNA damage response 1
Neu5Gc	N-glycolylneuraminic acid	ROS	reactive oxygen species
NeuN	neuronal nuclei	<b>S</b>	
NF-κB	nuclear factor-kappa B	SDF1	stromal cell-derived factor-1
NGS	normal goat serum	SEM	standard error of the mean
Nr3c1	nuclear receptor subfamily 3 group C member 1	Ser	serine
NRP-2	neuropilin-2	SHIP1	Src homology region 2 domain-containing inositol phosphatase-1
ns.	not significant	SHP1	Src homology region 2 domain-containing phosphatase-1
<b>P</b>		Siglec	sialic-acid-binding immunoglobulin-like lectin
PAMPs	pathogen-associated molecular patterns	SN pc	substantia nigra pars compacta
PBS	phosphate buffered saline	SN pr	substantia nigra pars reticulata
Pc	principle component	Sox9	SRA1 or SRY [sex determining region Y]-box 9
PCA	principle component analysis	sqRT-	semi-quantitative real-time
PCR	polymerase chain reaction	PCR	PCR
PD	Parkinson's disease	SynCAM	synaptic cell adhesion
PE	R-Phycoerythrin	-1	molecule-1
PEP	phosphoenolpyruvic acid		
Per1	period circadian clock 1		

---

<b>T</b>		TNF $\alpha$	tumor necrosis factor alpha
TBE	Tris/Borate/EDTA	TREM2	triggering receptor expressed on myeloid cells 2
TGF $\beta$	transforming growth factor beta	<b>U</b>	
TH	tyrosine hydroxylase	UDP	uridine diphosphate
Thr	Threonine	<b>W</b>	
Tmem119	transmembrane protein 119	WT	wildtype



# 1 Introduction

The brain is a highly complex organ with millions of neurons that control and regulate the body. The communication between each neuron as well as the crosstalk with glial cells, such as astrocytes and microglia, is essential for the proper function of the brain. The rich glycan-coated surface of every neuron, the neuronal glycocalyx, plays a central role in this network. However, in several diseases and during aging these cell-cell interactions undergo various changes and can become dysregulated. Thus, understanding the crosstalk between neurons and glial cells and its mediators at the level of the glycocalyx is an essential research goal.

## 1.1 The neuronal glycocalyx

### 1.1.1 The structure and function of the neuronal glycocalyx

The neuronal cell surface is the interface between the cell and its environment. It is covered with a dense array of different glycans that form a matrix, the glycocalyx. The complex composition of the glycocalyx varies among tissues and cell types and encodes a huge variety of information that is essential for health and in diseases.


Glycans like proteoglycans, glycoproteins, and glycolipids are glycosylated biopolymers with one or more carbohydrate chain(s). Glycosylation is a complex process of the secretory pathway and describes the modification of proteins, lipids or other organic molecules by adding sugars. These enzymatic processes are important for the structure, folding, stability, and function of the acceptor molecules (as reviewed in Schnaar et al., 2014a). Glycosylation starts in the endoplasmic reticulum with co- and posttranslational modifications of carbohydrate chains. The core structure of the glycoconjugates consists of the seven essential sugars: mannose, glucose, galactose, fucose, N-acetylgalactosamine, N-acetylglucosamine, and N-acetylneuraminic acid (sialic acid) as arranged in Figure 1 (Linnartz and Neumann, 2013). In contrast to nucleic acids or proteins, which are encoded by a DNA template, glycan structures are determined by its specific glycosyltransferases and can be tissue-dependent. Various sugar-specific glycosyltransferases mediate the transfer of sugar residues to an acceptor hydroxyl group on a serine or threonine (O-linked) or to nitrogen of an asparagine residue (N-linked) and determine their linkages. Further modifications like acetylation occur in the Golgi apparatus and can lead to a highly diverse structure of the glycocalyx (Ohtsubo and Marth, 2006; Varki and Schauer,

2009). This explains why a few building blocks are sufficient for the great diversity of the glycocalyx.

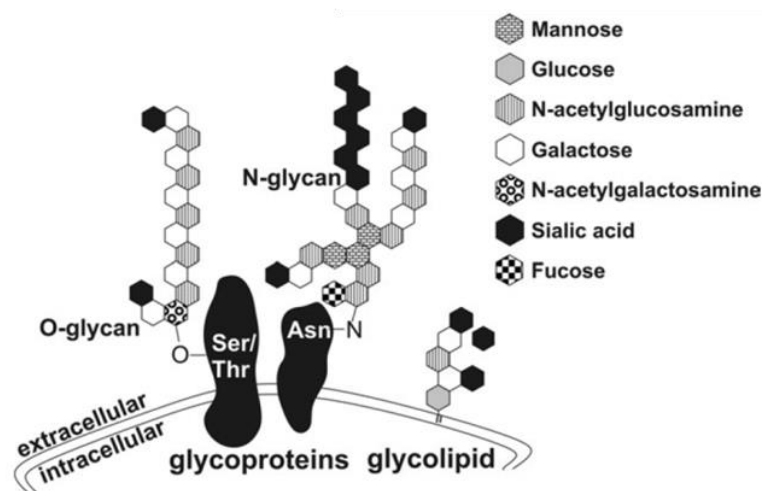


**Figure 1: Glycosylation pattern of the neuronal glycocalyx.** All secreted or cell-surface proteins in mammals are glycosylated. Oligosaccharide chains on the cell surface are formed in a specific order of sugars. Intact cells usually present sialic acids at the terminal ends of their glycoproteins or glycolipids. Thus, sialic acids are exposed at the cell surface. Asn, asparagine; Ser, serine; Thr, threonine. (Image was taken and modified from Linnartz and Neumann, 2013.)

The importance of glycosylation is shown by several human diseases with glycosylated defects that can be summarized by the term ‘congenital disorders of glycosylation’ (CDG). CDG studies show that correct N-glycosylation of proteins is essential for normal development, including the brain (Sato and Endo, 2010) and can result in severe developmental defects (Freeze, 2013). Alterations in glycosylation can not only lead to loss of function or altered cellular transport of proteins but might also result in misfolding and subsequent degradation by the proteasome.

The architecture of the glycocalyx is very dynamic and assumed to reflect the cellular well-being (Rachmilewitz, 2010; Varki, 2011a). The mostly hydrophilic and negatively charged surface likes to spread out in space and facilitates cell-cell interactions (Rudd et al., 2002). Glycans like heparin and chondroitin sulfate are one of the major cell surface structures and thus, dominate the physical and structural properties of the glycocalyx (Raman et al., 2005). In general, the glycosylation pattern of the glycocalyx regulates various functions within the local environment, like protein folding and stability within the cellular membrane, protein trafficking, or protein signaling. The specific function of each glycan is usually determined by the outermost sugars. In the mammalian glycocalyx it is sialic acid that is incorporated at the outermost ends of the glycostructures (black symbol , Figure 1). Due to this exposed position, sialic acids are considered to play a crucial role in cell-cell recognition and to mediate the initial

cellular interactions in physiological and pathological processes (Schauer, 2009; Cohen and Varki, 2010; Linnartz-Gerlach et al., 2014). Thus, sialic acids have a major impact on the neuronal glycocalyx. Furthermore, with their highly negative charges sialic acids contribute to protein hydration and thus, shield glycoproteins from enzymes and other receptors. This makes them an interesting therapeutic target on the neuronal cell surface.

### 1.1.2 The biosynthesis of sialic acids

Sialic acids are nine-carbon backbone sugars that form a diverse family of over 40 neuraminic acid derivatives (Schauer, 2000). Sialic acids are abundant in the deuterostome lineage (Angata and Varki, 2002) but rather an exception in other lineages. Thus, it happens that the expression of sialic acid is, for instance, exploited by a group of gram-negative bacteria that is associated with human or animal hosts and cause severe illness (Varki, 2008). The most abundant forms in mammals are N-acetylneuraminic acid (Neu5Ac) and N-glycolylneuraminic acid (Neu5Gc). They differ in their chemical structure only at carbon position C5 (Acetyl- or Glycolyl-group) as displayed in Figure 2. Humans are the only mammals that lost the ability to synthesize Neu5Gc. Two to three million years ago, a 92 base pair deletion in the cytidine monophospho-N-acetylneuraminic acid hydroxylase (CMAH) gene, the gene of the Neu5Gc converting enzyme, caused a frameshift and an inactivation in humans (Chou et al., 1998). This evolutionary event not only changed the ‘sialome’ in humans but was also followed by an evolutionary rise of sialic acid binding receptors (Varki, 2009).

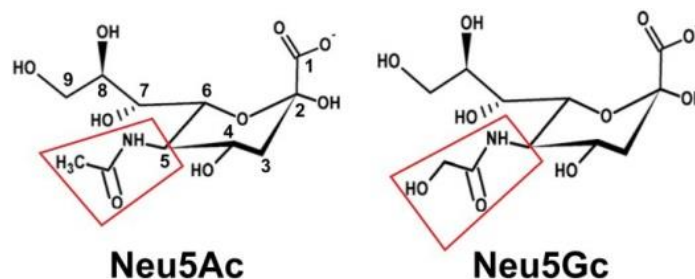


**Figure 2: The two major forms of sialic acids.** The chemical structures of N-acetylneuraminic acid (Neu5Ac) and N-glycolylneuraminic acid (Neu5Gc) are shown. Neu5Ac and Neu5Gc share the same chemical structures except of the chemical group at position C5 (red box). (Image was taken and modified from Bhide and Colley, 2017.)

However in the brain of mammals mainly exclusively Neu5Ac is expressed (Linnartz-Gerlach et al., 2014). It is synthesized in the cytosol from the precursor UDP-N-acetylglucosamine (UDP-GlcNAc) by four reactions (Figure 3). The two initial, essential reactions of the sialic acid biosynthesis are catalyzed by the bifunctional enzyme glucosamine (UDP-N-acetyl)-2-epimerase/N-acetylmannosamine kinase (GNE) in the cytosol. GNE is ubiquitously expressed

in all organs from early development onward (Horstkorte et al., 1999) and plays an important role in the sialic acid biosynthesis. It is the rate-limiting enzyme (Keppler, 1999). The complete inactivation of the GNE gene causes early embryonic lethality in mice (Schwarzkopf et al., 2002) emphasizing its fundamental role in development. The activity of GNE can be controlled on transcription level and is regulated on protein level via a feedback inhibition loop by CMP-sialic acid as shown in Figure 3, the end product of the sialic acid biosynthesis (Kornfeld et al., 1964). N-acetylmannosamine (ManNAc)-6-P, the product of GNE is further catalyzed by N-acetylneuraminic acid synthase (NANS) and N-acetylneuraminic acid phosphatase (NANP) to Neu5Ac in the cytosol (Figure 3).

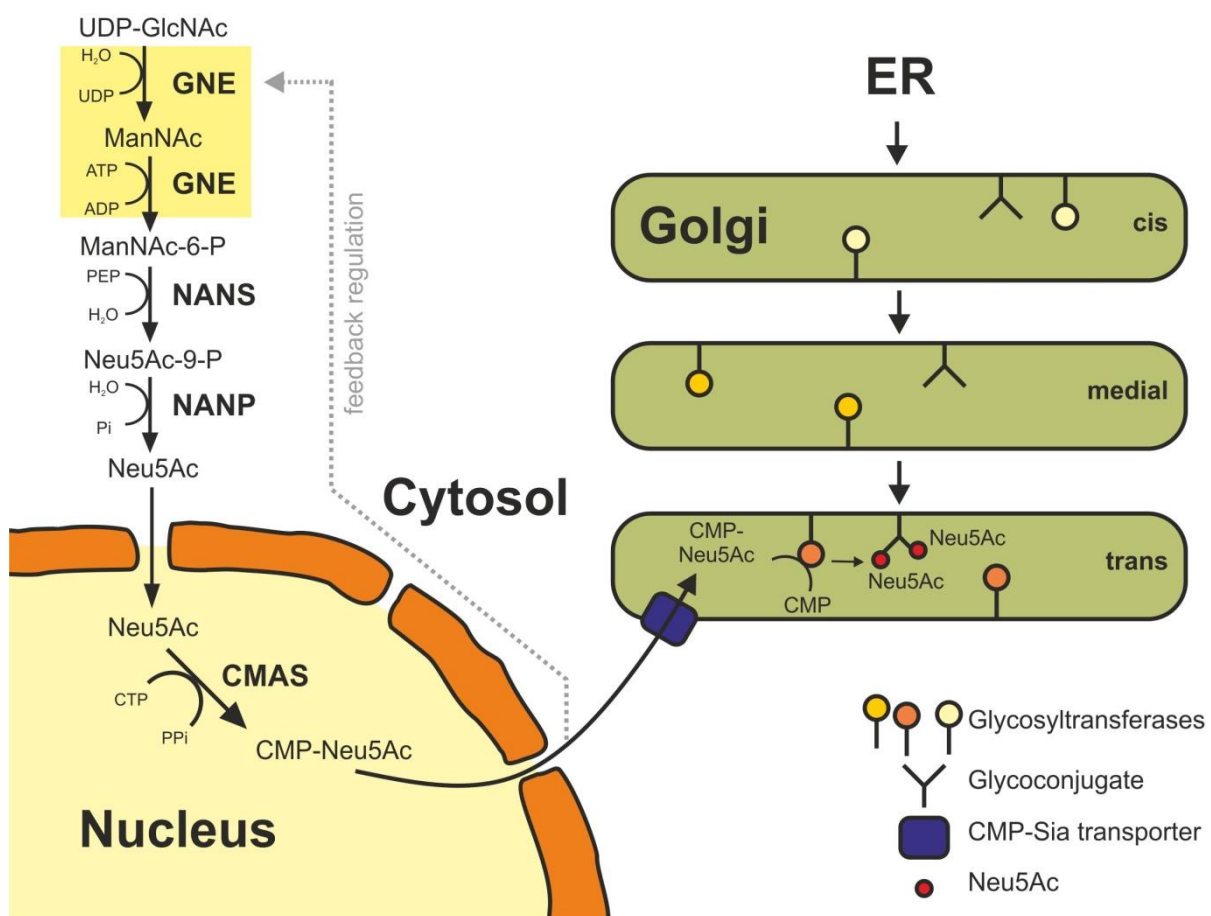


**Figure 3: Overview of the sialic acid biosynthesis.** N-acetylneuraminic acid (Neu5Ac) is synthesized from uridine diphosphate-N-acetylglucosamine (UDP-GlcNAc) in four different reactions in the cytosol. The two rate-limiting steps are catalyzed by the glucosamine (UDP-N-acetyl)-2-epimerase/N-acetylmannosamine kinase (GNE, yellow shaded box). The following steps are taken over by N-acetylneuraminic acid synthase (NANS) and N-acetylneuraminic acid phosphatase (NANP). The activation of Neu5Ac takes place in the nucleus by the cytidine monophosphate (CMP)-sialic acid synthetase (CMAS). Sialoglycoconjugates are formed in the Golgi apparatus by the transfer of the activated sialic acid molecule onto a glycoconjugate. CMP-Neu5Ac enters the Golgi complex via the specific CMP-Sia transporter. ADP - adenosine diphosphate; ATP - adenosine triphosphate; CTP - cytidine triphosphate; ER - endoplasmic reticulum; ManNAc - N-acetylmannosamine; PEP - phosphoenolpyruvic acid; P<sub>i</sub> (or PP<sub>i</sub>) - activated phosphate(s). (Image was adapted from a figure by Bhide and Colley, 2017.)

Neu5Ac is then transported into the nucleus. In the nucleus, the cytidine monophosphate (CMP)-sialic acid synthetase (CMAS) activates Neu5Ac by adding a nucleotide sugar donor

(‘CMP-‘; Figure 3). In the next step, the activated sialic acid molecules (CMP-Neu5Ac) are exported from the nucleus through the nuclear pores and are imported into the Golgi apparatus by the CMP-Sia transporters. In the *trans* cisternae of the Golgi apparatus sialyltransferases transfer the sialic acid from the activated nucleotide sugar donor (CMP-) to the terminus of an oligosaccharide chain of a glycolipid or -protein to form sialoglycoconjugates (Figure 3).

### 1.1.3 Sialoglycoconjugates and their regulation

Twenty different sialyltransferases are known in mammals, which differ in their linkage and saccharide acceptor specificity. They are all type II membrane proteins with a short N-terminal cytoplasmic part and a large proteolytic and catalytic luminal domain (Paulson and Colley, 1989) and share conserved sialylmotifs for binding. They can add mono-sialic acid (Neu5Ac<sub>1</sub>), di-sialic acids (Neu5Ac<sub>2</sub>), oligo-sialic acid (Neu5Ac<sub>3-7</sub>) or long sialic acid polymers (Neu5Ac<sub>8-90+</sub>). Polysialyltransferases (PolySTs) are specifically responsible for long polysialylation (homopolymers of  $n \geq 90$  Neu5Ac<sub>n</sub> molecules) of glycans. Polysialoconjugates have exceptional biochemical and physical properties. Interestingly, only a few polysialylation acceptors were discovered until now. Those include the neural cell adhesion molecule (NCAM; Hoffman et al., 1982; Rothbard et al., 1982; Finne et al., 1983), the synaptic cell adhesion molecule-1 (SynCAM-1; Galuska et al., 2010), neuropilin-2 (NRP-2; Curreli et al., 2007), the C–C chemokine receptor type 7 (CCR7; Kiermaier et al., 2016), E-selectin ligand-1 (Werneburg et al., 2016), the  $\alpha$  subunit of the voltage-dependent sodium channel (James and Agnew, 1987; Zuber et al., 1992), and the CD36 scavenger receptor in human milk (Yabe et al., 2003). Polysialylation is a widely occurring event in the developing brain but diminishes in the adult brain except for a few areas. It is essential for brain development and plays an important role in plasticity and regeneration in the adult brain. Polysialylation was also found on polySTs themselves, which has been referred to as autopolsialylation (Mühlenhoff et al., 1996; Close et al., 2000), but the function of this remains unknown so far.

However, the major sialoglycoconjugates in the brain are gangliosides (= sialoglycolipids) (Varki, 2008; Schnaar, 2016). Gangliosides share the same core structure but vary in their number of attached sialic acid molecules. Although gangliosides represent only 0.6 % of all brain lipids, they carry 75 % of the total brain sialic acids (Norton and Poduslo, 1973; Yu et al., 1988; Schnaar et al., 2014). The four major brain gangliosides are GM1, GD1a, GD1b, and GT1b (Figure 4) and comprise 97 % of all gangliosides (Tettamanti et al., 1973). Gangliosides are important for the development of the central nervous system (CNS; Yamashita et al., 2005) and for maintaining healthy cellular interactions during lifetime. While in *cis* interaction they

are involved in proper formation of lipid rafts, in *trans* they interact with possible binding partners, like the sialic acid-binding immunoglobulin-type lectins (Siglecs). For instance, they play a role in neuronal excitability, synaptic transmission, or axon-myelin interaction (detailed reviewed in Schnaar et al., 2014b; Palmano et al., 2015; Schnaar, 2016b). While in the developing brain rather simple gangliosides are expressed (e.g. GM3, GD3), the levels of more complex gangliosides, like GD1a and GT1b, rise after birth until mainly the four major complex gangliosides are present in the adult brain (Tettamanti et al., 1973; Schnaar, 2004). In the adult, gangliosides are differently distributed all over the brain (Kracun et al., 1991; Vajn et al., 2013; Saville et al., 2017). The enzymes being involved in synthesizing the different types of gangliosides are shown in Figure 4. Mutations in any of these enzymes results in severe cognitive decline as shown in diverse mouse models and human patients (Simpson et al., 2004; Yamashita et al., 2005; Boukhris et al., 2013).

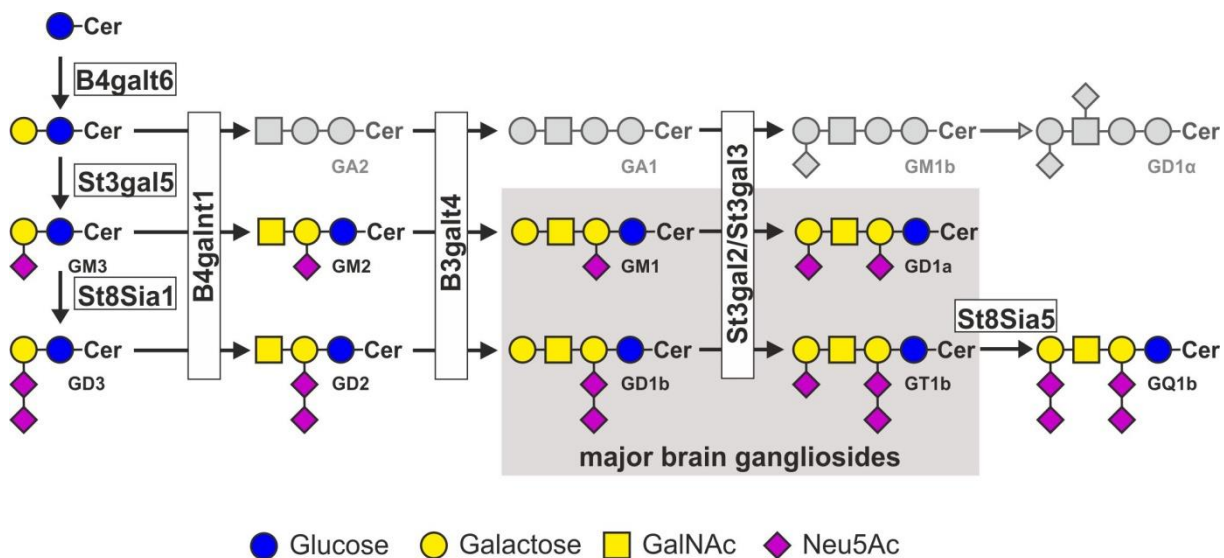


**Figure 4: Biosynthesis of the major brain gangliosides.** A set of different glycosyltransferases (white boxes) are responsible for the stepwise build-up of complex gangliosides. The building blocks of the brain gangliosides are glucose, galactose, N-acetylgalactosamine (GalNAc) and sialic acid (Neu5Ac). The major brain gangliosides comprise up to 97% of all brain gangliosides in the human CNS (shaded grey box). The structures are color-coded according to the widely accepted nomenclature of Svennerholm (Svennerholm, 1994; Varki et al., 2015). Cer, ceramide. (Design was adapted from Schnaar et al., 2014c).

The expression of sialic acids on the neuronal cell surface is regulated by its biosynthesis and its degradation. A good example for a well-regulated sialoglycoconjugate of neuronal cells is NCAM, the major protein-bound sialoglycan in the brain. NCAM shows a highly polysialylated form during embryogenesis, which peaks in the perinatal phase and is down regulated rapidly in the adult for mainly maintaining “neural plasticity” (Seki and Arai, 1993; Varki and Schauer, 2009). The removal of sialic acids from glycans is mediated via specific subcellular sialidases (also known as neuraminidases; Neu). In mammals, four sialidases are known (Neu1-Neu4) as

it was recently reviewed in details (Schnaar et al., 2014; Bhide and Colley, 2017). They differ mainly in their cellular localization and their substrate specificity. Sialidases are also necessary to degrade glycoconjugates. Patients and mice with mutations in sialidases develop severe lysosomal storage diseases (Bonten et al., 1996; Gowda et al., 2017; Pan et al., 2017). Additional knowledge about sialidases is based on research findings in the field of cancer. Cancer cells are often highly sialylated, which protects them from the removal by immune cells. Especially investigations on Neu1 and Neu3 show the direct involvement in cancer progression (Miyagi and Yamaguchi, 2012; Miyagi et al., 2012; Pearce and Läubli, 2016).

#### **1.1.4 The functions of sialic acids**

Sialic acids fulfill a wide range of different functions (Schauer, 2000; Varki, 2011b; Linnartz-Gerlach et al., 2014). Their function is mainly dependent on the linkage to the underlying sugars and glycan classes (glycolipid or glycoprotein). First, sialic acids are involved in the binding and transport of micro- and macromolecules and can influence the stability of the cellular membrane and its functions. Sialoglycan-rich microdomains were observed on the membrane, which are for instance important for the crosslink with extracellular lectins (Brewer et al., 2002; Boscher et al., 2011) as well as for the formation of membrane rafts (Simons and Sampaio, 2011). Secondly, sialic acids can prevent receptor binding by either masking underlying sugars or masking the receptor itself on the cellular surface. For example the coverage of mannose residues by sialic acids prevents the activation of the lectin pathway of the complement system (Murphy et al., 2008). The highly negatively charged and hydrophilic structure of sialic acids not only masks underlying structures but is even strong enough to cause repulsion from neighboring cells. Especially, polysialylation contributes strongly to the overall negative charge of glycans and is important in neural cell interactions, synaptic plasticity in the hippocampus and regulates neurotransmitter activity (Sato and Kitajima, 2013). Furthermore, the hydrophilic structures of polysialylation can serve as scavengers of soluble factors and thus, support ligand-receptor signaling. On the other hand, dysregulation of polysialylated NCAM was associated with psychiatric disorders (Vawter, 2000; Brennaman and Maness, 2010).

Most importantly, sialic acids can act as biological recognition sites and are described as “self” ligands or as a barometer of the cellular well-being. According to the model of Rachmilewitz (Rachmilewitz, 2010), a healthy cell displays a normal pattern of sialylation on the glycocalyx. This can be recognized and monitored by receptors like the inhibitory Siglecs on microglia and acts immunosuppressive. However, in the absence of sialic acids or after slight alterations of the glycocalyx (= removal of “self” ligands) the inhibition of immune cells is disrupted and

phagocytes become activated as it was observed in several studies (Meesmann et al., 2010; Linnartz et al., 2012b; Linnartz-Gerlach et al., 2016). Especially in the brain, microglial sensing of the glycocalyx is important to maintain homeostasis or to respond fast to altered cells under pathological conditions.

Furthermore, sialic acids as terminal caps of the neuronal glycocalyx are exposed to free radicals during oxidative stress. Oxidative stress plays an important role during aging and in a number of neurodegenerative diseases such as Parkinson's disease and Alzheimer's disease (Andersen, 2004). Several findings like site-specific degradation of sialoglycoconjugates after oxidative stress (Eguchi et al., 2002) or elevated serum level of sialic acids during inflammatory processes (Painbeni et al., 1997; Goswami et al., 2003) indicate that sialic acid caps are removed under pathological conditions. In addition, sialic acid supplementation was able to ameliorate oxidative stress in a rat model of puromycin aminonucleoside nephrosis (Pawluczyk et al., 2014) or in a rat model with high fat diet-induced oxidative stress (Yida et al., 2015).

All in all, the sialic acid pattern in the neuronal glycocalyx serves as a fine-tuned barometer of the cellular health's status and an interesting recognition site for microglia.

## **1.2 The innate immune system as sensor of the glycocalyx**

### **1.2.1 Microglia – the brain macrophages**

Microglia are the innate immune cells of the brain. They represent approximately 10 % of all brain cells (Lawson et al., 1992; Soulet and Rivest, 2008). Microglia express the common myeloid- and macrophage-specific markers: ionized calcium binding adapter molecule 1 (Iba1), F4/80, and fractalkine receptor and share the main features of phagocytes, such as phagocytosis, antigen presentation, or production and release of immunomodulatory factors (reviewed by Prinz and Priller, 2014). However, in contrast to peripheral macrophages, microglia arise from primitive myeloid progenitors in the yolk sac that appear around embryonic day (E) 7.5 and migrate to the brain at E9.5 (Ginhoux et al., 2010). Thus, microglia are distinct from macrophages with unique kinetic features, like being long-lived cells, not normally replaced by circulating peripheral myeloid cells, and able to self-renew in a context-dependent manner (Ajami et al., 2007). Microglia are much more than only immune cells. They play a key role in the brain development and in the maintenance of the adult brain. Thus, it is not surprising that microglial sensing of the neuronal glycocalyx is involved in many neurodegenerative diseases.



### 1.2.1.1 Microglial sensing in brain development

Microglia are essential in the development of the brain as reviewed in details by Frost and Schafer (2016). As professional phagocytes, they can remove entire cells, cellular debris, as well as cellular substructures like synapses (Figure 5). Microglia also recognize cells that already undergo apoptosis (e.g. via purinergic receptors). During brain development about 50 % of all synthesized neurons and glial cells are eliminated by microglia (Bilimoria and Stevens, 2015). Microglia mediate the migration and differentiation of neuronal precursor cells and control neurogenesis. To do so, they either actively initiate cell death as it was observed *in vitro* (Frade and Barde, 1998; Marín-Teva et al., 2004) as well as *in vivo* (Cunningham et al., 2013; Mazaheri et al., 2014) or promote neuronal survival and proliferation by secreting neural survival factors (Nagata et al., 1993; Chamak et al., 1994).

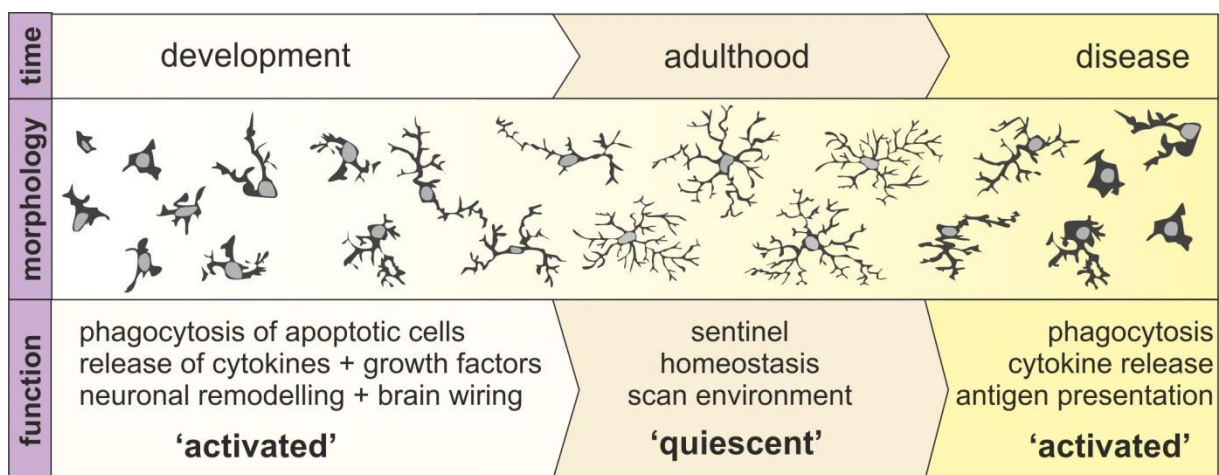


**Figure 5: Different microglial phenotypes during development and adulthood of the brain.** This schematic overview shows the different microglial states from early embryonic development until the fully developed brain. During this time microglia change their morphology from amoeboid forms to widely ramified cells. Upon activation and in the diseased brain microglia again adopt an amoeboid form. Functional modifications occur in parallel to morphological changes. (Scheme is based on a figure from Soulet and Rivest, 2008.)

The term ‘synaptic pruning’ describes the elimination of excess synaptic connections. Studies in the visual cortex could show how presynaptic inputs from retinal ganglion cells were tightly monitored by microglia in the dorsal lateral geniculate nucleus (Tremblay et al., 2010). In addition, mouse studies have implemented that the complement system is also involved in this process by possibly tagging unwanted synaptic structures that can then be recognized by the complement receptors expressed on microglia (Stevens et al., 2007; Schafer et al., 2012; Bialas and Stevens, 2013; Hong et al., 2016b). Later during postnatal development microglia still play a major role in synapse maturation and pruning. Furthermore, a study in the mouse hippocampus could show microglial engulfment of synapses via fractalkine (Paolicelli et al., 2011). Fractalkine (CX3CL1) is another essential mediator during development that is secreted

by neurons and can be recognized by the fractalkine receptor (CX3CR1) expressed on microglia (Ransohoff and El Khoury, 2015).

### 1.2.1.2 Microglial sensing in the adult and in the aging brain

During homeostasis ('resting' state), microglia permanently surveil the brain parenchyma for alterations with their highly motile processes (Nimmerjahn et al., 2005; Figure 5). Occasionally, microglial processes rest for a certain time and contact neuronal synapses. In the visual cortex, it was shown that these contacts were dependent on neuronal activity. Less active synapses were removed to support strong firing neuronal networks (Tremblay et al., 2010).

In a dangerous situation or upon ligand binding the so called 'quiescent' state (surveillance state) of microglia gets modulated into an 'activated' state (remodeling state; Figure 5), which must not be mixed up with the term 'polarization', the functional reprogramming of macrophages upon stimulation. This macrophage concept is not appropriate for microglia. Microglia 'activation' is normally accompanied by retraction of processes, increased proliferation, and expression and release of certain cytokines (Brown and Vilalta, 2015). Depending on the external trigger, microglia can develop numerous phenotypes. Microglia 'activation' was typically considered to induce inflammation by secreting signaling proteins that activate and recruit other immune cells. Recent *in situ* studies, in contrast, point out that the highly dynamic microglial states can be neurotoxic and neuroprotective at the same time and vary in a context- and tissue-dependent manner (Park et al., 2008; Shigemoto-Mogami et al., 2014). Microglia specificity is further achieved by a regional microglial heterogeneity that was first described in 1990 by Lawson and colleagues (Lawson et al., 1990) and by the observed differences in microglial density in different brain regions, being highest in the hippocampus, basal ganglia, substantia nigra and the olfactory bulbs (Yang et al., 2013).

A phenotype called 'microglial priming' defines the enhanced and prolonged response to homeostatic disturbances by microglia compared to naïve ones (Norden and Godbout, 2013; Perry and Holmes, 2014). Primed microglia show a more amoeboid morphology with enlarged soma and shorter processes. In parallel, cytokine release of pro- and anti-inflammatory factors like tumor necrosis factor alpha (TNF $\alpha$ ), interleukin 1 beta (IL1 $\beta$ ), IL6, IL10, transforming growth factor beta (TGF $\beta$ ), CD11c, major histocompatibility complex-II and AXL receptor tyrosine kinase are increased. Microglial priming occurs during normal aging but can also be induced by persistent neuroinflammation, chronic exposure to misfolded proteins and neuronal debris (e.g. in Alzheimer's disease, see Heneka et al., 2015). In human brain tissue, dystrophic

microglia are characterized by deramification, loss of fine cytoplasmic processes, cytoplasmic beading, and cytoplasmic fragmentation (reviewed in Streit and Xue, 2014). Presumably, the reduction of microglia-neuron interactions and the accompanied downregulation of neuronal ligands that normally activate microglial inhibitors (e.g. CX3CL1, CD42, or CD202) are the major underlying mechanisms that lead to this increased responsiveness to intrinsic and extrinsic stimuli in aging microglia. Consequences of brain aging are (1) increased neuronal loss, (2) neuroinflammation, and (3) increased oxidative stress due to mitochondrial damage and enhanced reactive oxygen species (ROS) production by microglia (von Bernhardi et al., 2015).

### **1.2.1.3 The role of microglia in diseases**

In neuroinflammatory diseases, such as multiple sclerosis (MS) or stroke, microglial activation is one of the major occurring events (Benakis et al., 2014; Bogie et al., 2014). In MS studies (mainly on mouse models), microglia become activated and proliferate already before onset of disease. They migrate to degenerating axons to remove myelin debris, which was shown to be beneficial in MS (Giunti et al., 2014). However, microglia also function as antigen-presenting cells and recruit T cells to the brain that increases the inflammation and leads to further neurotoxic events.

Hallmarks of neurodegenerative diseases (e.g. Alzheimer's disease, Parkinson's disease or amyotrophic lateral sclerosis) are aggregated and misfolded proteins and age-related deposition of debris (Heneka et al., 2014; Ransohoff and El Khoury, 2015). In Alzheimer's disease (AD) pathology, increasing numbers of proinflammatory microglia surround amyloid beta plaques. Single-nucleotide polymorphism in genes related to phagocytosis and cytokine signaling (e.g. TREM2 [= triggering receptor expressed on myeloid cells 2], CD33, CR1 [= complement receptor 1], APOE [= apolipoprotein E]) are associated with increased AD risks. Consensus agrees that insufficient protein degradation and decreasing microglia clearance capability correlates with amyloid beta plaques formation and that it is difficult to distinguish between age-related and purely AD-related microglial changes. Another major neurodegenerative disease is amyotrophic lateral sclerosis (ALS). While in early stages of ALS microglia are protecting the brain by increased release of brain-derived neurotrophic factor (BDNF), in later stages chronic activation of microglia becomes neurotoxic and finally results in a complete microglia impairment and accelerated disease progression (Brites and Vaz, 2014; Radford et al., 2015). Microglia activation also plays a central role in Parkinson's disease (PD). The occurrence of Lewy bodies and alpha-synuclein aggregates in the brain of PD patients goes

along with microglial phagocytosis and activation as it was observed in positron emission tomography imaging studies (Cicchetti et al., 2002; Bartels et al., 2010; Surendranathan et al., 2015). Beside the beneficial removal of the protein aggregates increasing cytokine release leads to enhanced stress and neuronal death in the substantia nigra of PD patients (Machado et al., 2016).

Microglia also play a central role in psychiatric disorders. In contrast to neuroinflammatory and neurodegenerative diseases the diagnoses of psychiatric disorders are more diffuse. In general, a dysbalance of the peripheral immune system drives neuroinflammation and microglia activation in the brain (Stertz et al., 2013; Leza et al., 2015; Inta et al., 2017). In schizophrenia, this is thought to interfere with the expression of local brain mediators, like serotonin, glutamate and dopamine. In autism spectrum disorders (ASD) microglia activation and/ or proliferation, and defective BDNF signaling was reported (Estes and McAllister, 2015; Koyama and Ikegaya, 2015; Petrelli et al., 2016). Similar to ASD, studies from postmortem brain of schizophrenia and bipolar disorders patients indicate abnormalities in regional microglia density and morphology that are changing during disease progression. Recently, genome-wide association studies linked microglial sensing receptors, like the major histocompatibility complex (Mokhtari and Lachman, 2016) and alleles of the complement component 4 (Sekar et al., 2016) with schizophrenia. Taken together, these data show that environmental risk factors combined with a genetic disposition might result in aberrant microglial activation or dysregulated synaptic pruning. The disruption of the fine interplay between microglia and the neuronal network might then develop into a psychiatric disorder.

#### **1.2.1.4 Microglial sensing of the neuronal glycocalyx**

Microglia have a diverse set of surface receptors to recognize the neuronal glycocalyx and to survey the brain parenchyma for foreign structures (reviewed in ElAli and Rivest, 2016). Some of these receptors belong to the group of pattern recognition receptors (PRRs), such as toll-like receptors, which recognize pathogen- as well as damage-associated molecular patterns (PAMPs and DAMPs). While PAMPs are normally found on microbes, DAMPs are generally released by damaged or dysfunctional cells as a result of aging or environmental risk factors (e.g. proteins like amyloid beta, alpha-synuclein, and hungtintin) and the activation of PRRs normally induces neuroinflammation. Scavenger receptors, like CD68 (also known as Macrosialin) are important for an innate immune response (Peiser et al., 2002). Under normal conditions, CD68 is expressed on the intracellular membrane of late endosomes and is actively involved in microglial phagocytosis. Its expression is increased upon activation by oxidized

low density lipoproteins (Ramprasad et al., 1996) and therefore, also seen as a typical microglia activation marker. Cytokine receptors play a crucial role in modulating microglial cell function. Microglia can be activated by cytokines from other cell types but also by their own released cytokines in a positive autocrine manner (Nadeau and Rivest, 2000; Kuno et al., 2005). Microglia are the main source of the proinflammatory cytokine TNF $\alpha$  in the brain (Dopp et al., 1997). IL1 $\beta$  signaling leads to nuclear factor-kappa B (NF- $\kappa$ B) pathway activation (Spörri et al., 2001), whereas IL4 and IL10 are potent anti-inflammatory modulators of microglial function (Ledeboer et al., 2000).

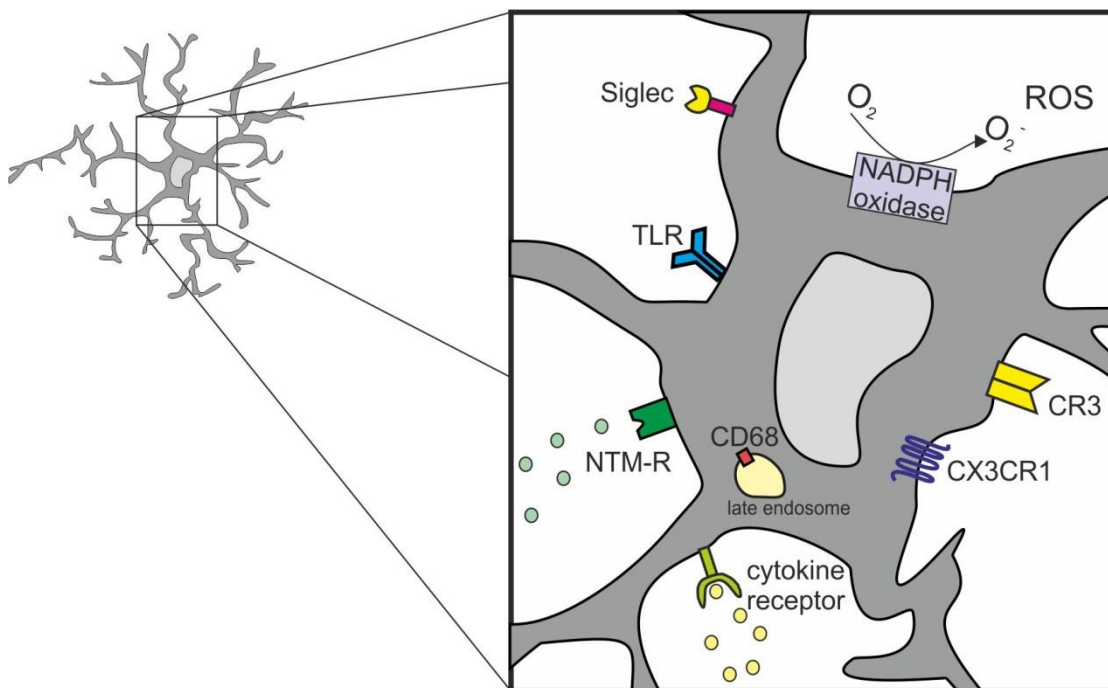


**Figure 6: A schematic overview of several microglial receptors.** Microglia express a diverse set of receptors on their cell surface. The location can be close to the soma as well as in the distant processes. The different surface receptors help microglia to communicate with other cells and to sense alterations in the brain. Internal receptors like CD68 are mainly involved in phagocytosis and degradation pathways. CR – complement receptor; CX3CR1 – fractalkine receptor; NADPH - nicotinamide adenine dinucleotide phosphate; NTM-R – neurotransmitter receptor; ROS – reactive oxygen species; Siglec - sialic acid-binding immunoglobulin-type lectins; TLR – toll-like receptors.

Chemokine signaling is another way of cell-cell communication in the brain. Chemokines are produced by different cell populations in the brain and are soluble mediators that function as chemoattractant and direct cell motility. One specific case is CX3CL1, which is produced by neurons. It can act either as soluble mediator or bound to the neuronal membrane (Fernandez and Lolis, 2002). CX3CL1-CX3CR1-signaling in neuron-microglia communication regulates microglial dynamics and migration during neuronal maintenance (Paolicelli et al., 2014). Microglia even express receptors for different neurotransmitters, like ATP, glutamate, gamma-aminobutyric acid (GABA), dopamine or acetylcholine to ensure an optimal neuron-microglia crosstalk (reviewed in Kettenmann et al., 2011).

To specifically recognize sialic acids on the neuronal glycoalyx microglia express Siglecs (reviewed in Linnartz and Neumann, 2013). Siglecs are type 1 transmembrane receptors and are only expressed on cells of the myeloid lineage (Crocker et al., 2007). These regulatory receptors tightly control the microglial immune function and can signal via the immunoreceptor tyrosine-based activation motif (ITAM) in their cytoplasmic tail or act as an inhibitory receptor via the immunoreceptor tyrosine-based inhibition motif (ITIM). Downstream of ITAM the Src and Syk tyrosine kinases are recruited (Daëron, 1997) that generate a mitogen-activated protein kinase (MAPK)-NF- $\kappa$ B response, while ITIM activation results in the recruitment and activation of Src homology region 2 domain-containing phosphatase-1 (SHP1) and Src homology region 2 domain-containing inositol phosphatase-1 (SHIP1) and thus, an inhibitory response (Billadeau and Leibson, 2002). Siglec signaling is mainly inhibitory and contributes to microglial cell adhesion, endocytosis, cytokine release and phagocytosis. The inhibitory mouse Siglec-E (or CD33) was proven to recognize sialic acids on the neuronal glycoalyx, which prevented phagocytic removal. Furthermore, this neuroprotective effect disappeared after enzymatic removal of sialic acids (Claude et al., 2013).

## **1.2.2 The complement system**

The complement system is one of the major mechanisms of effective host defense against initial infections as described in detail by Murphy and colleagues (Murphy et al., 2008). In short, the activation of the complement system by foreign structures leads to a rapidly amplifying cascade starting with the coating of the foreign structures (opsonization). Recognition of opsonized structures by complement-specific receptors on macrophages leads either to the uptake via phagocytosis or alternatively, to detrimental inflammatory downstream processes that result in the lysis of the opsonized cells (Figure 7). In contrast, recent publications also described the complement cascades as key system in brain homeostasis and is reviewed by Ricklin et al. (2010).

### **1.2.2.1 Complement components and its signaling pathways**

In general, the complement system consists of different plasma proteins, which can be activated either directly by pathogens or indirectly by antibodies bound to pathogens. These activated plasma proteins on the pathogen surface initiate a cascade of protease cleavage reactions with the active form of complement component 3b (C3b) as central event and three final defense strategies as described below.

Depending on the initial trigger three different pathways are discriminated: the classical pathway, the lectin pathway, and the alternative pathway (see Figure 7). In the classical pathway, the cascade is triggered directly by the pathogen itself or by pathogen-bound antibodies (lower pathway, Figure 7). The recognition protein C1q binds to the charged targets on the pathogen and activates the proteases C1r and C1s within the C1 complex (C1q:C1r<sub>2</sub>:C1s<sub>2</sub>). Activated C1s then cleaves C4 and C2, thereby generating a C3 convertase complex (C4b2a), which can cleave the complement component 3 (C3) into the active form C3b and the soluble mediator C3a (“Opsonization”, Figure 7). The lectin pathway is activated upon mannose-binding lectins (MBL) on the pathogen surface or upon the binding of carbohydrates through ficolins (middle pathway, Figure 7). Like the C1 complex, MBL or ficolin form a complex with MBL-associated serine proteases (MASPs). Upon binding, activated MASPs cleave and activate C4 and C2 resulting in the formation of a C3 convertase (C4b2a) as well. In the alternative pathway, the cleavage cascade is triggered by spontaneous hydrolysis of C3 into the active form C3b in the absence of a specific antibody (upper pathway, Figure 7). This alternative event is accompanied by binding of plasma protein factor B and a protease called factor D to form another active C3 convertase (C3bBb). Only if the active form C3b immediately tags the foreign cell, the pathway is amplified. Otherwise it will be directly deactivated. Thus, the alternative pathway provides a basic pattern recognition mechanism and an amplification loop for the other two pathways. After the initial activation, all three pathways converge on the convertase C3 that cleaves C3 into the active form C3b and a smaller soluble fragment C3a (see red square in Figure 7). The active form C3b binds directly to the pathogen (opsonization) and is the central event in the complement activation.

Abundant C3b opsonization of the pathogen is recognized by immune cells via complement receptors and is followed by phagocytic removal as one of three defense strategies. In addition, C3b can also form a C5 convertase (C4b2a3b or C3bBb3b) that cleaves C5 and produces the very potent inflammatory peptide C5a and the large fragment C5b. The active C5b recruits the terminal complement components. In the final phase (“Lysis”, Figure 7) the complement components C5b, C6, C7, C8, and C9 assemble the membrane-attack complex (MAC) to form a pore in the membrane of the pathogen surface, which leads to the lysis and the death of the pathogen (second defense strategy). The third defense strategy is accomplished by the small soluble cleavage fragments C4a, C3a, C5a (see Figure 7, encircled in orange). These fragments are powerful peptide mediators of inflammation contributing to the prompt initiation of the adaptive immune cells but also function as chemoattractant to recruit phagocytes to the site of infection.

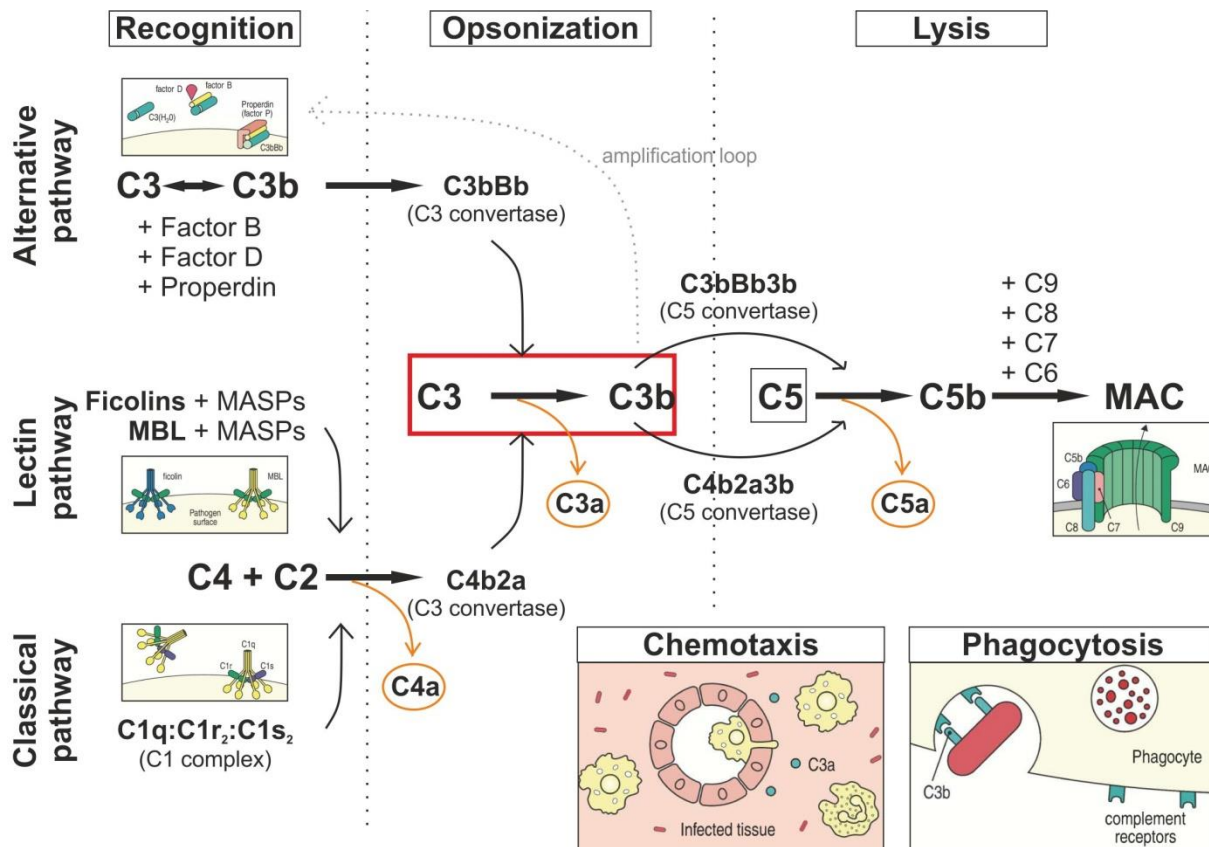


**Figure 7: Overview of the three complement signaling pathways.** The complement signaling pathways are cascades of protease cleavage reactions. Dependent on the initial trigger three different pathways can be distinguished: the classical pathway, the lectin pathway, and the alternative pathway. All three pathways can be divided into a recognition phase, an opsonization phase and a lysis phase. In the opsonization phase all three pathways converge on the central cleavage event of C3 into C3b and C3a (red box). This leads further downstream to either the assembly of the membrane-attack complex (MAC) with subsequent lysis, to the chemotactic recruitment of immune cells, and to phagocytosis (orange arrows). MBL - mannose-binding lectins (Images taken and modified from Murphy et al., 2008 and Mayilyan, 2012.)

The complement system is an amplifying cascade that can be initiated by only a small number of complement proteins but then turns rapidly into a large effective immune response. To prevent unintentional, spontaneous activation of the complement cascade and unnecessary tissue damage, several regulatory proteins have coevolved. Complement regulatory proteins can be found as soluble plasma proteins (e.g. factor H and Properdin) or bound to the host-cell membrane (e.g. decay-accelerating factor, DAF and CR1). These molecules ensure that correct complement activation only takes place close to the cell surface.

However, inappropriate activation of the complement system or defects in complement regulator proteins can lead to impaired host defense against certain pathogens and increased susceptibility to autoimmune diseases (Mayilyan, 2012). For instance, deficiency in early components of the cascade like C1, C2, C4 or MBL is often associated with systemic lupus erythematosus (Agnello et al., 1972; Day et al., 1973; Bowness et al., 1994; Pickering et al., 2000; Yang et al., 2004; Glesse et al., 2011), whereas recurrent invasive infections are more



associated with deficiencies in the terminal components C5, C6, C7, C8, and C9 (Mayilyan, 2012). Impaired neutrophil or monocyte recruitment can be due to mutations in complement receptor 3 (CR3; Springer et al., 1984, 1986) and a deficiency in the regulatory factor H contributes to age-related macular degeneration (AMD; Skerka et al., 2007).

#### **1.2.2.2 The role of complement system in homeostasis**

In the recent years, our view of the complement system has fundamentally changed as reviewed by Ricklin and colleagues (Ricklin et al., 2010). Beside immune surveillance the complement system seems to play a not negligible role in cell homeostasis and tissue development and repair. The involvement of the complement system in processes, like synapse maturation (Stevens et al., 2007; Kraft et al., 2016), clearance of immune complexes and endogenous debris, angiogenesis (Nozaki et al., 2006), mobilization of hematopoietic stem-progenitor cells (Shinjyo et al., 2009), neurogenesis, and tissue regeneration (Nozaki et al., 2006; Markiewski et al., 2009) are currently under investigations. Most homeostatic pathways are carried out by the classical complement pathway. In contrast to a normal immune response, the activation of the inflammatory C5a-C5aR-axis or the MAC formation (Gershov et al., 2000) are inhibited and tightly regulated during homeostasis. Pathways that normally lead to oxidative burst in macrophages are strictly downregulated. Additionally, a connection between the complement system and metabolism was recently pointed out (Hotamisligil, 2006; Kolev and Kemper, 2017). Data demonstrated that adipocytes communicate with macrophages (Wellen and Hotamisligil, 2005) and for instance, C3 was reported as a strong marker of insulin resistance in elderly patients (Muscari et al., 2007).

Likewise, failure in effective housecleaning (e.g. removal of apoptotic debris or immune complexes) not only impairs host homeostasis but can have detrimental consequences for the whole system. The complement system was linked to a number of neurological diseases, like AD (Fonseca et al., 2009), PD (Loeffler et al., 2006), glaucoma (Stevens et al., 2007), MS (Ingram et al., 2009; Michailidou et al., 2016), and schizophrenia (Mayilyan et al., 2008; Sekar et al., 2016). Furthermore, in a mouse model of repeated systemic challenge with lipopolysaccharides (LPS), inflammation induces neuronal loss in the substantia nigra by the activation of the microglial complement-phagosome pathway (Bodea et al., 2014).

These findings once more highlight the close interaction between the complement system and microglia in the brain and support the emerging view that the functions of the complement

system go beyond pure immune surveillance and might contribute substantially to the homeostasis in the brain.

### 1.3 Modelling alterations in the glycocalyx

Previous publications from Linnartz-Gerlach and colleagues (Linnartz et al., 2012b; Linnartz-Gerlach et al., 2016) showed that the removal of sialic acids from the glycocalyx, the “Don’t eat me”-signal, leads to neuronal removal *in vitro*. This complement-mediated phagocytosis by microglia was investigated in both, murine and human neuron-microglia/macrophage co-cultures. Blocking of the CR3 (but not of the additionally existing CR1 in the human system) was able to prevent the phagocytic removal of neurons by microglia *in vitro*. However, to understand how microglia deal with alterations of the glycocalyx in the complex *in vivo* situation a suitable model for mimicking an altered glycocalyx was needed. Enzymatic removal of sialic acid residues by sialidases as it was performed in these cell culture experiments was not an option for *in vivo* studies. In 2002, Schwarzkopf and colleagues engineered a mouse heterozygous for GNE ( $GNE^{+/-}$  mice), the essential enzyme of the sialic acid biosynthesis (Schwarzkopf et al., 2002). The inactivation of GNE was realized by targeted mutagenesis of exon 2 of the UDP-GlcNAc 2-epimerase gene. As mentioned before, GNE catalyzes the two initial steps in the sialic acid biosynthesis (see also Figure 3). However, the complete knockout of the GNE gene ( $GNE^{-/-}$ ) in mice leads to prenatal lethality between E8.5 and E9.5 and could only be fully investigated in embryonic stem cells (Schwarzkopf et al., 2002). Nevertheless, first studies showed that the mice heterozygous for GNE ( $GNE^{+/-}$ ) expressed decreased levels of sialic acids in different organs (Gagiannis et al., 2007). Gagiannis and colleagues described an overall reduction of membrane-bound sialic acids by 25 % in the otherwise healthy appearing  $GNE^{+/-}$  mice making them a suitable model for investigating the role of an altered glycocalyx.

### 1.4 Aims of this project

Neuronal loss is a central event in neurodegenerative diseases and during aging. Although thorough research investigations are taking place to understanding the principles of the neuronal loss, suitable therapies are still missing. As described before, sialic acids can be easily removed during oxidative stress and are shown to be decreased in the aged brain as well. Therefore, I addressed in this study the question whether such reduced levels of sialic acids can lead to

---

neuronal loss in the brain as proposed in the model based on *in vitro* data (Figure 8) and whether aging plays a role.

The first intention of this study was to set up an *in vivo* model to mimic an altered glycocalyx as shown previously *in vitro* (Linnartz et al., 2012b; Linnartz-Gerlach et al., 2016). Secondly, I wanted to understand if the neuronal loss *in vivo* is also mediated via microglia and the complement system as the *in vitro* data has shown and if this mechanism is causing neuroinflammation in the brain. Furthermore, I wanted to clarify if the neuronal loss can be prevented via inhibition of the complement system in such a complex system and what effect aging might play.

To solve these questions, I characterized the sialylation status in the brain of the transgenic  $GNE^{+/-}$  mice during aging in more depths and evaluated the  $GNE^{+/-}$  mice as model for an altered glycocalyx. The neuronal density was investigated in different brain regions of  $GNE^{+/-}$  mice at several time points and possible microglia alterations on transcription and protein levels were examined. Furthermore, the transcription analysis of inflammatory cytokines and investigations for astrogliosis helped to elucidate if neuroinflammation is occurring in the brain of these mice. I reconsidered the complement system as underlying pathway and checked for typical markers on transcription level. In addition, a transcriptome analysis was performed on adult mouse brains to understand the full impact of altered sialylation. Once the *in vitro* data were confirmed and I could show that *in vivo* reduced sialic acid levels lead to neuronal loss by microglia in a complement-dependent manner,  $GNE^{+/-}$  mice were crossed with mice deficient for the central complement factor C3 ( $C3^{-/-}$  mice) to rescue the neuronal loss *in vivo*.

In summary, with this project the previously discovered *in vitro* mechanisms were transferred into the living system to confirm and understand the impact of glycocalyx alterations. This study highlights the importance of sialic acids on the glycocalyx in prevention of neuronal loss especially during aging.

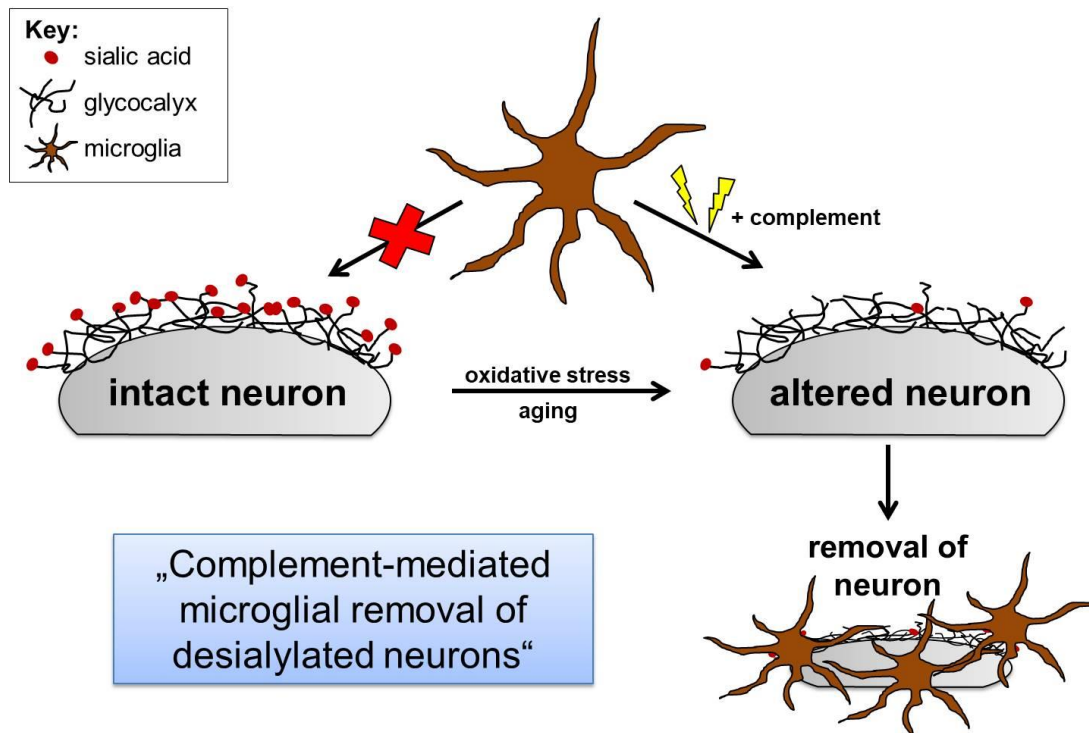


**Figure 8: Proposed model of glycoalyx alteration.** Sialic acids on the neuronal glycoalyx serve as “Don’t eat me”-signal and inhibit microglia via the inhibitory Siglecs. Environmental factors, like oxidative stress and aging can reduce the level of sialic acids. Consequently, an altered neuronal glycoalyx with reduced sialic acids misses the inhibitory signal and simultaneously is recognized by the complement system that activates microglial phagocytosis. This pathway leads to removal of desialylated neurons by microglia. The proposed model highlights the important function of sialic acids on the neuronal glycoalyx.

## 2 Materials and Methods

### 2.1 Materials

#### 2.1.1 Chemicals and Reagents

Name	Company
1,4-diazabicyclo[2.2.2]octane (DABCO)	Sigma, Germany
4',6-diamidino-2-phenylindole (DAPI)	Sigma, Germany
Agarose (PeqGOLD Universal)	PeqLab, Germany
AquaPoly/Mount	Polysciences Europe, Germany
Boric acid (H <sub>3</sub> BO <sub>3</sub> )	Roth, Germany
Bovine serum albumin (BSA)	Sigma, Germany
Double-distilled water (ddH <sub>2</sub> O)	autoclaved and filtered in the institute
Dulbecco's Phosphate Buffer Solution (PBS)	Gibco, Germany
Ethanol (C <sub>2</sub> H <sub>6</sub> O)	Roth, Germany
Ethidium Bromide (10g/l)	Roth, Germany
Ethylendiamintetraacetate (EDTA)	Roth, Germany
Glycerol	Sigma, Germany
Hexanucleotide Mix (10x)	Roche, Germany
Isopropanol	Roth, Germany
KETANEST <sup>®</sup> S (Ketamin)	Pfizer Pharma, Germany
Mowiol 4-88	Kremer Pigmente, Germany
Normal goat serum (NGS)	Sigma, Germany
O.C.T. <sup>™</sup> Compound, Tissue Tek <sup>®</sup>	Sakura, USA
Paraformaldehyde (PFA)	Sigma, Germany
QIAzol Lysis Reagent	Qiagen, Germany
Rompun <sup>®</sup> 2% (Xylazin)	Bayer, Germany
Sodium azide	Sigma, Germany
Sodium chloride (NaCl)	Roth, Germany
Sodium hydroxide (NaOH)	Roth, Germany
Sodiumhydrogenphosphate (NaH <sub>2</sub> PO <sub>4</sub> *7H <sub>2</sub> O)	Roth, Germany
Sodiumhydrogenphosphate (NaH <sub>2</sub> PO <sub>4</sub> *H <sub>2</sub> O)	Roth, Germany
Sucrose	Roth, Germany

SuperScript <sup>®</sup> III Reverse Transcriptase	Invitrogen, Germany
SYBR <sup>®</sup> Green ER <sup>™</sup> qPCR Super Mix	Invitrogen by Life Technologies, USA
Tert-amyl alcohol	Sigma, Germany
Trichloromethane/chloroform	Roth, Germany
Tris base	Roth, Germany
Tris buffer, 0.2 M	Roth, Germany
Triton X-100	Sigma, Germany

### 2.1.2 Consumables

Name	Company
1 ml syringe	Braun, Germany
10 µl, 100 µl, 1000 µl pipette tips	StarLab, Germany
15 ml plastic tubes	Greiner, Germany
5 ml, 10 ml, 25 ml plastic pipettes	Costar, Germany
50 ml plastic tubes	Sarstedt, Germany
Cell strainer 40 µm Nylon	BD Falcon, Germany
Cell strainer 70 µm Nylon	BD Falcon, Germany
Disposable vinyl specimen molds (Cryomold <sup>®</sup> , 25 x 20 x 5 mm)	Tissue-Tek <sup>®</sup> Sakura, USA
Erlenmeyer flask, 250 ml	Schott-Duran, Germany
Examination gloves (Micro-Touch)	Ansell Healthcare, Belgium
Glass cover slips (24 x 60 mm)	Thermo Scientific, USA
Injection needles	Braun, Germany
Polymerase chain reaction (PCR) tubes, 500 µl	Biozym Scientific GmbH, Germany
QPCR Seal optical clear film	PeqLab, Germany
QPCR Semi-skirted 96 Well PCR Plate	PeqLab, Germany
Stainless steel beads (7 mm)	Qiagen, Germany
SuperFrost <sup>®</sup> Plus microscope slides	Thermo Scientific, USA

### 2.1.3 Technical equipment

Name	Company
Agilent 2100 Bioanalyzer	Agilent, Luxembourg
AxioImager.Z1/ApoTome microscope	Zeiss, Germany

BD fluorescence-activated cell sorter (FACS) Calibur	BD Biosciences
Biofuge Fresco/ pico (centrifuges)	Heraeus, Germany
Electrophoresis Power Supply EPS-301	Amersham Bioscience, Germany
Fluoview1000 Confocal microscope	Olympus, Germany
Freezer -20 °C ProfiLine	Liebherr, Germany
Freezer -80 °C Herafreeze	Heraeus, Germany
GelDoc	BioRad, Germany
HI 9321 Microprocessor pH meter	Hanna Instruments, Germany
Mastercycler egradient S	Eppendorf, Germany
Megafuge, 1.0 R. (centrifuge)	Heraeus, Germany
Microm Cryo Star HM 560	Thermo Scientific, USA
NanoDrop 2000c spectrophotometer	Thermo Scientific, USA
NextSeq 500	Illumina, USA
Perfect Blue™ Horizontal Midi/Mini Gel Systems	PeqLab, Germany
Pumpdrive 5001 (perfusion pump)	Heidolph, Germany
Thermocycler T3 (PCRmaschine)	Biometra, Germany
Thermomixer compact (heating block)	Eppendorf, Germany
Tissue Lyser LT	Qiagen, Germany
Vortex Genie2	Scientific Industries Inc., USA

#### 2.1.4 Buffers and solutions

Name	Ingredients
1 % Agarose gel	0.6 g agarose 3 µl ethidium bromide 60 ml Tris/Borate/EDTA buffer (1x)
10x (0.125 M) phosphate buffered saline (PBS), pH 7.3	0.007 M NaH <sub>2</sub> PO <sub>4</sub> *H <sub>2</sub> O 0.034 M NaH <sub>2</sub> PO <sub>4</sub> *7H <sub>2</sub> O 0.6 M NaCl up to 1 liter ddH <sub>2</sub> O
10x BSA	10 g BSA in 100 ml 1x PBS

10x Tris/Borate/EDTA (TBE) buffer	1.78 M Tris base 1.78 M boric acid 0.04 M EDTA (pH 8.0) up to 2 litre ddH <sub>2</sub> O
30 % sucrose solution	30 g sucrose in 100 ml 1x PBS 0.1 % sodium azide
4 % paraformaldehyde (PFA), pH 7.3	20 g PFA + 30 ml NaOH + 50 ml PBS (1x) up to 1 litre ddH <sub>2</sub> O
Anaesthesia solution (Ketamin/Xylazin)	2 ml Ketanest 0.5 ml Rompun 2.5 ml ddH <sub>2</sub> O
Mowiol	4.8 g Mowiol 4-88 12 g Glycerol 24 ml 0.2 mM Tris buffer, pH 8.5 1.32 g DABCO 12 ml ddH <sub>2</sub> O
Tris buffer pH 8.5	50 mM Tris 150 mM NaCl Adjust pH with HCl to pH 8.5

### 2.1.5 Mice

Mouse line	Mouse strain	Origin/Provider
C57BL/6J	C57BL/6J	Charles River, Sulzfeld, Germany
C3 <sup>-/-</sup>	B6;129S4-C3tm1Crr/J	Charles River, Sulzfeld, Germany
GNE <sup>+/-</sup>	129/OLA and Balb/C mixed background mouse with heterozygous deletion of GNE gene (Schwarzkopf et al. 2002)	Animals were kindly provided by Prof. Horstkorte (University of Halle-Wittenberg, Halle [Saale], Germany).
GNE/C3	GNE <sup>+/-</sup> mice crossed with C3 <sup>-/-</sup> mice	

### 2.1.6 Primers



<b>Target</b>	<b>Orientation</b>	<b>Sequence</b>
37	forward	5' –CACCAGGCTCCACACGATTG– 3'
42	reverse	5' –GATTGAAATATGCCCAATACTTTG– 3'
Aif1	forward	5' –GAAGCGAATGCTGGAGAAAC– 3'
	reverse	5' –AAGATGGCAGATCTCTTGCC– 3'
A541	forward	5' –CGAAGGAGCAAAGCTGCTATTGGCC– 3'
C1qa	forward	5' –AGAGGGGAGCCAGGAGC– 3'
	reverse	5' –CTTTCACGCCCTTCAGTCCT– 3'
C1qb	forward	5' –GACTTCCGCTTTCTGAGGACA– 3'
	reverse	5' –CAGGGGCTTCCTGTGTATGGA– 3'
C1qc	forward	5' –GCCTGAAGTCCCTTACACCC– 3'
	reverse	5' –GGGATTCCTGGCTCTCCCTT– 3'
C3	forward	5' –TAGTGCTACTGCTGCTGTTGGC– 3'
	reverse	5' –GCTGGAATCTTGATGGAGACGCTT– 3'
C3geno	forward	5' –ATCTTGAGTGCACCAAGCC– 3'
C3mt	reverse	5' –GCCAGAGGCCACTTGTGTAG– 3'
C3wt	reverse	5' –GGTTGCAGCAGTCTATGAA– 3'
C4b	forward	5' –TGGAGGACAAGGACGGCTA– 3'
	reverse	5' –GGCCCTAACCCTGAGCTGA– 3'
Cd68	forward	5' –CAGGGAGGTTGTGACGGTAC– 3'
	reverse	5' –GAAACATGGCCCGAAGTATC– 3'
GAPDH (ms)	forward	5' –ACAACCTTTGGCATTGTGGAA– 3'
	reverse	5' –GATGCAGGGATGATGTTCTG– 3'
Gne	forward	5' –AAACTGGCCCCGATCATGTT– 3'
	reverse	5' –TCTACCATGGCCGCTTCATC– 3'
Il1b	forward	5' –CTTCCTTGTGCAAGTGTCTG– 3'
	reverse	5' –CAGGTCATTCTCATCACTGTC– 3'
Itgam	forward	5' –AATTGGGGTGGGAAATGCCT– 3'
	reverse	5' –TGGTACTTCCTGTCTGCGTG– 3'
Tmem119	forward	5' –GTGTCTAACAGGCCCCAGAA– 3'
	reverse	5' –AGCCACGTGGTATCAAGGAG– 3'
Tnfa	forward	5' –GGTGCCTATGTCTCAGCCTC– 3'
	reverse	5' –TGAGGGTCTGGGCCATAGAA– 3'

## 2.1.7 Antibodies

### 2.1.7.1 Primary antibodies

Antigen	host	company	dilution
A2B5	mouse	BD Pharmingen, #563775	1:200
CD56	rat	BD Pharmingen, #556325	1:200
CD68	rat	AbD Serotec, MCA1957	1:500
Glial fibrillary acidic protein (Gfap)	rabbit	DAKO, #Z0334	1:500
IgM kappa	mouse	BD Pharmingen, #557275	1:200
IgM kappa	rat	BD Pharmingen, #553940	1:200
Ionized calcium binding adaptor molecule 1 (Iba1)	rabbit	Wako, #019-19741	1:1000
Neuronal nuclei (NeuN)	mouse	Millipore, MAB377	1:500
Polysialylated neural cell adhesion molecule (PSA-NCAM)	mouse	Millipore, MAB5324	1:200
Tyrosine hydroxylase (TH)	rabbit	Sigma, # T8700	1:1000

### 2.1.7.2 Secondary antibodies

Fluorophore	reactivity	host	company	dilution
Alexa Fluor® 488	rabbit	goat	Invitrogen, #A11008	1:500
Alexa Fluor® 488	rat	goat	Invitrogen, #A11006	1:500
Cyanine 3 (Cy3)-conjugated F(ab') <sub>2</sub> fragment	mouse	goat	Dianova, #115-166-072	1:200
Cy3-conjugated F(ab') <sub>2</sub> fragment	rat	goat	Dianova, #112-166-072	1:200
R-Phycoerythrin (PE)-conjugated F(ab') <sub>2</sub> fragment	rat	goat	Jackson Immuno Research, #112-116-143	1:200
PE-conjugated F(ab') <sub>2</sub> fragment	mouse	goat	Jackson Immuno Research, #115-116-146	1:200

## 2.1.8 Kits and markers

Name	Company
100 base pair DNA ladder	Invitrogen, Germany

KAPA mouse genotyping Hot Start Kit	PeqLab, Germany
Qubit dsDNA HS assay Kit	Thermo Scientific, USA
RNase-Free DNase Set	Qiagen, Germany
RNeasy® Mini Kit	Qiagen, Germany
SuperScript First-Strand Synthesis System	Invitrogen, Germany
TruSeq Stranded mRNA Library Prep kit	Illumina, USA

### 2.1.9 Software

Name	Company
AxioVisio V4.8.2.0	Zeiss, Germany
Corel Draw® X5 + X8	Corel GmbH, Germany
Ensembl8 (GRCm38.p3, release 79)	EMBL-EBI, UK
FastQC v0.11.3	Babraham Bioinformatics, UK
FlowJo 8.6	Tree Star, USA
GraphPad QuickCalcs	GraphPad Software Inc., USA
IBM SPSS Statistics (v.22)	IBM Corporation, Germany
ImageJ 1.46h + NeuronJ plugin	National Institute of Health, USA
Ingenuity Pathway Analysis®	Qiagen, USA
Master cycler ep realplex	Eppendorf, Germany
Mendeley Desktop (v1.17.9)	Mendeley Ltd., USA
Microsoft Office 2010	Microsoft, USA
NanoDrop 2000/2000c	Thermo Fisher Scientific, USA
Olympus FluoView V3.1	Olympus, Germany
Prism 7 (v7.01)	GraphPad Software Inc., USA
QuantityOne	Bio-Rad, Germany
R (v3.4.0; free software)	R Core Team, <a href="https://www.R-project.org/">https://www.R-project.org/</a>
RStudio (v1.1; free software)	RStudio, <a href="http://www.rstudio.com/">http://www.rstudio.com/</a>
Spliced Transcripts Alignment to a Reference9 (STAR) v2.5.2b	Illumina, USA
STATA®/IC (v13.1 for Windows)	Stata Corp. LP, USA

## 2.2 Methods

### 2.2.1 Mice

For the characterization of an altered glycoalyx *in vivo*, mice heterozygous for the bifunctional enzyme GNE (referred as GNE<sup>+/-</sup> mice in the text) were kindly provided by Prof. Horstkorte (University of Halle-Wittenberg, Halle [Saale], Germany). The GNE<sup>+/-</sup> mice have a targeted deletion in exon 2 of the mouse Gne coding region by insertion of a neomycin cassette and were engineered by Schwarzkopf and colleagues (Schwarzkopf et al., 2002). The mice were subsequently backcrossed with C57BL/6J mice for at least ten generations in the institute's animal facility. For rescue experiments, GNE<sup>+/-</sup> mice were crossbred with B6;129S4-C3<sup>tm1Crr/J</sup> (referred as C3<sup>-/-</sup> mice in the text) to obtain GNE<sup>+/-</sup>C3<sup>-/-</sup> mice. The C3<sup>-/-</sup> mice have a targeted deletion of the nucleotides 1850-2214 within the mouse C3 coding region (AA 620-741, pro-C3 numbering) and were originally purchased from Charles River (Sulzfeld, Germany). For further offspring and to keep the GNE/C3 mouse line, breeding of GNE<sup>+/-</sup>C3<sup>-/-</sup> mice was performed. Animals were housed in the institute's animal facility in specific pathogen free environment with water and food *ad libitum* at 12 hours dark/night cycle. Housing and breeding of the animals were performed in accordance with the German guidelines of the animal care and use committee. All efforts were made to minimize the number of animals used and their suffering.

#### 2.2.1.1 Genotyping of mice

Tissue of either ear or tail was taken for the isolation of genomic DNA using the KAPA mouse genotyping Hot Start Kit according to the manufacturer's protocol. Genomic DNA was eluted in ddH<sub>2</sub>O. Then, PCR with the genotype-specific primers (see Table 1) was performed using the KAPA2G Fast Hot Start Genotyping Mix from the same kit as described in Table 2.

**Table 1: Genotyping primer mix**

Mouse line	Primer mix	Expected product length
GNE <sup>+/-</sup>	37 10 µM A541 10 µM 42 20 µM (modified from Weidemann et al., 2010)	wildtype allele (37/42) - 500 bp knockout allele (A541/42) - 750 bp heterozygous: both bands
C3 <sup>-/-</sup>	C3wt 7.8 µM C3mt 4.46 µM C3geno 7.8 µM	wildtype allele – 350 bp knockout allele – 500 bp heterozygous: both bands
GNE/C3	see primer mix for GNE <sup>+/-</sup> and for C3 <sup>-/-</sup>	

**Table 2: Genotyping PCR reaction mix**

<b>Master Mix for GNE</b>	<b>1x</b>	<b>Master Mix for C3</b>	<b>1x</b>
KAPA Genotyping Mix	10 $\mu$ l	KAPA Genotyping Mix	10 $\mu$ l
ddH <sub>2</sub> O	5 $\mu$ l	ddH <sub>2</sub> O	6 $\mu$ l
primer mix	4 $\mu$ l	primer mix	3 $\mu$ l
DNA	1 $\mu$ l	DNA	1 $\mu$ l

The two different settings for the thermocycler are described in Table 3.

**Table 3: Genotyping programs for thermocycler****GNE PCR**

Initial denature	94 °C	4:00 minutes	
Denature	94 °C	0:30 minutes	} 32x
Annealing	58 °C	0:45 minutes	
Elongation	72 °C	0:60 minutes	
Final elongation	72 °C	7:00 minutes	
	4 °C	$\infty$	

**C3 PCR**

Initial denature	94 °C	3:00 minutes	
Denature	94 °C	0:20 minutes	} 12x
Annealing	64 °C	0:30 minutes	
Elongation	72 °C	0:35 minutes	
Denature	94 °C	0:20 minutes	} 25x
Annealing	58 °C	0:30 minutes	
Elongation	72 °C	0:35 minutes	
Final elongation	72 °C	7:00 minutes	
	4 °C	$\infty$	

PCR products were loaded onto 1 % agarose gel containing ethidium bromide. A 100 base pair ladder was used as reference marker. The samples were run at 100-120 V and 110 mA for 45 minutes. The gels were visualized using GelDoc with QuantityOne software.

For mouse genotyping the presence of the knockout *gne* allele on the gel was important as shown in Figure 9. For wildtype mice the presence of only the wildtype allele with a band at

500 bp was detected. Heterozygous mice were determined by the presence of one wildtype and one knockout allele with two bands, at 500 bp and at 750 bp. The additional band for the knockout allele at around 2500 bp was not detectable within the normal number of PCR cycles and was therefore not taken into account.

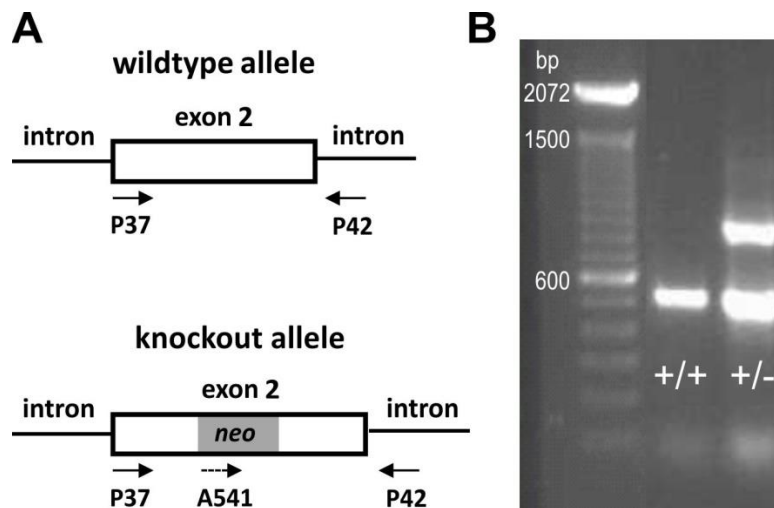


**Figure 9: GNE genotyping example.** (A) Illustration of the wildtype ( $GNE^{+/+}$ ) and the knockout ( $GNE^{+/-}$ ) allele showing the binding sites of GNE-specific primers (A541/42 – 750 bp; 37/42 – 500 bp or 2500 bp). In  $GNE^{+/-}$  mice a neomycin (neo) cassette was introduced in exon 2 of one allele. (Scheme was adapted and modified from Weidemann et al. 2010). (B) A 1 % agarose gel with the representative PCR products of both genotypes is shown. The genotypes were determined by the bands as following:  $GNE^{+/+}$  500 bp;  $GNE^{+/-}$  500 bp and 750 bp.

### 2.2.1.2 Tissue preparation

If not stated otherwise male animals were weighed routinely, followed by an anesthesia with 200  $\mu$ l per 10 g body weight anesthesia solution (Ketamin/Xylazin; for more details see 2.1.4) and then perfused with 1x PBS. The brain was directly removed and cut into both hemispheres. One hemisphere was directly used for RNA isolation, the other half was stored in 4 % PFA for 24 hours at 4  $^{\circ}$ C, followed by incubation in 30 % sucrose solution at 4  $^{\circ}$ C until the brain was fully soaked and sank to the bottom of the tube. The fixed brains were embedded in Tissue Tek<sup>®</sup> and stored at -80  $^{\circ}$ C for immunohistochemistry.

## 2.2.2 Analysis of gene transcription

### 2.2.2.1 RNA isolation of brain samples

RNA from freshly taken hemispheres of male transgenic mice or wildtype littermates (see section 2.2.1.2) was extracted using the RNeasy<sup>®</sup> Mini kit from Qiagen. Shortly, tissue was directly homogenized twice with 1 ml Qiazol Lysis Reagent and a stainless steel bead (mean diameter: 7 mm) in a Tissue Lyser LT for 3 minutes at 50 Hz. After 5 minutes incubation at room temperature, 200  $\mu$ l chloroform were added. The mixed suspension was again incubated

for 3 minutes at room temperature before centrifuging at 12000 x g for 15 minutes at 4 °C. The upper, aqueous phase was transferred into a new tube and 500 µl 70 % ethanol were added and mixed. Then, 600 µl of the solution were transferred into an RNeasy column and centrifuged at 8000 x g for 20 seconds at room temperature. The flow-through was discarded and the remaining solution was transferred in the same way until the complete lysate was loaded onto the column. The RNA isolation procedure was then continued according to the manufacturer's protocol. 50 µl eluted RNA was either stored at -80 °C or directly used for reverse transcription.

### 2.2.2.2 cDNA synthesis by reverse transcription of RNA

Reverse transcription of RNA was performed with SuperScript III reverse transcriptase and random hexanucleotide mix according to the Invitrogen protocol for SuperScript First-Strand Synthesis. The concentration of transcribed cDNA was measured using NanoDrop and was diluted to a working concentration of 100 ng/µl.

### 2.2.2.3 Semi-quantitative real-time polymerase chain reaction (sqRT-PCR)

Semi-qRT-PCR with specific oligonucleotides was performed using the SYBR<sup>®</sup> Green ER<sup>Tm</sup> qPCR Super Mix. Gene transcripts of the housekeeping gene glyceraldehyde-3-phosphate dehydrogenase (GAPDH) were applied as internal RNA loading control. For quantitative real-time PCR the following mix was prepared in a 96-well-plate:

12.5 µl SYBR Green Mix  
1 µl mix of forward and reverse primers  
(each 10 pmol/µl)  
2 µl cDNA  
9.5 µl ddH<sub>2</sub>O

For the non-template control cDNA was replaced with ddH<sub>2</sub>O. The plate was covered with a plastic lid and analyzed in a Mastercycler epgradient S with the following program:

Cover T° = 105 °C

Initial denature	95 °C	10:00 minutes
Denature	95 °C	00:15 minutes
Annealing	60 °C	00:30 minutes
Elongation	72 °C	00:30 minutes

Amplification for 40 cycles

To ensure that a specific product was obtained, a dissociation curve analysis was performed using the following program:

95 °C	01:00 minutes
55 °C	00:15 minutes
95 °C	00:15 minutes
ramp rate:	20:00 minutes

Amplification specificity was confirmed by analysis of the melting curves. Results were analyzed with the Master cycler ep realplex software after establishing the reaction efficiency for each primer pair. Values were normalized with their respective GAPDH values. Delta cycle threshold (CT) values were normalized to 3 months wildtype (=100 %) and quantification using the delta delta CT method was applied.

### **2.2.3 RNA sequencing**

#### **2.2.3.1 RNA isolation of brain samples for RNA sequencing**

Freshly taken hemispheres of female transgenic mice or wildtype littermates (see section 2.2.1.2) were directly homogenized twice with 1 ml Qiazol Lysis Reagent and a stainless-steel bead (mean diameter: 7 mm) in a Tissue Lyser LT for 3 minutes at 50 Hz. Homogenates were centrifuged for 10 minutes at 12000 x g and 4 °C. Supernatant was transferred into a new tube and incubated for 5 minutes at room temperature. Then, 200 µl chloroform were added to each sample, shaken well and again incubated for 3 minutes at room temperature before centrifuging for 15 minutes at 12000 x g and 4 °C. The upper, aqueous phase was transferred into a new tube and isopropanol was added in a 1:1 volume ratio. The samples were mixed well and incubated at -20 °C overnight to let also smaller RNA particles precipitate. On the following day, the samples were centrifuged for 20 minutes at 12000 x g and 4 °C. The supernatant was discarded. Then, 1 ml 75 % ethanol was added to the sample and gently mixed. After centrifugation for 5 minutes at 7500 x g and 4 °C the supernatant was discarded again, ethanol was added and the procedure was repeated. The remaining pellet was left for about 10 minutes at room temperature to dry. Subsequently, the pellet was resuspended in 50 µl RNase-free water and stored at -80 °C until usage. An RNA aliquot was kept separately for quality and quantity measurements at the NanoDrop and for reverse transcription into cDNA for further PCR controls (see paragraphs 2.2.2.2 and 2.2.2.3).

#### **2.2.3.2 RNA sequencing and analysis**



The sequencing and the analysis of the RNA samples was performed in collaboration with Dr. Sinkkonen and his Epigenetics Team at the University of Luxembourg (Belvaux, Luxembourg).

Libraries for the brain total RNA samples were built using the TruSeq Stranded mRNA Library Prep kit (Illumina) with 1 µg of RNA as starting material according to the manufacturer's protocol. The library quality was assessed using an Agilent 2100 Bioanalyzer and quantified using Qubit dsDNA HS assay Kit. Following this quantification, libraries were adjusted to 4 nM and sequenced on a NextSeq 500 (Illumina) following the manufacturer's instructions.

Library preparation and sequencing were performed at the Luxembourg Center for Systems Biomedicine Sequencing Facility. The quality of raw reads was checked by FastQC version 0.11.3 (<https://www.bioinformatics.babraham.ac.uk/projects/fastqc/>). Cutadapt6 version 1.8.1 was used to trim low quality reads (-q 30 parameter), remove Illumina adapters (-a parameter) and to remove reads shorter than 20 bases (-m 20 parameter) with an error tolerance of 10 % (-e 0.1 parameter). Additionally, reads mapping to ribosomal RNA species were removed using SortMeRNA7 with the parameters "--other; --log; -a; -v; --fastx enabled".

Lastly, the reads were processed by FastQC version 0.11.3 to control whether bias could have been. As no obvious bias were observed, the reads were mapped to the mouse genome mm10 by using the gene annotation downloaded from Ensembl8 (GRCm38.p3, release 79) and by using the Spliced Transcripts Alignment to a Reference9 (STAR) version 2.5.2b and the optimized parameters (Baruzzo et al., 2017). Briefly, the tweaked command arguments were:

```
--twopassMode Basic --outSAMunmapped Within --limitOutSJcollapsed 1000000 \  
--limitSjdbInsertNsj 1000000 --outFilterMultimapNmax 100 --outFilterMismatchNmax 33 \  
--outFilterMismatchNoverLmax 0.3 --seedSearchStartLmax 12 --alignSJoverhangMin 15 \  
--alignEndsType Local --outFilterMatchNminOverLread 0 --outFilterScoreMinOverLread 0.3  
--winAnchorMultimapNmax 50 --alignSJDBoverhangMin 3
```

The reads were further counted using the function featureCounts from the R package Rsubreads (v1.26; Liao et al., 2013) and the statistical analysis was performed using the R package DESeq2 (v1.15; Love et al., 2014). Most computation and plotting were done using R (v3.4.0; R Core Team, 2017) and RStudio (v1.1; RStudio Team, 2016). Principle component analysis was computed using the function plotPCA() from the DESeq2 package and plotted by the R package factoextra (v1.0.4; Kassambara and Mundt, 2017). Other plots were done using the R

package *ggplot2* (v2.1; Wickham, 2009) and the collection of packages *tidyverse* (v1.1; Wickham, 2017). For Ingenuity Pathway Analysis<sup>®</sup> (IPA), the list of differentially expressed genes in *GNE*<sup>+/-</sup>*C3*<sup>+/+</sup> mice (false discovery rate, FDR<0.1) was uploaded in the IPA tool (Ingenuity Systems, [www.ingenuity.com](http://www.ingenuity.com)). The significance of the association of the genes with a function or canonical pathway was measured by Fisher's exact test. For upstream regulator analysis only regulatory proteins were considered.

The sequencing data will be deposited in the European Nucleotide Archive (accession number not yet known).

#### **2.2.4 Flow cytometry analysis of *GNE*<sup>+/-</sup> mice**

Female *GNE*<sup>+/-</sup> mice and wildtype littermates were weighed routinely, consequently set under anesthesia with an anesthesia solution (Ketamin/Xylazin; for more details see 2.1.4) and then perfused with 1x PBS. The brain was directly removed, crushed through a 70 µm cell strainer into a falcon tube with 1x PBS and centrifuged for 3 minutes at 1500 rpm. The cell suspension was fixed with 4 % PFA for 10 minutes on ice. The cells were washed twice with 1x PBS and subsequently incubated in blocking solution (10 % BSA + 0.1 % Triton X-100 + 5 % NGS in PBS) for one hour on ice. Brain cells were taken up in 1x PBS and were separated into equal samples for the incubation with the primary antibodies (2.5 µg/ml) against PSA-NCAM, A2B5, and CD56, and their respective isotype controls for one hour on ice. After two washing steps, the cells were stained with PE-coated secondary antibodies for 30 minutes on ice in the dark. Cells were washed twice with 1x PBS and were resuspended in 500 µl 1x PBS. For each mouse one sample was kept on ice without any staining and was measured as blank sample. Analysis was done with a FACS Calibur flow cytometer and FlowJo Software. The main cell population in the blank sample was gated for each mouse data set, and then 1 %-positive cells in the isotype sample were gated and applied for the respective antibodies. For quantification the mean fluorescence intensity of the isotype controls were subtracted from the mean fluorescence intensity of PSA-NCAM, A2B5, and CD56. All samples were normalized to 3 months wildtype mice (=100 %).

#### **2.2.5 Immunohistochemistry of murine brains**

O.C.T.<sup>™</sup> Compound-embedded hemispheres of male transgenic mice or wildtype littermates (see section 2.2.1.2) were cut into 20 µm thick sagittal sections at a microtome and stored at -20 °C until usage.

### 2.2.5.1 Cell density quantification

For quantifying the cell density in the substantia nigra and the hippocampus, sections of lateral levels between 1.10 mm and 1.20 mm were immunohistochemically stained. Sections were washed once with 1x PBS and incubated in blocking solution (10 % BSA + 0.2 % Triton X-100 + 5 % NGS in PBS) in a wet chamber for one hour at room temperature, followed by incubation in primary antibodies directed against TH (1:500) and NeuN (1:500) in blocking solution for two hours at room temperature. After washing, sections were subsequently stained with the corresponding Alexa Fluor<sup>®</sup> 488- (1:500) or Cy3-conjugated antibodies (1:200) for two hours at room temperature. After two washing steps with 1x PBS, sections were stained for nuclei (DAPI, 1:10000) for 30 seconds and then covered with mowiol and a coverslip.

Three images per mouse were taken by an apotome microscope using AxioVisio (v4.8.2.0) with the MosaiX plugin and were analyzed using ImageJ. Either the area of the substantia nigra pars compacta (SN pc) or the Cornus Ammonis (CA) 3 region of the hippocampus was encircled and measured. Cells positive for either TH (applicable only in SN pc) or for NeuN in the selected area were counted only when their soma was completely visible. The co-staining with DAPI was used as additional reference. For the cell density the cell number was divided by the selected area and normalized to 3 months old wildtype mice.

Additionally the width of the CA3 region and of the dentate gyrus (DG) in the hippocampus was measured. For this, the DAPI-/NeuN-co-staining was used as orientation. For the CA3 region the width of the pyramidal cell layer (NeuN+ cells) located next to the most anterior part of the DG was chosen (indicated by the white left dotted line in Figure 15A). For the DG the granule cell layer (NeuN+ cells) was investigated anterior (DG1) and posterior (DG2). For DG1 the widths of both anterior “arms” located next to the end of the CA3 region (indicated by the middle white dotted line in Figure 15A) were measured and the mean was calculated. For the second DG region (DG2) the width of the posterior curvature of the DG was measured as shown in Figure 15A (white right bar). The mean per animal was normalized to 3 months old wildtype mice.

### 2.2.5.2 Astrocyte quantification

For quantifying the astrocytes in the substantia nigra, sections of lateral levels around 1.40 mm of 9 months old mice were immunohistochemically stained. Sections were treated in the same staining protocol as for the quantification of the cell density (see paragraph 2.2.5.1) with one

exception: Instead of the primary antibody against TH, an antibody against the astrocyte specific marker Gfap (1:500) was used.

Three z-stacks (3 x 2  $\mu\text{m}$ ) per mouse were taken in the substantia nigra pars reticulata by an inverted confocal laser scanning microscope. Maximum projection of the Gfap-/DAPI-double positive z-stack images were processed and used for analysis. Fluorescence intensity of Gfap per area was measured using ImageJ. Background intensity was subtracted. For the astrocyte number Gfap- and DAPI- double positive cells were counted in the selected area in each z-stack and the cell number per area was calculated. The resulting fluorescence intensity per area and the cell density of each animal were normalized to 9 months old wildtype mice.

### 2.2.5.3 Microglia quantification

For the quantification of the microglia, sections of lateral levels around 1.30 mm of 9 months old mice were immunohistochemically stained. Sections were washed once with 1x PBS and incubated in blocking solution (10 % BSA + 0.25 % Triton X-100 in PBS) in a wet chamber for two hours at room temperature, followed by incubation in primary antibodies directed against Iba1 (1:500) and Cd68 (1:500) in incubation solution (5 % BSA + 0.05 % Triton X-100 in PBS) overnight at 4 °C. On the following day sections were washed five times with incubation solution for 5 min. After washing, sections were subsequently stained with the corresponding Alexa Fluor<sup>®</sup> 488- (1:400) or Cy3-conjugated antibodies (1:200) in incubation solution for two hours at room temperature. After three washing steps with 1x PBS, sections were stained for nuclei (DAPI, 1:10000) for 30 seconds and then covered with Aqua-Polymount and a coverslip.

Three z-stacks (5x 2.5  $\mu\text{m}$  – 3  $\mu\text{m}$ ) per mouse were taken in the substantia nigra pars reticulata (SN pr) by an inverted confocal laser scanning microscope. Maximum projection of the Iba1-/Cd68-/DAPI-triple positive z-stack images were processed and used for analysis. Fluorescence intensity of Iba1 and Cd68 per area was measured using ImageJ. Background intensity was subtracted. Additionally, the soma area identified by Iba1 staining of each microglia was selected and measured. In addition, the fluorescence intensity of Iba1 and Cd68 of each selected soma was measured and calculated per soma area. For the microglia number Iba1- and DAPI-double positive cells were counted in the selected area in each z-stack. The resulting fluorescence intensities per area, the soma areas, and the cell numbers of each animal were normalized to 9 months old wildtype mice.

### 2.2.6 Statistical analysis

Results were presented as mean  $\pm$  SEM (= standard error of the mean) or mean + SEM of at least three independent experiments. Significant outliers were discovered by using the outlier calculator of GraphPad QuickCalcs and excluded from further analysis. Graphs were designed using Prism 7 (v7.01). For statistical analysis data with one variable (e.g. only genotype) were analyzed using the computer software IBM SPSS Statistics (v.22) and for more than one variable (e.g. age and genotype) the computer software STATA<sup>®</sup>/IC (v13.1) was used. In case of one variable, the Levene's test was used to assess the equality of variances for each data set. Then, comparison between two groups was performed using the Student's t-test (independent sample t-test) and multiple group comparisons were performed using one-way ANOVA followed by post hoc correction using the Bonferroni or the Dunnett's T3 method. For more than one variable, a linear model (multiple linear regression) including an interaction term was applied, followed by a pairwise comparison with LSD-post hoc correction. The Breusch-Pagan / Cook-Weisberg test for heteroscedasticity was performed to assess the equality of variances in the linear model. If variances were significantly different, a robust linear model including an interaction term was chosen for further analysis. Data were in general regarded as significant if  $p$ -values were below or equal 0.05 (\* $p \leq 0.050$ ; \*\* $p \leq 0.010$ ; \*\*\* $p \leq 0.001$ ).

## 3 Results

### 3.1 Characterization of the GNE<sup>+/-</sup> mice

In *in vitro* murine and human neuron-microglia/macrophage co-cultures our group could previously show that glycoalyx alterations lead to phagocytic removal by microglia/macrophages in a complement-dependent manner (Linnartz et al., 2012b; Linnartz-Gerlach et al., 2016). To investigate the role of an altered glycoalyx *in vivo*, I used a transgenic mouse heterozygous for GNE, the essential enzyme of sialic acid biosynthesis. According to Gagiannis and colleagues these mice show an overall reduction of membrane-bound sialic acids by 25 % but without having any obvious defects in organ architecture or function (Gagiannis et al., 2007). For further validation of this mouse line as a suitable model for an altered glycoalyx, extensive investigations for characterization were performed and in particular the influence of aging was analyzed.

#### 3.1.1 General observations

##### 3.1.1.1 Breeding and housing of mice

For general breeding and housing evaluation 38 mice (21x females, 16x males) were monitored for a period of 33 weeks according to the guidelines of the German Federal Institute for Risk Assessment (“Severity assessment of genetically altered animals”). Within this monitoring time period GNE<sup>+/-</sup> mice and wildtype littermates showed a normal housing behavior. No obvious effects in posture, behavior, or motor behavior could be monitored. The fur and the body's orifices looked normal and the reactions of the mice to animal handling were not disturbed. Breeding of female GNE<sup>+/-</sup> mice with male GNE<sup>+/-</sup> mice proceeded in a normal manner. Four to six pups per female mouse were usual. The pups developed normally and could be separated from their mother at an age of 21 days.

##### 3.1.1.2 Weight analysis of mice

Routinely, the weight of mice was measured directly before tissue collection for characterization. For the weight analysis in total 248 animals were analyzed (see Table 4). Sex and genotype were distinguished.

As shown in Figure 10 the weight of the mice increased with age. Overall, female mice weighed less than male mice. The mean sex-specific differences of all time points were  $7.0 \pm 0.2$  g in

GNE<sup>+/+</sup> mice and  $5.8 \pm 0.6$  g in GNE<sup>+/-</sup> mice. Male mice reached a steady weight at around 9 months, while this was not yet visible for female mice until the age of 12 months.

**Table 4: Number of measured mice for weight analysis**

sex	GNE <sup>+/+</sup>	GNE <sup>+/-</sup>	total:
female	55	74	129
male	49	70	119
<b>total:</b>	104	144	248

A linear model including an interaction term was applied to study the weight development during aging. For the female dataset a robust linear model was necessary. Both models revealed age-differences, whereas in female mice sex-specific differences were additionally present (♀:  $R^2 = 0.647$ , age effect:  $p < 0.001$ , genotype effect:  $p < 0.001$ ; ♂:  $R^2 = 0.873$ , age effect:  $p < 0.001$ , genotype effect:  $p = 0.274$ ) but without any effect modulations (age\*genotype: ♀  $p = 0.369$ ; ♂  $p = 0.800$ ). While the male mice gained equal weight (Figure 10B), female GNE<sup>+/-</sup> mice gained significantly higher weight at early time points compared to wildtype littermates (Figure 10A).

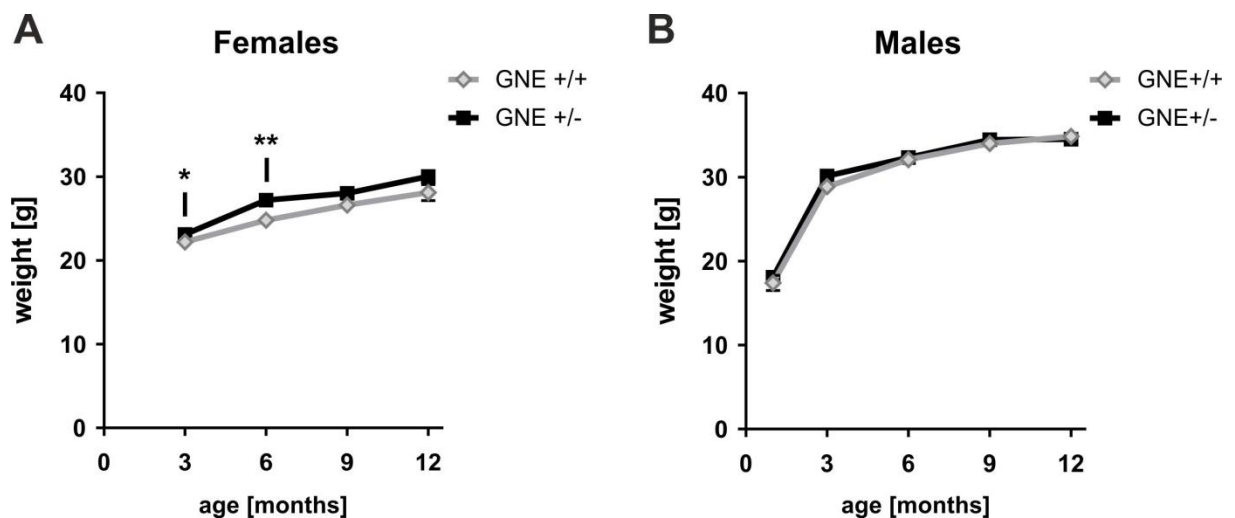


**Figure 10: Weight development of GNE mice during aging.** (A) Female GNE<sup>+/-</sup> mice showed significant higher weight development during aging compared to wildtype littermates from three to 12 months (genotype effect:  $p < 0.001$ ). Data shown as mean  $\pm$  SEM;  $n = 9-23$ ; pairwise comparison for GNE<sup>+/+</sup> vs. GNE<sup>+/-</sup> mice at different age, \* $p < 0.050$ , \*\* $p < 0.010$ . (B) Weight analysis from 1 month to 12 months old male mice did not show genotype-specific differences (genotype effect:  $p = 0.274$ ). Data shown as mean  $\pm$  SEM;  $n = 8-17$ , without significant differences for GNE<sup>+/-</sup> vs. GNE<sup>+/+</sup> at any time point.

In detail, female GNE<sup>+/+</sup> mice weighed  $22.2 \pm 0.3$  g (3 months),  $24.8 \pm 0.4$  g (6 months),  $26.6 \pm 0.8$  g (9 months), and  $28.1 \pm 1.0$  g (12 months) and female GNE<sup>+/-</sup> mice weighed  $23.1 \pm 0.3$  g (3 months),  $27.2 \pm 0.8$  g (6 months),  $28.0 \pm 0.6$  g (9 months), and  $30.0 \pm 0.7$  g (12 months). Pairwise comparisons between GNE<sup>+/+</sup> and GNE<sup>+/-</sup> at each time point revealed

significant differences at 3 months ( $*p = 0.044$ ) and at 6 months ( $**p = 0.004$ ). Male  $GNE^{+/+}$  mice weighed  $17.4 \pm 0.9$  g (1 month),  $28.9 \pm 0.6$  g (3 months),  $32.1 \pm 0.7$  g (6 months),  $34.0 \pm 0.8$  g (9 months), and  $34.8 \pm 0.8$  g (12 months) and male  $GNE^{+/-}$  mice weighed  $18.1 \pm 0.7$  g (1 month),  $30.1 \pm 0.5$  g (3 months),  $32.3 \pm 0.5$  g (6 months),  $34.5 \pm 0.7$  g (9 months), and  $34.5 \pm 0.5$  g (12 months). Pairwise comparisons between male  $GNE^{+/+}$  and  $GNE^{+/-}$  at each time point revealed no significant differences. For all following investigations either only male or only female mice were analyzed to avoid sex-specific genotype differences.

### 3.1.2 Sialic acid biosynthesis and sialylation status in the brain

#### 3.1.2.1 *Gne* gene transcription

The altered *gne* gene in  $GNE^{+/-}$  mice was not only tested by PCR during the standard genotyping procedure as described in the section “2.2.1.1 Materials and Methods” but was also specifically tested in the brain by sqRT-PCR.

To confirm an altered *gne* transcription in the brain, male mice at the age of 1 month, 3 months, 6 months, 9 months, and 12 months were screened by sqRT-PCR. Quantification of brain homogenates of transgenic mice showed an overall reduction of *gne* on mRNA levels by 54 % compared to wildtype littermates (see Figure 11). The robust linear model of *gne* transcript levels during aging revealed age- and genotype-specific differences ( $R^2 = 0.694$ , age effect:  $***p < 0.001$ , genotype effect:  $***p < 0.001$ ) and showed also effect modulations (age\*genotype:  $*p = 0.041$ ), meaning that age and genotype had an effect on each other. Pairwise comparison between  $GNE^{+/-}$  mice and wildtype littermates revealed strong significant differences between the genotypes (all time points:  $***p < 0.001$ ).

In detail, in 1 month old mice *gne* transcript levels were reduced from  $0.7 \pm 0.1$  fold change (FC) in  $GNE^{+/+}$  mice and to  $0.3 \pm 0.0$  FC in  $GNE^{+/-}$  mice, in 3 months old animals from  $1.0 \pm 0.1$  FC to  $0.4 \pm 0.0$  FC, in 6 months old animals from  $1.1 \pm 0.1$  FC to  $0.5 \pm 0.0$  FC, in 9 months old animals from  $1.0 \pm 0.1$  FC to  $0.4 \pm 0.1$  FC, and at the age of 12 months from  $1.0 \pm 0.1$  FC to  $0.5 \pm 0.0$  FC (Figure 11).



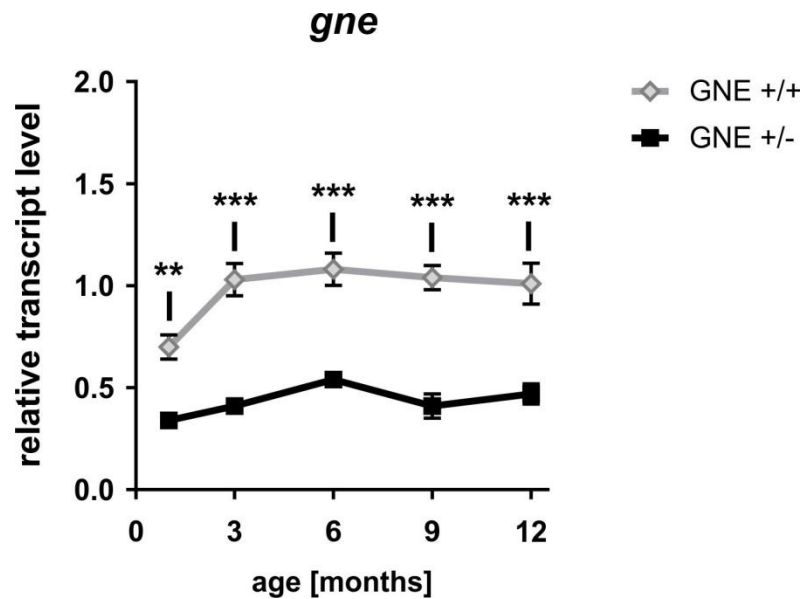


**Figure 11: Transcription analysis of *gne* mRNA levels.** Levels of *gne* transcripts in half brain homogenates of  $GNE^{+/-}$  mice at the age of 1 month, 3 months, 6 months, 9 months, and 12 months were significantly reduced compared to wildtype littermates. Data shown as mean  $\pm$  SEM; normalized to 3 months old  $GNE^{+/+}$  animals;  $n = 7-14$ , pairwise comparison for  $GNE^{+/+}$  vs.  $GNE^{+/-}$  mice at different age,  $**p \leq 0.010$ ,  $***p \leq 0.001$ .

Data confirmed that the heterozygous mice transcribed different alleles and that the wildtype allele is much lower transcribed in the  $GNE^{+/-}$  mice compared to wildtype littermates.

### 3.1.2.2 Sialic acid levels in the brain

Next, the overall sialic acid levels in brain homogenates at different age groups were investigated by flow cytometry. To assay different compositions of sialic acids, antibodies directed against polymers (NeuAc- $\alpha$ 2-8 $_n$ ,  $n > 10$ ; PSA-NCAM; Figure 12B) and oligomers (trimer; A2B5; Figure 12C) of sialic acids were used as shown in Figure 12. To further distinguish the embryonic form of polysialylated N-CAM from the adult form, which has normally decreased polysialic acid expression (Miller et al., 1993), an antibody for the 12F8 epitope was used (CD56; Figure 12D). In general, the relative mean fluorescence intensity was nearly always higher in wildtype animals compare to  $GNE^{+/-}$  mice and decreased with age, regardless of sialic acid chain lengths or genotype. While values of long and short sialic acid chain lengths decreased continuously (Figure 12B+D), overall levels of oligomers seemed to be more fluctuating (Figure 12C).

Linear modelling of PSA-NCAM data ( $R^2 = 0.227$ ) during aging did not reveal an age-dependent effect ( $p = 0.056$ ) but revealed a genotype-dependent effect ( $**p = 0.002$ ). For A2B5 during aging, multiple linear regression ( $R^2 = 0.102$ ) also showed no age-dependent effect ( $p = 0.473$ ) but a genotype-dependent effect ( $*p = 0.047$ ). In contrast, the linear model of CD56 data ( $R^2 = 0.253$ ) during aging showed a strong age-dependent effect ( $***p < 0.001$ ) but no

genotype-dependent effect ( $p = 0.369$ ). Effect modulations were not present for any dataset (age\*genotype: PSA-NCAM -  $p = 0.611$ ; A2B5 -  $p = 0.665$ ; CD56 -  $p = 0.396$ ). Pairwise comparison between  $GNE^{+/-}$  mice and wildtype littermates for each dataset resulted in the following  $p$ -values for the distinct time points: PSA-NCAM:  $p = 0.073$  (3 months),  $**p = 0.008$  (6 months),  $p = 0.137$  (9 months),  $p = 0.543$  (12 months); A2B5:  $p = 0.235$  (3 months),  $p = 0.857$  (6 months),  $p = 0.054$  (9 months),  $p = 0.443$  (12 months); CD56:  $p = 0.828$  (3 months),  $p = 0.089$  (6 months),  $p = 0.397$  (9 months),  $p = 0.638$  (12 months).

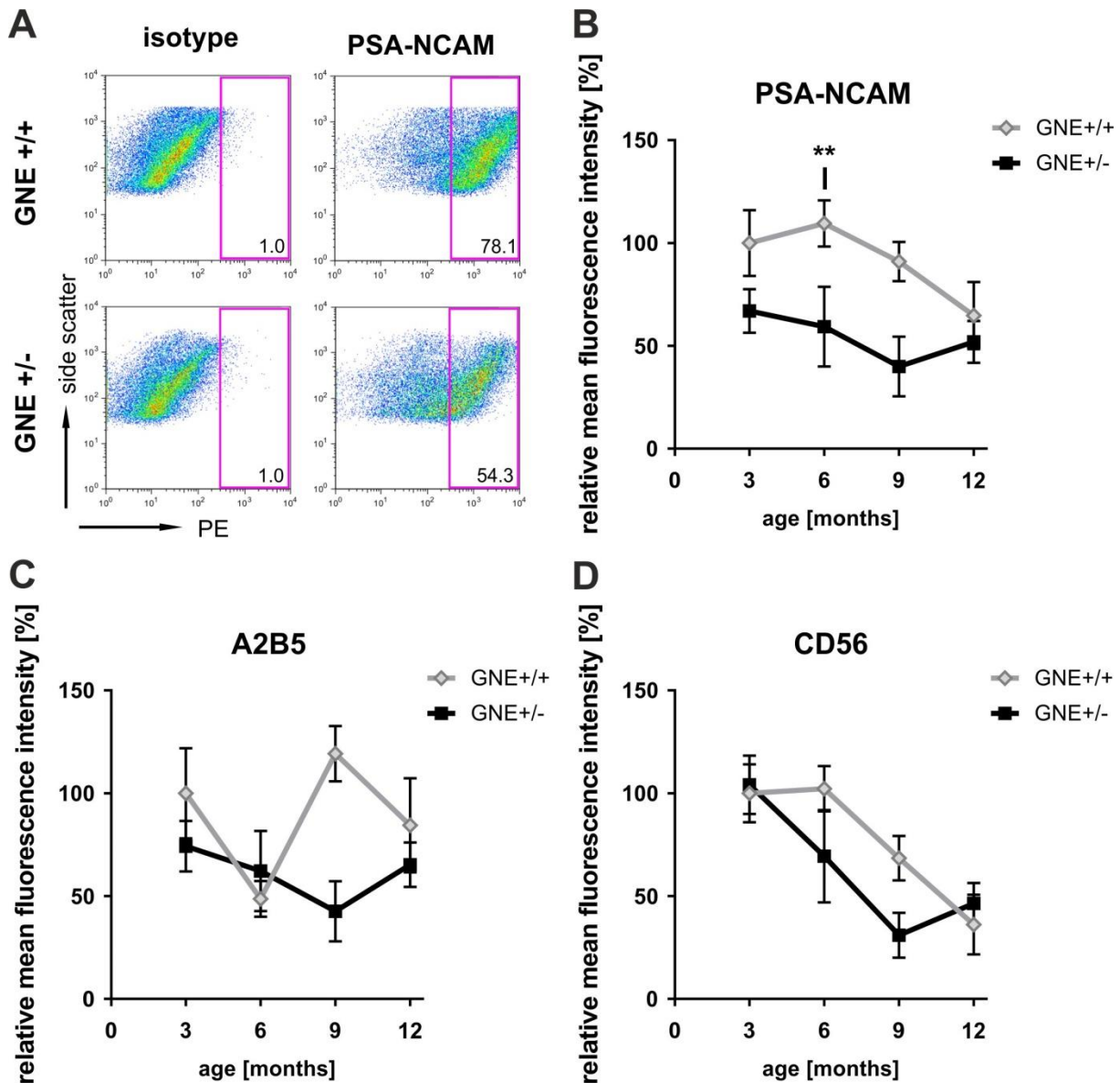


**Figure 12: Detection of different sialic acid lengths in the brain.** (A) Representative scatter plots of  $GNE^{+/+}$  and  $GNE^{+/-}$  mice for PSA-NCAM and the corresponding isotype control at 3 months are shown. PE - R-Phycoerythrin. (B-D) Flow cytometry revealed that the overall sialic acid levels in whole brain homogenates of  $GNE^{+/-}$  mice decreased with age. Long polymers (PSA-NCAM; B), oligomers (A2B5; C), and short polymers (CD56; D) of sialic acids were investigated. Especially long polymers were significantly decreased in  $GNE^{+/-}$  mice compared to wildtype littermates but also oligomers were significantly different between the genotypes. Data shown as mean  $\pm$  SEM; normalized to 3 months old  $GNE^{+/+}$  animals;  $n = 7-14$ , pairwise comparison for  $GNE^{+/+}$  vs.  $GNE^{+/-}$  mice at different age:  $**p \leq 0.010$ .

In detail, the detected relative mean fluorescence intensity of PSA-NCAM decreased in wildtype animals from  $100 \pm 16.0$  % at 3 months, over  $109.5 \pm 11.2$  % at 6 months, to  $91.0 \pm 9.5$  % at 9 months and ended at  $64.7 \pm 16.3$  % at 12 months (Figure 12B). In comparison, intensity levels in  $GNE^{+/-}$  mice varied from  $67.0 \pm 10.6$  % at 3 months, to  $59.3 \pm 19.4$  % at 6 months, to  $40.0 \pm 14.5$  % at 9 months and again to  $51.9 \pm 10.2$  % at 12 months. Quantification of A2B5 at the age of 3 months, 6 months, 9 months, and 12 months showed a mean fluorescence intensity of  $100.0 \pm 21.9$  %,  $48.4 \pm 8.7$  %,  $119.3 \pm 13.5$  %, and  $84.4 \pm 22.9$  % in wildtype animals compared to the mean fluorescence intensities of  $74.3 \pm 12.3$  %,  $62.2 \pm 19.5$  %,  $42.6 \pm 14.6$  %, and  $65.3 \pm 10.8$  % in transgenic mice, respectively (Figure 12C). The mean fluorescence intensity of CD56 (Figure 12D) in wildtype animals decreased from  $100.0 \pm 14.1$  % and  $102.2 \pm 11.0$  % at 3 months and 6 months, to  $68.4 \pm 10.8$  % and  $36.2 \pm 14.6$  % at the age of 9 months and 12 months, whereas in  $GNE^{+/-}$  mice the mean fluorescence intensity decreased from  $104.1 \pm 14.2$  %, over  $69.4 \pm 22.4$  %, to  $31.0 \pm 10.9$  %, and back to  $46.4 \pm 10.0$  % at the respective time points.

Data indicate that especially the polymers of sialic acids (NeuAc- $\alpha$ 2-8<sub>n</sub>) with a chain length of  $n > 10$  might be impaired or cannot be synthesized in the  $GNE^{+/-}$  mice to similar levels as in wildtype littermates.

### 3.1.3 Neurodegeneration in the brain

To prove the concept of phagocytosis of desialylated neurons by microglia/macrophages (Linnartz et al., 2012b; Linnartz-Gerlach et al., 2016),  $GNE^{+/-}$  mice were investigated for neurodegeneration in different brain regions. *In vitro*, the extent of neuronal loss was strongly dependent on the degree of sialic acid removal. Thus, I assumed that different brain regions might be differently regulated for sialic acid levels.

#### 3.1.3.1 Neurodegeneration analysis in the substantia nigra

Since oxidative stress can lead to sialic acid removal, I first investigated neurodegeneration in the substantia nigra, a brain region known for high levels of oxidative stress (Di Giovanni et al., 2012). Furthermore, dopaminergic neurons of the substantia nigra are more susceptible to inflammatory damage compared to other neuronal subtypes (Block et al., 2007).

Serial sagittal sections (lateral: 1.10 – 1.20 mm) of the substantia nigra pars compacta (SN pc) were analyzed by immunohistochemical antibody staining of the dopaminergic marker TH and the neuronal nuclei marker NeuN (see Figure 13A). Cells positive for TH or NeuN were counted

per area and the relative cell density in the SN pc was quantified at different time points to quantify the progression of the neuronal loss during aging (Figure 13B) including the latest time point investigated (12 months, Figure 13C).

In general, the overall neuronal cell density, as well as the dopaminergic (TH-positive) cell density started at higher levels in 1 month old animals compared to 3 months old animals regardless of the genotype of the mice. From 3 months onwards the neuronal cell density as well as the dopaminergic cell density stayed very stable during aging in wildtype mice. In contrast, the density levels of NeuN- and of TH-positive cells strongly decreased over the different time points in GNE<sup>+/-</sup> mice.

A robust multiple linear regression of the NeuN-positive cell density during aging revealed age- and genotype-specific differences ( $R^2 = 0.595$ , age effect:  $***p < 0.001$ , genotype effect:  $***p < 0.001$ ) as well as differences in effect modulations (age\*genotype:  $**p = 0.009$ ). Pairwise comparison between GNE<sup>+/-</sup> mice and wildtype littermates revealed no significant differences at 1 month ( $p = 0.749$ ), but increasingly significant differences between GNE<sup>+/-</sup> mice and wildtype littermates at all other time points (3 months:  $*p = 0.020$ ; 6 months:  $**p = 0.008$ ; 9 months:  $***p = 0.001$ ; 12 months:  $***p < 0.001$ ; Figure 14B upper graph). Multiple linear regression analysis of the TH-positive cell density during aging also resulted in age- and genotype-specific differences ( $R^2 = 0.598$ , age effect:  $***p < 0.001$ , genotype effect:  $***p < 0.001$ ) as well as effect modulations (age\*genotype:  $**p = 0.002$ ). Pairwise comparison between GNE<sup>+/-</sup> mice and wildtype littermates showed no significant differences at 1 month ( $p = 0.184$ ) and 3 months ( $p = 0.202$ ), but strong significant differences between GNE<sup>+/-</sup> mice and wildtype littermates at later time points (6 months:  $***p = 0.001$ ; 9 months:  $*p = 0.013$ ; 12 months:  $***p < 0.001$ ; Figure 14B lower graph).

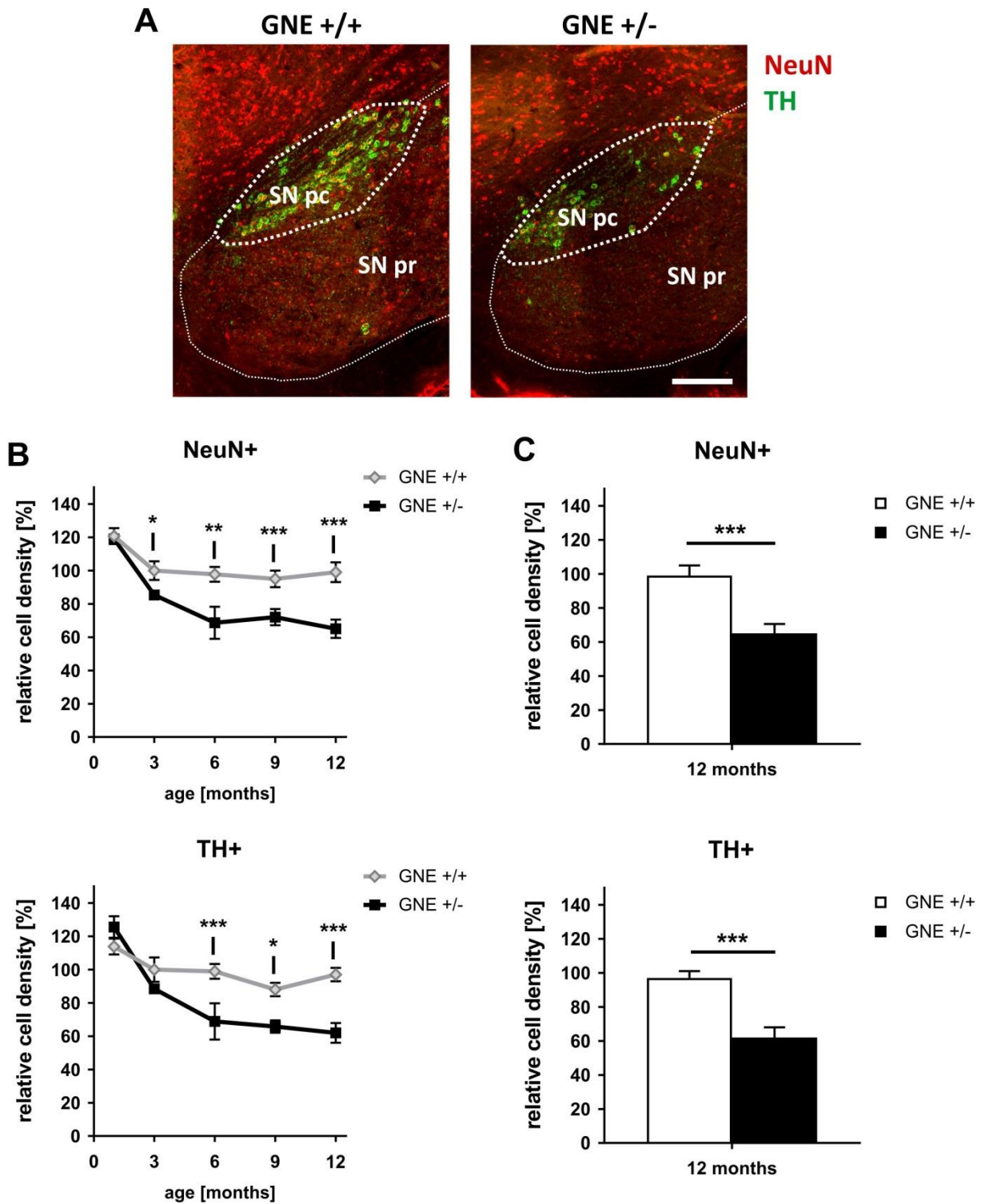


**Figure 13: Increasing neurodegeneration in the substantia nigra of GNE<sup>+/-</sup> mice with age.** (A) Representative images of the substantia nigra of 12 months old GNE<sup>+/+</sup> and GNE<sup>+/-</sup> mice at lateral sections between 1.10 mm and 1.20 mm are shown. Sagittal brain slices were stained with antibodies directed against tyrosine hydroxylase (TH, green) and neuronal nuclei (NeuN, red). SN pc – substantia nigra pars compacta, SN pr – substantia nigra pars reticulata. Scale bar: 200  $\mu$ m. (B) Quantification of the cell density of NeuN- (upper graph) and TH-positive cells (lower graph) showed increasing neuronal loss in GNE<sup>+/-</sup> mice compared to wildtype littermates with increasing age. Data shown as mean  $\pm$  SEM; normalized to 3 months old GNE<sup>+/+</sup> animals; n = 7-12, pairwise comparison for GNE<sup>+/+</sup> vs. GNE<sup>+/-</sup> mice at different age: \* $p \leq 0.050$ , \*\*\* $p \leq 0.001$ . (C) Quantification of the cell density of NeuN- (upper graph) and TH-positive cells (lower graph) at 12 months revealed a strong neuronal loss in GNE<sup>+/-</sup> mice compared to wildtype littermates. Data shown as mean + SEM; normalized to 3 months old GNE<sup>+/+</sup> animals; n = 9-12, Student's t-test, \*\*\* $p \leq 0.001$ .

The measured neuronal cell density at 1 month was almost identical between  $GNE^{+/-}$  mice and wildtype littermates ( $119.0 \pm 2.6\%$  vs.  $120.7 \pm 4.8\%$ ). While the relative neuronal cell density in wildtype mice stayed at a similar level between 3 months and 12 months ( $100.0 \pm 5.6\%$  vs.  $98.9 \pm 5.8\%$ ;  $p = 0.889$ ), it decreased by 29.9% in  $GNE^{+/-}$  mice from 3 months to 12 months ( $85.4 \pm 2.7\%$  vs.  $65.0 \pm 5.6\%$ ;  $**p = 0.002$ ) and by even 45.4% comparing 12 months to 1 month ( $65.0 \pm 5.6\%$  vs.  $119.0 \pm 2.6\%$ ;  $***p < 0.001$ ). In detail, the exact relative density levels for NeuN-positive cells changed from  $120.7 \pm 4.8\%$ , to  $100.0 \pm 5.6\%$ ,  $97.8 \pm 4.5\%$ ,  $95.3 \pm 4.7\%$ , and  $98.9 \pm 5.8\%$  in wildtype mice and from  $119.0 \pm 2.6\%$ , to  $85.4 \pm 2.7\%$ ,  $68.6 \pm 9.7\%$ ,  $72.0 \pm 4.9\%$ , and  $65.0 \pm 5.6\%$  in  $GNE^{+/-}$  mice starting from 1 month over 3 months, 6 months, 9 months to 12 months, respectively.

Similar trends were seen for the dopaminergic cell density, which started at  $113.8 \pm 4.8\%$  in  $GNE^{+/+}$  mice and at  $125.6 \pm 6.5\%$  in  $GNE^{+/-}$  mice. From 3 months to 12 months the dopaminergic cell density levels in wildtype mice varied only between  $100.0 \pm 7.3\%$  (3 months) and  $87.8 \pm 3.8\%$  (9 months), while the levels steadily decreased in  $GNE^{+/-}$  mice by overall 23.9% from 3 months to 12 months ( $88.4 \pm 2.4\%$  vs.  $62.0 \pm 6.0\%$ ;  $***p = 0.001$ ) and by even 50.6% comparing 12 months to 1 month ( $62.0 \pm 6.0\%$  vs.  $125.6 \pm 6.5\%$ ;  $***p < 0.001$ ). In detail, the exact relative density levels for TH-positive cells changed from  $113.8 \pm 4.8\%$ , to  $100.0 \pm 7.3\%$ ,  $98.9 \pm 4.5\%$ ,  $87.8 \pm 3.8\%$ , and  $96.8 \pm 4.1\%$  in wildtype mice and from  $125.6 \pm 6.5\%$ , to  $88.4 \pm 2.4\%$ ,  $68.9 \pm 10.9\%$ ,  $65.8 \pm 3.7\%$ , and  $62.0 \pm 6.0\%$  in  $GNE^{+/-}$  mice starting from 1 month over 3 months, 6 months, 9 months to 12 months, respectively.

Focusing only on the last time point of the characterization (12 months, Figure 13C), the direct comparison of  $GNE^{+/-}$  mice with wildtype littermates showed a significant reduction in the neuronal cell density by 34.3% ( $65.0 \pm 5.6\%$  vs.  $98.9 \pm 5.8\%$ ;  $***p < 0.001$ , Student's t-test) and a significant reduction in the dopaminergic cell density by 36.0% ( $62.0 \pm 6.0\%$  vs.  $96.8 \pm 4.1\%$ ;  $***p < 0.001$ , Student's t-test).

Taken together, data show a clear loss in neuronal density with aging in the SN pc of  $GNE^{+/-}$  mice compared to wildtype littermates, which, although not yet present in young mice, shows a strong difference in neuronal density at 12 months old mice.

### 3.1.3.2 Neurodegeneration analysis in the hippocampus

Based on its importance in mental health, the hippocampus was selected as second brain region for the characterization of possible neurodegeneration. Here, the CA3 region was particularly

interesting, as it is known for its specific role in memory processes, susceptibility to seizures, stress and neurodegeneration (Cherubini and Miles, 2015).

Serial sagittal sections (lateral: 1.10 mm to 1.20 mm) of the hippocampus were analyzed by immunohistochemical antibody staining of the neuronal nuclei marker NeuN and cellular nuclei marker DAPI (see Figure 14A). Cells positive for NeuN and DAPI were counted per area and the relative cell density in the CA3 region of the hippocampus was quantified at different time points to see the progression of the neuronal loss during aging (Figure 14B) and the status at the latest time point investigated (12 months, Figure 14C).

In general, the neuronal cell density in the CA3 region of the hippocampus was stable at 1 month and 3 months but then slowly decreased with increasing age. Interestingly, until 6 months the neuronal density was almost identical between both genotypes but diverged at later time points (Figure 14B). The linear model of the NeuN-positive cell density during aging revealed age- and genotype-specific differences ( $R^2 = 0.390$ , age effect:  $***p < 0.001$ , genotype effect:  $**p = 0.003$ ) but did not show any interactions between the effects (age\*genotype:  $p = 0.400$ ). Pairwise comparison between  $GNE^{+/-}$  mice and wildtype littermates detected no significant differences at 1 month ( $p = 0.584$ ), 3 months ( $p = 0.608$ ), and 6 months ( $p = 0.360$ ), but significant differences between  $GNE^{+/-}$  mice and wildtype littermates at 9 months ( $*p = 0.023$ ) and at 12 months ( $**p = 0.005$ ; Figure 14B).

Overall, the neuronal loss was stronger in the CA3 region of the  $GNE^{+/-}$  mice (3 months vs. 12 months:  $-24.1\%$ ;  $***p < 0.001$ ) compared to wildtype littermates (3 months vs. 12 months:  $-12.3\%$ ;  $*p = 0.030$ ). In detail, the relative density levels for NeuN-positive cells changed from  $98.9 \pm 4.6\%$ , to  $100.0 \pm 4.6\%$ ,  $93.4 \pm 5.0\%$ ,  $90.9 \pm 2.7\%$ , and  $87.7 \pm 6.2\%$  in wildtype mice and changed from  $95.6 \pm 2.7\%$ , to  $97.1 \pm 3.4\%$ ,  $88.4 \pm 2.1\%$ ,  $78.6 \pm 2.8\%$ , and  $73.7 \pm 2.0\%$  in  $GNE^{+/-}$  mice starting from 1 month over 3 months, 6 months, 9 months to 12 months, respectively.

Comparing only the 12 months old mice of both genotypes (Figure 14C), the differences in neuronal density already amounts to  $14\%$ . This is a significant reduction by  $16\%$  (Student's t-test:  $*p = 0.032$ ) and a clear neurodegeneration in the old  $GNE^{+/-}$  mice.

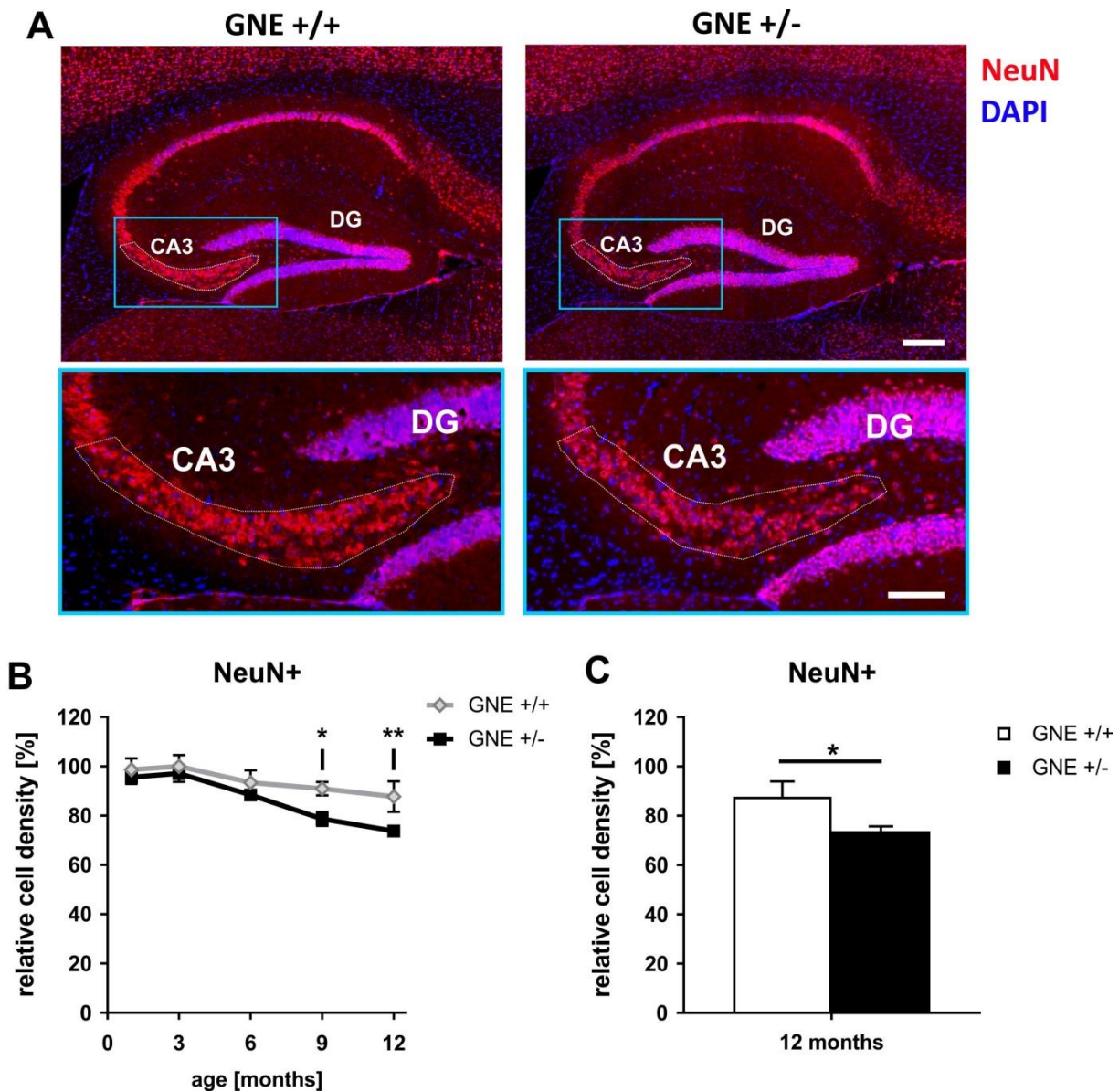


**Figure 14: Increasing neurodegeneration in the CA3 region of the hippocampus of GNE<sup>+/-</sup> mice with age.** (A) Representative images of the hippocampus of 12 months old GNE<sup>+/+</sup> and GNE<sup>+/-</sup> mice at lateral sections between 1.10 mm and 1.20 mm are shown. Lower images show a higher magnification of the analyzed CA3 region of the hippocampus (white dotted line). Sagittal brain slices were stained with antibodies directed against neuronal nuclei (NeuN, red) and DAPI (blue). DG – dentate gyrus. Scale bar: 200  $\mu$ m or 100  $\mu$ m (higher magnification). (B) Quantification of the cell density of NeuN- positive cells showed stronger neuronal loss in GNE<sup>+/-</sup> mice compared to wildtype littermates with increasing age. Data shown as mean  $\pm$  SEM; normalized to 3 months old GNE<sup>+/+</sup> animals; n = 7-12, pairwise comparison for GNE<sup>+/+</sup> vs. GNE<sup>+/-</sup> mice at different age: \* $p \leq 0.050$ , \*\* $p \leq 0.010$ . (C) Quantification of the cell density of NeuN-positive cells at 12 months for GNE<sup>+/-</sup> mice and wildtype littermates. Data shown as mean + SEM; normalized to 3 months old GNE<sup>+/+</sup> animals; n = 10-12, Student's t-test, \* $p \leq 0.050$ .

Since changes in neuronal numbers might influence tissue morphology, I further analyzed the width of the CA3 region as well as the width of the DG in the same sagittal sections (lateral: 1.10 mm to 1.20 mm), which were used for the neuronal density analysis. The immunohistochemical antibody staining of NeuN and DAPI were used for anatomical orientation. The different positions used for measuring the widths in the hippocampus are



shown in Figure 15A. For the DG, the anterior (mean of two positions; DG1) and the posterior part (DG2) were distinguished and separately analyzed (Figure 15A). The analysis of the width at different age points did not show any differences between the genotypes at any of the measured positions (DG1, DG2, and CA3). Interestingly, the width was similarly increasing for all regions from 1 month to 9 months, after which a sudden decline to almost the levels of 1 month was observed at 12 months.

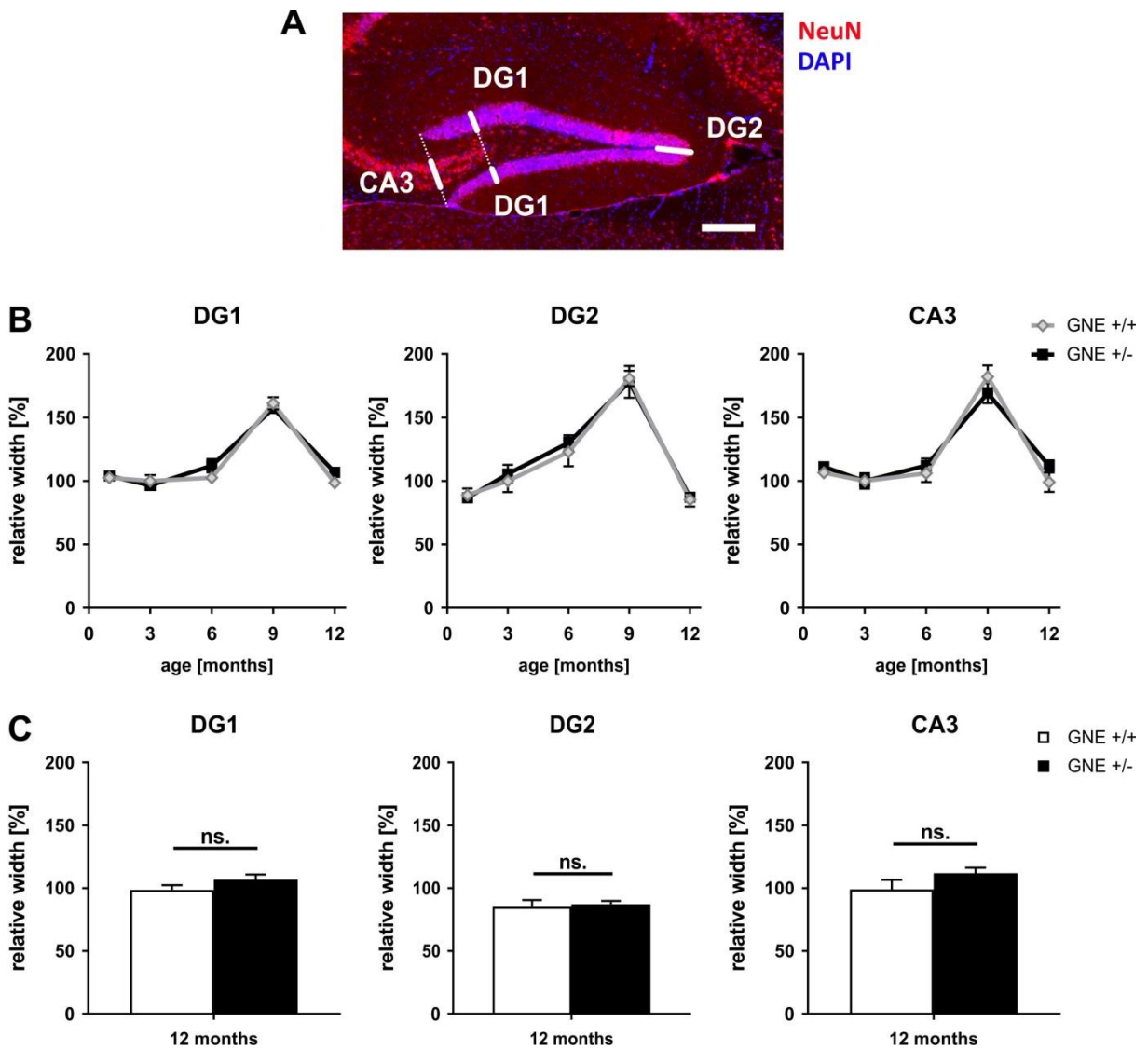


**Figure 15: No genotype-dependent differences in the width of the dentate gyrus (DG) and the CA3 region during aging.** (A) A representative image of the width analysis in the hippocampus of a 12 months old GNE<sup>+/+</sup> mouse at a lateral section between 1.10 mm and 1.20 mm is shown. The sagittal brain slice was stained with antibodies directed against neuronal nuclei (NeuN, red) and DAPI (blue). White bars show the measured width positions. Dotted white lines indicate how the positions were chosen. DG – dentate gyrus. Scale bar: 200  $\mu$ m. (B) Quantification of the relative width showed an age-dependent increase in DG1, DG2, and CA3 until 9 months (left to right). Data shown as mean  $\pm$  SEM; normalized to 3 months old GNE<sup>+/+</sup> animals; n = 7-12, pairwise comparison for GNE<sup>+/+</sup> vs. GNE<sup>+/-</sup> mice at different age showed no significant differences. (C) Quantification of the relative width for DG1, DG2, and CA3 at 12 months for GNE<sup>+/-</sup> mice and wildtype littermates (left to right). Data shown as mean + SEM; normalized to 3 months old GNE<sup>+/+</sup> animals; n = 10-12, Student's t-test, ns. = not significant.

The regression model for DG1 during aging revealed an age-dependent differences ( $R^2 = 0.799$ , age effect:  $***p < 0.001$ ) but no genotype-dependent differences (genotype effect:  $p = 0.381$ ). Pairwise comparison for DG1 between  $GNE^{+/-}$  mice and wildtype littermates did not detect any significant differences at 1 month ( $p = 0.836$ ), 3 months ( $p = 0.567$ ), 6 months ( $p = 0.116$ ), 9 months ( $p = 0.492$ ) or 12 months ( $p = 0.117$ ; Figure 15B). A robust linear model was applied for DG2 resulting in an age-dependent effect ( $R^2 = 0.750$ , age effect:  $***p < 0.001$ ) but again not in a genotype-dependent effect (genotype effect:  $p = 0.675$ ). Also here, pairwise comparison did not show any genotype-specific differences at 1 month ( $p = 0.718$ ), 3 months ( $p = 0.622$ ), 6 months ( $p = 0.573$ ), 9 months ( $p = 0.854$ ), or 12 months ( $p = 0.744$ ; Figure 15B). Even the robust linear model of the CA3 width could not detect a genotype-dependent effect (genotype effect:  $p = 0.599$ ) but only an age-dependent effect ( $R^2 = 0.721$ , age effect:  $***p < 0.001$ ). Pairwise comparison for the CA3 width between the genotypes showed no significant differences either (1 month:  $p = 0.415$ , 3 months:  $p = 0.876$ , 6 months:  $p = 0.493$ , 9 months:  $p = 0.286$ , 12 months:  $p = 0.145$ ). Effect modulations were not present for DG1, DG2, or CA3 width analysis (age\*genotype, DG1:  $p = 0.311$ , DG2:  $p = 0.941$ , CA3:  $p = 0.502$ ).

The age effect was strongest in the DG2 width. The width increased by 81 % in the  $GNE^{+/+}$  and by 69% in the  $GNE^{+/-}$  from 3 months to 9 months and even doubled comparing 9 months to 1 month. The increase in width of the CA3 region was similar strong (82.0 % in  $GNE^{+/+}$ , 69.4 % in  $GNE^{+/-}$ ) comparing 3 months with 9 months. Even the DG1 width showed still an increase around 60 % for both genotypes. Although the measured widths at 12 months were much lower than the levels at 9 months, there were still different trends visible. Interestingly, the DG1 width ( $p = 0.057$ ) and the CA3 width ( $p = 0.070$ ) increased comparing 3 months to 12 months, whereas the DG2 width significantly decreased ( $*p = 0.019$ ).

In detail, the relative DG1 widths were  $102.6 \pm 2.2$  % (1 month),  $100.0 \pm 4.6$  % (3 months),  $102.6 \pm 4.2$  % (6 months),  $161.1 \pm 4.8$  % (9 months), and  $98.6 \pm 3.8$  % (12 months) for  $GNE^{+/+}$  mice and  $103.9 \pm 4.2$  % (1 month),  $96.5 \pm 3.0$  % (3 month),  $112.0 \pm 5.2$  % (6 months),  $157.2 \pm 3.1$  % (9 months), and  $106.8 \pm 4.1$  % (12 months) for  $GNE^{+/-}$  mice. The measured relative DG2 widths were  $88.9 \pm 5.3$  % (1 month),  $100.0 \pm 8.7$  % (3 month),  $122.8 \pm 11.4$  % (6 months),  $180.7 \pm 6.1$  % (9 months), and  $85.2 \pm 5.4$  % (12 months) for  $GNE^{+/+}$  mice and  $86.7 \pm 3.0$  % (1 month),  $105.5 \pm 7.2$  % (3 month),  $130.6 \pm 6.0$  % (6 months),  $178 \pm 12.6$  % (9 months), and  $87.2 \pm 2.6$  % (12 months) for  $GNE^{+/-}$  mice. The mean values for the relative CA3 widths were  $106.5 \pm 4.0$  % (1 month),  $100.0 \pm 6.0$  % (3 month),  $106.1 \pm 7.0$  % (6 months),  $182.0 \pm 9.1$  % (9 months), and  $99.0 \pm 7.6$  % (12 months) for  $GNE^{+/+}$  mice and

111.1 ± 3.9 % (1 month), 99.8 ± 4.9 % (3 month), 112.2 ± 5.6 % (6 months), 169.1 ± 7.9 % (9 months), and 111.9 ± 4.4 % (12 months) for GNE<sup>+/-</sup> mice.

To investigate the old mice for neurodegeneration in particular, the relative mean widths at 12 months were plotted and statistically analyzed in a separate graph (Figure 15C). Although there is a slight tendency for a larger DG1 width and a larger CA3 width for GNE<sup>+/-</sup> mice, these differences were not significant (Student's t-test, DG1:  $p = 0.161$ , CA3:  $p = 0.145$ ).

Taken together, no genotype-dependent differences were detected in the width analysis of CA3 but the data showed slowly increasing neurodegeneration in the CA3 region of the hippocampus, which was stronger in the transgenic mice.

### 3.1.4 RNA sequencing of the brain

To better understand the underlying mechanisms and to identify key players in the observed neurodegeneration in the brain a transcriptome analysis was performed comparing GNE<sup>+/-</sup> mice with wildtype littermates. For a detailed characterization, whole brain RNA of 9 months old mice was chosen because at that age the neuronal loss in the GNE<sup>+/-</sup> mice was already progressed in the SN pc and was getting significantly different in the hippocampus.

RNA was isolated from four GNE<sup>+/-</sup> mice and four wildtype littermates. Quality controls and differences in *gne* transcription were validated by sqRT-PCR ( $***p \leq 0.001$ ; 1.0 ± 0.0 FC GNE<sup>+/+</sup> vs. 0.4 ± 0.0 FC GNE<sup>+/-</sup>; Figure 16A). The RNA sequencing, the processing and the analysis of the data were then performed by Dr. Sinkkonen and colleagues at the University of Luxembourg. Further in-depth analysis of the data was done in our lab in close collaboration.

After normalization of the RNA sequencing data in total 52832 separate genes (summarizing hits for transcript variants and isoforms under one gene name) with a detection threshold over 1 fragments per kilobase of transcripts per million mapped reads (> 1 FPKM) were detected. Then, statistical comparison using DeSeq2 was performed to detect differentially expressed genes (DEGs) between the groups. For this analysis it has to be taken into account that DeSeq2 cannot distinguish between isoforms but was considered to be the better tool to use for pairwise comparison and the biological question asked here. In total, 45 genes with a FDR < 0.1 and with an adjusted  $p$ -value < 0.1 were found differentially expressed in the GNE<sup>+/-</sup> group compared to the wildtype group (Table 8, Appendix). Interestingly, most of the 45 DEGs were downregulated with *Ppp1r3g*, *Ddit4*, and *Arl4d* as the most downregulated transcripts and only three genes were upregulated (*sox9*, *cxcl12*, *btg2*). Many of the genes were transcription factors

with several genes being involved in apoptotic pathways or regulation of neurogenesis. The snake plot in Figure 16B shows the 25 out of the 45 DEGs, which have the highest  $\log_2$  FC and an adjusted  $p$ -value  $< 0.05$ .

Next, I wanted to know if the detected DEGs hint towards a neuroinflammation in the brain. From studies by Bodea and colleagues (Bodea et al., 2014) it was known that systemic inflammation after LPS challenge not only leads to neuroinflammation but also to strong neurodegeneration in the substantia nigra. I wondered if similar mechanisms were also involved in the neurodegeneration discovered in the  $GNE^{+/-}$  mice or if at least similar key players could be detected. For this approach, the dataset was compared with the 45 DEGs (adjusted  $p < 0.1$ ). Strikingly, only six genes were shared with the 1467 genes changing in mouse brains upon LPS exposure (see Figure 16C). The six common genes are listed in Table 5 and only one of them (*dio2*) shared the same directionality indicating that the transcriptome analysis of  $GNE^{+/-}$  mice did not show a typical inflammatory signature.

**Table 5: List of the six shared genes of the GNE vs. LPS-induced neuroinflammation dataset**

Symbol	Gene name	Biological function <sup>1</sup>
<i>Acer2</i>	alkaline ceramidase 2	enzyme; involved e.g. in lipid metabolism, cell proliferation and death, and protein glycosylation in Golgi
<i>Bhlhe40</i>	basic helix-loop-helix family, member e40	transcriptional regulator; involved e.g. in circadian rhythm and control of cell differentiation
<i>Dio2</i>	deiodinase, iodothyronine, type II	thyroid enzyme; involved in thyroid hormone generation and metabolism, and myelination
<i>Frmd6</i>	FERM domain containing 6	regulator protein; involved in e.g. in actin-filament-based processes and cellular protein localization
<i>Nostrin</i>	nitric oxide synthase trafficker	transcriptional regulator; involved e.g. in endocytosis
<i>Per1</i>	period circadian clock 1	transcriptional regulator; involved mainly in circadian rhythm but also in e.g. regulation of cytokine production or glucocorticoid receptor signaling pathway

<sup>1</sup>taken and modified from BioGPS (Wu et al., 2009)

Nevertheless, I was interested to understand which other pathways might be involved. Therefore, an Ingenuity Pathway Analysis<sup>®</sup> (IPA, Qiagen<sup>®</sup>) was performed to explore general signs of biological functions related to the RNA sequencing data (FDR  $< 0.1$ ).

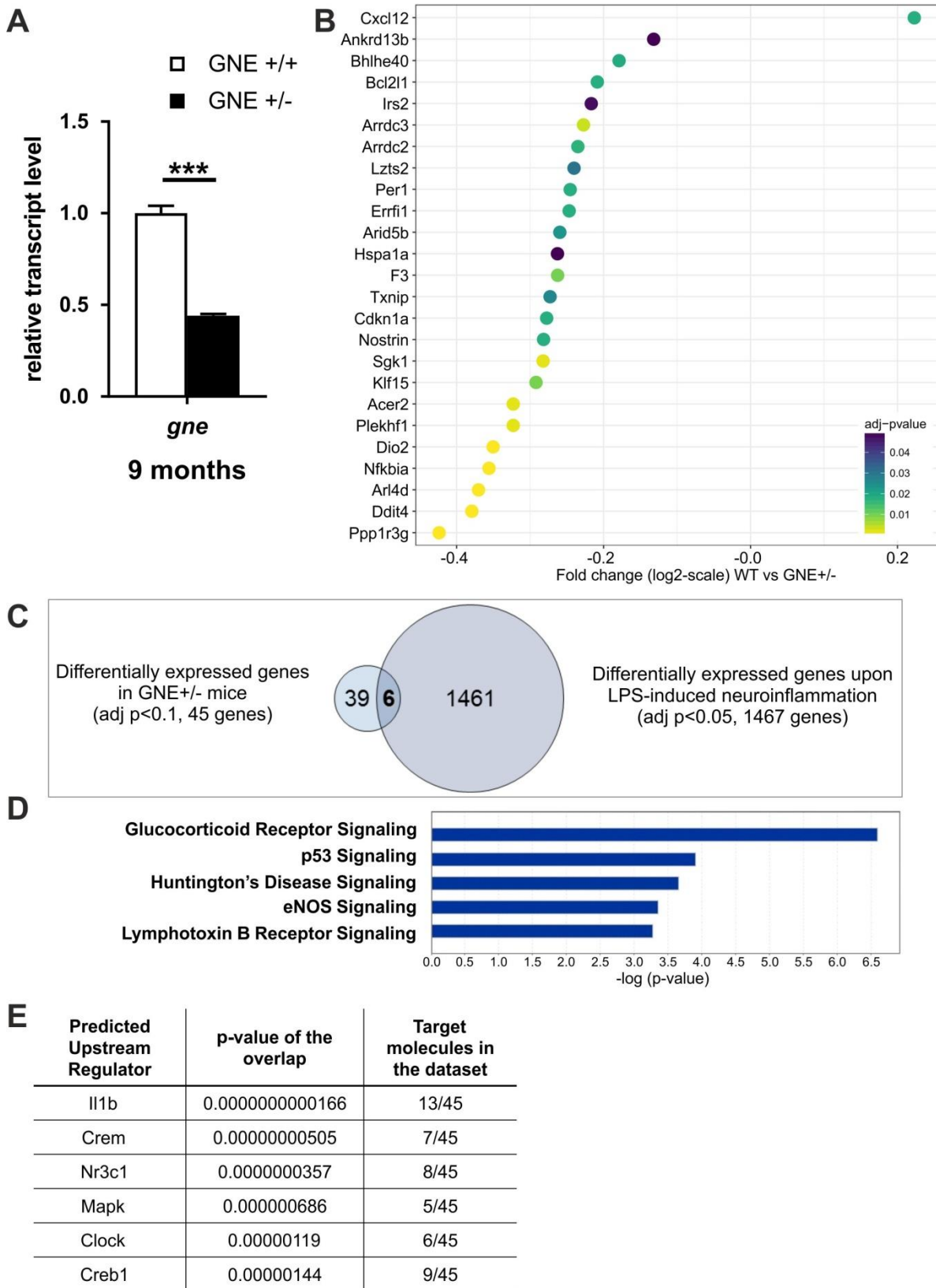


**Figure 16: RNA sequencing results of 9 months old GNE<sup>+/-</sup> mice compared to wildtype littermates.** RNA from brain homogenates was sequenced in collaboration with Dr. Sinkkonen, University of Luxembourg. (A) Confirmation of different *gne* transcription levels in the analyzed sample sets. Data shown as mean + SEM; normalized to 9 months old GNE<sup>+/+</sup> animals;  $n = 4$ , Student's t-test,  $***p \leq 0.001$ . (B) Snake plot of the 25 most differentially expressed genes (DEGs) in GNE<sup>+/-</sup> mice compared to wildtype (WT) littermates with an adjusted  $p$ -value (adj  $p$ )  $< 0.05$ . Genes are ranked by fold change (log<sub>2</sub>-scale) and color-coded for adj  $p$ . (C) Venn diagram comparing the total 45 DEGs (adj  $p < 0.1$ ) with 1467 DEGs of brain samples upon systemic 4 x LPS-induced

neuroinflammation (dataset from Bodea et al., 2014). Only six genes were shared pointing out the big differences in the responses of these mice. (D) Presentation of the top five canonical pathways enriched in the Ingenuity Pathway Analysis on the significantly 45 DEGs (false discovery rate, FDR < 0.1). (E) Table of predicted upstream molecules targeting most of the 45 DEGs. Il1b - interleukin-1 beta; Crem - cAMP responsive element modulator; Nr3c1 – nuclear receptor subfamily 3 group C member 1; Mapk – mitogen-activated protein kinase; Clock - clock circadian regulator; Creb1 - cAMP responsive element binding protein 1.

The top five canonical pathways that showed up in the IPA are listed in Figure 16D. The highest significant canonical pathway on the list was glucocorticoid receptor signaling. Almost 20 % of the DEGs are involved in this pathway. Glucocorticoid receptors are intracellular messengers and can directly or indirectly modulate the transcription of pro- and anti-inflammatory genes. Beside the canonical pathway analysis, IPA also predicted possible upstream regulators that could explain the 45 DEGs found in *GNE*<sup>+/-</sup> mice. A list of possible upstream regulators covering most of the 45 DEGs as target molecules can be found in Figure 16E. The regulator molecule having the most target molecules in the dataset was the cytokine Il1b. Nearly 30 % of the 45 DEGs interact with Il1b or are indirectly connected. Even 20 % of the DEGs can be regulated by the cAMP responsive element binding protein 1 (Creb1). Interestingly, the nuclear receptor subfamily 3 group C member 1 (Nr3c1), a member of the glucocorticoid receptor family, also showed up in the list of the predicted upstream regulator, connecting the upstream regulator with one of the canonical pathways.

Taken together, no clear signs of neuroinflammation could be found in the brains of *GNE*<sup>+/-</sup> mice compared to wildtype littermates. Nevertheless, some pathways like the glucocorticoid signaling pathway could be altered in the transgenic mice on transcriptional level.

### 3.1.5 Inflammation analysis on transcript level

To confirm the RNA sequencing data of 9 months old mouse brains but also to review other age points, some genes were reanalyzed by sqRT-PCR. Therefore, RNA was isolated from brains of *GNE*<sup>+/-</sup> mice and wildtype mice at the age of 1 month, 3 months, 6 months, 9 months, and 12 months and screened for cytokines, factors of the complement system and typical microglia marker.

#### 3.1.5.1 Cytokines

An indication for the activation of the innate immune system is the release of different cytokines. During inflammation mostly proinflammatory cytokines like Il1b and Tnfa are released. Therefore, I first investigated the relative transcript levels of the proinflammatory cytokines *il1b* and *tnfa* in more details (Figure 17). In Figure 17A the transcription levels at only 9 months are shown. While *tnfa* transcripts showed no difference ( $p = 0.624$ ;  $1.2 \pm 0.3$  FC

in  $GNE^{+/+}$  vs.  $1.3 \pm 0.1$  FC in  $GNE^{+/-}$ ) at 9 months, *illb* transcripts varied significantly in levels ( $*p = 0.041$ ;  $0.9 \pm 0.2$  FC in  $GNE^{+/+}$  vs.  $1.7 \pm 0.3$  FC in  $GNE^{+/-}$ ).

Comparing the findings at 9 months with the progression of the different transcript levels over age, they indeed reflected the time course quite well. The *illb* transcription levels increased much stronger with age than the *tnfa* transcript levels (increase of 100 % for  $GNE^{+/-}$  comparing 3 months to 12 months). However, while at 6 months until 12 months the levels were much higher in the  $GNE^{+/-}$  mice, they were still the same at 1 month and 3 months of age (Figure 17B, left graph). The *tnfa* transcription showed a slight increase with age (~20 %, 3 months vs. 12 months) but independently of the genotype (Figure 17B, right graph).

A robust multiple linear regression of *illb* transcription during aging revealed age- and genotype-specific differences ( $R^2 = 0.293$ , age effect:  $***p < 0.001$ , genotype effect:  $*p = 0.013$ ) but without any effect modulations (age\*genotype:  $p = 0.122$ ). Pairwise comparison between  $GNE^{+/-}$  mice and wildtype littermates revealed no significant differences at 1 month ( $p = 0.364$ ), 3 months ( $p = 0.491$ ) and at 12 months ( $p = 0.281$ ), but strong significant differences at 6 months ( $**p = 0.006$ ) and at 9 months ( $*p = 0.031$ ; Figure 17B, left graph). Multiple linear regression analysis of *tnfa* transcription during aging also resulted in age- but not in genotype-specific differences ( $R^2 = 0.168$ , age effect:  $***p < 0.001$ , genotype effect:  $p = 0.415$ ) as well as not in effect modulations (age\*genotype:  $p = 0.978$ ). Pairwise comparison between  $GNE^{+/-}$  mice and wildtype littermates showed no significant differences at any time point measured (1 month:  $p = 0.281$ ; 3 months:  $p = 0.753$ ; 6 months:  $p = 0.364$ ; 9 months:  $p = 0.672$ ; 12 months:  $p = 0.874$ ; Figure 17B, right graph).

In detail, the *illb* transcription levels increased from  $0.6 \pm 0.1$  FC (1 month) to  $1.1 \pm 0.2$  FC (3 months), back to  $0.4 \pm 0.1$  FC (6 months), and further to  $0.9 \pm 0.2$  FC (9 months) and  $1.5 \pm 0.3$  FC (12 months) in wildtype animals. The *illb* transcription levels of  $GNE^{+/-}$  mice started at  $0.7 \pm 0.1$  FC in 1 month and increased to  $1.0 \pm 0.2$  FC (3 months),  $0.8 \pm 0.1$  FC (6 months),  $1.7 \pm 0.3$  FC (9 months), and to  $2.0 \pm 0.4$  FC (12 months). The *tnfa* transcript levels changed from  $0.6 \pm 0.0$  FC (1 month), to  $1.1 \pm 0.2$  FC (3 months),  $0.9 \pm 0.1$  FC (6 months),  $1.2 \pm 0.3$  FC (9 months), and  $1.4 \pm 0.2$  FC (12 months) in wildtype mice and from  $0.7 \pm 0.1$  FC (1 month), to  $1.2 \pm 0.2$  FC (3 months),  $1.1 \pm 0.2$  FC (6 months),  $1.3 \pm 0.1$  FC (9 months), and  $1.3 \pm 0.2$  FC (12 months) in  $GNE^{+/-}$  mice.

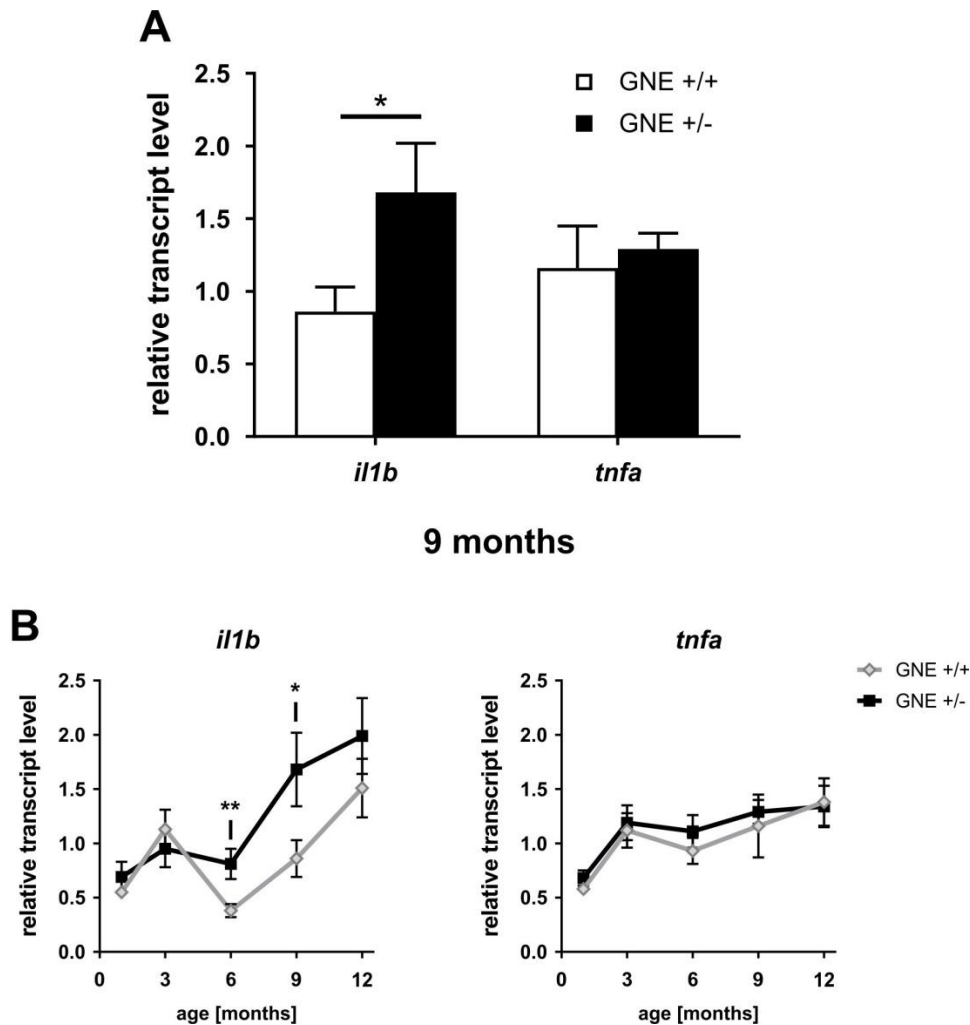


**Figure 17: Transcriptional profiles of the proinflammatory cytokines *Il1b* and *Tnfa*.** (A) Levels of interleukin 1 beta (*il1b*) and tumor necrosis factor alpha (*tnfa*) transcription in the brains of 9 months old GNE<sup>+/-</sup> mice and wildtype littermates are compared. Level of *il1b* is significantly higher in GNE<sup>+/-</sup> mice. Data shown as mean + SEM; normalized to 3 months old GNE<sup>+/+</sup> animals; n = 7-14, Student's t-test, \* $p \leq 0.050$ . (B) Progression of *il1b* (left graph) and *tnfa* (right graph) transcription levels in the brains from 1 month until 12 months. Levels are increasing with age and much stronger in GNE<sup>+/-</sup> mice for *il1b*. Data shown as mean  $\pm$  SEM; normalized to 3 months old GNE<sup>+/+</sup> animals; n = 7-15, pairwise comparison for GNE<sup>+/+</sup> vs. GNE<sup>+/-</sup> mice at different age: \* $p \leq 0.050$ , \*\* $p \leq 0.010$ .

Taken together, the levels of the proinflammatory cytokines *il1b* and *tnfa* at 9 months reflect the overall trend in transcript levels. Genotype-specific differences were found in *il1b* transcription levels but not in *tnfa* transcription levels during aging and while the levels for *tnfa* were only slightly increasing with age the levels for *il1b* showed a much stronger increase.

### 3.1.5.2 Complement system

In addition, I checked the transcription levels of different components of the complement system. The complement system is involved in not only neurodegenerative diseases, but also in development and homeostasis of the brain, to facilitate synaptic and neuronal clearance via microglial phagocytosis. To evaluate whether the complement cascade is altered in our



transgenic mouse model, I determined the transcript levels of the complement component 1 q subcomponent with alpha or beta polypeptide, or c chain (*c1qa*, *c1qb*, *c1qc*), the complement component 4b (*c4b*), the complement component 3 (*c3*), and the integrin alpha M (*itgam*, a subunit of complement receptor 3) in the brains of 1 month, 3 months, 6 months, 9 months, and 12 months old *GNE*<sup>+/-</sup> mice and wildtype littermates. A schematic drawing in Figure 18B describes complement interactions. The complement receptor 3 (*Itgam* + *Itgb2*) can be found on macrophages like microglia (not displayed in Figure 18B).

I first evaluated the 9 months old brains in more details (Figure 18). Here, a significant difference between the genotypes was found for *c1qb* (\*\**p* = 0.007; 1.0 ± 0.1 FC in *GNE*<sup>+/+</sup> vs. 0.8 ± 0.0 FC in *GNE*<sup>+/-</sup>). The level of *c1qc* was also strongly reduced in *GNE*<sup>+/-</sup> mice (*p* = 0.062; 2.2 ± 0.6 FC in *GNE*<sup>+/+</sup> vs. 0.9 ± 0.2 FC in *GNE*<sup>+/-</sup>). Similar transcript levels between *GNE*<sup>+/+</sup> and *GNE*<sup>+/-</sup> were detected for *c1qa*, *c4b*, and *c3*. For *c3* and *itgam* the levels were slightly elevated in *GNE*<sup>+/-</sup> mice compared to wildtype littermates.

Similar to the transcription levels of the cytokines, the 9 months data of the complement components reflected quite well the overall course of the transcription levels from 1 month to 12 months. For *c1qa* the levels were always minimally higher in the transgenic mice but were always reduced for *c1qb* and *c4b* levels. The levels of *c1qc* were also always between ~30 % to ~60 % reduced in the transgenic mice. The levels of *c3* and *itgam* showed slightly higher level in *GNE*<sup>+/-</sup> for 6 months and 9 months. Overall, a clear age-dependent increase was found for *c4b* and for *c3* transcripts but was also present for all other investigated components.

A robust multiple linear regression confirmed age-specific differences for all components (*c1qa*:  $R^2 = 0.150$ , age effect: \*\*\**p* < 0.001; *c1qb*:  $R^2 = 0.223$ , age effect: \**p* = 0.008; *c1qc*:  $R^2 = 0.206$ , age effect: \**p* = 0.013; *c4b*:  $R^2 = 0.330$ , age effect: \*\*\**p* < 0.001; *c3*:  $R^2 = 0.281$ , age effect: \*\*\**p* < 0.001; and *itgam*:  $R^2 = 0.094$ , age effect: \*\*\**p* < 0.001). A genotype-specific effect showed only the linear model for *c1qb* (genotype effect: \*\**p* = 0.009) and *c1qc* (genotype effect: \*\*\**p* < 0.001) and significant effect modulations (age\*genotype) were not present in any model. Pairwise comparison between *GNE*<sup>+/-</sup> and wildtype littermates detected significant differences for *c1qb* levels at 9 months (\*\**p* = 0.004), *c1qc* levels at 1 month (\**p* = 0.038) and 9 months (\**p* = 0.032), and for *c4b* levels at 6 months (\**p* = 0.012).

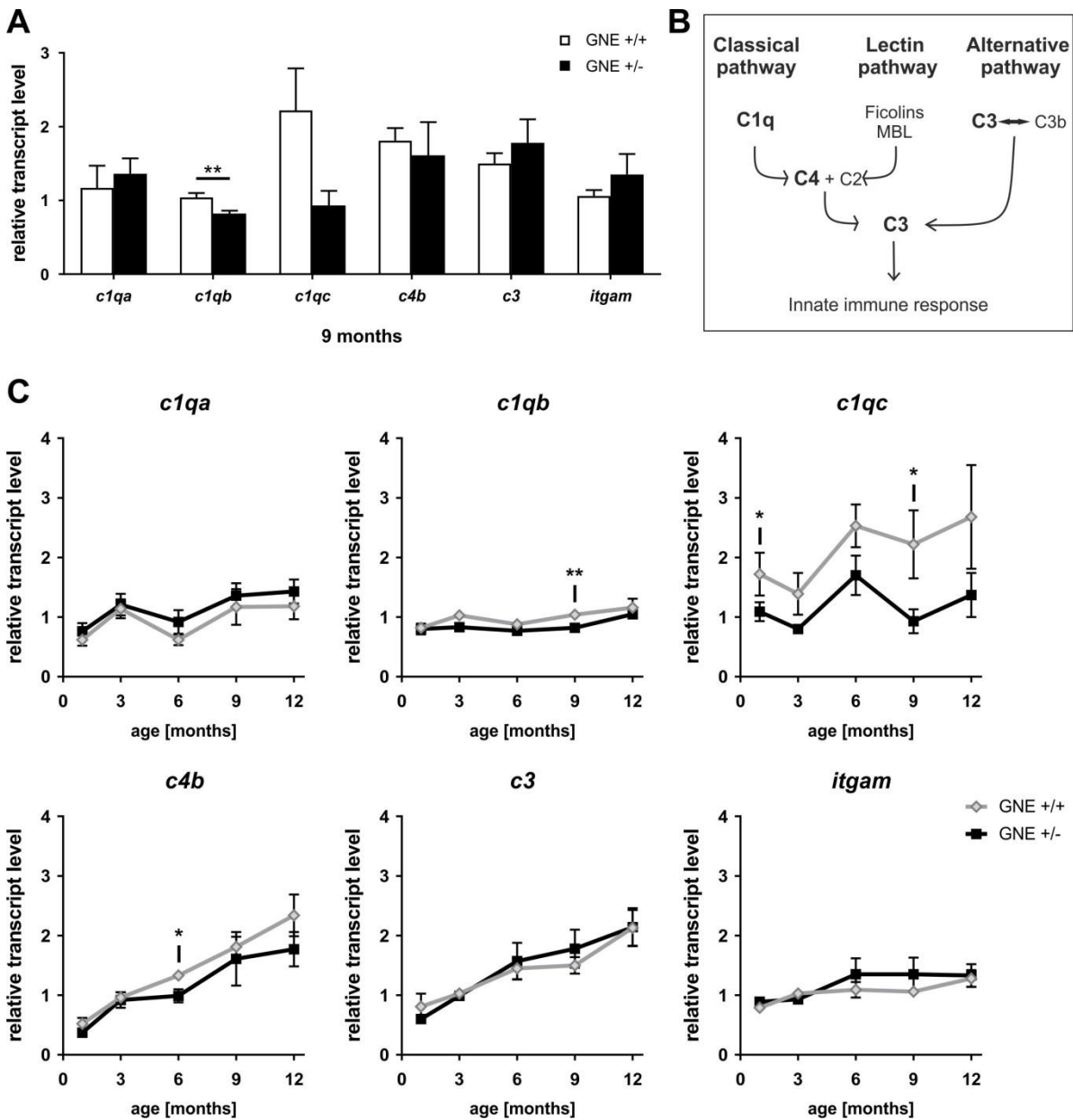


**Figure 18: Transcriptional profiles of components of the complement system.** (A) Transcription levels of complement component 1 with q subcomponent and alpha or beta polypeptide, or c chain (*c1qa*, *c1qb*, *c1qc*), complement component 4b (*c4b*), complement component 3 (*c3*), and integrin alpha M (*itgam*, a subunit of complement receptor 3) in the brains of 9 months old GNE<sup>+/-</sup> mice and wildtype littermates are compared. Data shown as mean + SEM; normalized to 3 months old GNE<sup>+/+</sup> animals; n = 8-14, Student's t-test, \*\**p* ≤ 0.010. (B) Schematic overview of all three pathways of the complement system showing some of the analyzed complement components in bold letters. (C) Progression of the transcription levels of the C1q subunits *c1qa*, *c1qb*, *c1qc* (upper graphs) and the complement components *c4b*, *c3*, and *itgam* (lower graphs) in the brains from 1 month until 12 months. Age-dependent upregulation was seen for *c4b* and *c3*. Higher levels in GNE<sup>+/-</sup> mice were detected for *c1qa*, *c3*, and *itgam*. Data shown as mean ± SEM; normalized to 3 months old GNE<sup>+/+</sup> animals; n = 7-15, pairwise comparison for GNE<sup>+/+</sup> vs. GNE<sup>+/-</sup> mice at different age: \**p* ≤ 0.050, \*\**p* ≤ 0.010.

In detail, the transcript levels of *c1qa* changed from  $0.6 \pm 0.1$  FC (1 month), to  $1.1 \pm 0.2$  FC (3 months),  $0.6 \pm 0.1$  FC (6 months),  $1.2 \pm 0.3$  FC (9 months), and  $1.2 \pm 0.2$  FC (12 months) in wildtype mice and from  $0.8 \pm 0.1$  FC (1 month), to  $1.2 \pm 0.2$  FC (3 months),  $0.9 \pm 0.2$  FC (6 months),  $1.4 \pm 0.2$  FC (9 months), and  $1.4 \pm 0.2$  FC (12 months) in GNE<sup>+/-</sup> mice. Levels of *c1qb* varied from  $0.8 \pm 0.0$  FC (1 month), to  $1.0 \pm 0.1$  FC (3 months),  $0.9 \pm 0.1$  FC (6 months),

1.0 ± 0.1 FC (9 months), and 1.2 ± 0.2 FC (12 months) in wildtype mice and from 0.8 ± 0.1 FC (1 month), to 0.8 ± 0.1 FC (3 months), 0.8 ± 0.0 FC (6 months), 0.8 ± 0.0 FC (9 months), and 1.0 ± 0.1 FC (12 months) in GNE<sup>+/-</sup> mice. Transcription of *c1qc* fluctuated between 1.7 ± 0.4 FC (1 month), to 1.4 ± 0.3 FC (3 months), 2.5 ± 0.4 FC (6 months), 2.2 ± 0.6 FC (9 months), and 2.7 ± 0.9 FC (12 months) in wildtype mice and between 1.1 ± 0.2 FC (1 month), 0.8 ± 0.1 FC (3 months), 1.7 ± 0.3 FC (6 months), 0.9 ± 0.2 FC (9 months), and 1.4 ± 0.4 FC (12 months) in GNE<sup>+/-</sup> mice. In contrast, the transcription levels of *c4b* steadily increased from 0.5 ± 0.1 FC (1 month) to 1.0 ± 0.1 FC (3 months), over 1.3 ± 0.1 FC (6 months), 1.8 ± 0.2 FC (9 months), to 2.3 ± 0.3 FC (12 months) in wildtype mice and increased similar from 0.4 ± 0.0 FC (1 month), over 0.9 ± 0.1 FC (3 months), 1.0 ± 0.1 FC (6 months), 1.6 ± 0.4 FC (9 months), to 1.8 ± 0.3 FC (12 months) in GNE<sup>+/-</sup> mice. The course of *c3* transcripts also increased from 0.8 ± 0.2 FC (1 month) to 1.0 ± 0.1 FC (3 months) over 1.5 ± 0.2 FC (6 months), 1.5 ± 0.1 FC (9 months), to 2.1 ± 0.3 FC (12 months) in wildtype mice and increased similar from 0.6 ± 0.0 FC (1 month), over 1.0 ± 0.1 FC (3 months), 1.6 ± 0.3 FC (6 months), 1.8 ± 0.3 FC (9 months), to 2.1 ± 0.3 FC (12 months) in GNE<sup>+/-</sup> mice. In addition, the levels of *itgam* stayed relatively constant with 0.8 ± 0.0 FC (1 month), 1.0 ± 0.1 FC (3 months), 1.1 ± 0.1 FC (6 months), 1.1 ± 0.1 FC (9 months), and 1.3 ± 0.1 FC (12 months) in wildtype mice and with 0.9 ± 0.1 FC (1 month), 0.9 ± 0.1 FC (3 months), 1.4 ± 0.3 FC (6 months), 1.3 ± 0.3 FC (9 months), and 1.3 ± 0.2 FC (12 months) in GNE<sup>+/-</sup> mice.

Taken together, transcription levels of different components of the complement system increased with age but to very diverse extents. Significant differences between GNE<sup>+/-</sup> mice and wildtype littermates were detected for *c1qb*, *c1qc*, and *c4b* transcription and with reduced levels in the transgenic mice. The overall findings were well reflected by the 9 months old results.

### 3.1.5.3 Microglia markers

To better understand if microglia sense an altered glycoalyx and sialic acid changes in the transgenic mouse model, the mRNA levels of the macrophage- and microglia-specific marker allograft inflammatory factor 1 (*aif1*; the *Iba1* encoding gene), the phagocytosis and activation marker CD68 antigen (*cd68*), and the newly identified microglia-specific marker transmembrane protein 119 (*tmem119*; described in Bennett et al., 2016) was determined in brain homogenates of GNE<sup>+/-</sup> mice and wildtype mice at the age of 1 month, 3 months, 6 months, 9 months, and 12 months (Figure 19).

First, in addition to the RNA sequencing results the transcription levels at 9 months were investigated in more details (Figure 19A). Overall, the transcript levels of *aif1*, *cd68*, and *tmem119* were always higher in  $GNE^{+/-}$  mice with differences in *aif1* transcripts at significant level ( $*p = 0.029$ ;  $0.9 \pm 0.1$  FC in  $GNE^{+/+}$  vs.  $1.7 \pm 0.3$  FC in  $GNE^{+/-}$ ).

Careful investigations of the time courses of all microglia markers showed similar tendencies (Figure 19B). While at 1 month and 3 months of age transcription levels were almost equal (except *cd68*, 3 months), detected levels for 6 months, 9 months, and 12 months were always higher in the transgenic mice. Furthermore, levels of *aif1* (left graph) and *tmem119* (right graph) were increasing with age with a discontinuum between 3 months and 6 months, while levels of *cd68* (middle graph) were rather decreasing after 3 months.

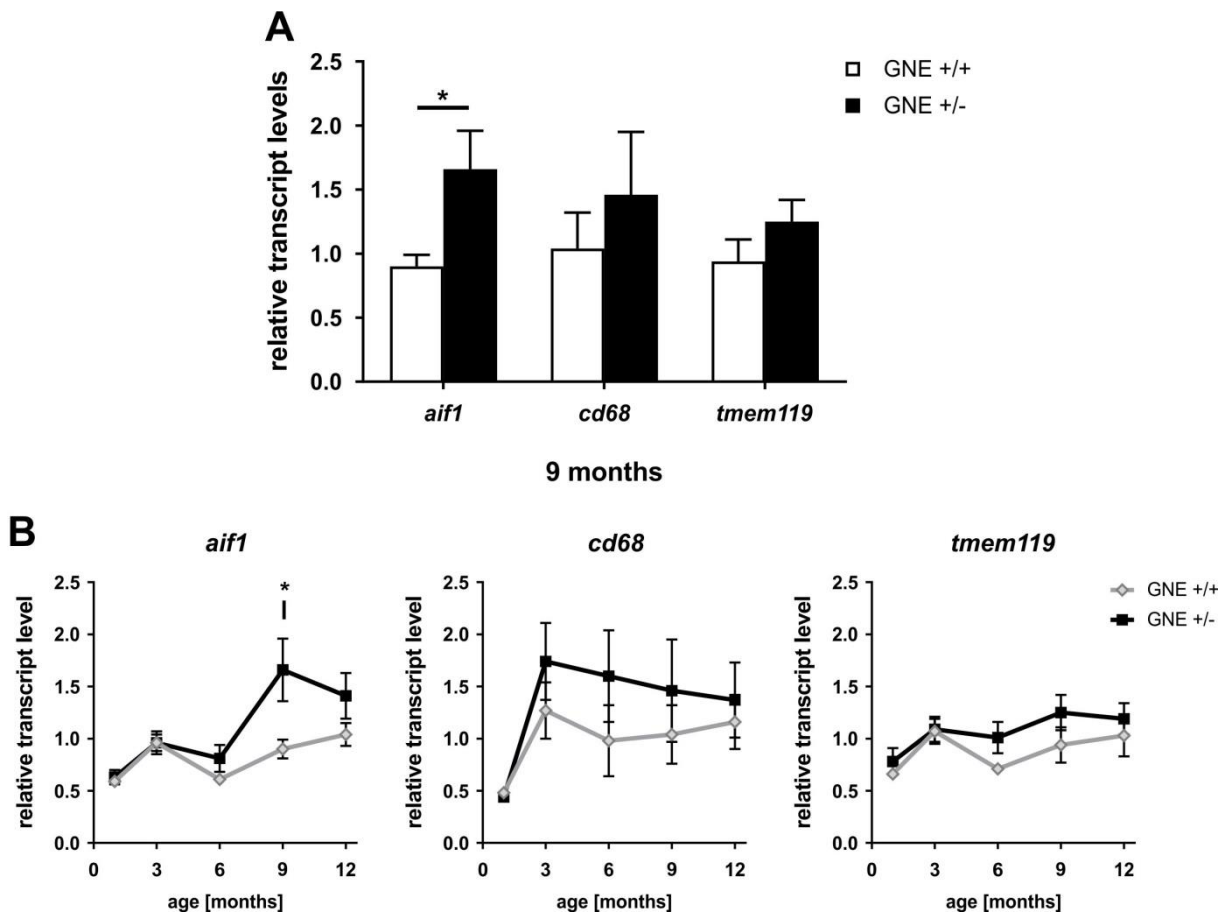


**Figure 19: Transcriptional profiles of microglial markers.** (A) Levels of allograft inflammatory factor 1 (*aif1*; gene of *Iba1*), the CD68 antigen (*cd68*), and the transmembrane protein 119 (*tmem119*) transcripts in the brains of 9 months old  $GNE^{+/-}$  mice and wildtype littermates are compared. Transcription of *il1b* is higher in  $GNE^{+/-}$  mice. Data shown as mean + SEM; normalized to 3 months old  $GNE^{+/+}$  animals;  $n = 8-14$ , Student's t-test,  $*p \leq 0.050$ . (B) Progression of *aif1* (left graph), *cd68* (middle graph), and *tmem119* (right graph) transcription levels in the brains from 1 month until 12 months. Levels of *il1b* increase with age. Transcription levels are mostly higher in  $GNE^{+/-}$  mice. Data shown as mean  $\pm$  SEM; normalized to 3 months old  $GNE^{+/+}$  animals;  $n = 7-15$ , pairwise comparison for  $GNE^{+/+}$  vs.  $GNE^{+/-}$  mice at different age:  $*p \leq 0.050$ .

A robust multiple linear regression during aging revealed age-specific differences for all three markers (*aif1*:  $R^2 = 0.278$ , age effect:  $***p < 0.001$ ; *cd68*:  $R^2 = 0.100$ , age effect:  $***p < 0.001$ ; *tmem119*:  $R^2 = 0.122$ , age effect:  $**p = 0.003$ ). A genotype-specific effect was seen in the model of *aif1* (genotype effect:  $**p = 0.003$ ) and of *tmem119* (genotype effect:  $*p = 0.040$ ) but not in the linear model of *cd68* (genotype effect:  $p = 0.109$ ). However, significant effect modulations (age\*genotype) were not present in any model (*aif1*:  $p = 0.130$ ; *cd68*:  $p = 0.416$ ; *tmem119*:  $p = 0.735$ ). Interestingly, pairwise comparison between GNE<sup>+/-</sup> and wildtype littermates detected only significant differences for *aif1* levels at 9 months ( $*p = 0.018$ ).

In detail, the transcript levels of *aif1* changed from  $0.6 \pm 0.1$  FC (1 month) to  $1.0 \pm 0.1$  FC (3 months), and from  $0.6 \pm 0.0$  FC (6 months), over  $0.9 \pm 0.1$  FC (9 months), to  $1.0 \pm 0.1$  FC (12 months) in wildtype mice and similar from  $0.6 \pm 0.1$  FC (1 month) to  $1.0 \pm 0.1$  FC (3 months), and from  $0.8 \pm 0.1$  FC (6 months), to  $1.7 \pm 0.3$  FC (9 months), to  $1.4 \pm 0.2$  FC (12 months) in GNE<sup>+/-</sup> mice. Transcription of *cd68* increased strongly from  $0.5 \pm 0.1$  FC (1 month) to  $1.3 \pm 0.3$  FC (3 months) and then decreased to  $1.0 \pm 0.3$  FC (6 months),  $1.0 \pm 0.3$  FC (9 months), and  $1.2 \pm 0.3$  FC (12 months) in wildtype mice. In GNE<sup>+/-</sup> mice transcription of *cd68* increased also from  $0.4 \pm 0.0$  FC (1 month) to  $1.7 \pm 0.4$  FC (3 months) and steadily decreased from  $1.6 \pm 0.4$  FC (6 months), to  $1.5 \pm 0.5$  FC (9 months), and to  $1.4 \pm 0.4$  FC (12 months). Mean levels of *tmem119* changed from  $0.7 \pm 0.0$  FC (1 month), to  $1.1 \pm 0.1$  FC (3 months),  $0.7 \pm 0.0$  FC (6 months),  $0.9 \pm 0.2$  FC (9 months), and  $1.0 \pm 0.2$  FC (12 months) in wildtype mice and from  $0.8 \pm 0.1$  FC (1 month), to  $1.1 \pm 0.1$  FC (3 months),  $1.0 \pm 0.2$  FC (6 months),  $1.3 \pm 0.2$  FC (9 months), and  $1.2 \pm 0.2$  FC (12 months) in GNE<sup>+/-</sup> mice.

Altogether, differences in the transcription levels of microglial markers were minor but present. Especially at 6 months and 9 months levels were increased in the brain of GNE<sup>+/-</sup> mice compared to wildtype littermates.

### 3.1.6 Inflammation analysis on protein level

Although no typical inflammatory signature was found in the brain transcriptome analysis, neuroinflammation occurring on protein level could not automatically be excluded. Typical sensors of neuronal stress are glial cells, like microglia and astrocytes. Changes in the brain parenchyma might be sensed and lead to activation and morphological changes in these cells. Over-activation and dysregulation of these cells can have detrimental effects on the neurons, like neuroinflammation.

### 3.1.6.1 Microglia analysis

As described by Linnartz-Gerlach and colleagues (Linnartz et al., 2012b; Linnartz-Gerlach et al., 2016) sialylation serves as an inhibitory flag for the innate immune system. Thus, an altered sialylation in the brain can lead to the activation of microglia. Inflammatory microglia activation is often described along with morphological changes. Activation markers like Cd68 are upregulated and microglia retract their processes, which normally results in a larger soma area. To quantify some of these parameters, sagittal sections of the SN pr of 9 months old mice were stained with antibodies against the microglial membrane receptor Iba1 and the activation/lysosomal marker Cd68. Z-stack images were acquired to consider the three-dimensional stretch of a microglia.

As displayed in Figure 20A, the microglia morphology was not obviously altered in the  $GNE^{+/-}$  mice compared to wildtype littermates. The lysosomal protein Cd68 was often co-stained with Iba1-positive structures and could be observed in the soma as well as in microglial processes. Microglia were equally distributed in the sagittal sections investigated and the density of Iba1-/DAPI-positive cells was not significantly different between the genotypes ( $p = 0.075$ ; Figure 20B). The overall fluorescence intensity of Iba1 was slightly higher in the  $GNE^{+/-}$  mice ( $p = 0.244$ ). In contrast, the overall Cd68 fluorescence intensity per area was minor but significantly decreased in  $GNE^{+/-}$  mice ( $*p = 0.013$ ; Figure 20C).

In detail, the relative density of Iba1-/DAPI-positive cells was  $100.0 \pm 13.4$  % in  $GNE^{+/+}$  mice and  $68.1 \pm 3.4$  % in  $GNE^{+/-}$  mice. As quantified in Figure 20C, the measured Iba1 fluorescence intensity per area was  $100.0 \pm 10.1$  % in  $GNE^{+/+}$  mice and  $125.0 \pm 49.7$  % in  $GNE^{+/-}$  mice and the measured Cd68 fluorescence intensity per area was  $100.0 \pm 1.3$  % in  $GNE^{+/+}$  mice compared to  $86.7 \pm 4.1$  % in  $GNE^{+/-}$  mice.

Additionally, the microglial soma area was selected and quantified separately. As shown in Figure 20D no genotype-specific differences in the soma area were detected ( $p = 0.571$ ). The Iba1 fluorescence intensity of the soma did also not show any genotype-specific differences ( $p = 0.776$ ; Figure 20E, left graph). In contrast, the Cd68 fluorescence intensity was again reduced, but not significantly in  $GNE^{+/-}$  mice compared to wildtype littermates ( $p = 0.134$ ; Figure 20E, right graph).

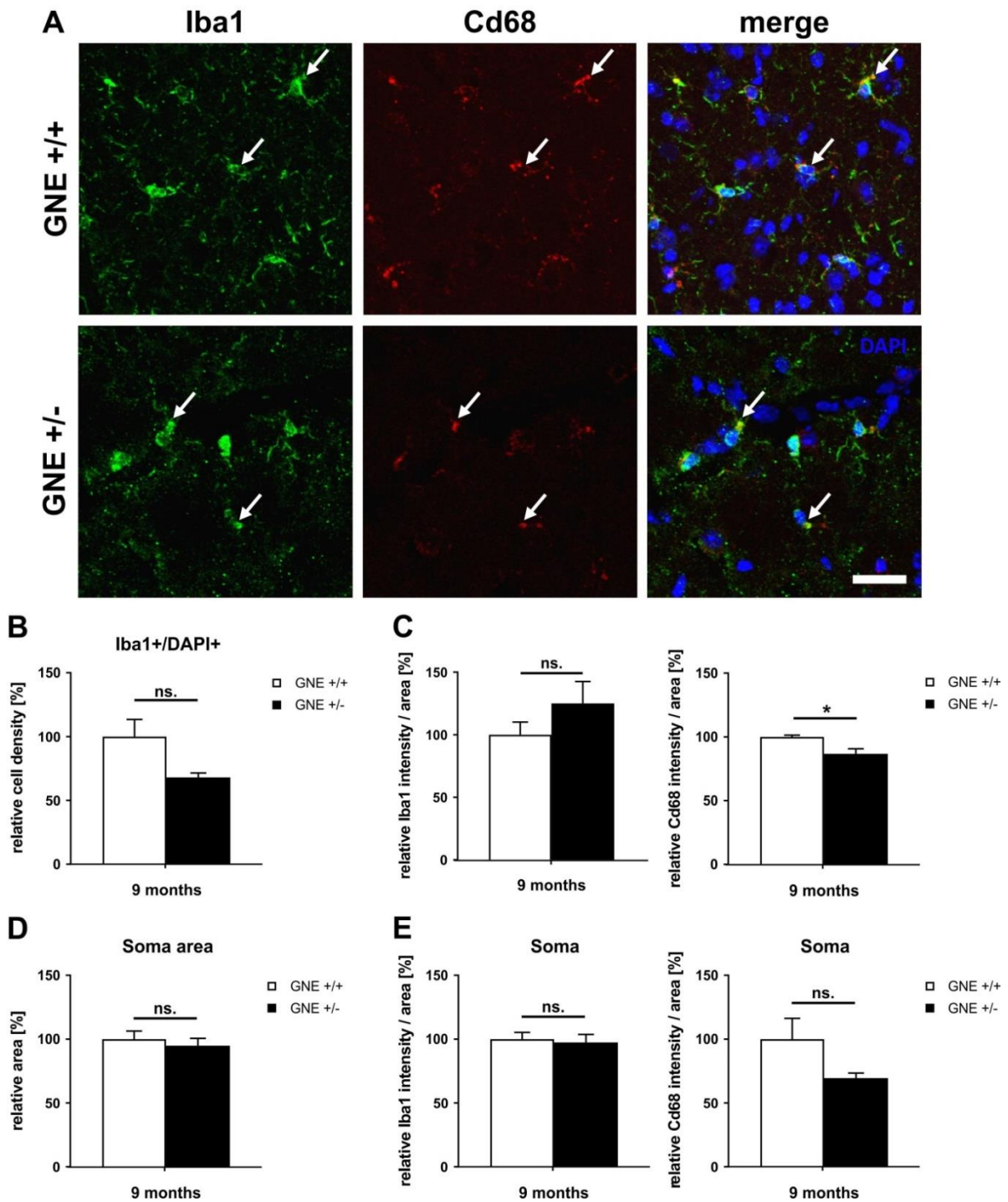


**Figure 20: No genotype-dependent differences in the microglia morphology of 9 months old mice.** (A) Representative z-stack images of the microglia in the SN pr of 9 months old GNE<sup>+/-</sup> mice and wildtype littermates at lateral sections of ~1.30 mm are shown. The sagittal brain slices were stained with antibodies directed against the microglial marker ionized calcium binding adaptor molecule 1 (Iba1; green), the microglial activation marker Cd68 (red) and the nucleus marker DAPI (blue). White arrows indicate some representative Iba1-/Cd68 co-staining. Scale bar: 50 μm. (B) Quantification of the relative microglial (Iba+/DAPI+) cell density showed a slight decrease for GNE<sup>+/-</sup> mice. Data shown as mean + SEM; n = 5-8, Student's t-test, ns. = not significant. (C) Quantification of the relative fluorescence intensity per area of Iba1 (left graph) and of Cd68 (right graph) revealed no differences in Iba1 and a slight decrease in Cd68 in GNE<sup>+/-</sup> mice. Data shown as mean + SEM; n = 4-8, Student's t-test, ns. = not significant, \**p* ≤ 0.050. (D) Quantification of the relative soma area of Iba-/DAPI-positive cells showed no difference. Data shown as mean + SEM; n = 5-8, Student's t-test, ns. = not significant. (E) Quantification of the relative fluorescence intensity per soma area of Iba1 (left graph) and of Cd68 (right graph) revealed no difference for Iba1 and a decrease in Cd68 for GNE<sup>+/-</sup> mice. Data shown as mean + SEM; n = 4-8, Student's t-test, ns. = not significant.

In detail, the relative soma area was  $100.0 \pm 6.3$  % in  $GNE^{+/+}$  mice and  $94.8 \pm 5.9$  % in  $GNE^{+/-}$  mice. The measured Iba1 fluorescence intensity per soma was  $100.0 \pm 5.2$  % in  $GNE^{+/+}$  mice compared to  $97.4 \pm 6.3$  % in  $GNE^{+/-}$  mice and the measured Cd68 fluorescence intensity per soma was  $100.0 \pm 16.3$  % in  $GNE^{+/+}$  mice compared to  $69.4 \pm 4.1$  % in  $GNE^{+/-}$  mice.

### 3.1.6.2 Astrocytes analysis

Astrocytes are star-shaped glial cells in the brain that originate from precursor cells of the neuronal lineage and do not belong to the innate immune system such as microglia. Nevertheless, astrocytes closely interact with the neuronal tissue like microglia. Beside a range of different functions, they can support neurons by provisions of nutrients, regulating transmitter and ion concentrations in the extracellular space and are closely associated with synaptic activity modulation. In inflammatory brains, astrogliosis can be detected by increased fluorescence intensity of the glial fibrillary acidic protein (Gfap) and increased numbers of astrocytes. To investigate astrogliosis as possible inflammatory sign in the brain of  $GNE^{+/-}$  mice, sagittal sections of the SN pr of 9 months old mice were stained with antibodies directed against the astroglial marker Gfap and the nucleus marker DAPI. Z-stack images were acquired to consider the three-dimensional stretch of an astrocyte.

Representative z-stacks of the Gfap-positive cells are shown in Figure 21A. More and thicker processes branch from the soma of astrocytes compared to microglia, which gives them a star-like shape. All z-stacks investigated show a rather equal cell distribution and no differences in cell density between the genotypes could be observed in the SN pr of 9 months old mice ( $p = 393$ ; Figure 21B). The Gfap fluorescence intensity per area was slightly but not significantly reduced in  $GNE^{+/-}$  mice ( $p = 250$ ; Figure 21C).

In detail, the measured relative density of Gfap-/DAPI-positive cells was  $100.0 \pm 4.9$  % in  $GNE^{+/+}$  mice compared to  $93.2 \pm 6.0$  % in  $GNE^{+/-}$  mice. The overall Gfap fluorescence intensity per area was  $100.0 \pm 16.1$  % in  $GNE^{+/+}$  mice and  $77.3 \pm 9.2$  % in  $GNE^{+/-}$  mice.

Taken together, the analyzed data on protein level showed no typical inflammatory changes in the morphology of microglia and astrocytes. Only minor genotype-dependent differences could be observed.



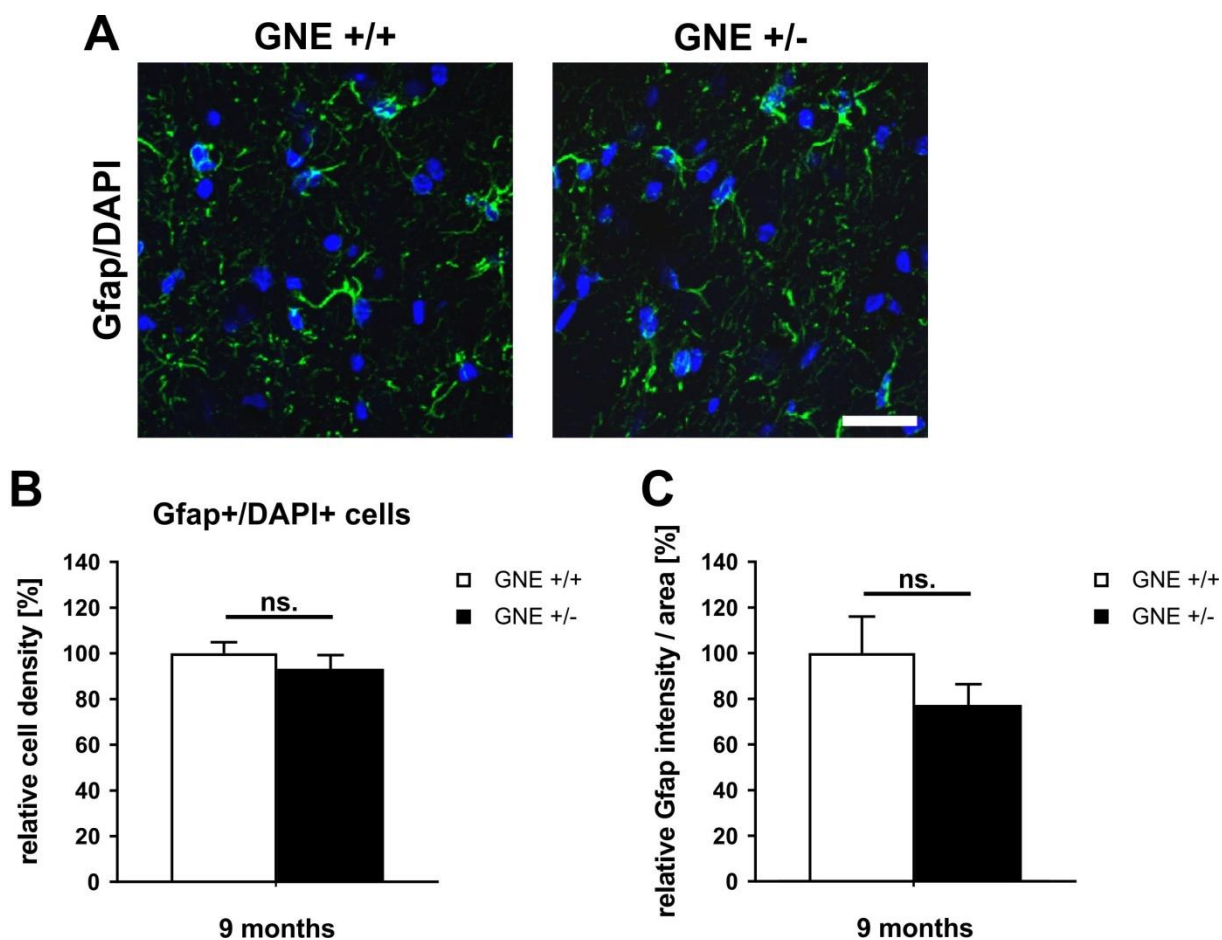


**Figure 21: No genotype-dependent differences in astrocytes in the SN pr.** (A) Representative z-stack images of the astrocytes in the SN pr of 9 months old  $GNE^{+/-}$  mice and wildtype littermates at lateral sections of  $\sim 1.40$  mm are shown. The sagittal brain slices were stained with antibodies directed against the astrocytic marker glial fibrillary acidic protein (Gfap; green) and the nucleus marker DAPI (blue). Scale bar: 25  $\mu$ m. (B) Quantification of the relative astrocyte (Gfap+/DAPI+) cell density in the SN pr of 9 months old animals revealed no difference. Data shown as mean + SEM;  $n = 9-10$ , Student's t-test, ns. = not significant. (C) Quantification of the relative Gfap fluorescence intensity per area in the SN pr of 9 months old animals showed a slight but not significant decrease for  $GNE^{+/-}$  mice. Data shown as mean + SEM;  $n = 9-10$ , Student's t-test, ns. = not significant.

### 3.2 Rescue of the $GNE^{+/-}$ -specific phenotype

The characterization of the transgenic mouse model indicated major changes in the homeostasis of the brains of these mice probably due to the altered sialylation. Neuronal loss correlates with microglial activation and supported the hypothesis of Linnartz-Gerlach and colleagues (Linnartz et al., 2012b; Linnartz-Gerlach et al., 2016) that in the absence of sialic acids, complement-mediated phagocytosis is initiated. To confirm that the above described neuronal loss is indeed dependent on the activation of the complement cascade, I crossbred  $GNE$  mice with mice deficient for C3. The complement component C3 is the central player in the complement cascade and a C3 knockout prevents complement activation. The  $GNE/C3$  offspring were investigated with similar parameters as used for the characterization of the  $GNE^{+/-}$  mice.

### 3.2.1 RNA sequencing

First, a transcriptome analysis on 9 months old brains was performed in direct comparison to the  $GNE^{+/-}$  mice (now written as  $GNE^{+/-}C3^{+/+}$ ). The direct comparison should enable to detect the rescue of even small changes. In addition to the samples described in section 3.1.4, RNA was isolated from four  $GNE^{+/-}C3^{-/-}$  mice and four  $GNE^{+/+}C3^{-/-}$  mice. The RNA sequencing, the processing and the analysis of the data were again performed by Dr. Sinkkonen and colleagues at the University of Luxembourg. Further in-depth analysis of the data was carried out in our lab in close collaboration.

To compare the overall gene expression profiles between the four different genotypes, a principle component analysis (PCA) was performed. The PCA displayed in Figure 22A demonstrated that in general the RNA sequencing analysis was successful because all four groups were distinguishable by their genotype. The PCA plot shows that samples with C3 wildtype background clustered strongly together as well as samples with C3-deficient background. Furthermore, all  $GNE^{+/+}$  samples were located together regarding the principle component (Pc) 2 ( $Pc2 < 0$ ), while the  $GNE^{+/-}$  samples were rather located above  $Pc2 = 0$ . Interestingly, the samples with  $GNE^{+/+}$  background clustered closer together than samples with a  $GNE^{+/-}$  background and those samples seemed to be more diverse. Still, the C3 background was dividing the samples strongest ( $C3^{-/-}$ :  $Pc1 < -2$ ;  $C3^{+/+}$ :  $Pc1 > 2$ ). Noteworthy, the sample G5 was most different to all other samples according to the PCA but without being a significant outlier. Thus, it was not excluded from further investigations. In Figure 22B volcano plots were used to visualize the comparison of  $GNE^{+/+}C3^{-/-}$  samples (upper graph) and of  $GNE^{+/-}C3^{-/-}$  samples (lower graph) with the wildtype samples ( $GNE^{+/+}C3^{+/+}$ ). Each dot of the volcano plot represents a gene and the overall distribution gives an idea of the extent of changes in the C3-deficient samples. Plenty of genes were affected in both directions but with modest fold change ( $\leq 2$  -fold) except for C3, which was located in the far upper left corner of the volcano plots. This furthermore confirmed that the analysis was working and that the modest changes in  $GNE^{+/-}$  are biological and not some technical artifacts. Overall, 64 % of the DEGs in  $GNE^{+/+}C3^{-/-}$  mice and 62 % in  $GNE^{+/-}C3^{-/-}$  mice were downregulated. Additional quality controls and differences in *gne* and *c3* transcription were validated by sqRT-PCR (\*\* $p \leq 0.001$ ; Figure 22C).

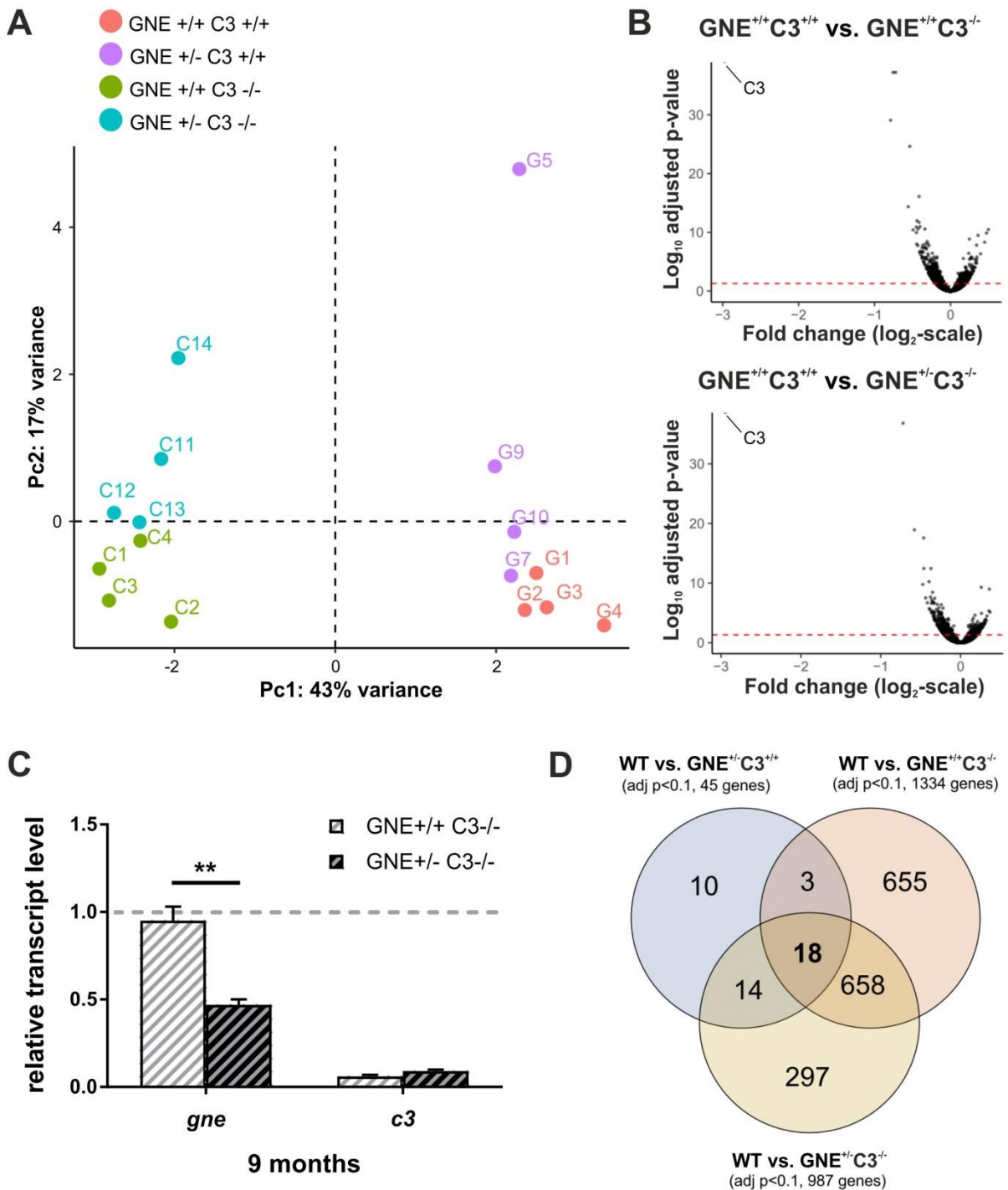


**Figure 22: RNA sequencing results of 9 months old GNE<sup>+/-</sup>C3<sup>-/-</sup> mice compared to wildtype controls.** RNA from brain homogenates was sequenced in collaboration with Dr. Sinkkonen, University of Luxembourg. (A) A principle component (Pc) analysis of all 4 genotype groups represented by a color code is shown. Dashed lines indicate zero for both x- and y-axis.  $n = 4$ . (B) Volcano plots displaying the extent of the changes in the C3-deficient mice compared to wildtype mice with C3 highly downregulated. Each dot represents a gene. The order of the plots indicates that the baseline value is that from wildtype samples and the indicated fold change happens in the compared condition. Red dotted line represents adjusted  $p$ -value  $< 0.05$ .  $n = 4$ . (C) Confirmation of different *gne* and *c3* transcription levels in the analyzed sample sets by sqRT-PCR. Data shown as mean + SEM; normalized to 3 months old GNE<sup>+/+</sup>C3<sup>+/+</sup> animals (indicated as grey dashed line).  $n = 4$ ; Student's t-test,  $**p \leq 0.010$  (D) Venn diagram comparing the differentially expressed genes (DEGs; adj  $p < 0.1$ ) of each genotype group in regard to the wildtype group (WT = GNE<sup>+/+</sup>C3<sup>+/+</sup>) with each other. Overlapping areas show number of shared genes.  $n = 4$ .

While the transcript levels of *gne* of the  $GNE^{+/-}C3^{-/-}$  mice were reduced by 50% ( $0.5 \pm 0.0$  FC),  $GNE^{+/+}C3^{-/-}$  mice showed similar *gne* levels as the wildtype mice ( $0.9 \pm 0.1$  FC). Transcription of *c3* was almost undetectable ( $0.1 \pm 0.0$  FC in  $GNE^{+/+}C3^{-/-}$  and  $0.1 \pm 0.0$  FC in  $GNE^{+/-}C3^{-/-}$ ) in the C3-deficient mice.

The analysis of the RNA sequencing data revealed that while in the  $GNE^{+/-}C3^{+/+}$  group 45 genes were differentially expressed compared to the wildtype group as mentioned before, the C3-deficient mice showed much more DEGs. In detail, the sample group  $GNE^{+/+}C3^{-/-}$  had 1334 DEGs compared to the wildtype group (Table 9, Appendix) and the group of  $GNE^{+/-}C3^{-/-}$  samples had 987 DEGs (Table 10, Appendix) compared to the wildtype group. Comparing the different data sets in form of a Venn diagram (see Figure 22D) it becomes obvious that 21 DEGs of the “ $GNE^{+/-}C3^{+/+}$  vs. WT” group were also present independently in the “ $GNE^{+/+}C3^{-/-}$  vs. WT” group and 18 genes out of them remained dysregulated in the “ $GNE^{+/-}C3^{-/-}$  vs. WT” group. Furthermore, 14 genes out of the 45 DEGs in  $GNE^{+/-}C3^{+/+}$  remained also dysregulated in  $GNE^{+/-}C3^{-/-}$  mice. Consequently, there were ten DEGs that were specific to  $GNE^{+/-}C3^{+/+}$  and those got partially or fully corrected in  $GNE^{+/-}C3^{-/-}$  (listed in Table 6). In addition, there are three genes that were dysregulated in both the  $GNE^{+/-}C3^{+/+}$  and in the  $GNE^{+/+}C3^{-/-}$  group that returned closer to the wildtype group in  $GNE^{+/-}C3^{-/-}$  (listed in Table 7).

**Table 6: List of the ten DEGs unique for  $GNE^{+/-}C3^{+/+}$**

Symbol	Gene name	Biological function <sup>1</sup>	log <sub>2</sub> fold change	adjusted p-value
<i>Arrdc2</i>	arrestin domain containing 2	not exactly known yet	-0,235	0,018
<i>Pdk4</i>	pyruvate dehydrogenase kinase, isoenzyme 4	mitochondrial protein; helps to decrease metabolism and conserve glucose; involved e.g. in ROS metabolism; regulated by glucocorticoids	-0,239	0,099
<i>Mknk2</i>	MAPK-interacting serine/ threonine kinase 2	transcriptional regulator; involved in e.g. apoptotic processes, intracellular signal transduction, and hemopoiesis	-0,172	0,062
<i>Trp53inp1</i>	transformation related protein 53 inducible nuclear protein 1	SIP or "stress inducible protein"; involved e.g. in autophagosome assembly, apoptotic processes, and transcriptional regulation	-0,231	0,096
<i>Acer2</i>	alkaline ceramidase 2	enzyme; involved e.g. in lipid metabolism, cell proliferation and death, and protein glycosylation in Golgi	-0,322	0,002
<i>Klf13</i>	Kruppel-like factor 13	transcriptional regulator; associated with obesity and	-0,190	0,073

		orexigenic processes; negative regulator of cell proliferation		
<i>Kdm3a</i>	lysine (K)-specific demethylase 3A	demethylase; involved in hormone-dependent transcriptional activation	-0,138	0,094
<i>1810011</i> <i>O10Rik</i>	RIKEN cDNA 1810011O10 gene	positive regulator of the Wnt / beta-catenin signaling pathway; involved e.g. in apoptotic processes and immune response	-0,195	0,094
<i>Myh1</i>	myosin, heavy polypeptide 1, skeletal muscle, adult	unique protein for striated muscle; important in muscle contraction	-0,126	0,052
<i>Numb1</i>	numb-like	protein; involved e.g. in neurogenesis, cytokine-mediated signaling pathway, and protein metabolic processes	-0,131	0,094

<sup>1</sup>taken and modified from BioGPS (Wu et al., 2009)

Overall, the Venn diagram showed that the C3-deficiency caused much greater changes on transcription level than the Gne-heterozygosity. The 13 DEGs described in Table 6 and Table 7 were the most likely genes to explain any transcriptional correction of GNE<sup>+/-</sup>-induced dysregulation by deletion of the C3 gene. The low number was consistent with the absence of major overall transcriptome changes described before. Indeed, the differences between the individual biological replicates were sometimes bigger than the differences between the different genotypes.

**Table 7: List of the 3 DEGs common in GNE<sup>+/-</sup>C3<sup>+/+</sup> and GNE<sup>+/-</sup>C3<sup>-/-</sup>**

Symbol	Gene name	Biological function <sup>3</sup>	log <sub>2</sub> fold change	adjusted <i>p</i> -value
<i>Per1</i>	period circadian clock 1	important for the maintenance of circadian rhythms in cells	-0,245 <sup>1</sup>	0,019 <sup>1</sup>
			-0,138 <sup>2</sup>	0,173 <sup>2</sup>
<i>Mxi1</i>	MAX interactor 1, dimerization protein	transcriptional repressor thought to negatively regulate c-myc function, and therefore a potential tumor suppressor	-0,151 <sup>1</sup>	0,062 <sup>1</sup>
			-0,078 <sup>2</sup>	0,321 <sup>2</sup>
<i>Arl4d</i>	ADP-ribosylation factor-like 4D	GTP-binding proteins; may play a role in membrane-associated intracellular trafficking; mutations in this gene have been associated with Bardet–Biedl syndrome	-0,370 <sup>1</sup>	0,000 <sup>1</sup>
			-0,156 <sup>2</sup>	0,116 <sup>2</sup>

<sup>1</sup>Wildtype vs. GNE<sup>+/-</sup>C3<sup>+/+</sup>    <sup>2</sup>Wildtype vs. GNE<sup>+/-</sup>C3<sup>-/-</sup>

<sup>3</sup>taken and modified from BioGPS (Wu et al., 2009)

Furthermore, some of the top five canonical pathways mentioned in Figure 16D, like the glucocorticoid receptor signaling pathway did not show up anymore in the IPA of GNE<sup>+/-</sup>C3<sup>-/-</sup> mice. The same was true for some of the predicted upstream regulators, like Il1b.

### 3.2.2 Inflammation analysis on transcript level

Specific transcription analysis of the brain of the GNE<sup>+/-</sup>C3<sup>+/+</sup> mice showed that some genes were still affected more strongly than the RNA sequencing approach revealed and thus, are of particular interest. Therefore, the transcript levels of the cytokines, the complement components and the microglia markers as described earlier were re-evaluated in the C3-deficient mice by sqRT-PCR.

The cytokine analysis (Figure 23A) showed no differences in *tnfa* transcript levels but it showed GNE-dependent differences in *il1b* levels. Transcription of *il1b* was decreased after C3-knockout indicating a possible rescue effect. In detail, the *il1b* levels were 1.1 + 0.2 FC (GNE<sup>+/+</sup>C3<sup>+/+</sup>), 2.2 + 0.4 FC (GNE<sup>+/-</sup>C3<sup>+/+</sup>), 1.3 + 0.2 FC (GNE<sup>+/+</sup>C3<sup>-/-</sup>), and 1.6 + 0.2 FC (GNE<sup>+/-</sup>C3<sup>-/-</sup>) and the transcription levels of *tnfa* were 0.9 + 0.2 FC (GNE<sup>+/+</sup>C3<sup>+/+</sup>), 1.0 + 0.1 FC (GNE<sup>+/-</sup>C3<sup>+/+</sup>), 0.9 + 0.2 FC (GNE<sup>+/+</sup>C3<sup>-/-</sup>), and 1.0 + 0.1 FC (GNE<sup>+/-</sup>C3<sup>-/-</sup>).

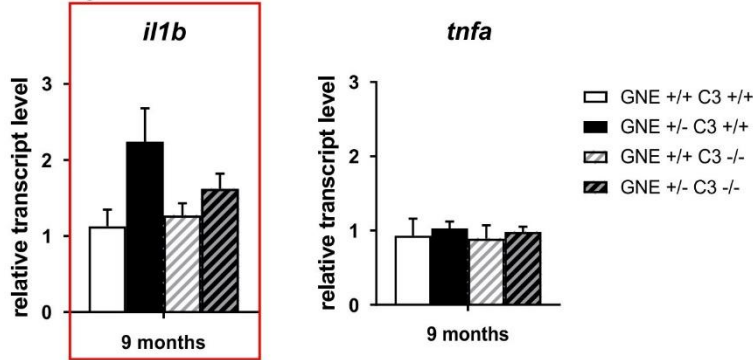
As representative complement components the transcripts of the c1q subunits *c1qa*, *c1qb*, and *c1qc* were investigated, as well as the transcription of the soluble factor *c4b*, the central player *c3*, and one of the genes of the complement receptor 3 (*itgam*; Figure 23B). First, the *c3* transcription was clearly downregulated and almost undetectable in the C3-deficient samples, whereas the transcription of *c1qa* and of *c4b* seemed not to be affected by the C3-deficiency. Levels of *c1qc* reduced to levels of GNE<sup>+/-</sup>C3<sup>+/+</sup> mice independently of the GNE-genotype. Interestingly, the significant reduction of *c1qb* transcript levels in GNE<sup>+/-</sup>C3<sup>+/+</sup> samples (\*\**p* = 0.009) were not present anymore after C3-knockout (ns. *p* = 1). A similar tendency was observed for *itgam* levels. The slightly elevated levels in GNE<sup>+/-</sup>C3<sup>+/+</sup> mice compared to wildtype littermates were not observed any more in C3-deficient mice. In detail, the *c1qa* levels differed between 1.3 + 0.3 FC (GNE<sup>+/+</sup>C3<sup>+/+</sup>), 1.5 + 0.2 FC (GNE<sup>+/-</sup>C3<sup>+/+</sup>), 1.4 + 0.3 FC (GNE<sup>+/+</sup>C3<sup>-/-</sup>), and 1.6 + 0.2 FC (GNE<sup>+/-</sup>C3<sup>-/-</sup>). The transcription levels of *c1qb* differed between 1.0 + 0.1 FC (GNE<sup>+/+</sup>C3<sup>+/+</sup>), 0.8 + 0.0 FC (GNE<sup>+/-</sup>C3<sup>+/+</sup>), 1.0 + 0.0 FC (GNE<sup>+/+</sup>C3<sup>-/-</sup>), and 0.9 + 0.0 FC (GNE<sup>+/-</sup>C3<sup>-/-</sup>) and the transcription levels of *c1qc* differed between 1.4 + 0.4 FC (GNE<sup>+/+</sup>C3<sup>+/+</sup>), 0.6 + 0.1 FC (GNE<sup>+/-</sup>C3<sup>+/+</sup>), 0.5 + 0.1 FC (GNE<sup>+/+</sup>C3<sup>-/-</sup>), and 0.4 + 0.1 FC (GNE<sup>+/-</sup>C3<sup>-/-</sup>). The detected levels of *c4b* were at 1.0 + 0.1 FC (GNE<sup>+/+</sup>C3<sup>+/+</sup>), 0.9 + 0. FC (GNE<sup>+/-</sup>C3<sup>+/+</sup>), 0.9 + 0.2 FC (GNE<sup>+/+</sup>C3<sup>-/-</sup>), and 0.8 + 0.1 FC (GNE<sup>+/-</sup>C3<sup>-/-</sup>) and for

*c3* at 1.0 + 0.1 FC (GNE<sup>+/+</sup>C3<sup>+/+</sup>), 1.2 + 0.2 FC (GNE<sup>+/-</sup>C3<sup>+/+</sup>), 0.1 + 0.0 FC (GNE<sup>+/+</sup>C3<sup>-/-</sup>), and 0.1 + 0.0 FC (GNE<sup>+/-</sup>C3<sup>-/-</sup>). Levels of *itgam* varied from 1.0 + 0.1 FC (GNE<sup>+/+</sup>C3<sup>+/+</sup>) and 1.3 + 0.3 FC (GNE<sup>+/-</sup>C3<sup>+/+</sup>) and stayed similar at 0.8 + 0.1 FC (GNE<sup>+/+</sup>C3<sup>-/-</sup>), and 0.8 + 0.0 FC (GNE<sup>+/-</sup>C3<sup>-/-</sup>).

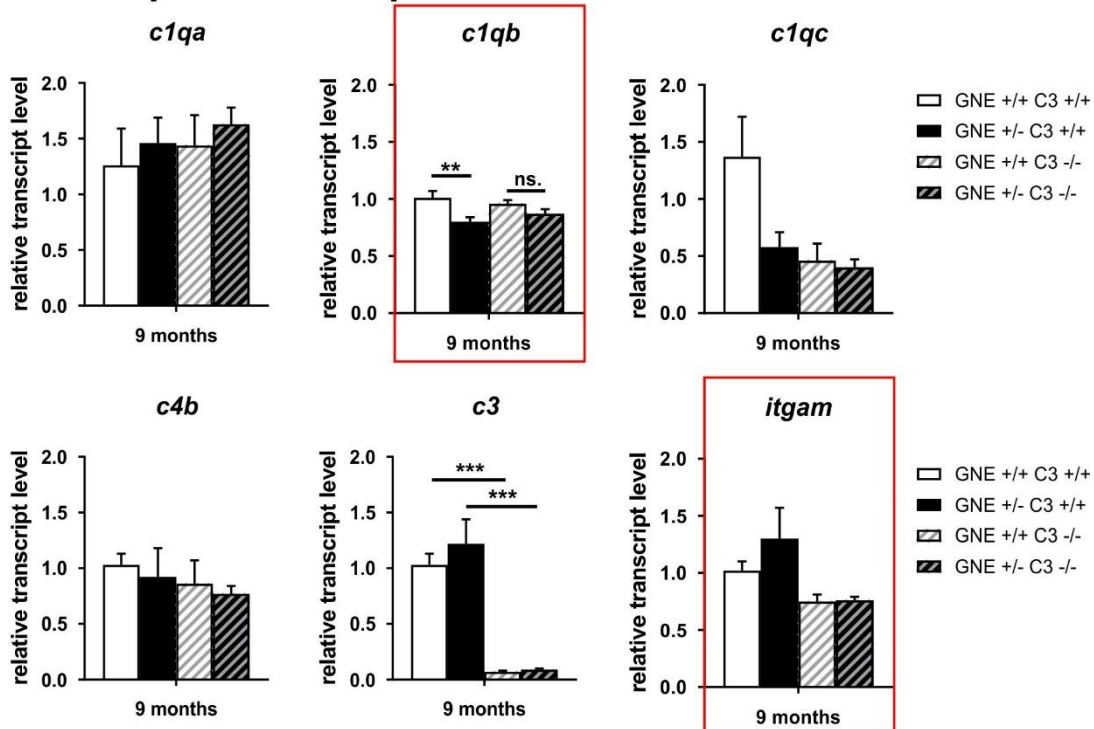
Microglia markers were re-evaluated on transcription levels (Figure 23C). The increase in *aif* levels in GNE<sup>+/-</sup>C3<sup>+/+</sup> mice ( $p = 0.147$ ) was not visible any more in GNE<sup>+/-</sup>C3<sup>-/-</sup> samples and the level was almost reduced back to wildtype level. The slight increase of *cd68* transcription was also gone in C3-deficient mice. Interestingly, the overall levels were very much reduced after C3-knockout. Transcript levels of *tmem119* were equal in GNE<sup>+/+</sup>C3<sup>-/-</sup> and GNE<sup>+/-</sup>C3<sup>-/-</sup> mice and similar to GNE<sup>+/-</sup>C3<sup>+/+</sup> mice. In detail, the *aif1* levels were 1.0 + 0.1 FC (GNE<sup>+/+</sup>C3<sup>+/+</sup>), 1.9 + 0.3 FC (GNE<sup>+/-</sup>C3<sup>+/+</sup>), 0.8 + 0.1 FC (GNE<sup>+/+</sup>C3<sup>-/-</sup>), and 1.1 + 0.1 FC (GNE<sup>+/-</sup>C3<sup>-/-</sup>) and the transcription levels of *cd68* were at 1.2 + 0.3 FC (GNE<sup>+/+</sup>C3<sup>+/+</sup>), 1.7 + 0.6 FC (GNE<sup>+/-</sup>C3<sup>+/+</sup>), 0.4 + 0.1 FC (GNE<sup>+/+</sup>C3<sup>-/-</sup>), and at 0.5 + 0.0 FC (GNE<sup>+/-</sup>C3<sup>-/-</sup>). Levels of *tmem119* varied between 1.1 + 0.2 FC (GNE<sup>+/+</sup>C3<sup>+/+</sup>), 1.5 + 0.2 FC (GNE<sup>+/-</sup>C3<sup>+/+</sup>), 1.5 + 0.4 FC (GNE<sup>+/+</sup>C3<sup>-/-</sup>), and 1.5 + 0.1 FC (GNE<sup>+/-</sup>C3<sup>-/-</sup>).

Taken together, some transcript levels that were altered in GNE<sup>+/-</sup>C3<sup>+/+</sup> mice compared to wildtype mice do not show these differences anymore in GNE<sup>+/-</sup>C3<sup>-/-</sup> mice compared to GNE<sup>+/+</sup>C3<sup>+/+</sup> mice and thus, might be rescued by the C3-knockout.

## A cytokines



## B complement components



## C microglia markers

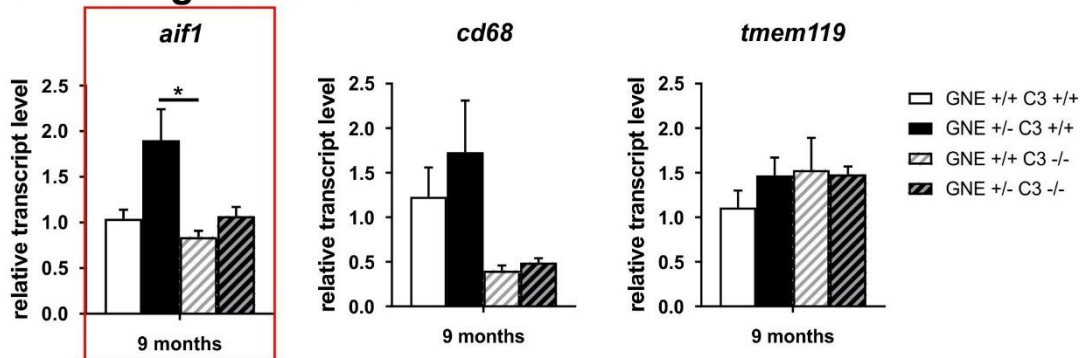


**Figure 23: Transcriptional profiles of 9 months old GNE mice in comparison with C3-deficient background.** Transcript levels of cytokines (A), complement components (B), and microglia markers (C) were measured in brain homogenates from GNE<sup>+/+</sup>C3<sup>-/-</sup> and GNE<sup>+/-</sup>C3<sup>-/-</sup> mice and were compared to GNE mice with C3-wildtype background. Red rectangles label graphs with a possible phenotype-rescue. Data shown as mean + SEM; normalized to 9 months old GNE<sup>+/+</sup>C3<sup>+/+</sup> animals. n = 4-14; one-way ANOVA with Bonferroni or Dunnett's T3 post hoc correction, ns. = not significant, \* $p \leq 0.050$ , \*\* $p \leq 0.010$ , \*\*\* $p \leq 0.001$ . (A) Levels of interleukin 1 beta



(*il1b*) and tumor necrosis factor alpha (*tnfa*) transcription were almost equal after knockout of C3. (B) Transcription levels of complement component 1 with q subcomponent and alpha or beta polypeptide, or c chain (*c1qa*, *c1qb*, *c1qc*), complement component 4b (*c4b*), complement component 3 (*c3*), and integrin alpha M (*itgam*, one of the genes of complement receptor 3) are shown. Levels of *c1qa* and *c4b* were similar in all groups. Differences in *c1qb*, *c1qc* and *itgam* levels were rescued by knockout of C3, whereas *c3* levels were undetectable. (C) Levels of allograft inflammatory factor 1 (*aif1*; gene of Iba1), the CD68 antigen (*cd68*), and the transmembrane protein 119 (*tmem119*) transcripts in the brains of 9 months old GNE<sup>+/-</sup> mice and wildtype littermates showed no GNE-dependent difference anymore after knockout of C3.

### 3.2.3 Neuronal loss in the brain

The characterization of the GNE<sup>+/-</sup> mice revealed not only an altered sialylation in the brain but was also accompanied by increasing neuronal loss in different brain regions compared to wildtype littermates. Based on the introduced concept of Linnartz-Gerlach and colleagues (Linnartz et al., 2012b; Linnartz-Gerlach et al., 2016) it should be possible to prevent the neuronal loss in mice with reduced sialic acid levels by inhibiting the complement system. Therefore, the neuronal density was also investigated in the substantia nigra and in the hippocampus of GNE<sup>+/-</sup>C3<sup>-/-</sup> mice and as control also in GNE<sup>+/+</sup>C3<sup>-/-</sup> mice.

#### 3.2.3.1 Neuronal loss analysis in the substantia nigra

Serial sagittal sections (lateral: 1.10 – 1.20 mm) of the SN pc were again analyzed by immunohistochemical antibody staining of the dopaminergic marker TH and the neuronal nuclei marker NeuN in 12 months old mice (see Figure 24A). Cells positive for TH or NeuN were counted per area and the relative cell density in the SN pc was quantified in all four genotypes (Figure 24B).

Strikingly, the strong overall neuronal loss seen in the SN pc of 12 months old GNE<sup>+/-</sup>C3<sup>+/+</sup> mice (34 % reduction; \*\*\* $p \leq 0.001$  vs. GNE<sup>+/+</sup>C3<sup>+/+</sup>) was not present anymore in 12 months old GNE<sup>+/-</sup>C3<sup>-/-</sup> mice ( $p = 1.000$  vs. GNE<sup>+/+</sup>C3<sup>-/-</sup>). The neuronal cell density of GNE<sup>+/-</sup>C3<sup>-/-</sup> mice (93.8 + 5.2 %) reached almost the same levels as those of GNE<sup>+/+</sup>C3<sup>+/+</sup> mice (100.0 + 5.9 %) and of GNE<sup>+/+</sup>C3<sup>-/-</sup> mice (103.6 + 4.6 %) compared to 65.8 + 5.7 % in GNE<sup>+/-</sup>C3<sup>+/+</sup> mice (left graph; Figure 24B). The same strong rescue-effect was seen for the dopaminergic cell density in the SN pc (right graph; Figure 24B). While in GNE<sup>+/-</sup>C3<sup>+/+</sup> mice the relative cell density of TH-positive cells was at 64.1 + 6.2 % compared to 100.0 + 4.2 % in GNE<sup>+/+</sup>C3<sup>+/+</sup> mice (34 % reduction; \*\*\* $p \leq 0.001$ ), the density was back at wildtype levels after C3-knockout (95.5 + 4.1 % in GNE<sup>+/-</sup>C3<sup>-/-</sup> and 104.2 + 5.7 % in GNE<sup>+/+</sup>C3<sup>-/-</sup>).

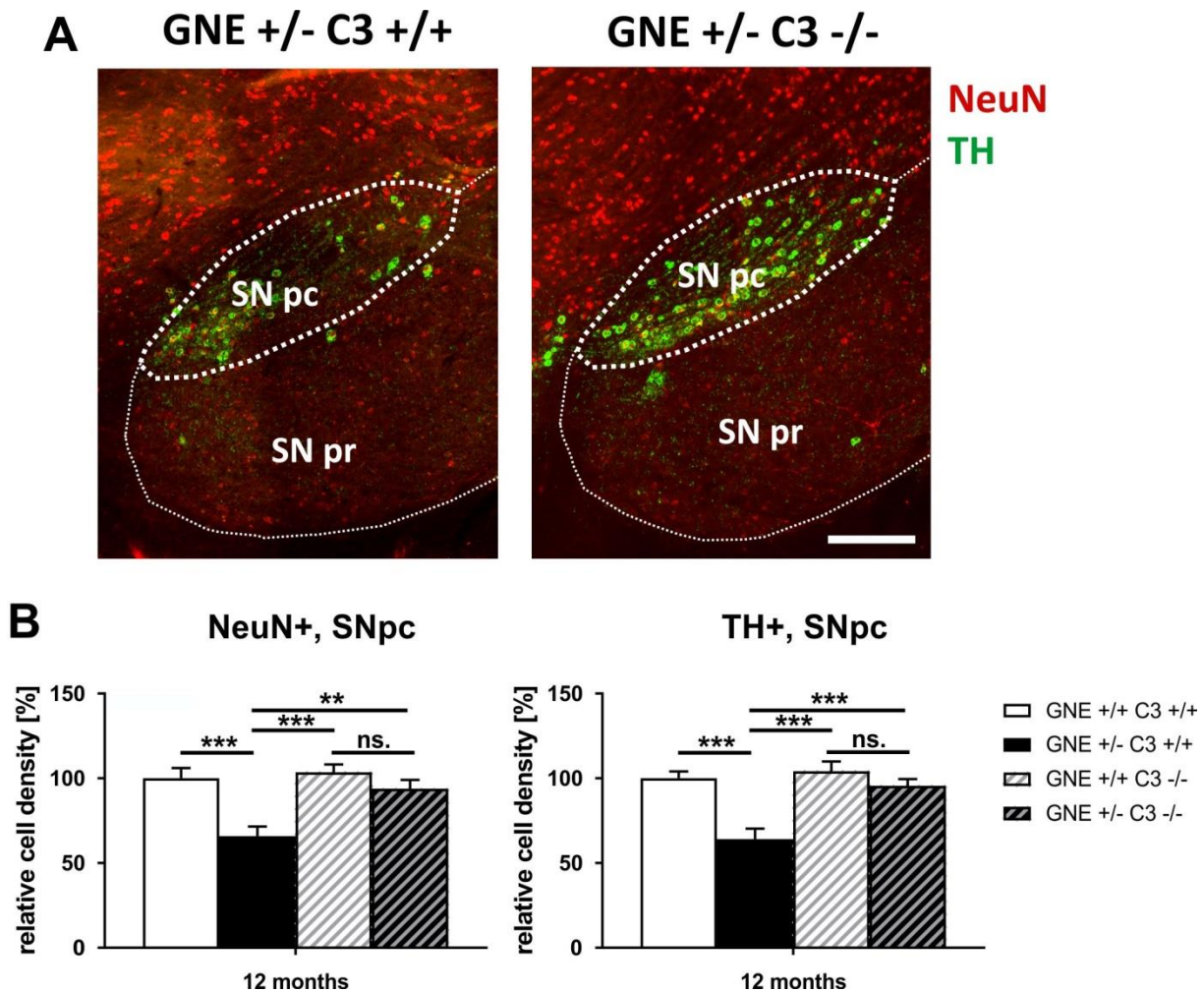


**Figure 24: Neuronal loss in the substantia nigra of GNE<sup>+/-</sup>C3<sup>+/+</sup> mice was rescued in GNE<sup>+/-</sup>C3<sup>-/-</sup> mice.** (A) Representative images of the substantia nigra of 12 months old GNE<sup>+/-</sup>C3<sup>+/+</sup> and GNE<sup>+/-</sup>C3<sup>-/-</sup> mice at lateral sections between 1.10 mm and 1.20 mm are shown. Sagittal brain slices were stained with antibodies directed against tyrosine hydroxylase (TH, green) and neuronal nuclei (NeuN, red). SN pc – substantia nigra pars compacta, SN pr – substantia nigra pars reticulata. Scale bar: 200  $\mu$ m. (B) Quantification of the cell density of NeuN- (left graph) and TH-positive cells (right graph) in 12 months old brain section revealed almost a complete rescue of the GNE<sup>+/-</sup>-dependent neuronal loss. Data shown as mean + SEM; normalized to 12 months old GNE<sup>+/+</sup>C3<sup>+/+</sup> animals; n = 9-13, one-way ANOVA with Bonferroni post hoc correction, ns. = not significant, \*\* $p \leq 0.010$ , \*\*\* $p \leq 0.001$ .

Data of the neuronal density in the SN pc strongly showed that the GNE-dependent neurodegeneration was prevented under C3-deficient background.

### 3.2.3.2 Neuronal loss analysis in the hippocampus

Serial sagittal sections (lateral: 1.10 mm to 1.20 mm) of the hippocampus were analyzed by immunohistochemical antibody staining of the neuronal nuclei marker NeuN and the cellular nuclei marker DAPI (see Figure 25A). The cell density was determined by counting the cells positive for NeuN per area in the CA3 region of 12 months old brain of all four genotypes as shown in Figure 25B.

Although the neuronal loss in the CA3 region was not as strong as in the SN pc, there was still a significant difference in the  $GNE^{+/-}C3^{+/+}$  mice compared to the wildtype mice (~16 % reduction;  $*p = 0.045$ ) that was absent in the  $GNE^{+/-}C3^{-/-}$  mice compared to  $GNE^{+/+}C3^{-/-}$  mice ( $p = 1.000$ ). Comparing the  $GNE^{+/-}$ -genotypes with each other, the C3-knockout showed a significant rescue-effect on the neurodegeneration ( $**p = 0.003$   $GNE^{+/-}C3^{+/+}$  vs.  $GNE^{+/-}C3^{-/-}$ ). In detail, the neuronal density in the CA3 region was quantified with  $100.0 \pm 9.3$  % ( $GNE^{+/+}C3^{+/+}$ ),  $84.1 \pm 2.3$  % ( $GNE^{+/-}C3^{+/+}$ ),  $96.9 \pm 2.6$  % ( $GNE^{+/+}C3^{-/-}$ ), and  $104.3 \pm 3.0$  % ( $GNE^{+/-}C3^{-/-}$ ).

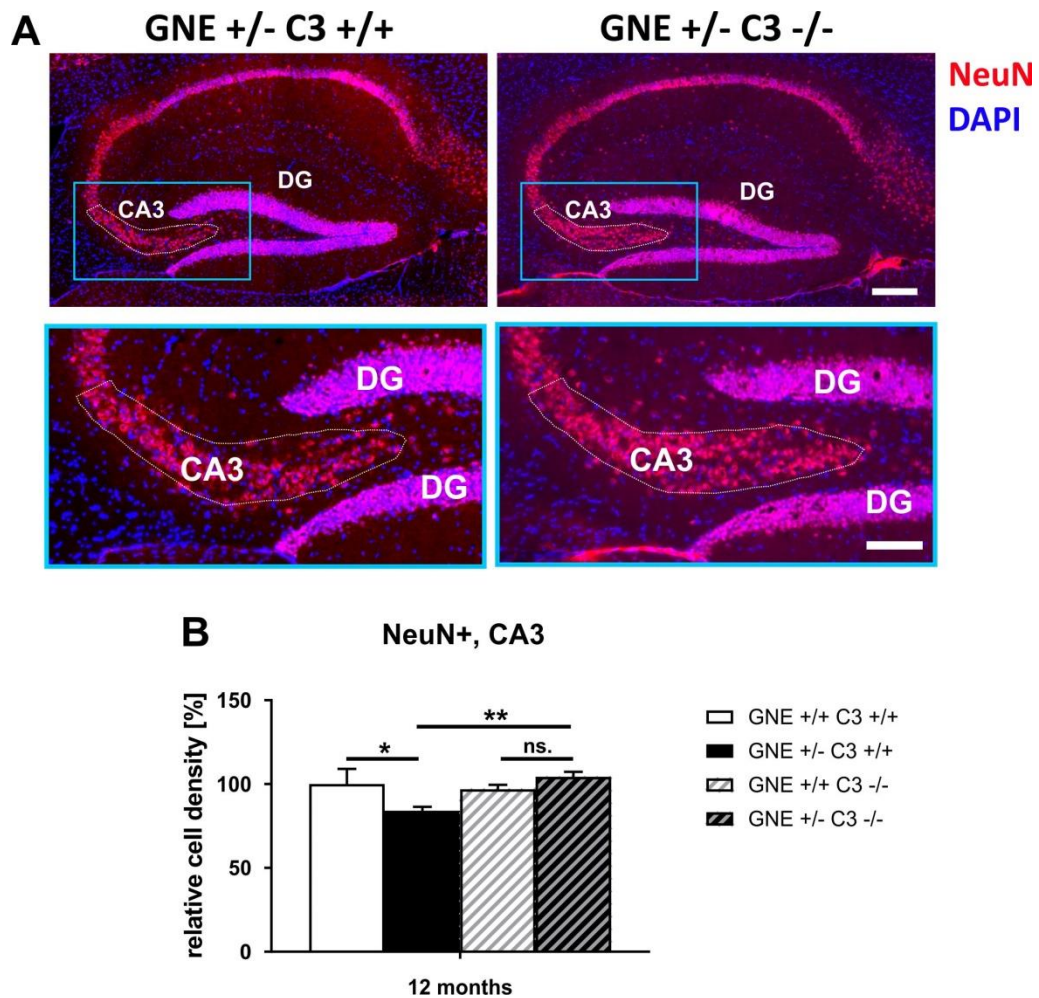


**Figure 25: Neuronal loss in the CA3 region of the hippocampus of  $GNE^{+/-}C3^{+/+}$  mice was rescued in  $GNE^{+/-}C3^{-/-}$  mice.** (A) Representative images of the hippocampus of 12 months old  $GNE^{+/-}C3^{+/+}$  and  $GNE^{+/-}C3^{-/-}$  mice at lateral sections between 1.10 mm and 1.20 mm are shown. Lower images show a higher magnification of the CA3 region in the hippocampus (white dotted line). Sagittal brain slices were stained with antibodies directed against neuronal nuclei (NeuN, red) and DAPI (blue). DG – dentate gyrus. Scale bar: 200  $\mu$ m or 100  $\mu$ m (higher magnification). (B) Quantification of the cell density of NeuN-positive cells at 12 months old brain sections revealed the complete rescue of neuronal cell density by knockout of C3. Data shown as mean + SEM; normalized to 12 months old  $GNE^{+/+}C3^{+/+}$  animals;  $n = 10-13$ , one-way ANOVA with Bonferroni post hoc correction, ns. = not significant,  $*p \leq 0.050$ ,  $**p \leq 0.010$ .

The same immunohistochemical staining was also used to measure the width of the CA3 region and the DG at different positions as described before. The mice deficient for C3 showed similar

mean widths for all three positions as the C3-wildtype mice (Figure 26). The only difference was found in the width of the CA3 region in  $GNE^{+/+}C3^{-/-}$  mice, which was slightly increased compared to  $GNE^{+/+}C3^{+/+}$  mice. In detail, the relative measured widths of the DG1 position were  $100.0 \pm 3.9\%$  ( $GNE^{+/+}C3^{+/+}$ ),  $108.4 \pm 4.2\%$  ( $GNE^{+/-}C3^{+/+}$ ),  $110.5 \pm 4.1\%$  ( $GNE^{+/+}C3^{-/-}$ ), and  $108.3 \pm 3.3\%$  ( $GNE^{+/-}C3^{-/-}$ ) and the measured widths for the DG2 position was  $100.0 \pm 6.3\%$  ( $GNE^{+/+}C3^{+/+}$ ),  $102.3 \pm 3.1\%$  ( $GNE^{+/-}C3^{+/+}$ ),  $100.4 \pm 4.4\%$  ( $GNE^{+/+}C3^{-/-}$ ), and  $111.3 \pm 3.7\%$  ( $GNE^{+/-}C3^{-/-}$ ). The relative width of the CA3 region was  $100.0 \pm 7.7\%$  ( $GNE^{+/+}C3^{+/+}$ ),  $113.1 \pm 4.4\%$  ( $GNE^{+/-}C3^{+/+}$ ),  $130.0 \pm 9.2\%$  ( $GNE^{+/+}C3^{-/-}$ ), and  $110.8 \pm 6.4\%$  ( $GNE^{+/-}C3^{-/-}$ ).

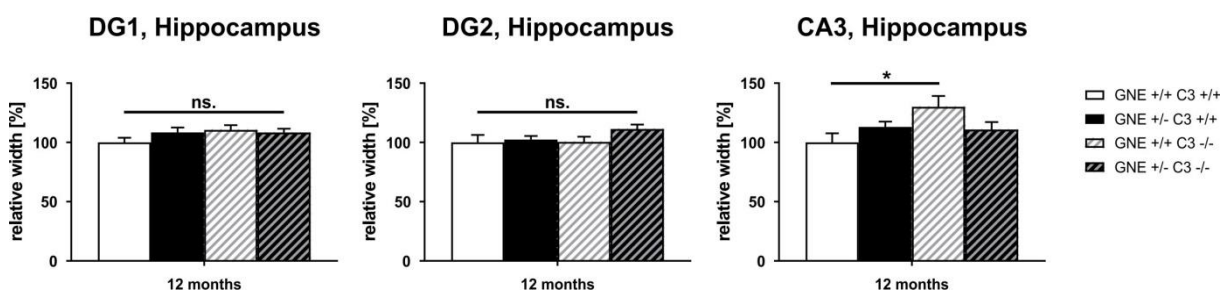


**Figure 26: Minor changes in the width of the dentate gyrus (DG) and of the CA3 region in C3-deficient mice.** Quantification of the relative width for DG1, DG2, and CA3 at 12 months old sagittal brain sections (left to right) revealed significant differences in CA3 for  $GNE^{+/+}C3^{-/-}$  vs.  $GNE^{+/+}C3^{+/+}$ . Data shown as mean  $\pm$  SEM; normalized to 12 months old  $GNE^{+/+}C3^{+/+}$  animals;  $n = 9-13$ , one-way ANOVA with post hoc correction, ns. = not significant,  $*p \leq 0.050$ .

Taken together, knocking out C3 prevented the increased neuronal loss in the hippocampus of  $GNE^{+/-}C3^{-/-}$  mice but did not alter the width in these mice compared to wildtype animals.

---

## 4 Discussion

Strong improvements in medical care and hygiene have allowed an increasingly aging population worldwide. At the same time neurodegenerative diseases, like AD, PD or dementia are emerging tremendously (Bishop et al., 2010). One of the key events of these diseases and during aging is a general or cell-type specific neuronal loss. Although enormous research investigations have been carried out to unravel the underlying mechanisms leading to neuronal loss and to develop suitable drugs for therapy, still, rather the symptoms but not the causes can be treated by now. Meanwhile glial research is postulating microglia as a key mediator in most of the neurodegenerative diseases in the aging population (Lull and Block, 2010; Šišková and Tremblay, 2013; von Bernhardi et al., 2015). Being the only immune cells in the immune-privileged brain, microglia not only work as policemen but also as nannies. Maintaining the homeostasis involves close interaction with neurons and other cell types, like astrocytes. This important crosstalk is mediated by the cellular glycocalyx, a dense network of receptors, signaling proteins and lipids on the cell surface that is covered by a fine regulated glycosylation structure. The tight regulation of this interface enables precise communication between neurons or neuron-glial cells in the brain.

Studying the neuronal glycocalyx *in vitro* has demonstrated that even small alterations like the removal of sialic acids, which form the terminal caps, can lead to a dysregulated crosstalk between microglia and neurons. This resulted in phagocytic removal by microglia of otherwise viable neurons. Furthermore, it was proven that phagocytosis was mediated by the complement system in a CR3-dependent manner. Desialylated but not sialylated neuronal structures were opsonized by C1q. Moreover, inhibition of CR3 prevented the microglia-mediated phagocytosis. This mechanism was not only proven in mouse microglia-neuron co-cultures (Linnartz et al., 2012b) but was demonstrated in human microglia/macrophage-neuron co-cultures as well (Linnartz-Gerlach et al., 2016).

However, many *in vitro* studies lack validation *in vivo* or even worse, *in vitro* results cannot be confirmed in the complex *in vivo* situation as discussed by Ransohoff and Perry (2009). To confirm the complement-mediated phagocytosis of desialylated neuronal structures by microglia *in vivo*, the brains of mice heterozygous for GNE were thoroughly characterized in this study and were evaluated as possible model for an altered glycocalyx *in vivo*. Furthermore, the need of transgenic mouse models and the clinical relevance of mutations in GNE will be discussed.

## 4.1 Characterization of the GNE<sup>+/-</sup> mice

Gagiannis and colleagues reported that GNE<sup>+/-</sup> mice have an overall reduction of membrane-bound sialic acids by 25 % but do not have any obvious defects in organ architecture or function compared to wildtype mice (Gagiannis et al., 2007). In the present study, I investigated the brain of these mice in more detail and discovered some additional genotype-specific differences.

First of all, routinely mouse monitoring indeed did not identify differences in the appearance or in the behavior of the mice but female GNE<sup>+/-</sup> mice were significantly heavier than their wildtype littermates. Male mice did not show these genotype-specific differences in weight. Because GNE has other roles beside the sialic acid biosynthesis (Wang et al., 2006; Grover and Arya, 2014), I assume that the GNE-heterozygosity might influence the female metabolism more than the male metabolism. However, deeper investigations on metabolism were beyond this study.

In general, sex-specific differences are not yet routinely tested in scientific experiments. Recent publications that compared sex-specific transcriptomes of female and male brains discovered notable differences between microglia and neuroimmune signaling (Lenz and McCarthy, 2015; Hanamsagar et al., 2017; Mangold et al., 2017). Furthermore, not only the signaling but also microglia numbers vary significantly between sexes and female mice show a more inflammatory neuroimmune milieu than males, which is increasing with age (Nissen, 2017). Hormones like estradiol have a potential influence on the brain anatomy and are capable of promoting neurite outgrowth and thus, shaping the local environment (Amateau and McCarthy, 2002; McCarthy, 2008). Considering these findings, it was not surprising that the X chromosome was found to have the highest concentration of immune-related genes compared to the whole genome (Bianchi et al., 2012). This once more explains the stronger immune-imprint in the female brain and is possibly also the reason why autoimmune disorders (e.g. MS) mostly occur in females. Nevertheless, studies with PD mouse models revealed that female mice are less sensitive for the loss of dopaminergic neurons and exhibit a higher variability (Przedborski et al., 2001). In addition, estrogen levels in female mice seem to be neuroprotective in PD mouse models (Miller et al., 1998) and thus, male mice are preferentially chosen for neurodegeneration analysis. These findings highlight how important it is to clearly distinguish between sexes in brain research.

Taken this into account, I strictly distinguished between male and female data in the experiments of this study. Female mice were mainly used for the sialylation status and male mice were investigated for neuronal loss and transcription levels. The only exception was the RNA sequencing data that was performed in female mice but were confirmed in male mice after discovering sex-specific differences.

#### 4.1.1 Evaluation of the sialylation status

Sialylation of proteins or lipids on the cell surface belongs to the most common posttranslational modification in the mammalian brain and is highly dynamic. The biosynthesis as well as the incorporation of sialic acids as terminal caps is essential for the cell-cell interaction and is tightly regulated by a number of enzymes, like GNE being a rate-limiting enzyme.

In the  $GNE^{+/-}$  mice the mRNA levels of GNE were reduced by about 50% compared to wildtype as it was also shown for the heterozygous embryonic stem cell line generated by Schwarzkopf and colleagues (Schwarzkopf et al., 2002). This clearly demonstrated that one copy of the wildtype allele of GNE is not sufficient to produce the wildtype transcription levels (haploinsufficiency). Schwarzkopf and colleagues even measured reduced protein levels of GNE and reduced enzyme activity. However, the transcription analysis did only account for the two most known isoforms of GNE. At the time of the study, 14 transcripts of the mouse GNE gene (ENSMUSG00000028479) were listed at ensembl annotations (v.89) with eight transcripts listed for protein coding (Yates et al., 2016). From these eight protein coding transcripts only two transcripts were validated in more details and listed in NCBI GenBank (5384 bp: NM\_015828 and 2920 bp: NM\_001190414) and NCBI GenPept (753aa: NP\_056643 and 722aa: NP\_001177343). Therefore, differences in transcription level of other GNE variants cannot be ruled out and it remains unclear, which effects they may have.

On protein level, the sialylation of the whole brain was significantly altered in the  $GNE^{+/-}$  mice. Greatest differences were detected in long polymers of sialic acids ( $n > 10$ ). At 3 months, I found an overall reduction of 33% in PSA-NCAM levels, which confirms the study of Gagiannis and colleagues (Gagiannis et al., 2007) that showed 32% reduction in membrane-bound sialic acids in the brain. The data is also in line with the study of the heterozygous GNE embryonic stem cell line from Schwarzkopf and colleagues (Schwarzkopf et al., 2002). Heterozygous cells expressed much lower amounts of polysialic acids on NCAM than the wildtype cells. PSA-NCAM levels of GNE wildtype mice were increasing until about 6 months

and then were steadily decreasing. Similar results were shown for muscle sialylation in mice (Hanisch et al., 2013).

In comparison, levels of oligomers were reduced by 26% at 3 months, whereas levels of the embryonic form of NCAM were the same between genotypes and only lower in older  $GNE^{+/-}$  mice. The epitope of CD56 distinguishes the embryonic form of NCAM from the adult, less sialylated form. The measured decline in CD56 levels with aging, corresponds to the decline I saw for PSA-NCAM and is also described for polysialic acids in literature (Miller et al., 1993; Sato and Endo, 2010). While overall polysialylation decreases in the adult brain, some plastic regions like the olfactory bulb, the hypothalamus or the hippocampus remain highly positive for polysialic acids (Seki and Arai, 1993; Kuhn et al., 1996). Altogether, data indicate that mostly long sialic acid chains are affected by the reduced or altered sialic acid supply in the mice. This is in agreement with data shown by Kreuzmann and colleagues suggesting that the intracellular sialic acid concentration regulates polysialylation on NCAM *in vivo* (Kreuzmann et al., 2016). These findings support my idea that polysialyltransferases need higher concentrations of CMP-sialic acids than normal alpha-2,3- und alpha-2,6-sialyltransferases, which are necessary for surface sialylation.

Nevertheless, it remains unclear whether the levels of membrane-bound sialic acids are equally affected all over the brain. Sialylation might be differently regulated in different organs and even in different brain regions. Murray and colleagues have shown for example that the distribution of PSA-NCAM in post-mortem human brain tissue is very abundant in cortical regions (especially in layers II and III) but is sparsely distributed in the cerebellum (Murray et al., 2016). Furthermore, variable intensity of PSA-NCAM staining was found in the visual cortex and throughout the substantia nigra. In the hippocampus, the CA1 region showed the strongest staining for PSA-NCAM. Due to these regional differences, I assume that some brain regions might also be more affected by the  $GNE$ -heterozygosity than others. A specific analysis of membrane-bound sialic acids in different brain regions  $GNE^{+/-}$  mice and wildtype littermates could clarify if such an effect is occurring.

Polysialylation of NCAM is directly connected with learning and memory formation. NCAM-deficient mice as well as mice deficient for polysialyltransferases, which are responsible for the polysialylation, show deficits in learning and memory formation but otherwise no phenotype differences compared to wildtype mice (Cremer et al., 1994; Eckhardt et al., 2000). Thus, to clarify if the reduced levels of polysialylation in the  $GNE^{+/-}$  mice have already an impact on



memory and cognitive functions, behavior tests for spatial and temporal learning, like the Morris-Water-Maze or the novel object recognition test could be used.

Desialylation can also be seen as first step of protein turnover and consequently as “protein aging”. The life span of secreted proteins is regulated by glycosylation. Endogenous glycosidases like neuraminidase 1, beta-galactosidase and hexosaminidase have been shown to progressively remodel glycosylated proteins with aging. Removal of sialic acids leads to exposure of different saccharides that are then recognized by phagocytes resulting in protein degradation (Yang et al., 2015). Similar control mechanisms were shown in the turnover of blood cells and platelets (Grozovsky et al., 2014; Li et al., 2015; Qiu et al., 2016), concluding that unwanted desialylation is a form of accelerated aging and might activate or enhance aging processes in the organism as observed in the  $GNE^{+/-}$  mice.

#### **4.1.2 Evaluation of the transcriptional and morphological changes in the brain**

##### **4.1.2.1 Loss of neurons in different brain regions**

One of the major questions of the study was whether an altered glycocalyx with reduced sialylation is sufficient to cause neuronal loss *in vivo*. In the *in vitro* studies it was clearly demonstrated that microglia remove desialylated neurites (Linnartz et al., 2012b; Linnartz-Gerlach et al., 2016). However, it was not described at which level of desialylation microglia are able to significantly change the neuronal density.

In the  $GNE^{+/-}$  mice a clear reduction in neuronal density was observed during aging in the SN pc as well as in the CA3 region of the hippocampus compared to wildtype littermates. This loss of neurons further progressed with decreasing sialic acid levels. Worth to mention, the neuronal density was not different in 1 month old mice, suggesting that the neuronal loss in the substantia nigra and the hippocampus of older  $GNE^{+/-}$  mice is likely not a result of abnormal neuronal development or a developmental artefact. Interestingly, the findings in the substantia nigra and the hippocampus show distinct neurodegeneration progression. While the neuronal density in  $GNE^{+/-}$  mice decreased much earlier in the substantia nigra than in the hippocampus, in contrast, the neuronal density of wildtype animals was more stable in the substantia nigra than in the hippocampus. In the hippocampus even for wildtype mice (3 months *vs.* 12 months) a significant neuronal decline was measured, although to a lower extent than in  $GNE^{+/-}$  mice. Nevertheless, this neuronal decline is in line with findings in other wildtype mice reported by

Shi and colleagues (Shi et al., 2015). They saw a significant reduction in neuronal numbers at 16 months but not at 4 months.

From the obtained data I cannot judge whether the neuronal loss seen in the hippocampus is delayed compared to the substantia nigra due to more protective sialic acids. As mentioned before, sialic acid levels of different brain regions have not yet been investigated in  $GNE^{+/-}$  mice but might help to understand the regional differences in neuronal loss. Alternatively, the neuronal loss seen in the hippocampus is simply slower progressing than in the substantia nigra. One aspect supporting this hypothesis is the microglial density. The substantia nigra is the brain region with the highest microglia density (Lawson et al., 1990). This could explain why the neuronal loss in the  $GNE^{+/-}$  mice is progressing faster and earlier in the substantia nigra compared to the hippocampus. However, it was also described that the otherwise stable microglia number is increasing exceptionally in the hippocampus, the visual and auditory cortices, and in the retina with age (Mouton et al., 2002; Damani et al., 2011; Tremblay et al., 2012). Thus, with increasing number of microglia in the aged hippocampus the neuronal loss might accelerate to a degree seen in the substantia nigra. In addition, the sensitivity to inflammatory stimuli varies across different brain regions. It even differs within a brain region as it was shown for the hippocampus by Shi and colleagues (Shi et al., 2015), where only the CA3 region but not the CA1 region or the DG was affected by the age-dependent neuronal loss. At the same time, no neuronal loss was detected in the V1 region of the cortex or the cerebellum in these mice (Shi et al., 2015).

Taken together, age-dependent neuronal loss is normal but varies strongly between brain regions and even sub-regions and apparently, can be accelerated by reduced sialic acid levels. Therefore, it would be interesting to understand at which level of sialic acids or at which age a cognitive decline can be measured. One study from Vidal and colleagues showed that the neuronal density in the CA1 region of AD patients decreases with progressing Braak stages and resulted in 38% reduction at Braak stages V/VI compared to age-matched controls with Braak stage 0 (Vidal et al., 2016). These findings are in line with a study from Padurariu and colleagues who analyzed different CA regions in the hippocampus of postmortem human brains. CA1 showed the strongest decline in neuronal density (-34%), while in the CA3 the neuronal loss was about 25% (Padurariu et al., 2012), suggesting that the neuronal decline in the CA3 region of the 12 months old  $GNE^{+/-}$  mice might be similar severe as for AD patients with advanced cognitive decline. Additional learning and memory tests in 12 months or older mice might further clarify the cognitive status of the  $GNE^{+/-}$  mice. It might also help to

understand at which time point reduced sialic acid levels can result in cognitive deficits and thus, can have a major impact on aging.

I also measured the width of hippocampal regions because neuronal loss might lead to atrophy and shrinkage of the tissue or at the opposite, inflammatory processes could lead to swellings and increased volume of the affected areas. Width measurements were previously introduced as a valid and affordable method for detecting the levels of neurodegeneration and neuroprotection in the hippocampus (Öz and Saybaşı, 2017). In an earlier study in diabetic mice, selective deficits in spatial memory were correlating with increased width of the DG and CA1 region in the hippocampus and reduced spine densities in CA1 neurons (Taylor et al., 2015). Indeed, I saw an increase in width in the CA3 region and the DG, which peaked at 9 months but it occurred independently of the genotype. Strikingly, the increase was greatly diminished in 12 months old mice. These findings could hint towards a tissue remodeling. Increasing swelling might precede final atrophy of the tissue. Still, these width changes stay elusive.

Oxidative stress might also play a major role in the neuronal loss seen in this study. In particular the neurons in the substantia nigra are very susceptible to oxidative stress compared to other neurons. First of all, the dopamine biosynthesis in the dopaminergic neurons is associated with elevated ROS production (Di Giovanni et al., 2012), which is in fact a highly regulated process. It is assumed that regulatory mechanisms fail during aging. Furthermore, dopaminergic neurons express less glutathione. Glutathione normally works as a buffer against ROS (Loeffler et al., 1994) by neutralizing the radicals. Reduced levels of glutathione decrease the potential of regulating ROS in the substantia nigra. Besides, oxidative stress supports the release of membrane-bound sialic acids (Goswami et al., 2003) because sialic acids are good scavengers and possible antioxidants. This might amplify the phenotype in  $GNE^{+/-}$  mice, which have a reduced capacity of building up sialic acids in the glycocalyx, and might reduce the levels of membrane-bound sialic acid even further. For a follow-up study it would be interesting to analyze the correlation of oxidative stress and sialic acid levels in the brain. Two possible options for an indirect measurement of oxidative stress in tissue is the quantification of malondialdehyde (MDA) or 4-hydroxynonenal (4-HNE), which are both natural bi-products of lipid peroxidation. Lipid peroxidation is the result of free radicals and therefore, quantification of MDA and 4-HNE can be used as marker for oxidative stress (Ho et al., 2009; Wu et al., 2013; Zhang et al., 2016a; Kleniewska and Pawliczak, 2017).

Neurodegeneration in the substantia nigra is a major hallmark of PD. PD is characterized by progressive loss of dopaminergic neurons in the SN pc and the nerve terminals in the striatum (Dauer and Przedborski, 2003). The clinical symptoms are mainly motor impairment like bradykinesia, rigidity, tremors, and postural instability but also non-motor symptoms including disorganized speech and altered moods were described (Fakhoury, 2016). Precise analysis of postmortem brains of PD patients showed around 80% loss of dopaminergic cells compared to age-matched controls (Damier et al., 1999), which is double as much as I have seen in the SN pc of 12 months old GNE<sup>+/-</sup> mice (-36% loss in TH-positive neurons) and hence, explains why I did not observe any obvious motor impairment. It is possible that progressing neuronal loss with further age might be strong enough to develop clear clinical symptoms in GNE<sup>+/-</sup> mice and might be worth to test.

Beside the appearance of neuronal loss, abnormal intracytoplasmic filamentous aggregates, so called Lewy bodies, are found in somas and axons of PD patients. These aggregates consist of phosphorylated neurofilament, parkin, alpha-synuclein and components of the proteasomic-ubiquitin pathway (Orr et al., 2002). It is conceivable that sialylation is involved in the normal folding of proteins, suggesting that impaired sialylation results in aggregation. Recently, the study of Oikawa and colleagues showed that an imbalance of ganglioside (sialoglycoconjugates) composition triggered amyloid beta deposition (Oikawa et al., 2015) and altered sialylation of proteins in AD was already discussed before (Schedin-Weiss et al., 2014). However, the underlying cause is not completely understood. PD has also been suggested as accelerated form of aging but neuronal loss in normal aging is not sufficient to cause PD. Similar conclusions were drawn for neuronal loss in aging *versus* AD (Morrison and Hof, 2002). Additional confirmed etiological factors for the neurodegeneration in PD are environmental toxins like herbicides (1-Methyl-4-phenyl-1,2,3,6-tetrahydropyridin, MPTP), insecticides (Rotenone), or metals and genetic factors. Mutations in alpha-synuclein and parkin but also mitochondrial dysfunction and oxidative stress can lead to the accumulation of misfolded proteins and aggregates (reviewed in Ramirez et al., 2017).

#### **4.1.2.2 The absence of neuroinflammation**

The composition and function of the brain is much more complex than a cell culture dish with defined cell types. Transcriptomic studies are a helpful tool to understand complex pathways and provide an overview of the expression levels of all genes and functional elements in the CNS. Nowadays, high-throughput RNA sequencing technology enables to map and quantify a large number of transcripts simultaneously and cost-effectively. In direct comparison to the

former predominantly used method of microarrays, RNA sequencing has the advantage to discover novel transcripts, alternative splicing events, and even genetic variations. Thus, nowadays RNA sequencing is more quantitative, accurate and comprehensive than a microarray approach (Dong et al., 2015).

In this study we used the RNA sequencing approach to study the effects of altered sialic acid levels on gene transcription. Interestingly, the transcriptome analysis of whole brain RNA revealed no major changes between the genotypes. This was not entirely unexpected, as we have a modest perturbation of GNE (heterozygote) and used total brain tissue RNA. Even if there would be robust changes in some cell types, they can easily be masked by other cell types in the tissue. Also opposite directions in different cell types might neutralize each other in whole brain homogenate analysis. However, robust effects are normally seen by this approach suggesting that indeed, the GNE heterozygosity had no deeper effect on gene expression. Inconsistent with this statement is the finding that *gne* did not appear within the 45 DEGs in GNE<sup>+/-</sup> mice, although I was able to confirm reduced transcription levels by sqRT-PCR. This discrepancy is probably due to the primer design and the statistical analysis we applied. The primers used for *gne* detection are exon 2 – exon 3 spanning and were designed to distinguish between the wildtype and the knockout allele. This primer pair was further confirmed to recognize the two main known protein coding isoforms published by NCBI (mGne1: NM\_001190414 and mGne2: NM\_015828) but probably does not recognize all possible splice variants (e.g. see Ensembl: Gne, ENSMUSG00000028479; Yates et al., 2016) as mentioned earlier. Since only the two major isoforms of these 14 listed transcripts are confirmed to be protein coding (Reinke et al., 2009; Yardeni et al., 2013) it remains unclear if and how many of the other splice variants are functional and should be taken into account. However, as mentioned before DeSeq2 is not distinguishing between transcript variants and is counting all identified isoforms of Gne. In contrast, CuffLinks and CuffDiff, two alternative statistical approaches that has been tested for the RNA sequencing data (data not shown), distinguish between variants. The analysis using CuffLinks and CuffDiff revealed that not all *gne* variants were downregulated in GNE<sup>+/-</sup> mice explaining why the summarized levels of all *gne* variants are not listed as differentially expressed in the DeSeq2 analysis. Nevertheless, based on quality checks these statistical approaches were not as appropriate for the dataset as DeSeq2.

Furthermore, no typical inflammatory signature could be found in the brain, which typically accompanies a neuronal loss seen in neurodegeneration. We compared our dataset with a study of inflammatory neurodegeneration sharing the neuronal loss in the substantia nigra. In this

study the neuronal loss was mediated by the activation of the microglial complement-phagosome pathway (Bodea et al., 2014) and the neuronal loss was already observed 14 days after a systemic repeated LPS challenge (on four consecutive days). Furthermore, already within five days of treatment, inflammatory response pathways were enriched in the brain of these mice and increased production of proinflammatory cytokines like Tnfa or Il1b was measured. However, a similar upregulation of inflammatory markers was not seen in  $GNE^{+/-}$  mice. Furthermore, the number of DEGs in the brains of  $GNE^{+/-}$  mice was only 3 % of the number of altered genes in the LPS-challenged brains. Almost all shared genes differed in directionality, except the deiodinase, iodothyronine, type II (Dio2). Dio2 being downregulated in both datasets is normally mentioned as activator of thyroid hormone synthesis but also indirectly promotes myelination via thyroxine upregulation. Interestingly, Dio2 was found to be a risk factor for late-onset AD and was confirmed to be downregulated in late-onset AD patients similar as in the  $GNE^{+/-}$  mice (Humphries et al., 2015).

Taken together, the direct comparison with the whole genome transcriptome analysis of the brain with inflammatory neurodegeneration demonstrated clearly that an inflammatory profile was not present in  $GNE^{+/-}$  mice, suggesting that inflammation is not the underlying mechanism for the neuronal loss observed in this study. Furthermore, the transcriptional profile of 9 months could be validated for several genes and transcriptional time series of these genes confirmed similar trends at earlier time points.

Yet, minor changes in transcription were at least discovered for 45 DEGs. Most of these genes were surprisingly downregulated in  $GNE^{+/-}$  mice, whereas only three genes were significantly upregulated (Cxcl12, Btg2, and Sox9). C-X-C Motif Chemokine Ligand 12 (Cxcl12), also known as stromal cell-derived factor-1 (SDF1), is a chemoattractant for immune cells such as microglia and has anti-inflammatory properties (Azizi et al., 2014). Its receptor is the C-X-C Motif Chemokine Receptor 4 (Cxcr4). Cxcl12/Cxcr4 signaling plays an important role in adult neurogenesis and was shown to be upregulated after stroke (Cui et al., 2013). In the rat cochlea, Cxcl12 was found to be highly expressed in degenerating spiral ganglion neurons and promoted the migration of Cxcr4-expressing neural stem cells to the degenerated site (Zhang et al., 2013). In line with Cxcl12, the B cell translocation gene 2 (Btg2) was described as regulator of neuron differentiation during embryonic development (Canzoniere et al., 2004) and plays a role in adult neurogenesis in the subventricular zone and in the DG of the hippocampus (Farioli-Vecchioli et al., 2008). These findings suggest that the upregulation of Cxcl12 and Btg2 levels in  $GNE^{+/-}$  is an attempt to counteract the neuronal loss by promoting neurogenesis. Puzzling is the

upregulation of Sox9 (also known as SRA1 or sex determining region Y-box 9). Sox9 plays a pivotal role in male sexual development and inhibits the formation of the female reproductive system (De Santa Barbara et al., 1998; Moniot et al., 2009). Why a transcript supporting male sexual development is upregulated in female  $GNE^{+/-}$  mice cannot be explained.

Among the 45 DEGs the protein phosphatase 1 regulatory subunit 3G (*Ppp1r3g*) was the strongest downregulated gene. It is a glucose metabolism-related enzyme that regulates postprandial glucose homeostasis and lipid metabolism (Zhang et al., 2017). Liver-specific overexpression of *Ppp1r3g* in mice enhanced postprandial blood glucose clearance and mice showed a reduced fat mass (Zhang et al., 2014b). Therefore, reduced *ppp1r3g* transcription might be a sign of a changed metabolism and might account for the increased weight in female  $GNE^{+/-}$  mice. Another strongly downregulated gene was DNA-damage-inducible transcript 4 (*Ddit4*), also known as protein regulated in development and DNA damage response 1 (*REDD1*) or under the name “RTP801”. It regulates a variety of cellular functions such as growth, proliferation and autophagy by inhibiting the mammalian target of rapamycin complex-1 (mTORC1; Corradetti et al., 2005; Sofer et al., 2005; Ota et al., 2014). Interestingly, in the substantia nigra of postmortem PD brains highly elevated levels of *Ddit4* were measured but not in cerebellar neurons. It was concluded that elevated *Ddit4* may mediate degeneration and death of substantia nigral neurons (Malagelada et al., 2006) meaning that the downregulation of *Ddit4* in the brains of  $GNE^{+/-}$  mice is another unsuccessful attempt to counteract the neuronal loss and to maintain homeostasis. Why the ADP-ribosylation factor-like protein 4D (*Arl4d*), the third most downregulated DEG, was also downregulated is unclear. *Arl4d* was identified as neuroprotective molecule by Dai and colleagues (Dai et al., 2010) and is normally upregulated during BDNF dependent long-term potentiation and promotes adaptive neuronal plasticity in the brain (Alme et al., 2007). The downregulation of *Arl4d* might be a first sign that the ability of neuronal plasticity such as synapse formation is impaired.

Interestingly, the proinflammatory cytokine *Il1b* was predicted as most possible upstream regulator in  $GNE^{+/-}$  mice and was confirmed to be upregulated in  $GNE^{+/-}$  mice at several ages. Although *Il1b* is an important mediator between the brain and the immune system, it has also been shown to play a role in a number of homeostatic functions, including fever (Morimoto et al., 1986; Blatteis and Sehic, 1998; Netea et al., 2000), sleep (Ingiosi et al., 2015), feeding and drinking behavior (De Castro E Silva et al., 2006; Luz et al., 2006, 2009), and cardiovascular control, such as body temperature, blood pressure, and fluid homeostasis (Takahashi et al., 1992; Yamamoto et al., 1994; Cerqueira et al., 2016). Furthermore, *Il1b* was shown to be

negatively affected by gangliosides, the sialic acid-containing glycosphingolipids. Gangliosides are considered to play an important role in tissue homeostasis and repair in the CNS. Via protein kinase A (PKA)-mediated phosphorylation gangliosides can activate the cAMP response element binding protein (CREB), which was also among the predicted upstream regulators (Chandra et al., 1995; Min et al., 2004). In addition, the promoter region of the gene encoding *Il1b* contains a CREB binding site (Stylianou and Saklatvala, 1998). Thus, gangliosides are able to regulate *il1b* levels via several second messengers, such as the transcription factor CREB. Considering that most sialic acids are found on gangliosides in the brain, it is most likely that the ganglioside composition is altered in *GNE*<sup>+/-</sup> mice and affects *il1b* transcription. Similar upregulation of *il1b* was shown for other transgenic mouse models affecting the ganglioside composition in the cerebellum and in the spinal cord (Ohmi et al., 2011, 2014). The transcription of *il1b* was upregulated with increasing severity of ganglioside ablation. Furthermore, increasing *il1b* levels were observed during aging, similar to our study. In another study from Ba and colleagues it was shown that the treatment with the ganglioside GM1 was able to reduce elevated *il1b* levels in a rat model of PD (Ba, 2016). Taken together, these publications draw a link between altered sialic acids, ganglioside and *il1b* levels.

In the canonical pathway analysis the glucocorticoid signaling pathway appeared as first hit. Glucocorticoids are hormones that are secreted from the adrenal glands in response to acute stress signals deriving from the hypothalamus and from the pituitary gland and help to maintain homeostasis or to adapt to a stress situation (reviewed in Hall et al., 2015). Lately, glucocorticoids were also found to be involved in synaptic plasticity. Endogenous glucocorticoid oscillations promoted spine formations and were required for spine stabilization, whereas chronic excessive glucocorticoid signaling eliminated new spines (Liston et al., 2013). Chronic elevation and prolonged exposure to glucocorticoids were also measured in several psychiatric disorders like depression (Carroll et al., 1976; Starkman et al., 1992). Thus, quantification of the synaptic density in different brain regions would be interesting. Glucocorticoid signaling is mediated by glucocorticoid receptors and mineralocorticoid receptors. While mineralocorticoid receptors are mainly expressed in neurons as well as in glial cells (Sierra 2008, see Herrero 2015), glucocorticoid receptors are almost ubiquitously expressed in the brain (Herrero et al., 2015). If glucocorticoid signaling is significantly altered in *GNE*<sup>+/-</sup> mice it is not unexpected that the glucocorticoid receptor *Nr3c1* is among the predicted upstream regulators. These data are also in line with the decreased glucocorticoid receptor levels reported in the substantia nigra of a PD patient and in a PD mouse model (Ros-Bernal et al., 2011). Unfortunately, the activity of *Nr3c1* as well as of *Creb1* is not really



regulated on transcription levels but usually by ligand binding (glucocorticoid levels for Nr3c1) or phosphorylation (in response to cAMP signaling), respectively. Thus, levels cannot be verified by sqRT-PCR. To validate their predicted activity it would be necessary to measure glucocorticoid protein levels or CREB1 phosphorylation by Western blot.

Taken these findings and the fact that glucocorticoids can also act on microglia rhythms by inducing the expression of period circadian clock 1 (Per1; Fonken et al., 2016), which is also among the 45 DEGs, glucocorticoid signaling plays clearly a role in the brain of the GNE<sup>+/-</sup> mice. Nonetheless, further investigations are needed to better understand its specific function here. It is even possible that the differences in glucocorticoids are a hint of a starting muscle weakness in the GNE<sup>+/-</sup> mice because glucocorticoids were reported to regulate muscle atrophy (Schakman et al., 2013; Bodine and Furlow, 2015). Furthermore, muscle atrophy correlates with muscle weakness as it was observed in a transgenic mouse model expressing the human p.D207V mutant *GNE* but not their own *Gne* anymore (Malicdan et al., 2008).

For a more in-depths understanding of the underlying pathway a single cell analysis of microglia or neurons or RNA sequencing of different brain regions might be suitable to unravel any hidden differences. In fact, a regional transcriptome analysis by Mangold and colleagues detected very different transcriptional profiles comparing hippocampus with cortex (Mangold et al., 2017). Single-cell RNA sequencing helps to elucidates biological complexity (Zhang et al., 2014a; Dong et al., 2015; Grabert et al., 2016; Wes et al., 2016) but nevertheless, it must be taken into account that sample isolation can alter gene expression and data sets might not be comparable.

#### 4.1.2.3 Involvement of microglia and the complement system

The second challenge of this study was to validate the involvement of the complement system and of microglia in the neuronal loss and to confirm the underlying mechanism known from the *in vitro* studies (Linnartz et al., 2012b; Linnartz-Gerlach et al., 2016). *In vitro*, it was demonstrated that C1q binds to desialylated neurites and that blocking of CR3 on microglia prevents the uptake of desialylated neuronal structures by microglia. The transcriptome analysis at 9 months did not clearly hint towards a microglia-mediated mechanism that could explain the neuronal loss in the brain. A typical inflammatory process mediated by microglia was also excluded, which was in line with the non-inflammatory *in vitro* situation.

However, transcription levels of specific microglial markers (*aif1*, *cd68*, and *tmem119*) were consistently upregulated in brains of GNE<sup>+/-</sup> mice throughout aging (6 months to 12 months)

compared to wildtype mice. Especially the general increase of wildtype *aif1* (gene encoding Iba1) levels with aging were in line with the findings of Mangold and colleagues (Mangold et al., 2017) and was also reported by other researchers (Mouton et al., 2002; Tremblay et al., 2012). *Tmem119* is a rather new microglia-specific marker for a protein with so far unknown function (Sato et al., 2015; Bennett et al., 2016). Its specificity has the advantage that microglia differences are not masked by *tmem119* transcription on other cell types in the brain. Thus, the observed increased *tmem119* transcription levels in  $GNE^{+/-}$  mice during aging could either indicate higher microglia numbers or morphological changes. Remodeling of the membrane surface might require increased receptor expression.

Iba1 is expressed by all mononuclear phagocytes and is a widely used marker for microglia and macrophages in the brain. Immunohistochemistry with an antibody against Iba1 allows detection of all morphological and functional forms of microglia in both rodent and human preparations. It further allows direct comparison of microglia in translational studies, and between species (Ito et al., 1998; Hirasawa et al., 2005). Therefore, tissue from 9 months old mice (highest *aif1* transcript levels) was chosen and microglia in the SN pr, the region with the higher neuronal loss was investigated. Here, I could confirm the significant increase in *aif1* transcription levels at 9 months also on protein level. Surprisingly, the number of Iba1-positive cells was slightly reduced in 9 months old  $GNE^{+/-}$  mice. Although not fully investigated, changes in microglial number with age are still controversially discussed. In some studies no changes in microglial numbers were described for mice (Long et al., 1998; Askew et al., 2017) and rats (VanGuilder et al., 2011), but in other publications lower numbers in mice were found with age (Hayakawa et al., 2007), or an increase in female mice but not in male mice was reported (Mouton et al., 2002). The discrepancy in microglial number might also be a result of different markers used for microglia staining (e.g. isolectin B4, Mac-1, Iba1) and different counting techniques, and thus, needs to be carefully revised. As mentioned before, Iba1 staining can also be used for morphology analysis. Microglia activation is often described as amoeboid cell morphology with enlarged soma and shorter processes. In this study such differences in soma area were not found between the genotypes and also the Iba1 intensity in the soma was not stronger expressed in the  $GNE^{+/-}$  mice.

The lysosomal membrane protein Cd68 is associated with microglia activation and phagocytosis (Ramprasad et al., 1996) and was shown to be increased in  $GNE^{+/-}$  mice on transcription level. However, immunohistochemical staining of Cd68 was rather reduced in  $GNE^{+/-}$  mice and in particular in the soma, even though only slightly. Thus, from this basic

morphological analysis a clear conclusion was not possible. Variations were often higher than differences. Therefore, I conclude that either a morphological change occurred earlier and at 9 months microglia do not differ anymore in shape or alternatively, the expected changes in microglia morphology and function change in a homeostatic range and consequently, are too small to be captured by the methods applied here. In addition, microglia morphology was only investigated in the substantia nigra. If the underlying mechanism for the neuronal loss seen in the substantia nigra is occurring before 9 months and as proposed, if the neuronal loss in the hippocampus appears much later than in the substantia nigra, it is likely that at 9 months changes in microglia morphology can be seen in the hippocampus but not in the substantia nigra anymore. Interestingly, Bodea and colleagues were only able to see differences in Iba1 fluorescence one day after the final LPS injection but not two weeks later when the neuronal loss was present (Bodea et al., 2014). This was an unexpected finding considering that systemic LPS challenge has a major impact on the brain transcriptome and inflammatory processes as it was mentioned before. Similar data were also shown for Cd68 immunohistochemical staining. This indicates again that changes in microglia morphology not necessarily occur in parallel with neuronal loss and might need strong inflammatory input. Thus, for a detailed morphology analysis a 3D reconstruction of microglia in different brain regions is recommended. This analysis is more precise and might clarify the circumstances.

It has to be kept in mind that the *in vitro* studies were a reduced model system meaning that it is likely, that in the *in vivo* situation other cells types are involved as well. Astrocytes are also involved in the complex regulation of the CNS inflammation and tightly interact with microglia. Under pathological conditions astrocytes and microglia can orchestrate together and induce an inflammatory response. For instance, after brain injury, astrocytes produce cytokines and chemokines that activate microglia and recruit peripheral immune cells to the CNS (Ramirez et al., 2017). Furthermore, Il1b secreted by microglia was shown to be a potent activator of astrogliosis (Lee et al., 1993; Giulian et al., 1994). Reactive astrogliosis is a physiological response to destruction of nearby neurons in all forms of CNS injury and diseases and considered as a protective reaction at first place (De Strooper and Karran, 2016). Typically, an abnormal increase in the number of astrocytes and increased GFAP fluorescence can be seen (Sofroniew and Vinters, 2010; Sofroniew, 2014) but was not detected in the tissue of GNE<sup>+/-</sup> mice. This is in line with the absence of neuroinflammation on transcriptional level and argues against an inflammatory crosstalk between microglia and astrocytes via Il1b. However, under pathological conditions atypical activation of gliosis was already observed. In PD, for instance, microglia are highly activated by the disease, whereas astrogliosis is often largely absent

(Ramirez et al., 2017). Nevertheless, similar to the microglia data only astrocytes in the substantia nigra were analyzed in this study and thus, astrogliosis cannot be excluded for other brain regions.

The complement system is a part of the innate immune system. Beside its immune function it is essential for refining the neuronal network in the developing brain via microglia-mediated synaptic pruning. Removal of pathogens and cellular debris as well as removal of inappropriate synapses are the basic functions. Later in life, complement proteins still play a role in the adult and aging brain. The increase in the expression of complement components I found is supported by human data of aged hippocampus (Cribbs et al., 2012) and studies in male mice (Stephan et al., 2013). Increasing levels were especially seen for old mice (18-24 months). A significant increase of the initiation factor C1q was also seen in both, human and mouse brains (Stephan et al., 2013) and increasing *c4b* transcript levels with age were, for example, demonstrated by Bonasera and colleagues in the mouse cerebellum (Bonasera et al., 2016). Remarkably, the measured transcription levels of the C1q genes were fluctuating over time, in particular *c1qc* levels showed an oscillating pattern. In comparison, the study of Kraft and colleagues measured the transcription levels of *c1qa*, *c1qb*, and *c1qc* in response to induced death of dentate granule neurons in the hippocampus (Kraft et al., 2016). The transcription levels of all three complement factors were increasing with the severity of neuronal loss. Similar to our findings, their data also showed the highest response levels for *c1qc* and the lowest for *c1qb* transcripts, whereas in the study of Mangold and colleagues, differences between *c1qa* and *c1qc* were minor in male hippocampi but higher for *c1qa* in female hippocampi (Mangold et al., 2017). Surprisingly, *itgam*, one of the genes encoding the CR3, is expressed on the surface of many leukocytes, including macrophages and microglia and was barely altered with age. Yet, levels were slightly increased in  $GNE^{+/-}$  mice and corresponded to the transcript levels of the microglial marker *tmem119*.

Considering the fact that the complement system is involved in normal synapse formation and regulation, an altered expression of complement components most likely plays a significant role in synapse loss with aging and neurodegenerative diseases as it was discussed before (Stevens et al., 2007; Stephan et al., 2012). With exception of *c1qc*, most genotype-specific transcription differences occurred after 3 months but it remains unclear why transcript levels of *c1qb*, *c1qc* and *c4b* were higher in wildtype mice, whereas transcript levels of *c1qa*, *c3* and *itgam* were higher in  $GNE^{+/-}$  mice. Again, regional differences might be masked when analyzing overall brain tissue and might only be visible when analyzing distinct brain regions as described for

instance for the neocortex and the cerebellum (Lee et al., 2000). Moreover, the lack of major differences speaks in favor for a homeostatic regulation on protein level.

#### 4.1.2.4 Rescue of the GNE<sup>+/-</sup>-dependent phenotype

Crossbreeding with C3-deficient mice enabled us to confirm the involvement of the complement system in microglia-mediated neuronal loss as observed *in vitro*. The knockout of C3 prevented neuronal loss in different brain regions of aged GNE<sup>+/-</sup> mice. Furthermore, even for some important markers, like *il1b* and *aif1* transcription levels were reduced similar to wildtype levels. Also the predicted pathways, which were altered in GNE<sup>+/-</sup> mice were rescued and did not show up in IPA anymore after knockout of C3, suggesting that these pathways did not play a major role anymore. The increased width I found in GNE<sup>+/-</sup>C3<sup>-/-</sup> mice might be explained by the C3 deficiency. C3-deficient mice were reported to have in general more synapses and thus, maybe have an higher brain volume (Kalm et al., 2016). As mentioned before, the quantification of the synaptic density in different brains regions could unveil whether synapses are being excessively removed in GNE<sup>+/-</sup> mice and whether this removal can be prevented in GNE<sup>+/-</sup>C3<sup>-/-</sup> mice.

In double knockout mice of ganglioside GM2/GD2 synthase (B4ganlt1) and GD3 synthase (St8sia1), another mouse model of glycoalyx alterations, a similar rescue was possible (Ohmi et al., 2011, 2014). In these mice progressive deterioration with aging was observed in in the spinal cord and in the cerebellum accompanied by increased complement-related genes. The double-knockout mouse developed an even more severe phenotype but mating with C3-deficient mice was able to restore the neuronal numbers and the complement transcription levels as it was shown in GNE<sup>+/-</sup>C3<sup>-/-</sup> mice. These studies not only confirm our findings but also support the important role of the complement system in neuronal loss.

#### 4.1.3 Reactivation of developmental synaptic pruning

Bodea and colleagues discovered that systemic LPS leads to inflammatory neurodegeneration and a complement-mediated response that activates microglia via CR3 and ITAM-associated signaling. This signaling results in the formation of the nicotinamide adenine dinucleotide phosphate (NADPH) oxidase and presumably in the production of neurotoxic ROS (Bodea et al., 2014). In contrast to the inflammatory proposed mechanism by Bodea and colleagues, I propose a non-inflammatory and homeostatic removal of neurons as underlying mechanism of this study. Silent phagocytosis of desialylated neurons is one of the main beneficial functions of microglia (Neumann et al., 2009; Linnartz et al., 2012a) and might be aberrantly regulated

in  $GNE^{+/-}$  mice. Under normal conditions sialic acids mask important “eat me” signals on neurons that are essential for synaptic pruning and consequently, are highly controlled. Especially the long polysialic acid chains are necessary for a proper inhibitory Siglec signaling. In  $GNE^{+/-}$  mice this inhibition is simply gone or at least reduced. Further hints come from the ganglioside-based literature showing that the ganglioside composition is crucial for synapse regulation (Palmano et al., 2015; Zhang et al., 2016b). Synaptic degeneration was described to be an early hallmark of aging as well as of neurodegenerative diseases and followed by neuronal loss (reviewed in Morrison and Baxter, 2012). It is already under current debate if the developmental synaptic pruning is recapitulated in the aging brain (Zabel and Kirsch, 2013). Under normal conditions, microglia can clearly distinguish between wanted and unwanted synapses. They selectively remove axosomatic inhibitory synapses while leaving excitatory synapses intact (Wolf et al., 2017) but during aging microglia-mediated synaptic development might transform into pathological alterations. An aberrantly reactivated synapse pruning in the aged brain was confirmed to contribute to the synapse loss seen in AD (Hong et al., 2016a). However, if microglia actively initiate synapse remodeling or clear synapses passively, this remains unsolved.

Here, I show that reduced masking of the neuronal surface in  $GNE^{+/-}$  mice accelerated the normal aging process and possibly provokes increased and unwanted synaptic pruning by microglia. As suggested previously (Shi et al., 2015), in aging early synapse loss in neurons precedes late neuronal loss. That implies that the age-dependent loss of neurons in either the substantia nigra or the hippocampus might be a result of post-developmental complement-mediated synapse elimination in the adult brain and in fact, occurs much earlier in the  $GNE^{+/-}$  mice than in wildtype littermates.

In summary, I hypothesize that the early neuronal loss I observed in the  $GNE^{+/-}$  mice might be due to unwanted accelerated synapse elimination. To further clarify the synaptic loss, brain region-specific investigations on synaptic density and synaptic turnover are essential.

## 4.2 Transgenic mice for modeling an altered glycoalyx

As previously mentioned most *in vitro* data lack confirmation *in vivo* and this has a huge impact on data validation or clinical trials. Therefore, it is important to find suitable animal models to reproduce pathways in a complex organism that were obtained in a limited cell culture dish. Nevertheless, the reduction of complexity is necessary to understand a basic concept before transferring it to a more complex organism and it is important to understand the limitation of each applied model.

### 4.2.1 GNE<sup>+/-</sup> mice as model for an altered glycoalyx

To model an altered glycoalyx *in vivo*, a mouse heterozygous for the enzyme GNE was used that was described with an overall reduction of membrane-bound sialic acid by 32% in the brain (Gagiannis et al., 2007). As mentioned before the complete knockout of the GNE enzyme results in embryonic lethality (Schwarzkopf et al., 2002) and could not be used. Surprisingly, the introduced loss-of function mutation into only one allele was enough to reduce the total sialic acid production. Although GNE is described to be ubiquitously expressed in all cells, regional differences in GNE function (summarized in Willems et al., 2016) and different sialic acid regulation might result in regional or global differences.

In direct comparison, GNE<sup>+/-</sup> mice are a good model for an altered glycoalyx and a good translation of both *in vitro* models. Only some minor differences occur. First of all, *in vitro* the sialic acid residues were removed enzymatically by a combination of an exo- and an endo- $\alpha$ -sialidase and only at the neuronal cell surface (Linnartz et al., 2012b; Linnartz-Gerlach et al., 2016), whereas *in vivo*, reduced sialic acid levels were achieved by systemic reduction of the *de novo* biosynthesis of sialic acids. Secondly, *in vitro* the effect of the altered glycoalyx was investigated at a particular time point because enzymatic removal is a temporary situation. In contrast, the systemic reduction of the sialic acid synthesis *in vivo* provides the option to study long-term effects and in addition, sialic acid levels further decreased with age in the mouse brain and enhanced the phenotype. The increasing neuronal loss in the brain of the GNE<sup>+/-</sup> mice was in line with the documented neuronal loss of desialylated neurites in both *in vitro* studies (Linnartz et al., 2012b; Linnartz-Gerlach et al., 2016). Furthermore, I could show small alterations in transcription and on protein levels of microglial markers that hinted towards a microglial involvement. However, to confirm the microglial phagocytosis of desialylated neuronal debris as it was shown in the cell culture experiments, *in vivo* imaging would be the necessary follow-up experiment. The thinned-skull imaging method by two-photon laser

microscopy might be an appropriate method (Guo et al., 2017) that could be realized in form of a collaboration but it has to be kept in mind that this method needs the crossbreeding with a microglia reporter line. Nevertheless, even with *in vivo* imaging it will be difficult to prove the new concept of silent phagocytosis.

Importantly, I could prove the involvement of the complement system *in vivo*. By genetic inhibition of the complement system, the neuronal loss was prevented in the GNE<sup>+/-</sup> mice. In contrast to the *in vitro* studies that used blocking antibodies against CR3 to inhibit microglial phagocytosis, in the *in vivo* situation, the complete downstream signaling pathway of the complement system was inhibited by C3 knockout. This approach is much stronger but might also cause some additional effects in the mice.

Although the mouse model was reflecting nicely most of the *in vitro* data some limitations have to be taken into account. First of all, sexual dimorphism is not yet a question *in vitro* but it is a not negligible environmental factor *in vivo*, especially when addressing microglia-specific questions. Also the sexual dimorphism of the brain anatomy has to be considered and possible differences in immune functions. In particular, when it comes to aging, male and female mice develop different phenotypes (Hanamsagar et al., 2017; Mangold et al., 2017). Furthermore, it was observed that the GNE heterozygosity leads to dynamic variabilities between generations and also litters (data not shown). Different protein expression might have a large impact on the phenotype. As a consequence, only global effects will be visible in GNE<sup>+/-</sup> mice but smaller effects might be masked by these variations. When studying neuronal loss in these mice, it also has to be taken into account that dependent on the brain region of interest a certain age is mandatory to detect and investigate significant neuronal loss. However, the slowly developing phenotype in the GNE<sup>+/-</sup> mice might in fact reflect much better an age-dependent neuronal loss. Another limitation of studying an altered glycoalyx in mice is the difference in sialic acid monomers. While in the mouse both monomers, Neu5Ac and Neu5Gc, are synthesized, in humans only Neu5Ac is synthesized. As a consequence, the SIGLEC composition and binding preferences in humans had to adapt to these changes (Sonnenburg et al., 2004; Varki and Angata, 2006). Therefore, the mouse as model organism might not be suitable for some human diseases related to SIGLEC signaling.

In general, the reduced sialic acid levels and thus, an altered glycoalyx were confirmed in the mouse model and the neuronal loss could not only be successfully recapitulated in the brain of the GNE<sup>+/-</sup> mice but was also rescued via inhibition of the complement system. Therefore, the GNE<sup>+/-</sup> mouse was validated as suitable model for an altered glycoalyx.



## 4.2.2 Other transgenic mouse models with glycoalyx alterations

$GNE^{+/-}$  mice are not the only transgenic mice for studying an altered glycoalyx. Other mouse models have been engineered to modify specific sialoglycoconjugates, like gangliosides and to study the role of sialic acids in different pathologies. All these models develop comparable pathologies as the  $GNE^{+/-}$  mice but with different degrees of severity (Sheikh et al., 1999; Sugiura et al., 2005; Furukawa et al., 2014).

Mutations in enzymes of the early ganglioside biosynthesis can result in the disruption of complex gangliosides and the impairment of nervous tissue integrity. Thus, modifying the ganglioside composition in the brain can shed light on their specific functions in brain development and maintenance. For instance, the *B4galnt1* mutant mice (“complex ganglioside KO”) are deficient for the GM2/GD2 synthase and cannot synthesize the major brain gangliosides GM1, GD1b, GD1a, and GT1b. They only express GM3 and GD3 (Sheikh et al., 1999; Pan et al., 2005). The absence of complex brain gangliosides in these mice leads to strong CNS disorders, including motor impairment, depletion of striatal dopamine, selective loss of TH-expressing neurons, and aggregation of alpha-synuclein (Chiavegatto et al., 2000; Wu et al., 2012). Similar to the  $GNE^{+/-}$  mice these mutants are viable and show a normal development at young age. However, with increasing age these mice develop heavy neurodegeneration accompanied by motor defects and dysmyelination in the CNS, which was partially observed in  $GNE^{+/-}$  mice but less severe. In contrast, mice expressing only GM3 as major brain ganglioside establish strong epileptic seizures and die already early after birth (Kawai et al., 2001). Strikingly, the only structural difference between GM3 and GD3 is a mono-sialic acid residue (for GM3) instead of a di-sialic acid residue (for GD3) on galactose but the absence of one sialic acid residue on the ganglioside seems to have a major effect on the glycoalyx structure and its function. This is further confirmed by mice that lack even mono-sialic acid gangliosides (GM3) and die at E7.5 (Yamashita et al., 1999).

Sialyltransferases are necessary for transferring sialic acids to their final carrier and to build more complex gangliosides (see introduction, Figure 4). Moreover, they also sialylate glycoproteins. The sialyltransferases ST3Gal-II and ST3Gal-III are mainly responsible for the biosynthesis of GD1a, GT1b, and GQ1b that form half of all ganglioside types in the mammalian brain. Mice deficient for *St3gal2* have a 50% reduction in GD1a/GT1b/GQ1b but higher levels of the gangliosides GM1 and GD1b, while mice deficient for *St3gal3* show 50% reduction in sialoglycoproteins. Double-knockout of *St3gal* and *St3gal3* in mice blocked two of the four major brain gangliosides (GD1a and GT1b) almost completely and resulted in strong

dysmyelination, reduction in hippocampal neurons and impaired motor functions (Yoo et al., 2015). In the brains of mice deficient for polysialyltransferases (St8SiaII<sup>-/-</sup>, St9SiaIV<sup>-/-</sup>) polysialylated glycoconjugates are completely absent. The mice show major defects in long-term depression and long-term potentiation in the hippocampus (Eckhardt et al., 2000). These findings are in line with the neurological abnormalities in NCAM-deficient mice (Bork et al., 2007; Sato and Endo, 2010). Those mice have reduced long-term potentiation in the CA3 region of the hippocampus and show a decreased ability for spatial memory and cell migration. In combination, the different mouse models confirm that mice need at least simple sialylated gangliosides in early development of the brain but complex sialylation and as a consequence complex gangliosides for the correct maturation and maintenance of the brain.

Not only the sialic acid synthesis is crucial for maintenance in the brain but also the functional regulation and degradation of sialoglycoconjugates is essential. Important findings were obtained in mice lacking the neuraminidases 3 and 4. Impaired degradation of gangliosides can result in GM3 storage in microglia, neurons, and vascular pericytes causing memory loss, neuroinflammation and the accumulation of lipofuscin bodies (Pan et al., 2017). Aggregation of alpha-synuclein was also detected in GM1-deficient mice (Wu et al., 2012). These findings draw a link to the reduced polysialylation that has been described for patients with PD or AD (Murray et al., 2016) and in schizophrenia (Sato et al., 2016).

Although other mutations can result in similar pathologies as shown in the GNE<sup>+/-</sup> mouse, the GNE<sup>+/-</sup> mouse is a distinct model for aging. While the other mouse models are useful to understand the functions of specific sialoglycoconjugates in the glycocalyx, the GNE<sup>+/-</sup> mice mimic the natural overall decline in sialic acid levels with aging and thus, are a good model of studying the effects of aging based on glycocalyx alterations.

### 4.2.3 Further implications for GNE<sup>+/-</sup> mice

The GNE<sup>+/-</sup> mouse model was proven to be a good model to study alterations in the neuronal glycocalyx in the brain, especially in aging. However, alterations in gangliosides have been demonstrated to play a major role in several other brain diseases, including ALS (Rapport, 1990) and PD (Wu et al., 2012). It is very likely that glycocalyx alterations are also involved in a wide range of other age-related diseases, including retinal diseases, such as age-related macular degeneration (AMD) and glaucoma. AMD is an inflammatory, degenerative disease of the eye resulting in a gradual loss of vision. More than 30 million people worldwide are affected with increasing numbers. Therapy of AMD is limited and the available treatments help

only temporary (Rofagha et al., 2013). Although the mechanism for developing AMD is not fully understood, activation of the complement system and release of ROS play a central role in the disease (Ambati and Fowler, 2012; Harvey and Durant, 2014). Highly reactive phagocytes can be found in the retina of AMD patients (Gupta et al., 2003) and in mouse model of light-damaged retinas (Scholz et al., 2015). Based on the important role of complement factors in the retina it is very likely that the reduced sialic acid levels in  $GNE^{+/-}$  mice can also facilitate neurodegeneration of photoreceptors in the retina during aging. From another approach, it was already shown that sialic acid treatment inhibits complement activation and reduces the reactivity of phagocytes in the retina of an AMD mouse model (Karlstetter et al., 2017). At this point, I would also like to highlight the common mechanisms of AMD with AD. Both, the complement system as immunological player as well as the microglia as neuronal supporting cells are involved in these diseases. During aging something fundamental must turn wrong in these two players leading to the neurological pathology. Using insights of one neurodegenerative disease might help to understand the other (Harvey and Durant, 2014; Ramirez et al., 2017) and could also be applied on the  $GNE^{+/-}$  mice.

Another neuronal pathology worth to investigate in  $GNE^{+/-}$  mice is acquired hearing loss. About half of the 700 million cases of hearing loss worldwide are not heritable but develop during aging, or are caused by increased noise exposure or by ototoxic substances like aminoglycosides (antibiotics). The degeneration of hair cells, the sensory receptors in the cochlea and the vestibular organ lead to a gradual loss of hearing. Hair cell loss precedes neuronal loss in the spiral ganglion but not much is known about the initial cause of the degeneration. Similar as in the retina the release of radicals is one of the suggested mechanisms and inhibition of the tissue macrophages in the cochlea was able to prevent ototoxicity-induced hair cell degeneration (Sun et al., 2014). Recent findings propose changes in cochlear synaptopathy after acoustic overexposure as initial event to induce hair cell loss (Liberman et al., 2015) and currently new attempts are made to explore the clinical potential of these findings (summarized in Hickox et al., 2017). Furthermore, two aminoglycoside treatments with different ototoxic potentials were shown to reduce the expression of sialoglycoconjugates on the glycocalyx of hair cells (Groot et al., 2005). Sialic acids are known to play an important function as “Don’t eat me signal” but also as scavenger molecules. Age-dependent reduction of sialic acid levels in the cochlea or release of membrane-bound sialic acids to neutralize free radicals after noise exposure or ototoxicity might be the first occurring step in this disease, followed by synaptic changes that finally turn into neurodegeneration. Consequently, the  $GNE^{+/-}$  mice present a suitable model to

unravel the underlying mechanism of neuronal loss in the inner ear and to clarify the potential role of sialic acids in neuronal maintenance.

Last but not least, the  $GNE^{+/-}$  mice are also useful to understand the role of sialic acids in embryonic development.  $GNE^{-/-}$  embryos die between E8.5 and E9.5 (Schwarzkopf et al., 2002). The developmental time frame until around E9.5 can be used to study the essential role of sialic acid in embryogenesis and brain development. So far, it is not clear why the embryos die around E9.5 and not earlier or later. One suggestion is the immigration of microglia into the brain during that crucial time period (Ginhoux et al., 2010), once again highlighting the importance of microglia in recognizing the neuronal glycoalyx. Similar findings were made in mice deficient for CMAS. These mice lack the ability to activate sialic acid to CMP-sialic acid for successful glycosylation.  $Cmas^{-/-}$  embryos were shown to be embryonic lethal similar to  $GNE^{-/-}$  mice and die at a similar time point (Abeln et al., unpublished data). In earlier studies it was shown that desialylation of embryos by neuraminidase treatment led to a fast complement-mediated lysis (Klemke and Weitlauf, 1993; Kircheis et al., 1996) suggesting the complement system as important mediator. Furthermore, it seems that sialylation is crucial to prevent early rejection of the blastocyst by the immune system, which is in line with a study from Whyte and Loke (1978) that showed that trophoblasts are much stronger sialylated than the inner cell mass. Still, it remains unclear if the complement system induces the death of the embryo or if its main function is to remove the dead embryo.  $GNE^{-/-}$  mice could be an alternative model to study the role of sialic acids in early embryogenesis.

### **4.3 Clinical relevance of GNE mutations and mouse models**

Mutations in GNE have important clinical relevance. By now, two completely different diseases caused by GNE mutations are known: GNE myopathy (OMIM #605820) and sialuria (OMIM #269921). Their pathomechanisms are not fully understood yet and different mice models are currently under investigations to find suitable drug therapies.

#### **4.3.1 GNE myopathy**

GNE myopathy is an autosomal, bi-allelic recessive genetic disorder of GNE. A number of different mutations in GNE have been detected that lead to reduced enzyme activity and result in reduced sialic acid biosynthesis. GNE myopathy manifests predominantly in progressive muscle atrophy and weakness, mainly at the distal muscles (Mirabella et al., 2000; Broccolini et al., 2002) and was first described as Nonaka myopathy in Japan (Nonaka et al., 1981). In

some populations, e.g. the Iranian-Jewish population, the frequency of GNE myopathy is greater than one in every 1500 individuals (Jay et al., 2009) and recently 154 reported and novel GNE variants associated with GNE myopathy were published (Celeste et al., 2014). The different mutations in GNE display a variety of different pathological features and thus, it is not surprising that alternative names for the same genetic disorder emerged, like distal myopathy with rimmed vacuoles (DMRV; Nonaka et al., 1981), hereditary inclusion body myopathy (HIBM; Askanas and Engel, 1995), or rimmed vacuole myopathy (Argov and Yarom, 1984) that are now summarized as 'GNE myopathy' (Huizing et al., 2014). Unfortunately, there are other hereditary inclusion body myopathies having different genetic defects but sharing also common features of pathology and thus, make a clear diagnosis difficult (Murnyák et al., 2015).

In general, the pathology starts in early adulthood with weakness in the anterior tibialis muscles. Within ten to twenty years it progresses from the distal to the proximal skeletal muscles in the lower, then in the upper extremities and leads to wheelchair-bound patients. Interestingly, most reports of patients describe sparing of the quadriceps even in advanced stage of GNE myopathy. However, the severity of the disease varies highly and even among siblings (Boyden et al., 2011; Mori-Yoshimura et al., 2012; Cho et al., 2014; Huizing et al., 2014). In a subset of patients, weakness of respiratory muscles appears at advanced stage or dilated cardiomyopathies have been observed as well (Celeste et al., 2014). The histopathological features are decreased sialylation of specific muscle proteins and 'rimmed' vacuole inclusions in the affected muscle tissue. Some of the degenerating muscle fibers contain even abnormal accumulations of amyloid beta protein (Argov and Yarom, 1984) but no protein aggregates have so far been described in the CNS. In addition, no indication for neuronal loss as I have observed in the GNE<sup>+/-</sup> mice has been described so far either. At least, there was one case report with mild ptosis on one eye and diminished neuronal sensation in the feet, which might be an early sign of neuropathy (Weihl et al., 2011). However, most patients probably die too early to develop clear cognitive symptoms, neuronal loss or any abnormal accumulations of amyloid beta protein in the CNS. In some patients hyposialylated NCAM1 was detected in degenerating muscles but not in normal muscles (Ricci et al., 2006). This was also confirmed in other patients, where many vacuolated muscle fibers showed immunoreactivity to NCAM1 and were at the same time immunoreactive for amyloid beta protein, ubiquitin, and tau protein (Murakami et al., 1995). In fact, the question remains, whether AD might share some common pathogenic mechanisms with GNE myopathy. However, similarities such as for the formation of rimmed vacuoles can be found in different neurodegenerative diseases not only in AD (Mizuno et al., 2003) and might be based on a common mechanism.

In GNE myopathy, the huge phenotype variations make it difficult to draw a direct link to the genotype and thus, to fully understand the underlying mechanisms. As mentioned before, the general pathomechanism is hyposialylation, which could be due to reduced CMP-sialic acid levels in serum. However, serum transferrin glycosylation, a standard diagnostic assay for GNE patients is normal in patients (Sparks et al., 2007). Hyposialylation is tissue- and protein-specific and depends on the loci of the GNE mutation (Saito et al., 2004). Comparison with patients having different GNE mutations suggested that mutations in the epimerase domain impair sialylation, while most mutations in the kinase domain lower enzyme activity but not cellular sialylation. It is likely that the kinase function can be substituted by other kinases and most variations might occur due to the sialic acid salvage pathway that can bypass GNE. The bypassing efficiency, indeed, varies in some patients more than in others (Willems et al., 2016).

To better understand the pathology of GNE myopathy, mice models for the different subtypes are meanwhile under investigations, like the mouse model of DMRV that expresses the human GNE D176V mutation (Malicdan et al., 2007; Anada et al., 2014; Cho et al., 2017) or the knock-in mouse carrying the human GNE M712T mutation (Galeano et al., 2007). Nevertheless, the limitation for a mouse model of human GNE myopathy is that in humans meanwhile eight functional isoforms have been detected compared to the two functional murine isoforms (Yardeni et al., 2011, 2013). The additional isoforms might have additional cellular functions that cannot be modelled in mice.

However, studying the Gne-deficient mice expressing the human D176V-GNE mutation revealed hyposialylation in serum, muscle tissue, and organs (Malicdan et al., 2007). The motor performance of these mice markedly decreased after 20 weeks (~5 months) of age (Malicdan et al., 2008) and 10 weeks later amyloid beta deposition was discovered, followed by rimmed vacuoles formation at 40 weeks of age (Malicdan et al., 2009). With these results the Gne-deficient mice expressing the human D176V-GNE mutation resemble quite well the histological and pathological findings of many GNE myopathy patients and present a promising human disease model. In a follow-up study, Malicdan and colleagues used these GNE myopathy mice to test the supplementation of sialic acid precursor molecules and successfully provided evidence that the prophylactic oral administration of ManNAc, Neu5Ac, and sialyllactose can increase sialic acid levels in blood and tissue (Malicdan et al., 2009). Importantly, the therapy improved the motor performance of these mice. Even after disease onset (50 weeks old) treatment of GNE myopathy mice with sialyllactose was able to ameliorated the myopathic phenotype (Yonekawa et al., 2014). The promising results of the

preclinical studies in mice have meanwhile realized a number of clinical trials for human patients: phase 1 (NCT01359319, sialic acid, completed 2012; NCT01634750, ManNAc, completed 2017), phase 2 (NCT01517880, sialic acid, completed 2016; NCT02346461, ManNAc, still ongoing), and a phase 3 (NCT02377921, sialic acid, completed 2017). This once more highlights the importance of using mouse models. Even if they cannot completely recapitulate the human disease they might still be very useful to investigate the underlying mechanisms and to develop suitable treatment strategies.

### 4.3.2 Sialuria

Sialuria is a completely different congenital disorder based on GNE mutations. In contrast to GNE myopathies, the human mutations (R266W, R266Q, and R263L) in sialuria affect the allosteric feedback site of GNE and prevent the regulating feedback by CMP-sialic acids (Kamerling et al., 1979; Seppala et al., 1999; Leroy et al., 2001). This gene defect causes excessive sialic acid synthesis. Sialuria is a rare autosomal dominant disorder starting at early age and the main symptoms are hepatomegaly, coarse facies, and varying skeletal and cognitive developmental delays (Enns et al., 2001; Leroy et al., 2001). So far, only eight individuals are diagnosed for sialuria (Champaigne et al., 2016) but the real number is probably underestimated because heterozygous mutations cause much milder cognitive delays and thus, might be misdiagnosed. The physiopathology is not well understood. Recently, the group from Kaya Bork developed a transgenic mouse model of sialuria using the human sialuria GNE mutation R263L (Kreuzmann et al., 2016). Their transgenic mice excreted up to 400 times more Neu5Ac than wildtype mice due to the missing feedback regulation in GNE and showed increased polysialylation in the brain. However, further investigations showed that the sialic acid levels increased mainly in the blood and not in peripheral organs and after 6 months the differences in polysialylation were not significantly different anymore. So far, the attempt to model sialuria in mice has not been successful and this explains why no clinical trial was realized until now.

Taken together, these two different GNE disorders exhibit completely different pathologies but exhibit both a rather underestimated clinical prevalence. Although GNE might have additional functions in humans, the attempt to find suitable treatments for clinical therapy by modelling the human pathology in mice should not be underestimated. At least for GNE myopathy it was proven that mouse models can be very helpful for a successful therapy of human patients. This once more highlights the importance of using mouse models to understand the underlying mechanisms of human diseases.

## 4.4 Summary and further prospects

The present study describes a new model for glycoalyx alteration. Mice heterozygous for GNE have only been described for reduced sialylation in several organs so far. No further investigations were performed in aging mice. In this study, thorough characterization of the brains of GNE<sup>+/-</sup> mice could now demonstrate that *gne* transcription is reduced by 50% during lifetime and reduced sialylation levels further decrease with age in the brain. In addition, it was shown that polysialylation is more affected by the genotype than shorter sialic acid oligomers.

Furthermore, the model was used to successfully transfer the previously published *in vitro* findings from Linnartz and colleagues into a complex living organism. Linnartz and colleagues showed the removal of desialylated neurons by complement-mediated microglial phagocytosis (Linnartz et al., 2012b; Linnartz-Gerlach et al., 2016). Similar to that, GNE<sup>+/-</sup> mice started to lose neurons from the age of 3 months to 6 months. Aging and simultaneous loss of sialic acids accelerated the neuronal loss in different brain regions. Furthermore, crossbreeding with C3-deficient mice could prevent the neuronal loss with aging and confirmed that also *in vivo* removal of desialylated neurons is mediated by the complement system. Surprising was the absence of any neuroinflammation aside of the proceeding neuronal loss. Neither on transcription level, nor on protein levels could a typical activation profile be confirmed. Slightly elevated microglia marker indicated the involvement of microglia but a typical activatory phenotype was not found. These findings went along with the minor transcriptome differences found at 9 months of age and encouraged me to extend the *in vitro* model to a model of homeostatic removal of desialylated neurons by complement-mediated microglial phagocytosis.

In line with a recent publication demonstrating a role of the complement system in synaptic pruning in an AD mouse model (Hong et al., 2016b), I now postulate that the neuronal loss observed in the GNE<sup>+/-</sup> mice is a false reactivation of developmental synaptic pruning. Aberrant loss of sialic acids on the glycoalyx during aging can cause this reactivation. High-resolution microscopy will help to proof the direct involvement of microglia in this synaptic plasticity and will help to correlate sialic acid levels with synapse density.

One question that turned up during this study was not addressed yet and might be applied to future projects: Are mice with reduced sialic acids more susceptible to oxidative stress? Several hints from literature were given that connect sialic acids with oxidative stress in neurodegenerative diseases. Sialic acid as a known antioxidant on the glycoalyx is likely to be



---

affected by enhanced oxidative stress in tissue assuming that in a chronic stress situation elevated ROS levels might possibly effect the glycocalyx composition. Consequently, increased removal of sialic acids from the glycocalyx will result in neuronal loss similar as it has been seen in the  $GNE^{+/-}$  mice. Furthermore, it is easily conceivable that  $GNE^{+/-}$  mice having an altered glycocalyx might be more susceptible to systemic inflammation. While in general the substantia nigra seems to be very sensitive to LPS-induced neuronal death, the hippocampus, for instance, appeared to be more resistant to LPS (Espinosa-Oliva et al., 2011). Thus, LPS treatment of  $GNE^{+/-}$  mice could provide new insights how vulnerable the glycocalyx might be during systemic inflammation, especially in certain types of neurons. By this idea, I would like to point out that the glycocalyx composition in general should be more the focus of investigation in any model of oxidative stress and in neurodegenerative diseases.

For future therapy purpose it is helpful that sialic acids belong to the group of metabolites. As it was already shown in several studies, sialic acid precursor molecules can be used to treat mice and increase sialylation in different organs. However, the uptake and incorporation of sialic acids lacks optimization. The  $GNE^{+/-}$  mice offer a suitable model to understand the uptake of sialic acid precursor molecules, like ManNAc or sialyllactose, to optimize its therapeutic function and to test the treatment effects in the suggested disease models (e.g. AMD, hearing loss, or AD). Successful reconstitution of a normal glycocalyx and thus, preventing neurodegeneration in different organs can then be transferred to a successful treatment for a number of neurodegenerative diseases.

## 5 References

- Agnello V, De Bracco MM, Kunkel HG (1972) Hereditary C2 deficiency with some manifestations of systemic lupus erythematosus. *J Immunol* 108:837–840.
- Ajami B, Bennett JL, Krieger C, Tetzlaff W, Rossi FM V (2007) Local self-renewal can sustain CNS microglia maintenance and function throughout adult life. *Nat Neurosci* 10:1538–1543.
- Alme MN, Wibrand K, Dagestad G, Bramham CR (2007) Chronic Fluoxetine Treatment Induces Brain Region-Specific Upregulation of Genes Associated with BDNF-Induced Long-Term Potentiation. *Neural Plast* 2007:1–9.
- Amateau SK, McCarthy MM (2002) A novel mechanism of dendritic spine plasticity involving estradiol induction of prostaglandin-E2. *J Neurosci* 22:8586–8596.
- Ambati J, Fowler BJ (2012) Mechanisms of Age-Related Macular Degeneration. *Neuron* 75:26–39.
- Anada RP, Wong KT, Malicdan MC, Goh KJ, Hayashi Y, Nishino I, Noguchi S (2014) Absence of beta-amyloid deposition in the central nervous system of a transgenic mouse model of distal myopathy with rimmed vacuoles. *Amyloid* 21:138–139.
- Andersen JK (2004) Oxidative stress in neurodegeneration: cause or consequence? *Nat Med* 10 Suppl:S18-25.
- Angata T, Varki A (2002) Chemical diversity in the sialic acids and related alpha-keto acids: an evolutionary perspective. *Chem Rev* 102:439–469.
- Argov Z, Yarom R (1984) "Rimmed vacuole myopathy"; sparing the quadriceps. A unique disorder in Iranian Jews. *J Neurol Sci* 64:33–43.
- Askanas V, Engel WK (1995) New advances in the understanding of sporadic inclusion-body myositis and hereditary inclusion-body myopathies. *Curr Opin Rheumatol* 7:486–496.
- Askew K, Li K, Olmos-Alonso A, Garcia-Moreno F, Liang Y, Richardson P, Tipton T, Chapman MA, Riecken K, Beccari S, Sierra A, Molnár Z, Cragg MS, Garaschuk O, Perry VH, Gomez-Nicola D (2017) Coupled Proliferation and Apoptosis Maintain the Rapid Turnover of Microglia in the Adult Brain. *Cell Rep* 18:391–405.
- Azizi G, Khannazer N, Mirshafiey A (2014) The Potential Role of Chemokines in Alzheimer's Disease Pathogenesis. *Am J Alzheimer's Dis Other Dementiasr* 29:415–425.
- Ba X (2016) Therapeutic effects of GM1 on Parkinson's disease in rats and its mechanism. *Int J Neurosci* 126:163–167.
- Bartels AL, Willemsen ATM, Doorduyn J, de Vries EFJ, Dierckx RA, Leenders KL (2010) [11C]-PK11195 PET: quantification of neuroinflammation and a monitor of anti-inflammatory treatment in Parkinson's disease? *Parkinsonism Relat Disord* 16:57–59.
- Baruzzo G, Hayer KE, Kim EJ, Di Camillo B, FitzGerald GA, Grant GR (2017) Simulation-based comprehensive benchmarking of RNA-seq aligners. *Nat Methods* 14:135–139.

- Benakis C, Garcia-Bonilla L, Iadecola C, Anrather J (2014) The role of microglia and myeloid immune cells in acute cerebral ischemia. *Front Cell Neurosci* 8:461.
- Bennett ML, Bennett FC, Liddel SA, Ajami B, Zamanian JL, Fernhoff NB, Mulinyawe SB, Bohlen CJ, Adil A, Tucker A, Weissman IL, Chang EF, Li G, Grant GA, Hayden Gephart MG, Barres BA (2016) New tools for studying microglia in the mouse and human CNS. *Proc Natl Acad Sci U S A* 113:E1738-46.
- Bhide GP, Colley KJ (2017) Sialylation of N-glycans: mechanism, cellular compartmentalization and function. *Histochem Cell Biol* 147:149–174.
- Bialas AR, Stevens B (2013) TGF- $\beta$  signaling regulates neuronal C1q expression and developmental synaptic refinement. *Nat Neurosci* 16:1773–1782.
- Bianchi I, Lleo A, Gershwin ME, Invernizzi P (2012) The X chromosome and immune associated genes. *J Autoimmun* 38:J187–J192.
- Bilimoria PM, Stevens B (2015) Microglia function during brain development: New insights from animal models. *Brain Res* 1617:7–17.
- Billadeau DD, Leibson PJ (2002) ITAMs versus ITIMs: striking a balance during cell regulation. *J Clin Invest* 109:161–168.
- Bishop NA, Lu T, Yankner BA (2010) Neural mechanisms of ageing and cognitive decline. *Nature* 464:529–535.
- Blatteis CM, Sehic E (1998) Cytokines and fever. *Ann N Y Acad Sci* 840:608–618.
- Block ML, Zecca L, Hong JS (2007) Microglia-mediated neurotoxicity: uncovering the molecular mechanisms. *Nat Rev Neurosci* 8:57–69.
- Bodea L-GL-G, Wang Y, Linnartz-Gerlach B, Kopatz J, Sinkkonen L, Musgrove R, Kaoma T, Muller A, Vallar L, Di Monte DA, Balling R, Neumann H (2014) Neurodegeneration by Activation of the Microglial Complement-Phagosome Pathway. *J Neurosci* 34:8546–8556.
- Bodine SC, Furlow JD (2015) Glucocorticoids and Skeletal Muscle. In: *Advances in experimental medicine and biology*, pp 145–176.
- Bogie JFJ, Stinissen P, Hendriks JJA (2014) Macrophage subsets and microglia in multiple sclerosis. *Acta Neuropathol* 128:191–213.
- Bonasera SJ, Arikath J, Boska MD, Chaudoin TR, DeKorver NW, Goulding EH, Hoke TA, Mojtahedzadeh V, Reyelts CD, Sajja B, Schenk AK, Tecott LH, Volden TA (2016) Age-related changes in cerebellar and hypothalamic function accompany non-microglial immune gene expression, altered synapse organization, and excitatory amino acid neurotransmission deficits. *Aging (Albany NY)* 8:2153–2181.
- Bonten E, van der Spoel A, Fornerod M, Grosveld G, d’Azzo A (1996) Characterization of human lysosomal neuraminidase defines the molecular basis of the metabolic storage disorder sialidosis. *Genes Dev* 10:3156–3169.
- Bork K, Gagiannis D, Orthmann A, Weidemann W, Kontou M, Reutter W, Horstkorte R (2007) Experimental approaches to interfere with the polysialylation of the neural cell adhesion molecule in vitro and in vivo. *J Neurochem* 103 Suppl:65–71.

- Boscher C, Dennis JW, Nabi IR (2011) Glycosylation, galectins and cellular signaling. *Curr Opin Cell Biol* 23:383–392.
- Boukhris A et al. (2013) Alteration of Ganglioside Biosynthesis Responsible for Complex Hereditary Spastic Paraplegia. *Am J Hum Genet* 93:118–123.
- Bowness P, Davies KA, Norsworthy PJ, Athanassiou P, Taylor-Wiedeman J, Borysiewicz LK, Meyer PA, Walport MJ (1994) Hereditary C1q deficiency and systemic lupus erythematosus. *QJM* 87:455–464.
- Boyden SE, Duncan AR, Estrella EA, Lidov HGW, Mahoney LJ, Katz JS, Kunkel LM, Kang PB (2011) Molecular diagnosis of hereditary inclusion body myopathy by linkage analysis and identification of a novel splice site mutation in GNE. *BMC Med Genet* 12:87.
- Brenneman LH, Maness PF (2010) NCAM in Neuropsychiatric and Neurodegenerative Disorders. In: *Advances in experimental medicine and biology*, pp 299–317.
- Brewer CF, Miceli MC, Baum LG (2002) Clusters, bundles, arrays and lattices: novel mechanisms for lectin-saccharide-mediated cellular interactions. *Curr Opin Struct Biol* 12:616–623.
- Brites D, Vaz AR (2014) Microglia centered pathogenesis in ALS: insights in cell interconnectivity. *Front Cell Neurosci* 8:117.
- Broccolini A, Pescatori M, D'Amico A, Sabino A, Silvestri G, Ricci E, Servidei S, Tonali PA, Mirabella M (2002) An Italian family with autosomal recessive inclusion-body myopathy and mutations in the GNE gene. *Neurology* 59:1808–1809.
- Brown GC, Vilalta A (2015) How microglia kill neurons. *Brain Res* 1628:288–297.
- Canzoniere D, Farioli-Vecchioli S, Conti F, Ciotti MT, Tata AM, Augusti-Tocco G, Mattei E, Lakshmana MK, Krizhanovsky V, Reeves SA, Giovannoni R, Castano F, Servadio A, Ben-Arie N, Tirone F (2004) Dual Control of Neurogenesis by PC3 through Cell Cycle Inhibition and Induction of Math1. *J Neurosci* 24:3355–3369.
- Carroll BJ, Curtis GC, Mendels J (1976) Neuroendocrine regulation in depression. II. Discrimination of depressed from nondepressed patients. *Arch Gen Psychiatry* 33:1051–1058.
- Celeste F V, Vilboux T, Ciccone C, de Dios JK, Malicdan MC V, Leoyklang P, McKew JC, Gahl WA, Carrillo-Carrasco N, Huizing M (2014) Mutation update for GNE gene variants associated with GNE myopathy. *Hum Mutat* 35:915–926.
- Cerqueira DR, Ferreira HS, Moiteiro ALBB, Fregoneze JB (2016) Physiology & Behavior Effects of interleukin-1 beta injections into the subfornical organ and median preoptic nucleus on sodium appetite, blood pressure and body temperature of sodium-depleted rats. *Physiol Behav* 163:149–160.
- Chamak B, Morandi V, Mallat M (1994) Brain macrophages stimulate neurite growth and regeneration by secreting thrombospondin. *J Neurosci Res* 38:221–233.
- Champaigne NL, Leroy JG, Kishnani PS, Decaestecker J, Steenkiste E, Chaubey A, Li J, Verslype C, Van Dorpe J, Pollard L, Goldstein JL, Libbrecht L, Basehore M, Chen N, Hu H, Wood T, Friez MJ, Huizing M, Stevenson RE (2016) New observation of sialuria

- prompts detection of liver tumor in previously reported patient. *Mol Genet Metab* 118:92–99.
- Chandra G, Cogswell JP, Miller LR, Godlevski MM, Stinnett SW, Noel SL, Kadwell SH, Kost TA, Gray JG (1995) Cyclic AMP signaling pathways are important in IL-1 beta transcriptional regulation. *J Immunol* 155:4535–4543.
- Cherubini E, Miles R (2015) The CA3 region of the hippocampus: how is it? What is it for? How does it do it? *Front Cell Neurosci* 9:19.
- Chiavegatto S, Sun J, Nelson RJ, Schnaar RL (2000) A Functional Role for Complex Gangliosides: Motor Deficits in GM2/GD2 Synthase Knockout Mice. *Exp Neurol* 166:227–234.
- Cho A, Hayashi YK, Monma K, Oya Y, Noguchi S, Nonaka I, Nishino I (2014) Mutation profile of the GNE gene in Japanese patients with distal myopathy with rimmed vacuoles (GNE myopathy). *J Neurol Neurosurg Psychiatry* 85:914–917.
- Cho A, Malicdan MC V., Miyakawa M, Nonaka I, Nishino I, Noguchi S (2017) Sialic acid deficiency is associated with oxidative stress leading to muscle atrophy and weakness in the GNE myopathy. *Hum Mol Genet* 274:19792–19798.
- Chou HH, Takematsu H, Diaz S, Iber J, Nickerson E, Wright KL, Muchmore EA, Nelson DL, Warren ST, Varki A (1998) A mutation in human CMP-sialic acid hydroxylase occurred after the Homo-Pan divergence. *Proc Natl Acad Sci U S A* 95:11751–11756.
- Cicchetti F, Brownell AL, Williams K, Chen YI, Livni E, Isacson O (2002) Neuroinflammation of the nigrostriatal pathway during progressive 6-OHDA dopamine degeneration in rats monitored by immunohistochemistry and PET imaging. *Eur J Neurosci* 15:991–998.
- Claude J, Linnartz-Gerlach B, Kudin AP, Kunz WS, Neumann H (2013) Microglial CD33-related Siglec-E inhibits neurotoxicity by preventing the phagocytosis-associated oxidative burst. *J Neurosci* 33:18270–18276.
- Close BE, Tao K, Colley KJ (2000) Polysialyltransferase-1 autopolysialylation is not requisite for polysialylation of neural cell adhesion molecule. *J Biol Chem* 275:4484–4491.
- Cohen M, Varki A (2010) The Sialome—Far More Than the Sum of Its Parts. *Omi A J Integr Biol* 14:455–464.
- Corradetti MN, Inoki K, Guan K-L (2005) The stress-induced proteins RTP801 and RTP801L are negative regulators of the mammalian target of rapamycin pathway. *J Biol Chem* 280:9769–9772.
- Cremer H, Lange R, Christoph A, Plomann M, Vopper G, Roes J, Brown R, Baldwin S, Kraemer P, Scheff S, Barthels D, Rajewsky K, Wille W (1994) Inactivation of the N-CAM gene in mice results in size reduction of the olfactory bulb and deficits in spatial learning. *Nature* 367:455–459.
- Cribbs DH, Berchtold NC, Perreau V, Coleman PD, Rogers J, Tenner AJ, Cotman CW (2012) Extensive innate immune gene activation accompanies brain aging, increasing vulnerability to cognitive decline and neurodegeneration: a microarray study. *J Neuroinflammation* 9:179.

- Crocker PR, Paulson JC, Varki A (2007) Siglecs and their roles in the immune system. *Nat Rev Immunol* 7:255–266.
- Cui L, Qu H, Xiao T, Zhao M, Jolkkonen J, Zhao C (2013) Stromal cell-derived factor-1 and its receptor CXCR4 in adult neurogenesis after cerebral ischemia. *Restor Neurol Neurosci* 31:239–251.
- Cunningham CL, Martínez-Cerdeño V, Noctor SC (2013) Microglia regulate the number of neural precursor cells in the developing cerebral cortex. *J Neurosci* 33:4216–4233.
- Curreli S, Arany Z, Gerardy-Schahn R, Mann D, Stamatou NM (2007) Polysialylated neuropilin-2 is expressed on the surface of human dendritic cells and modulates dendritic cell-T lymphocyte interactions. *J Biol Chem* 282:30346–30356.
- Daëron M (1997) Fc receptor biology. *Annu Rev Immunol* 15:203–234.
- Dai C, Liang D, Li H, Sasaki M, Dawson TM, Dawson VL (2010) Functional identification of neuroprotective molecules. *PLoS One* 5:e15008.
- Damani MR, Zhao L, Fontainhas AM, Amaral J, Fariss RN, Wong WT (2011) Age-related alterations in the dynamic behavior of microglia. *Aging Cell* 10:263–276.
- Damier P, Hirsch EC, Agid Y, Graybiel AM (1999) The substantia nigra of the human brain. II. Patterns of loss of dopamine-containing neurons in Parkinson's disease. *Brain* 122 (Pt 8):1437–1448.
- Dauer W, Przedborski S (2003) Parkinson's disease: mechanisms and models. *Neuron* 39:889–909.
- Day NK, Geiger H, McLean R, Michael A, Good RA (1973) C2 deficiency. Development of lupus erythematosus. *J Clin Invest* 52:1601–1607.
- De Castro E Silva E, Luz PA, Magrani J, Andrade L, Miranda N, Pereira V, Fregoneze JB (2006) Role of the central opioid system in the inhibition of water and salt intake induced by central administration of IL-1beta in rats. *Pharmacol Biochem Behav* 83:285–295.
- De Santa Barbara P, Bonneaud N, Boizet B, Desclozeaux M, Moniot B, Sudbeck P, Scherer G, Poulat F, Berta P (1998) Direct interaction of SRY-related protein SOX9 and steroidogenic factor 1 regulates transcription of the human anti-Müllerian hormone gene. *Mol Cell Biol* 18:6653–6665.
- De Strooper B, Karran E (2016) The Cellular Phase of Alzheimer's Disease. *Cell* 164:603–615.
- Di Giovanni G, Pessia M, Di Maio R (2012) Redox sensitivity of tyrosine hydroxylase activity and expression in dopaminergic dysfunction. *CNS Neurol Disord Drug Targets* 11:419–429.
- Dong X, You Y, Wu JQ (2015) Building an RNA Sequencing Transcriptome of the Central Nervous System. *Neuroscientist*:1073858415610541-.
- Dopp JM, Mackenzie-Graham A, Otero GC, Merrill JE (1997) Differential expression, cytokine modulation, and specific functions of type-1 and type-2 tumor necrosis factor receptors in rat glia. *J Neuroimmunol* 75:104–112.

- Eckhardt M, Bukalo O, Chazal G, Wang L, Goridis C, Schachner M, Gerardy-Schahn R, Cremer H, Dityatev A (2000) Mice deficient in the polysialyltransferase ST8SiaIV/PST-1 allow discrimination of the roles of neural cell adhesion molecule protein and polysialic acid in neural development and synaptic plasticity. *J Neurosci* 20:5234–5244.
- Eguchi H, Ikeda Y, Koyota S, Honke K, Suzuki K, Gutteridge JMC, Taniguchi N (2002) Oxidative damage due to copper ion and hydrogen peroxide induces GlcNAc-specific cleavage of an Asn-linked oligosaccharide. *J Biochem* 131:477–484.
- ElAli A, Rivest S (2016) Microglia Ontology and Signaling. *Front cell Dev Biol* 4:72.
- Enns GM, Seppala R, Musci TJ, Weisiger K, Ferrell LD, Wenger DA, Gahl WA, Packman S (2001) Clinical course and biochemistry of sialuria. *J Inherit Metab Dis* 24:328–336.
- Espinosa-Oliva AM, de Pablos RM, Villarán RF, Argüelles S, Venero JL, Machado A, Cano J (2011) Stress is critical for LPS-induced activation of microglia and damage in the rat hippocampus. *Neurobiol Aging* 32:85–102.
- Estes ML, McAllister AK (2015) Immune mediators in the brain and peripheral tissues in autism spectrum disorder. *Nat Rev Neurosci* 16:469–486.
- Fakhoury M (2016) Immune-mediated processes in neurodegeneration: where do we stand? *J Neurol* 263:1683–1701.
- Farioli-Vecchioli S, Saraulli D, Costanzi M, Pacioni S, Cinà I, Aceti M, Micheli L, Bacci A, Cestari V, Tirone F (2008) The Timing of Differentiation of Adult Hippocampal Neurons Is Crucial for Spatial Memory Goodell MA, ed. *PLoS Biol* 6:e246.
- Fernandez EJ, Lolis E (2002) Structure, function, and inhibition of chemokines. *Annu Rev Pharmacol Toxicol* 42:469–499.
- Finne J, Finne U, Deagostini-Bazin H, Goridis C (1983) Occurrence of alpha 2-8 linked polysialosyl units in a neural cell adhesion molecule. *Biochem Biophys Res Commun* 112:482–487.
- Fonken LK, Kitt MM, Gaudet AD, Barrientos RM, Watkins LR, Maier SF (2016) Diminished circadian rhythms in hippocampal microglia may contribute to age-related neuroinflammatory sensitization. *Neurobiol Aging* 47:102–112.
- Fonseca MI, Ager RR, Chu S-H, Yazan O, Sanderson SD, LaFerla FM, Taylor SM, Woodruff TM, Tenner AJ (2009) Treatment with a C5aR antagonist decreases pathology and enhances behavioral performance in murine models of Alzheimer's disease. *J Immunol* 183:1375–1383.
- Frade JM, Barde YA (1998) Microglia-derived nerve growth factor causes cell death in the developing retina. *Neuron* 20:35–41.
- Freeze HH (2013) Understanding human glycosylation disorders: biochemistry leads the charge. *J Biol Chem* 288:6936–6945.
- Frost JL, Schafer DP (2016) Microglia: Architects of the Developing Nervous System. *Trends Cell Biol* 26:587–597.
- Furukawa K, Ohmi Y, Ohkawa Y, Tajima O, Furukawa K (2014) Glycosphingolipids in the regulation of the nervous system. *Adv Neurobiol* 9:307–320.

- Gagiannis D, Orthmann A, Danßmann I, Schwarzkopf M, Weidemann W, Horstkorte R (2007) Reduced sialylation status in UDP-N-acetylglucosamine-2-epimerase/N-acetylmannosamine kinase (GNE)-deficient mice. *Glycoconj J* 24:125–130.
- Galeano B, Klootwijk R, Manoli I, Sun M, Ciccone C, Darvish D, Starost MF, Zervas PM, Hoffmann VJ, Hoogstraten-Miller S, Krasnewich DM, Gahl W a, Huizing M (2007) Mutation in the key enzyme of sialic acid biosynthesis causes severe glomerular proteinuria and is rescued by N-acetylmannosamine. *J Clin Invest* 117:1585–1594.
- Galuska SP, Rollenhagen M, Kaup M, Eggers K, Oltmann-Norden I, Schiff M, Hartmann M, Weinhold B, Hildebrandt H, Geyer R, Mühlenhoff M, Geyer H (2010) Synaptic cell adhesion molecule SynCAM 1 is a target for polysialylation in postnatal mouse brain. *Proc Natl Acad Sci U S A* 107:10250–10255.
- Gershov D, Kim S, Brot N, Elkon KB (2000) C-Reactive protein binds to apoptotic cells, protects the cells from assembly of the terminal complement components, and sustains an antiinflammatory innate immune response: implications for systemic autoimmunity. *J Exp Med* 192:1353–1364.
- Ginhoux F, Greter M, Leboeuf M, Nandi S, See P, Gokhan S, Mehler MF, Conway SJ, Ng LG, Stanley ER, Samokhvalov IM, Merad M (2010) Fate mapping analysis reveals that adult microglia derive from primitive macrophages. *Science* 330:841–845.
- Giulian D, Li J, Li X, George J, Rutecki PA (1994) The impact of microglia-derived cytokines upon gliosis in the CNS. *Dev Neurosci* 16:128–136.
- Giunti D, Parodi B, Cordano C, Uccelli A, Kerlero de Rosbo N (2014) Can we switch microglia's phenotype to foster neuroprotection? Focus on multiple sclerosis. *Immunology* 141:328–339.
- Glesse N, Monticeliolo OA, Mattevi VS, Brenol JCT, Xavier RM, da Silva GK, Dos Santos BP, Rucatti GG, Chies JAB (2011) Association of mannose-binding lectin 2 gene polymorphic variants with susceptibility and clinical progression in systemic lupus erythematosus. *Clin Exp Rheumatol* 29:983–990.
- Goswami K, Nandakumar DN, Koner BC, Bobby Z, Sen SK (2003) Oxidative changes and desialylation of serum proteins in hyperthyroidism. *Clin Chim Acta* 337:163–168.
- Gowda VK, Srinivasan VM, Benakappa N, Benakappa A (2017) Sialidosis Type 1 with a Novel Mutation in the Neuraminidase-1 (NEU1) Gene. *Indian J Pediatr* 84:403–404.
- Grabert K, Michoel T, Karavolos MH, Clohisey S, Baillie JK, Stevens MP, Freeman TC, Summers KM, McColl BW (2016) Microglial brain region-dependent diversity and selective regional sensitivities to aging. *Nat Neurosci* 19:504–516.
- Groot JCMJ De, Hendriksen EGJ, Smoorenburg GF (2005) Reduced expression of sialoglycoconjugates in the outer hair cell glycocalyx after systemic aminoglycoside administration. 205:68–82.
- Grover S, Arya R (2014) Role of UDP-N-Acetylglucosamine-2-Epimerase/N-Acetylmannosamine Kinase (GNE) in  $\beta$ 1-Integrin-Mediated Cell Adhesion. *Mol Neurobiol* 50:257–273.
- Grozovsky R, Begonja AJ, Liu K, Visner G, Hartwig JH, Falet H, Hoffmeister KM (2014) The Ashwell-Morell receptor regulates hepatic thrombopoietin production via JAK2-



- STAT3 signaling. *Nat Med* 21:47–54.
- Guo D, Zou J, Rensing N, Wong M (2017) In Vivo Two-Photon Imaging of Astrocytes in GFAP-GFP Transgenic Mice. Dunaevsky A, ed. *PLoS One* 12:e0170005.
- Gupta N, Brown KE, Milam AH (2003) Activated microglia in human retinitis pigmentosa, late-onset retinal degeneration, and age-related macular degeneration. *Exp Eye Res* 76:463–471.
- Hall BS, Moda RN, Liston C (2015) Neurobiology of Stress Glucocorticoid mechanisms of functional connectivity changes in stress-related neuropsychiatric disorders. *Neurobiol Stress* 1:174–183.
- Hanamsagar R, Alter MD, Block CS, Sullivan H, Bolton JL, Bilbo SD (2017) Generation of a microglial developmental index in mice and in humans reveals a sex difference in maturation and immune reactivity. *Glia* 65:1504–1520.
- Hanisch F, Weidemann W, Großmann M, Joshi PR, Holzhausen H-J, Stoltenburg G, Weis J, Zierz S, Horstkorte R (2013) Sialylation and muscle performance: sialic acid is a marker of muscle ageing. Arendt T, ed. *PLoS One* 8:e80520.
- Harvey H, Durant S (2014) The role of glial cells and the complement system in retinal diseases and Alzheimer’s disease: common neural degeneration mechanisms. *Exp Brain Res* 232:3363–3377.
- Hayakawa N, Kato H, Araki T (2007) Age-related changes of astrocytes, oligodendrocytes and microglia in the mouse hippocampal CA1 sector. *Mech Ageing Dev* 128:311–316.
- Heneka MT et al. (2015) Neuroinflammation in Alzheimer’s disease. *Lancet Neurol* 14:388–405.
- Heneka MT, Kummer MP, Latz E (2014) Innate immune activation in neurodegenerative disease. *Nat Rev Immunol* 14:463–477.
- Herrero M-T, Estrada C, Maatouk L, Vyas S (2015) Inflammation in Parkinson’s disease: role of glucocorticoids. *Front Neuroanat* 9:32.
- Hickox AE, Larsen E, Heinz MG, Shinobu L, Whitton JP (2017) Translational issues in cochlear synaptopathy. *Hear Res* 349:164–171.
- Hirasawa T, Ohsawa K, Imai Y, Ondo Y, Akazawa C, Uchino S, Kohsaka S (2005) Visualization of microglia in living tissues using Iba1-EGFP transgenic mice. *J Neurosci Res* 81:357–362.
- Ho C-H, Hsu S-P, Yang C-C, Lee Y-H, Chien C-T (2009) Sialic acid reduces acute endotoxemia-induced liver dysfunction in the rat. *Shock* 32:228–235.
- Hoffman S, Sorkin BC, White PC, Brackenbury R, Mailhammer R, Rutishauser U, Cunningham BA, Edelman GM (1982) Chemical characterization of a neural cell adhesion molecule purified from embryonic brain membranes. *J Biol Chem* 257:7720–7729.
- Hong S, Beja-Glasser VF, Nfonoyim BM, Frouin A, Li S, Ramakrishnan S, Merry KM, Shi Q, Rosenthal A, Barres BA, Lemere CA, Selkoe DJ, Stevens B (2016a) Complement and microglia mediate early synapse loss in Alzheimer mouse models. *Science* (80- )

8373:1–9.

- Hong S, Dissing-Olesen L, Stevens B (2016b) New insights on the role of microglia in synaptic pruning in health and disease. *Curr Opin Neurobiol* 36:128–134.
- Horstkorte R, Nöhring S, Wiechens N, Schwarzkopf M, Danker K, Reutter W, Lucka L (1999) Tissue expression and amino acid sequence of murine UDP-N-acetylglucosamine-2-epimerase/N-acetylmannosamine kinase. *Eur J Biochem* 260:923–927.
- Hotamisligil GS (2006) Inflammation and metabolic disorders. *Nature* 444:860–867.
- Huizing M, Carrillo-Carrasco N, Malicdan MC V., Noguchi S, Gahl WA, Mitrani-Rosenbaum S, Argov Z, Nishino I (2014) GNE myopathy: New name and new mutation nomenclature. *Neuromuscul Disord* 24:387–389.
- Humphries CE, Kohli MA, Nathanson L, Whitehead P, Beecham G, Martin E, Mash DC, Pericak-Vance MA, Gilbert J (2015) Integrated whole transcriptome and DNA methylation analysis identifies gene networks specific to late-onset Alzheimer's disease. *J Alzheimers Dis* 44:977–987.
- Ingiosi AM, Raymond RM, Pavlova MN, Opp MR (2015) Selective contributions of neuronal and astroglial interleukin-1 receptor 1 to the regulation of sleep. *Brain Behav Immun* 48:244–257.
- Ingram G, Hakobyan S, Robertson NP, Morgan BP (2009) Complement in multiple sclerosis: its role in disease and potential as a biomarker. *Clin Exp Immunol* 155:128–139.
- Inta D, Lang UE, Borgwardt S, Meyer-Lindenberg A, Gass P (2017) Microglia Activation and Schizophrenia: Lessons From the Effects of Minocycline on Postnatal Neurogenesis, Neuronal Survival and Synaptic Pruning. *Schizophr Bull* 43:493–496.
- Ito D, Imai Y, Ohsawa K, Nakajima K, Fukuuchi Y, Kohsaka S (1998) Microglia-specific localisation of a novel calcium binding protein, Iba1. *Brain Res Mol Brain Res* 57:1–9.
- James WM, Agnew WS (1987) Multiple oligosaccharide chains in the voltage-sensitive Na channel from *Electrophorus electricus*: evidence for alpha-2,8-linked polysialic acid. *Biochem Biophys Res Commun* 148:817–826.
- Jay CM, Levonyak N, Nemunaitis G, Maples PB, Nemunaitis J (2009) Hereditary Inclusion Body Myopathy (HIBM2). *Gene Regul Syst Bio* 3:181–190.
- Kalm M, Andreasson U, Björk-Eriksson T, Zetterberg H, Pekny M, Blennow K, Pekna M, Blomgren K (2016) C3 deficiency ameliorates the negative effects of irradiation of the young brain on hippocampal development and learning. *Oncotarget* 7:19382–19394.
- Kamerling JP, Strecker G, Farriaux JP, Dorland L, Haverkamp J, Vliegthart JF (1979) 2-Acetamidoglucal, a new metabolite isolated from the urine of a patient with sialuria. *Biochim Biophys Acta* 583:403–408.
- Karlstetter M, Kopatz J, Aslanidis A, Shahrzad A, Caramoy A, Linnartz-Gerlach B, Lin Y, Lückoff A, Fauser S, Düker K, Claude J, Wang Y, Ackermann J, Schmidt T, Hornung V, Skerka C, Langmann T, Neumann H (2017) Polysialic acid blocks mononuclear phagocyte reactivity, inhibits complement activation, and protects from vascular damage in the retina. *EMBO Mol Med* 9:154–166.

- Kassambara A, Mundt F (2017) factoextra: Extract and Visualize the Results of Multivariate Data Analyses.
- Kawai H, Allende ML, Wada R, Kono M, Sango K, Deng C, Miyakawa T, Crawley JN, Werth N, Bierfreund U, Sandhoff K, Proia RL (2001) Mice expressing only monosialoganglioside GM3 exhibit lethal audiogenic seizures. *J Biol Chem* 276:6885–6888.
- Keppler OT (1999) UDP-GlcNAc 2-Epimerase: A Regulator of Cell Surface Sialylation. *Science* (80- ) 284:1372–1376.
- Kettenmann H, Hanisch U-K, Noda M, Verkhratsky A (2011) Physiology of Microglia. *Physiol Rev* 91:461–553.
- Kiermaier E, Moussion C, Veldkamp CT, Gerardy-Schahn R, de Vries I, Williams LG, Chaffee GR, Phillips AJ, Freiberger F, Imre R, Taleski D, Payne RJ, Braun A, Förster R, Mechtler K, Mühlenhoff M, Volkman BF, Sixt M (2016) Polysialylation controls dendritic cell trafficking by regulating chemokine recognition. *Science* 351:186–190.
- Kircheis R, Kircheis L, Oshima H, Kohchi C, Soma G, Mizuno D (1996) Selective lysis of early embryonic cells by the alternative pathway of complement--a possible mechanism for programmed cell death in embryogenesis. *In Vivo* 10:389–403.
- Klemke RL, Weitlauf HM (1993) Comparison of the ontogeny of specific cell surface determinants on normal and delayed implanting mouse embryos. *J Reprod Fertil* 99:167–172.
- Kleniewska P, Pawliczak R (2017) Influence of Synbiotics on Selected Oxidative Stress Parameters. *Oxid Med Cell Longev* 2017:1–8.
- Kolev M, Kemper C (2017) Keeping It All Going-Complement Meets Metabolism. *Front Immunol* 8:1.
- Kornfeld S, Kornfeld R, Neufeld EF, O'Brien PJ (1964) The feedback control of sugar nucleotide biosynthesis in liver. *Proc Natl Acad Sci U S A* 52:371–379.
- Koyama R, Ikegaya Y (2015) Microglia in the pathogenesis of autism spectrum disorders. *Neurosci Res* 100:1–5.
- Kracun I, Rosner H, Drnovsek V, Heffer-Lauc M, Cosović C, Lauc G (1991) Human brain gangliosides in development, aging and disease. *Int J Dev Biol* 35:289–295.
- Kraft AD, McPherson CA, Harry GJ (2016) Association Between Microglia, Inflammatory Factors, and Complement with Loss of Hippocampal Mossy Fiber Synapses Induced by Trimethyltin. *Neurotox Res*.
- Kreuzmann D, Horstkorte R, Kohla G, Kannicht C, Bennmann D, Thate A, Bork K (2016) Increased Polysialylation of the Neural Cell Adhesion Molecule in a Transgenic Mouse Model of Sialuria. *Chembiochem*.
- Kuhn HG, Dickinson-Anson H, Gage FH (1996) Neurogenesis in the dentate gyrus of the adult rat: age-related decrease of neuronal progenitor proliferation. *J Neurosci* 16:2027–2033.
- Kuno R, Wang J, Kawanokuchi J, Takeuchi H, Mizuno T, Suzumura A (2005) Autocrine

- activation of microglia by tumor necrosis factor- $\alpha$ . *J Neuroimmunol* 162:89–96.
- Lawson LJ, Perry VH, Dri P, Gordon S (1990) Heterogeneity in the distribution and morphology of microglia in the normal adult mouse brain. *Neuroscience* 39:151–170.
- Lawson LJ, Perry VH, Gordon S (1992) Turnover of resident microglia in the normal adult mouse brain. *Neuroscience* 48:405–415.
- Ledeboer A, Brevé JJ, Poole S, Tilders FJ, Van Dam AM (2000) Interleukin-10, interleukin-4, and transforming growth factor- $\beta$  differentially regulate lipopolysaccharide-induced production of pro-inflammatory cytokines and nitric oxide in co-cultures of rat astroglial and microglial cells. *Glia* 30:134–142.
- Lee CK, Weindruch R, Prolla TA (2000) Gene-expression profile of the ageing brain in mice. *Nat Genet* 25:294–297.
- Lee SC, Liu W, Dickson DW, Brosnan CF, Berman JW (1993) Cytokine production by human fetal microglia and astrocytes. Differential induction by lipopolysaccharide and IL-1  $\beta$ . *J Immunol* 150:2659–2667.
- Lenz KM, McCarthy MM (2015) A starring role for microglia in brain sex differences. *Neurosci* 21:306–321.
- Leroy JG, Seppala R, Huizing M, Dacremont G, De Simpel H, Van Coster RN, Orvisky E, Krasnewich DM, Gahl WA (2001) Dominant inheritance of sialuria, an inborn error of feedback inhibition. *Am J Hum Genet* 68:1419–1427.
- Leza JC, García-Bueno B, Bioque M, Arango C, Parellada M, Do K, O'Donnell P, Bernardo M (2015) Inflammation in schizophrenia: A question of balance. *Neurosci Biobehav Rev* 55:612–626.
- Li J et al. (2015) Desialylation is a mechanism of Fc-independent platelet clearance and a therapeutic target in immune thrombocytopenia. *Nat Commun* 6:7737.
- Liao Y, Smyth GK, Shi W (2013) The Subread aligner: fast, accurate and scalable read mapping by seed-and-vote. *Nucleic Acids Res* 41:e108.
- Liberman LD, Liberman MC, Liberman MC (2015) Dynamics of cochlear synaptopathy after acoustic overexposure. *J Assoc Res Otolaryngol* 16:205–219.
- Linnartz-Gerlach B, Mathews M, Neumann H (2014) Sensing the neuronal glycocalyx by glial sialic acid binding immunoglobulin-like lectins. *Neuroscience* 275C:113–124.
- Linnartz-Gerlach B, Schuy C, Shahraz A, Tenner AJ, Neumann H (2016) Sialylation of neurites inhibits complement-mediated macrophage removal in a human macrophage-neuron Co-Culture System. *Glia* 64:35–47.
- Linnartz B, Bodea L, Neumann H (2012a) Microglial carbohydrate-binding receptors for neural repair. *Cell Tissue Res* 349:215–227.
- Linnartz B, Kopatz J, Tenner AJ, Neumann H (2012b) Sialic Acid on the Neuronal Glycocalyx Prevents Complement C1 Binding and Complement Receptor-3-Mediated Removal by Microglia. *J Neurosci* 32:946–952.
- Linnartz B, Neumann H (2013) Microglial activatory (immunoreceptor tyrosine-based activation motif)- and inhibitory (immunoreceptor tyrosine-based inhibition motif)-

- signaling receptors for recognition of the neuronal glycocalyx. *Glia* 61:37–46.
- Liston C, Cichon JM, Jeanneteau F, Jia Z, Chao M V, Gan W (2013) Circadian glucocorticoid oscillations promote learning- dependent synapse formation and maintenance. *Nat Publ Gr* 16:698–705.
- Loeffler DA, Camp DM, Conant SB (2006) Complement activation in the Parkinson's disease substantia nigra: an immunocytochemical study. *J Neuroinflammation* 3:29.
- Loeffler DA, DeMaggio AJ, Juneau PL, Havaich MK, LeWitt PA (1994) Effects of enhanced striatal dopamine turnover in vivo on glutathione oxidation. *Clin Neuropharmacol* 17:370–379.
- Long JM, Kalehua AN, Muth NJ, Calhoun ME, Jucker M, Hengemihle JM, Ingram DK, Mouton PR (1998) Stereological analysis of astrocyte and microglia in aging mouse hippocampus. *Neurobiol Aging* 19:497–503.
- Love MI, Huber W, Anders S (2014) Moderated estimation of fold change and dispersion for RNA-seq data with DESeq2. *Genome Biol* 15:550.
- Lull ME, Block ML (2010) Microglial activation and chronic neurodegeneration. *Neurotherapeutics* 7:354–365.
- Luz PA, Andrade L, Miranda N, Pereira V, Fregoneze J, De Castro e Silva E (2006) Inhibition of water intake by the central administration of IL-1 $\beta$  in rats: Role of the central opioid system. *Neuropeptides* 40:85–94.
- Luz PA, Saraiva R, Almeida T, Fregoneze JB, De Castro e Silva E (2009) Blockade of central kappa-opioid receptors inhibits the antidipsogenic effect of interleukin-1beta. *Neuropeptides* 43:93–103.
- Machado V, Zöller T, Attaai A, Spittau B (2016) Microglia-Mediated Neuroinflammation and Neurotrophic Factor-Induced Protection in the MPTP Mouse Model of Parkinson's Disease-Lessons from Transgenic Mice. *Int J Mol Sci* 17:151.
- Malagelada C, Ryu EJ, Biswas SC, Jackson-Lewis V, Greene LA (2006) RTP801 is elevated in Parkinson brain substantia nigral neurons and mediates death in cellular models of Parkinson's disease by a mechanism involving mammalian target of rapamycin inactivation. *J Neurosci* 26:9996–10005.
- Malicdan MC V., Noguchi S, Nonaka I, Hayashi YK, Nishino I (2007) A Gne knockout mouse expressing human GNE D176V mutation develops features similar to distal myopathy with rimmed vacuoles or hereditary inclusion body myopathy. *Hum Mol Genet* 16:2669–2682.
- Malicdan MC V, Noguchi S, Hayashi YK, Nishino I (2008) Muscle weakness correlates with muscle atrophy and precedes the development of inclusion body or rimmed vacuoles in the mouse model of DMRV/hIBM. *Physiol Genomics* 35:106–115.
- Malicdan MC V, Noguchi S, Hayashi YK, Nonaka I, Nishino I (2009) Prophylactic treatment with sialic acid metabolites precludes the development of the myopathic phenotype in the DMRV-hIBM mouse model. *Nat Med* 15:690–695.
- Mangold CA, Wronowski B, Du M, Masser DR, Hadad N, Bixler G V., Brucklacher RM, Ford MM, Sonntag WE, Freeman WM (2017) Sexually divergent induction of

- microglial-associated neuroinflammation with hippocampal aging. *J Neuroinflammation* 14:141.
- Marín-Teva JL, Dusart I, Colin C, Gervais A, van Rooijen N, Mallat M (2004) Microglia promote the death of developing Purkinje cells. *Neuron* 41:535–547.
- Markiewski MM, DeAngelis RA, Strey CW, Foukas PG, Gerard C, Gerard N, Wetsel RA, Lambris JD (2009) The regulation of liver cell survival by complement. *J Immunol* 182:5412–5418.
- Mayilyan KR (2012) Complement genetics, deficiencies, and disease associations. *Protein Cell* 3:487–496.
- Mayilyan KR, Weinberger DR, Sim RB (2008) The complement system in schizophrenia. *Drug News Perspect* 21:200.
- Mazaheri F, Breus O, Durdu S, Haas P, Wittbrodt J, Gilmour D, Peri F (2014) Distinct roles for BAI1 and TIM-4 in the engulfment of dying neurons by microglia. *Nat Commun* 5:4046.
- McCarthy MM (2008) Estradiol and the Developing Brain. *Physiol Rev* 88:91–134.
- Meesmann HM, Fehr E-M, Kierschke S, Herrmann M, Bilyy R, Heyder P, Blank N, Krienke S, Lorenz H-M, Schiller M (2010) Decrease of sialic acid residues as an eat-me signal on the surface of apoptotic lymphocytes. *J Cell Sci* 123:3347–3356.
- Michailidou I, Naessens DMP, Hametner S, Guldenaar W, Kooi E-J, Geurts JJG, Baas F, Lassmann H, Ramaglia V (2017) Complement C3 on microglial clusters in multiple sclerosis occur in chronic but not acute disease: Implication for disease pathogenesis. *Glia* 65:264–277.
- Miller DB, Ali SF, O’Callaghan JP, Laws SC (1998) The impact of gender and estrogen on striatal dopaminergic neurotoxicity. *Ann N Y Acad Sci* 844:153–165.
- Miller PD, Chung WW, Lagenaur CF, DeKosky ST (1993) Regional distribution of neural cell adhesion molecule (N-CAM) and L1 in human and rodent hippocampus. *J Comp Neurol* 327:341–349.
- Min K-J, Pyo H-K, Yang M-S, Ji K-A, Jou I, Joe E-H (2004) Gangliosides activate microglia via protein kinase C and NADPH oxidase. *Glia* 48:197–206.
- Mirabella M, Christodoulou K, Di Giovanni S, Ricci E, Tonali P, Servidei S (2000) An Italian family with autosomal recessive quadriceps-sparing inclusion-body myopathy (ARQS-IBM) linked to chromosome 9p1. *Neurol Sci* 21:99–102.
- Miyagi T, Takahashi K, Moriya S, Hata K, Yamamoto K, Wada T, Yamaguchi K, Shiozaki K (2012) Altered Expression of Sialidases in Human Cancer. In: *Advances in experimental medicine and biology*, pp 257–267.
- Miyagi T, Yamaguchi K (2012) Mammalian sialidases: Physiological and pathological roles in cellular functions. *Glycobiology* 22:880–896.
- Mizuno Y, Hori S, Kakizuka A, Okamoto K (2003) Vacuole-creating protein in neurodegenerative diseases in humans. *Neurosci Lett* 343:77–80.
- Mokhtari R, Lachman HM (2016) The Major Histocompatibility Complex (MHC) in

- Schizophrenia: A Review. *J Clin Cell Immunol* 7.
- Moniot B, Declosmenil F, Barrionuevo F, Scherer G, Aritake K, Malki S, Marzi L, Cohen-Solal A, Georg I, Klattig J, Englert C, Kim Y, Capel B, Eguchi N, Urade Y, Boizet-Bonhoure B, Poulat F (2009) The PGD2 pathway, independently of FGF9, amplifies SOX9 activity in Sertoli cells during male sexual differentiation. *Development* 136:1813–1821.
- Mori-Yoshimura M, Monma K, Suzuki N, Aoki M, Kumamoto T, Tanaka K, Tomimitsu H, Nakano S, Sonoo M, Shimizu J, Sugie K, Nakamura H, Oya Y, Hayashi YK, Malicdan MC V, Noguchi S, Murata M, Nishino I (2012) Heterozygous UDP-GlcNAc 2-epimerase and N-acetylmannosamine kinase domain mutations in the GNE gene result in a less severe GNE myopathy phenotype compared to homozygous N-acetylmannosamine kinase domain mutations. *J Neurol Sci* 318:100–105.
- Morimoto A, Ono T, Watanabe T, Murakami N (1986) Activation of brain regions of rats during fever. *Brain Res* 381:100–105.
- Morrison JH, Baxter MG (2012) The ageing cortical synapse: hallmarks and implications for cognitive decline. *Nat Rev Neurosci* 13:240–250.
- Morrison JH, Hof PR (2002) Selective vulnerability of corticocortical and hippocampal circuits in aging and Alzheimer's disease. *Prog Brain Res* 136:467–486.
- Mouton PR, Long JM, Lei D-L, Howard V, Jucker M, Calhoun ME, Ingram DK (2002) Age and gender effects on microglia and astrocyte numbers in brains of mice. *Brain Res* 956:30–35.
- Mühlenhoff M, Eckhardt M, Bethe A, Frosch M, Gerardy-Schahn R (1996) Autocatalytic polysialylation of polysialyltransferase-1. *EMBO J* 15:6943–6950.
- Murakami N, Ihara Y, Nonaka I (1995) Muscle fiber degeneration in distal myopathy with rimmed vacuole formation. *Acta Neuropathol* 89:29–34.
- Murnyák B, Bodoki L, Vincze M, Griger Z, Csonka T, Szepesi R, Kurucz A, Dankó K, Hortobágyi T (2015) Inclusion body myositis - pathomechanism and lessons from genetics. *Open Med (Warsaw, Poland)* 10:188–193.
- Murphy K, Travers P, Walport M (2008) *Janeway's Immunobiology*, 7th ed. CT, United States: Garland Science, Taylor & Francis Inc.
- Murray HC, Low VF, Swanson ME V, Dieriks B V., Turner C, Faull RLM, Curtis MA (2016) Distribution of PSA-NCAM in normal, Alzheimer's and Parkinson's disease human brain. *Neuroscience* 330:359–375.
- Muscari A, Antonelli S, Bianchi G, Cavrini G, Dapporto S, Ligabue A, Ludovico C, Magalotti D, Poggiopollini G, Zoli M, Pianoro Study Group (2007) Serum C3 is a stronger inflammatory marker of insulin resistance than C-reactive protein, leukocyte count, and erythrocyte sedimentation rate: comparison study in an elderly population. *Diabetes Care* 30:2362–2368.
- Nadeau S, Rivest S (2000) Role of microglial-derived tumor necrosis factor in mediating CD14 transcription and nuclear factor kappa B activity in the brain during endotoxemia. *J Neurosci* 20:3456–3468.

- Nagata K, Nakajima K, Takemoto N, Saito H, Kohsaka S (1993) Microglia-derived plasminogen enhances neurite outgrowth from explant cultures of rat brain. *Int J Dev Neurosci* 11:227–237.
- Netea MG, Kullberg BJ, Van der Meer JW (2000) Circulating cytokines as mediators of fever. *Clin Infect Dis* 31 Suppl 5:S178-84.
- Neumann H, Kotter MR, Franklin RJM (2009) Debris clearance by microglia: An essential link between degeneration and regeneration. *Brain* 132:288–295.
- Nimmerjahn A, Kirchhoff F, Helmchen F (2005) Resting microglial cells are highly dynamic surveillants of brain parenchyma in vivo. *Neuroforum* 11:95–96.
- Nissen JC (2017) Microglial Function across the Spectrum of Age and Gender. *Int J Mol Sci* 18:561.
- Nonaka I, Sunohara N, Ishiura S, Satoyoshi E (1981) Familial distal myopathy with rimmed vacuole and lamellar (myeloid) body formation. *J Neurol Sci* 51:141–155.
- Norden DM, Godbout JP (2013) Review: microglia of the aged brain: primed to be activated and resistant to regulation. *Neuropathol Appl Neurobiol* 39:19–34.
- Norton WT, Poduslo SE (1973) Myelination in rat brain: changes in myelin composition during brain maturation. *J Neurochem* 21:759–773.
- Nozaki M, Raisler BJ, Sakurai E, Sarma JV, Barnum SR, Lambris JD, Chen Y, Zhang K, Ambati BK, Baffi JZ, Ambati J (2006) Drusen complement components C3a and C5a promote choroidal neovascularization. *Proc Natl Acad Sci U S A* 103:2328–2333.
- Ohmi Y, Ohkawa Y, Tajima O, Sugiura Y, Furukawa K, Furukawa K (2014) Ganglioside deficiency causes inflammation and neurodegeneration via the activation of complement system in the spinal cord. *J Neuroinflammation* 11:61.
- Ohmi Y, Tajima O, Ohkawa Y, Yamauchi Y, Sugiura Y, Furukawa K, Furukawa K (2011) Gangliosides are essential in the protection of inflammation and neurodegeneration via maintenance of lipid rafts: elucidation by a series of ganglioside-deficient mutant mice. *J Neurochem* 116:926–935.
- Ohtsubo K, Marth JD (2006) Glycosylation in cellular mechanisms of health and disease. *Cell* 126:855–867.
- Oikawa N, Matsubara T, Fukuda R, Yasumori H (2015) Imbalance in Fatty-Acid-Chain Length of Gangliosides Triggers Alzheimer Amyloid Deposition in the Precuneus. :1–19.
- Orr CF, Rowe DB, Halliday GM (2002) An inflammatory review of Parkinson's disease. *Prog Neurobiol* 68:325–340.
- Ota KT, Liu R-J, Voleti B, Maldonado-Aviles JG, Duric V, Iwata M, Dutheil S, Duman C, Boikess S, Lewis DA, Stockmeier CA, DiLeone RJ, Rex C, Aghajanian GK, Duman RS (2014) REDD1 is essential for stress-induced synaptic loss and depressive behavior. *Nat Med* 20:531–535.
- Öz P, Saybaşı H (2017) Data on pharmacological applications and hypothermia protection against in vitro oxygen-glucose-deprivation-related neurodegeneration of adult rat CA1



- region. *Data Br* 10:373–376.
- Padurariu M, Ciobica A, Mavroudis I, Fotiou D, Baloyannis S (2012) Hippocampal neuronal loss in the CA1 and CA3 areas of Alzheimer's disease patients. *Psychiatr Danub* 24:152–158.
- Painbeni T, Gamelin E, Cailleux A, Le Bouil A, Boisdron-Celle M, Daver A, Larra F, Allain P (1997) Plasma sialic acid as a marker of the effect of the treatment on metastatic colorectal cancer. *Eur J Cancer* 33:2216–2220.
- Palmano K, Rowan A, Guillermo R, Guan J, Mcjarrow P (2015) The Role of Gangliosides in Neurodevelopment. :3891–3913.
- Pan B, Fromholt SE, Hess EJ, Crawford TO, Griffin JW, Sheikh KA, Schnaar RL (2005) Myelin-associated glycoprotein and complementary axonal ligands, gangliosides, mediate axon stability in the CNS and PNS: neuropathology and behavioral deficits in single- and double-null mice. *Exp Neurol* 195:208–217.
- Pan X, De Aragão CDBP, Velasco-Martin JP, Priestman DA, Wu HY, Takahashi K, Yamaguchi K, Sturiale L, Garozzo D, Platt FM, Lamarche-Vane N, Morales CR, Miyagi T, Pshezhetsky A V. (2017) Neuraminidases 3 and 4 regulate neuronal function by catabolizing brain gangliosides. *FASEB J* 31:3467–3483.
- Paolicelli RC, Bisht K, Tremblay M-È (2014) Fractalkine regulation of microglial physiology and consequences on the brain and behavior. *Front Cell Neurosci* 8:129.
- Paolicelli RC, Bolasco G, Pagani F, Maggi L, Scianni M, Panzanelli P, Giustetto M, Ferreira TA, Guiducci E, Dumas L, Ragozzino D, Gross CT (2011) Synaptic pruning by microglia is necessary for normal brain development. *Science* 333:1456–1458.
- Park KW, Baik HH, Jin BK (2008) Interleukin-4-induced oxidative stress via microglial NADPH oxidase contributes to the death of hippocampal neurons in vivo. *Curr Aging Sci* 1:192–201.
- Paulson JC, Colley KJ (1989) Glycosyltransferases. Structure, localization, and control of cell type-specific glycosylation. *J Biol Chem* 264:17615–17618.
- Pawluczyk IZA, Ghaderi Najafabadi M, Patel S, Desai P, Vashi D, Saleem MA, Topham PS (2014) Sialic acid attenuates puromycin aminonucleoside-induced desialylation and oxidative stress in human podocytes. *Exp Cell Res* 320:258–268.
- Pearce OMT, Läubli H (2016) Sialic acids in cancer biology and immunity. *Glycobiology* 26:111–128.
- Peiser L, Mukhopadhyay S, Gordon S (2002) Scavenger receptors in innate immunity. *Curr Opin Immunol* 14:123–128.
- Perry VH, Holmes C (2014) Microglial priming in neurodegenerative disease. *Nat Rev Neurol* 10:217–224.
- Petrelli F, Pucci L, Bezzi P (2016) Astrocytes and Microglia and Their Potential Link with Autism Spectrum Disorders. *Front Cell Neurosci* 10:21.
- Pickering MC, Botto M, Taylor PR, Lachmann PJ, Walport MJ (2000) Systemic lupus erythematosus, complement deficiency, and apoptosis. *Adv Immunol* 76:227–324.

- Prinz M, Priller J (2014) Microglia and brain macrophages in the molecular age: from origin to neuropsychiatric disease. *Nat Rev Neurosci* 15:300–312.
- Przedborski S, Przedborski S, Naini AB, Naini AB, Akram M, Akram M (2001) The parkinson toxin 1-methyl-4-phenyl-1,2,3,6-tetrahydropyridine (MPTP): a technical review of its utility and safety. *J Neurochem*:1265–1274.
- Qiu J, Liu X, Li X, Zhang X, Han P, Zhou H, Shao L, Hou Y, Min Y, Kong Z, Wang Y, Wei Y, Liu X, Ni H, Peng J, Hou M (2016) CD8+ T cells induce platelet clearance in the liver via platelet desialylation in immune thrombocytopenia. *Sci Rep* 6:27445.
- Rachmilewitz J (2010) Glycosylation: an intrinsic sign of “Danger.” *Self Nonsel* 1:250–254.
- R Core Team (2017) R: A language and environment for statistical computing.
- Radford RA, Morsch M, Rayner SL, Cole NJ, Pountney DL, Chung RS (2015) The established and emerging roles of astrocytes and microglia in amyotrophic lateral sclerosis and frontotemporal dementia. *Front Cell Neurosci* 9:414.
- Raman R, Sasisekharan V, Sasisekharan R (2005) Structural insights into biological roles of protein-glycosaminoglycan interactions. *Chem Biol* 12:267–277.
- Ramirez AI, de Hoz R, Salobar-Garcia E, Salazar JJ, Rojas B, Ajoy D, López-Cuenca I, Rojas P, Triviño A, Ramírez JM (2017) The Role of Microglia in Retinal Neurodegeneration: Alzheimer’s Disease, Parkinson, and Glaucoma. *Front Aging Neurosci* 9:214.
- Ramprasad MP, Terpstra V, Kondratenko N, Quehenberger O, Steinberg D (1996) Cell surface expression of mouse macrosialin and human CD68 and their role as macrophage receptors for oxidized low density lipoprotein. *Proc Natl Acad Sci U S A* 93:14833–14838.
- Ransohoff RM, El Khoury J (2015) Microglia in Health and Disease. *Cold Spring Harb Perspect Biol* 8:a020560.
- Ransohoff RM, Perry VH (2009) Microglial Physiology: Unique Stimuli, Specialized Responses. *Annu Rev Immunol* 27:119–145.
- Rapport MM (1990) Implications of altered brain ganglioside profiles in amyotrophic lateral sclerosis (ALS). *Acta Neurobiol Exp (Wars)* 50:505–513.
- Reinke SO, Eidenschink C, Jay CM, Hinderlich S (2009) Biochemical characterization of human and murine isoforms of UDP-N-acetylglucosamine 2-epimerase/N-acetylmannosamine kinase (GNE). *Glycoconj J* 26:415–422.
- Ricci E, Broccolini A, Gidaro T, Morosetti R, Gliubizzi C, Frusciante R, Di Lella GM, Tonali PA, Mirabella M (2006) NCAM is hyposialylated in hereditary inclusion body myopathy due to GNE mutations. *Neurology* 66:755–758.
- Ricklin D, Hajishengallis G, Yang K, Lambris JD (2010) Complement: a key system for immune surveillance and homeostasis. *Nat Immunol* 11:785–797.
- Rofagha S, Bhisitkul RB, Boyer DS, Sadda SR, Zhang K, SEVEN-UP Study Group (2013) Seven-Year Outcomes in Ranibizumab-Treated Patients in ANCHOR, MARINA, and HORIZON. *Ophthalmology* 120:2292–2299.

- Ros-Bernal F, Hunot S, Herrero MT, Parnadeau S, Corvol J-C, Lu L, Alvarez-Fischer D, Carrillo-de Sauvage MA, Saurini F, Coussieu C, Kinugawa K, Prigent A, Hoglinger G, Hamon M, Tronche F, Hirsch EC, Vyas S (2011) Microglial glucocorticoid receptors play a pivotal role in regulating dopaminergic neurodegeneration in parkinsonism. *Proc Natl Acad Sci* 108:6632–6637.
- Rothbard JB, Brackenbury R, Cunningham BA, Edelman GM (1982) Differences in the carbohydrate structures of neural cell-adhesion molecules from adult and embryonic chicken brains. *J Biol Chem* 257:11064–11069.
- RStudio Team (2016) RStudio: Integrated Development for R.
- Rudd PM, Merry AH, Wormald MR, Dwek RA (2002) Glycosylation and prion protein. *Curr Opin Struct Biol* 12:578–586.
- Saito F, Tomimitsu H, Arai K, Nakai S, Kanda T, Shimizu T, Mizusawa H, Matsumura K (2004) A Japanese patient with distal myopathy with rimmed vacuoles: missense mutations in the epimerase domain of the UDP-N-acetylglucosamine 2-epimerase/N-acetylmannosamine kinase (GNE) gene accompanied by hyposialylation of skeletal muscle glycoproteins. *Neuromuscul Disord* 14:158–161.
- Sato C, Hane M, Kitajima K (2016) Relationship between ST8SIA2, polysialic acid and its binding molecules, and psychiatric disorders. *Biochim Biophys Acta* 1860:1739–1752.
- Sato C, Kitajima K (2013) Disialic, oligosialic and polysialic acids: distribution, functions and related disease. *J Biochem* 154:115–136.
- Sato Y, Endo T (2010) Alteration of brain glycoproteins during aging. *Geriatr Gerontol Int* 10 Suppl 1:S32-40.
- Satoh J ichi, Kino Y, Asahina N, Takitani M, Miyoshi J, Ishida T, Saito Y (2015) TMEM119 marks a subset of microglia in the human brain. *Neuropathology* 36:n/a-n/a.
- Saville JT, Thai HN, Lehmann RJ, Derrick-Roberts ALK, Fuller M (2017) Subregional brain distribution of simple and complex glycosphingolipids in the mucopolysaccharidosis type I (Hurler syndrome) mouse: impact of diet. *J Neurochem*:1–9.
- Schafer DP, Lehrman EK, Kautzman AG, Koyama R, Mardinly AR, Yamasaki R, Ransohoff RM, Greenberg ME, Barres BA, Stevens B (2012) Microglia sculpt postnatal neural circuits in an activity and complement-dependent manner. *Neuron* 74:691–705.
- Schakman O, Kalista S, Barbé C, Loumaye A, Thissen JP (2013) Glucocorticoid-induced skeletal muscle atrophy. *Int J Biochem Cell Biol* 45:2163–2172.
- Schauer R (2000) Achievements and challenges of sialic acid research. *Glycoconj J* 17:485–499.
- Schauer R (2009) Sialic acids as regulators of molecular and cellular interactions. *Curr Opin Struct Biol* 19:507–514.
- Schedin-Weiss S, Winblad B, Tjernberg LO (2014) The role of protein glycosylation in Alzheimer disease. *FEBS J* 281:46–62.
- Schnaar RL (2004) Glycolipid-mediated cell-cell recognition in inflammation and nerve regeneration. *Arch Biochem Biophys* 426:163–172.

- Schnaar RL (2016) Gangliosides of the vertebrate nervous system. *J Mol Biol* 428:3325–3336.
- Schnaar RL, Gerardy-Schahn R, Hildebrandt H (2014) Sialic acids in the brain: gangliosides and polysialic acid in nervous system development, stability, disease, and regeneration. *Physiol Rev* 94:461–518.
- Scholz R, Sobotka M, Caramoy A, Stempf T, Moehle C, Langmann T (2015) Minocycline counter-regulates pro-inflammatory microglia responses in the retina and protects from degeneration. *J Neuroinflammation* 12:209.
- Schwarzkopf M, Knobloch K-P, Rohde E, Hinderlich S, Wiechens N, Lucka L, Horak I, Reutter W, Horstkorte R (2002) Sialylation is essential for early development in mice. *Proc Natl Acad Sci U S A* 99:5267–5270.
- Sekar A, Bialas AR, de Rivera H, Davis A, Hammond TR, Kamitaki N, Tooley K, Presumey J, Baum M, Van Doren V, Genovese G, Rose SA, Handsaker RE, Daly MJ, Carroll MC, Stevens B, McCarroll SA (2016) Schizophrenia risk from complex variation of complement component 4. *Nature*:1–17.
- Seki T, Arai Y (1993) Distribution and possible roles of the highly polysialylated neural cell adhesion molecule (NCAM-H) in the developing and adult central nervous system. *Neurosci Res* 17:265–290.
- Seppala R, Lehto VP, Gahl WA (1999) Mutations in the human UDP-N-acetylglucosamine 2-epimerase gene define the disease sialuria and the allosteric site of the enzyme. *Am J Hum Genet* 64:1563–1569.
- Sheikh KA, Sun J, Liu Y, Kawai H, Crawford TO, Proia RL, Griffin JW, Schnaar RL (1999) Mice lacking complex gangliosides develop Wallerian degeneration and myelination defects. *Proc Natl Acad Sci U S A* 96:7532–7537.
- Shi Q, Colodner KJ, Matousek SB, Merry K, Hong S, Kenison JE, Frost JL, Le KX, Li S, Dodart J-C, Caldarone BJ, Stevens B, Lemere CA (2015) Complement C3-Deficient Mice Fail to Display Age-Related Hippocampal Decline. *J Neurosci* 35:13029–13042.
- Shigemoto-Mogami Y, Hoshikawa K, Goldman JE, Sekino Y, Sato K (2014) Microglia enhance neurogenesis and oligodendrogenesis in the early postnatal subventricular zone. *J Neurosci* 34:2231–2243.
- Shinjyo N, Ståhlberg A, Dragunow M, Pekny M, Pekna M (2009) Complement-derived anaphylatoxin C3a regulates in vitro differentiation and migration of neural progenitor cells. *Stem Cells* 27:2824–2832.
- Simons K, Sampaio JL (2011) Membrane Organization and Lipid Rafts. *Cold Spring Harb Perspect Biol* 3:a004697–a004697.
- Simpson MA, Cross H, Proukakis C, Priestman DA, Neville DCA, Reinkensmeier G, Wang H, Wiznitzer M, Gurtz K, Verganelaki A, Pryde A, Patton MA, Dwek RA, Butters TD, Platt FM, Crosby AH (2004) Infantile-onset symptomatic epilepsy syndrome caused by a homozygous loss-of-function mutation of GM3 synthase. *Nat Genet* 36:1225–1229.
- Šišková Z, Tremblay M-È (2013) Microglia and synapse: interactions in health and neurodegeneration. *Neural Plast* 2013:425845.

- Skerka C, Lauer N, Weinberger AAWA, Keilhauer CN, Sühnel J, Smith R, Schlötzer-Schrehardt U, Fritsche L, Heinen S, Hartmann A, Weber BHF, Zipfel PF (2007) Defective complement control of factor H (Y402H) and FHL-1 in age-related macular degeneration. *Mol Immunol* 44:3398–3406.
- Sofer A, Lei K, Johannessen CM, Ellisen LW (2005) Regulation of mTOR and cell growth in response to energy stress by REDD1. *Mol Cell Biol* 25:5834–5845.
- Sofroniew M V (2014) Astrogliosis. *Cold Spring Harb Perspect Biol* 7:a020420.
- Sofroniew M V, Vinters H V (2010) Astrocytes: biology and pathology. *Acta Neuropathol* 119:7–35.
- Sonnenburg JL, Altheide TK, Varki A (2004) A uniquely human consequence of domain-specific functional adaptation in a sialic acid-binding receptor. *Glycobiology* 14:339–346.
- Soulet D, Rivest S (2008) Microglia. *Curr Biol* 18:R506-8.
- Sparks S, Rakocevic G, Joe G, Manoli I, Shrader J, Harris-Love M, Sonies B, Ciccone C, Dorward H, Krasnewich D, Huizing M, Dalakas MC, Gahl WA (2007) Intravenous immune globulin in hereditary inclusion body myopathy: a pilot study. *BMC Neurol* 7:3.
- Spörri B, Bickel M, Dobbelaere D, Machado J, Lottaz D (2001) Soluble interleukin-1 receptor--reverse signaling in innate immunoregulation. *Cytokine Growth Factor Rev* 12:27–32.
- Springer TA, Miller LJ, Anderson DC (1986) p150,95, the third member of the Mac-1, LFA-1 human leukocyte adhesion glycoprotein family. *J Immunol* 136.
- Springer TA, Thompson WS, Miller LJ, Schmalstieg FC, Anderson DC (1984) Inherited deficiency of the Mac-1, LFA-1, p150,95 glycoprotein family and its molecular basis. *J Exp Med* 160:1901–1918.
- Starkman MN, Gebarski SS, Berent S, Scheingart DE (1992) Hippocampal formation volume, memory dysfunction, and cortisol levels in patients with Cushing's syndrome. *Biol Psychiatry* 32:756–765.
- Stephan AH, Barres BA, Stevens B (2012) The complement system: an unexpected role in synaptic pruning during development and disease. *Annu Rev Neurosci* 35:369–389.
- Stephan AH, Madison D V, Mateos JM, Fraser DA, Lovelett EA, Coutellier L, Kim L, Tsai H-H, Huang EJ, Rowitch DH, Berns DS, Tenner AJ, Shamloo M, Barres BA (2013) A dramatic increase of C1q protein in the CNS during normal aging. *J Neurosci* 33:13460–13474.
- Stertz L, Magalhães PVS, Kapczinski F (2013) Is bipolar disorder an inflammatory condition? The relevance of microglial activation. *Curr Opin Psychiatry* 26:19–26.
- Stevens B, Allen NJ, Vazquez LE, Howell GR, Christopherson KS, Nouri N, Micheva KD, Mehalow AK, Huberman AD, Stafford B, Sher A, Litke AM, Lambris JD, Smith SJ, John SWMM, Barres BA (2007) The classical complement cascade mediates CNS synapse elimination. *Cell* 131:1164–1178.
- Streit WJ, Xue Q-S (2014) Human CNS immune senescence and neurodegeneration. *Curr*

- Opin Immunol 29:93–96.
- Stylianou E, Saklatvala J (1998) Interleukin-1. *Int J Biochem Cell Biol* 30:1075–1079.
- Sugiura Y, Furukawa K, Tajima O, Mii S, Honda T, Furukawa K (2005) Sensory nerve-dominant nerve degeneration and remodeling in the mutant mice lacking complex gangliosides. *Neuroscience* 135:1167–1178.
- Sun S, Yu H, Yu H, Honglin M, Ni W (2014) Inhibition of the Activation and Recruitment of Microglia-Like Cells Protects Against Neomycin-Induced Ototoxicity. *Mol Neurobiol*:252–267.
- Surendranathan A, Rowe JB, O’Brien JT (2015) Neuroinflammation in Lewy body dementia. *Parkinsonism Relat Disord* 21:1398–1406.
- Svennerholm L (1994) Designation and Schematic Structure of Gangliosides and Allied Glycosphingolipids. In: *Progress in brain research*, pp xi–xiv. Elsevier.
- Takahashi H, Nishimura M, Sakamoto M, Ikegaki I, Nakanishi T, Yoshimura M (1992) Effects of interleukin-1 beta on blood pressure, sympathetic nerve activity, and pituitary endocrine functions in anesthetized rats. *Am J Hypertens* 5:224–229.
- Taylor SL, Trudeau D, Arnold B, Wang J, Gerrow K, Summerfeldt K, Holmes A, Zamani A, Brocardo PS, Brown CE (2015) VEGF can protect against blood brain barrier dysfunction, dendritic spine loss and spatial memory impairment in an experimental model of diabetes. *Neurobiol Dis* 78:1–11.
- Tettamanti G, Bonali F, Marchesini S, Zambotti V (1973) A new procedure for the extraction, purification and fractionation of brain gangliosides. *Biochim Biophys Acta* 296:160–170.
- Tremblay M-È, Lowery RL, Majewska AK (2010) Microglial interactions with synapses are modulated by visual experience. *Dalva M, ed. PLoS Biol* 8:e1000527.
- Tremblay M-È, Zettel ML, Ison JR, Allen PD, Majewska AK (2012) Effects of aging and sensory loss on glial cells in mouse visual and auditory cortices. *Glia* 60:541–558.
- Vajn K, Viljetić B, Degmečić IV, Schnaar RL, Heffer M (2013) Differential Distribution of Major Brain Gangliosides in the Adult Mouse Central Nervous System. *PLoS One* 8:1–11.
- VanGuilder HD, Bixler G V, Brucklacher RM, Farley JA, Yan H, Warrington JP, Sonntag WE, Freeman WM (2011) Concurrent hippocampal induction of MHC II pathway components and glial activation with advanced aging is not correlated with cognitive impairment. *J Neuroinflammation* 8:138.
- Varki A (2008) Sialic acids in human health and disease. *Trends Mol Med* 14:351–360.
- Varki A (2009) Multiple changes in sialic acid biology during human evolution. *Glycoconj J* 26:231–245.
- Varki A (2011a) Evolutionary Forces Shaping the Golgi Glycosylation Machinery: Why Cell Surface Glycans Are Universal to Living Cells. *Cold Spring Harb Perspect Biol* 3:a005462–a005462.
- Varki A (2011b) Since there are PAMPs and DAMPs, there must be SAMPs? Glycan “self-

- associated molecular patterns” dampen innate immunity, but pathogens can mimic them. *Glycobiology* 21:1121–1124.
- Varki A et al. (2015) Symbol Nomenclature for Graphical Representations of Glycans. *Glycobiology* 25:1323–1324.
- Varki A, Angata T (2006) Siglecs - The major subfamily of I-type lectins. *Glycobiology* 16:1R–27R.
- Varki A, Schauer R (2009) Sialic Acids. In: *Essentials of Glycobiology*, 2nd editio. (Varki A, Cummings R, Esko J, Freeze H, Stanley P, Bertozzi C, Hart G, Etzler M, eds). Cold Spring Harbor (NY): Cold Spring Harbor Laboratory Press.
- Vawter MP (2000) Dysregulation of the neural cell adhesion molecule and neuropsychiatric disorders. *Eur J Pharmacol* 405:385–395.
- Vidal B, Sebti J, Verdurand M, Fieux S, Billard T, Streichenberger N, Troakes C, Newman-Tancredi A, Zimmer L (2016) Agonist and antagonist bind differently to 5-HT 1A receptors during Alzheimer’s disease: A post-mortem study with PET radiopharmaceuticals. *Neuropharmacology* 109:88–95.
- von Bernhardt R, Eugenín-von Bernhardt L, Eugenín J (2015) Microglial cell dysregulation in brain aging and neurodegeneration. *Front Aging Neurosci* 7:124.
- Wang Z, Sun Z, Li A V., Yarema KJ (2006) Roles for UDP-GlcNAc 2-epimerase/ManNAc 6-kinase outside of sialic acid biosynthesis: modulation of sialyltransferase and BiP expression, GM3 and GD3 biosynthesis, proliferation, and apoptosis, and ERK1/2 phosphorylation. *J Biol Chem* 281:27016–27028.
- Weidemann W, Klukas C, Klein A, Simm A, Schreiber F, Horstkorte R (2010) Lessons from GNE-deficient embryonic stem cells: Sialic acid biosynthesis is involved in proliferation and gene expression. *Glycobiology* 20:107–117.
- Weihl CC, Miller SE, Zaidman CM, Pestronk A, Baloh RH, Al-Lozi M (2011) Novel GNE mutations in two phenotypically distinct HIBM2 patients. *Neuromuscul Disord* 21:102–105.
- Wellen KE, Hotamisligil GS (2005) Inflammation, stress, and diabetes. *J Clin Invest* 115:1111–1119.
- Werneburg S, Buettner FFR, Erben L, Mathews M, Neumann H, Mühlhoff M, Hildebrandt H (2016) Polysialylation and lipopolysaccharide-induced shedding of E-selectin ligand-1 and neuropilin-2 by microglia and THP-1 macrophages. *Glia* 64:1314–1330.
- Wes PD, Holtman IR, Boddeke EWGM, Möller T, Eggen BJL (2016) Next generation transcriptomics and genomics elucidate biological complexity of microglia in health and disease. *Glia* 64:197–213.
- Whyte A, Loke YW (1978) Increased sialylation of surface glycopeptides of human trophoblast compared with fetal cells from the same conceptus. *J Exp Med* 148:1087–1092.
- Wickham H (2009) *ggplot2: Elegant Graphics for Data Analysis*. New York, NY: Springer-Verlag.

- Wickham H (2017) tidyverse: Easily Install and Load “Tidyverse” Packages.
- Willems AP, van Engelen BGM, Lefeber DJ (2016) Genetic defects in the hexosamine and sialic acid biosynthesis pathway. *Biochim Biophys Acta* 1860:1640–1654.
- Wolf SA, Boddeke HWGM, Kettenmann H (2017) Microglia in Physiology and Disease. *Annu Rev Physiol* 79:619–643.
- Wu C, Orozco C, Boyer J, Leglise M, Goodale J, Batalov S, Hodge CL, Haase J, Janes J, Huss JW, Su AI (2009) BioGPS: an extensible and customizable portal for querying and organizing gene annotation resources. *Genome Biol* 10:R130.
- Wu G, Lu Z-H, Kulkarni N, Ledeen RW (2012) Deficiency of ganglioside GM1 correlates with Parkinson’s disease in mice and humans. *J Neurosci Res* 90:1997–2008.
- Wu N-C, Chen T-H, Yang Y-C, Liao F-T, Wang J-C, Wang J-J (2013) N-acetylcysteine Improves Cardiac Contractility and Ameliorates Myocardial Injury in a Rat Model of Lung Ischemia and Reperfusion Injury. *Transplant Proc* 45:3550–3554.
- Yabe U, Sato C, Matsuda T, Kitajima K (2003) Polysialic acid in human milk. CD36 is a new member of mammalian polysialic acid-containing glycoprotein. *J Biol Chem* 278:13875–13880.
- Yamamoto T, Kimura T, Ota K, Shoji M, Inoue M, Ohta M, Sato K, Funyu T, Abe K (1994) Effects of interleukin-1 beta on blood pressure, thermoregulation, and the release of vasopressin, ACTH and atrial natriuretic hormone. *Tohoku J Exp Med* 173:231–245.
- Yamashita T, Wada R, Sasaki T, Deng C, Bierfreund U, Sandhoff K, Proia RL (1999) A vital role for glycosphingolipid synthesis during development and differentiation. *Proc Natl Acad Sci U S A* 96:9142–9147.
- Yamashita T, Wu Y-P, Sandhoff R, Werth N, Mizukami H, Ellis JM, Dupree JL, Geyer R, Sandhoff K, Proia RL (2005) Interruption of ganglioside synthesis produces central nervous system degeneration and altered axon-glia interactions. *Proc Natl Acad Sci U S A* 102:2725–2730.
- Yang T-T, Lin C, Hsu C-T, Wang T-F, Ke F-Y, Kuo Y-M (2013) Differential distribution and activation of microglia in the brain of male C57BL/6J mice. *Brain Struct Funct* 218:1051–1060.
- Yang WH, Aziz P V, Heithoff DM, Mahan MJ, Smith JW, Marth JD (2015) An intrinsic mechanism of secreted protein aging and turnover. *Proc Natl Acad Sci U S A* 112:13657–13662.
- Yang Y, Chung EK, Zhou B, Lhotta K, Hebert LA, Birmingham DJ, Rovin BH, Yu CY (2004) The intricate role of complement component C4 in human systemic lupus erythematosus. *Curr Dir Autoimmun* 7:98–132.
- Yardeni T, Choekyi T, Jacobs K, Ciccone C, Patzel K, Anikster Y, Gahl WA, Kurochkina N, Huizing M (2011) Identification, tissue distribution, and molecular modeling of novel human isoforms of the key enzyme in sialic acid synthesis, UDP-GlcNAc 2-epimerase/ManNAc kinase. *Biochemistry* 50:8914–8925.
- Yardeni T, Jacobs K, Niethamer TK, Ciccone C, Anikster Y, Kurochkina N, Gahl W a., Huizing M (2013) Murine isoforms of UDP-GlcNAc 2-epimerase/ManNAc kinase:



- Secondary structures, expression profiles, and response to ManNAc therapy. *Glycoconj J* 30:609–618.
- Yates A et al. (2016) Ensembl 2016. *Nucleic Acids Res* 44:D710–6.
- Yida Z, Imam MU, Ismail M, Ismail N, Ideris A, Abdullah MA (2015) High fat diet-induced inflammation and oxidative stress are attenuated by N-acetylneuraminic acid in rats. *J Biomed Sci* 22:96.
- Yonekawa T, Malicdan MC V, Cho A, Hayashi YK, Nonaka I, Mine T, Yamamoto T, Nishino I, Noguchi S (2014) Sialyllactose ameliorates myopathic phenotypes in symptomatic GNE myopathy model mice. *Brain* 137:2670–2679.
- Yoo S-W, Motari MG, Susuki K, Prendergast J, Mountney A, Hurtado A, Schnaar RL (2015) Sialylation regulates brain structure and function. *FASEB J* 29:3040–3053.
- Yu RK, Macala LJ, Taki T, Weinfield HM, Yu FS (1988) Developmental changes in ganglioside composition and synthesis in embryonic rat brain. *J Neurochem* 50:1825–1829.
- Zabel MK, Kirsch WM (2013) From development to dysfunction: microglia and the complement cascade in CNS homeostasis. *Ageing Res Rev* 12:749–756.
- Zhang B, Bailey WM, McVicar AL, Gensel JC (2016a) Age increases reactive oxygen species production in macrophages and potentiates oxidative damage after spinal cord injury. *Neurobiol Aging* 47:157–167.
- Zhang P, He Y, Jiang X, Chen F, Chen Y, Xue T, Zhou K, Li X, Wang Y, Wu Y, Mi W, Qiu J (2013) Up-regulation of stromal cell-derived factor-1 enhances migration of transplanted neural stem cells to injury region following degeneration of spiral ganglion neurons in the adult rat inner ear. *Neurosci Lett* 534:101–106.
- Zhang Y, Chen K, Sloan SA, Bennett ML, Scholze AR, O’Keeffe S, Phatnani HP, Guarnieri P, Caneda C, Ruderisch N, Deng S, Liddelow SA, Zhang C, Daneman R, Maniatis T, Barres BA, Wu JQ (2014a) An RNA-sequencing transcriptome and splicing database of glia, neurons, and vascular cells of the cerebral cortex. *J Neurosci* 34:11929–11947.
- Zhang Y, Gu J, Wang L, Zhao Z, Pan Y, Chen Y (2017) Ablation of PPP1R3G reduces glycogen deposition and mitigates high-fat diet induced obesity. *Mol Cell Endocrinol* 439:133–140.
- Zhang Y, Xu D, Huang H, Chen S, Wang L, Zhu L, Jiang X, Ruan X, Luo X, Cao P, Liu W, Pan Y, Wang Z, Chen Y (2014b) Regulation of glucose homeostasis and lipid metabolism by PPP1R3G-mediated hepatic glycogenesis. *Mol Endocrinol* 28:116–126.
- Zhang Z, Chu S, Mou Z, Gao Y, Wang Z, Wei G, Chen N (2016b) Molecular and Cellular Neuroscience Ganglioside GQ1b induces dopamine release through the activation of Pyk2. *Mol Cell Neurosci* 71:102–113.
- Zuber C, Lackie PM, Catterall WA, Roth J (1992) Polysialic acid is associated with sodium channels and the neural cell adhesion molecule N-CAM in adult rat brain. *J Biol Chem* 267:9965–9971.

## 6 Appendix

### 6.1 Lists of differentially expressed genes (DEGs)

**Table 8: List of all 45 DEGs in GNE<sup>+/-</sup> vs. wildtype**

Symbol	Gene name	Symbol	Gene name
1810011 O10Rik	RIKEN cDNA 1810011O10 gene	Klf13	Kruppel-like factor 13
Acer2	alkaline ceramidase 2	Klf15	Kruppel-like factor 15
Ankrd13b	ankyrin repeat domain 13b	Lzts2	leucine zipper, putative tumor suppressor 2
Arid5b	AT rich interactive domain 5B (MRF1-like)	Mat2a	methionine adenosyltransferase II, alpha
Arl4d	ADP-ribosylation factor-like 4D	Mknk2	MAPK-interacting serine/threonine kinase 2
Arrdc2	arrestin domain containing 2	Mxi1	MAX interactor 1, dimerization protein
Arrdc3	arrestin domain containing 3	Nfkbia	nuclear factor of kappa light polypeptide gene enhancer in B cells inhibitor, alpha
Bcl2l1	BCL2-like 1	Nostrin	nitric oxide synthase trafficker
Bhlhe40	basic helix-loop-helix family, member e40	Numbl	numb-like
Btg2	B cell translocation gene 2, anti- proliferative	Pdk4	pyruvate dehydrogenase kinase, isoenzyme 4
Cdkn1a	cyclin-dependent kinase inhibitor 1A (P21)	Per1	period circadian clock 1
Chka	choline kinase alpha	Plekhf1	pleckstrin homology domain containing, family F (with FYVE domain) member 1
Cxcl12	chemokine (C-X-C motif) ligand 12	Ppp1r3g	protein phosphatase 1, regulatory (inhibitor) subunit 3G
Dbp	D site albumin promoter binding protein	Rtn4rl1	reticulon 4 receptor-like 1
Ddit4	DNA-damage-inducible transcript 4	Sgk1	serum/glucocorticoid regulated kinase 1
Dio2	deiodinase, iodothyronine, type II	Sox9	SRY (sex determining region Y)-box 9
Errfi1	ERBB receptor feedback inhibitor 1	Spns2	spinster homolog 2
F3	coagulation factor III	Trp53inp 1	transformation related protein 53 inducible nuclear protein 1
Frmd6	FERM domain containing 6	Tsc22d3	TSC22 domain family, member 3
Fst	follistatin	Txnip	thioredoxin interacting protein
Hspa1a	heat shock protein 1A		
Hspa1b	heat shock protein 1B		
Irs2	insulin receptor substrate 2		
Kdm3a	lysine (K)-specific demethylase 3A		

Table 9: List of the 50 most differently expressed genes of all 1334 DEGs in GNE<sup>+/+</sup>C3<sup>-/-</sup> vs. wildtype

<b>Top 25 downregulated genes:</b>		<b>Top 25 upregulated genes:</b>	
<b>Symbol</b>	<b>Gene</b>	<b>Symbol</b>	<b>Gene</b>
C3	complement component 3	Pkd2l1	polycystic kidney disease 2-like 1
Hddc3	HD domain containing 3	Chaf1a	chromatin assembly factor 1, subunit A (p150)
Iqgap1	IQ motif containing GTPase activating protein 1	Pla2g4e	phospholipase A2, group IVE
Rps3a3	ribosomal protein S3A3	Rec8	REC8 meiotic recombination protein
Folh1	folate hydrolase 1	Rnf169	ring finger protein 169
Hspa1b	heat shock protein 1B	Wnt9a	wingless-type MMTV integration site family, member 9A
Dio2	deiodinase, iodothyronine, type II	Gstm6	glutathione S-transferase, mu 6
Btaf1	B-TFIID TATA-box binding protein associated factor 1	Ighm	immunoglobulin heavy constant mu
Homer1	homer scaffolding protein 1	Ighm	immunoglobulin heavy constant mu
Manf	mesencephalic astrocyte-derived neurotrophic factor	Zc3h6	zinc finger CCCH type containing 6
Gm15506	predicted gene 15506	Heyl	hairy/enhancer-of-split related with YRPW motif-like
Nptx2	neuronal pentraxin 2	Zkscan2	zinc finger with KRAB and SCAN domains 2
Xbp1	X-box binding protein 1	Gm9866	predicted gene 9866
Gm6969	cytochrome c oxidase subunit VIIa polypeptide 2-like pseudogene	Tnni1	troponin I, skeletal, slow 1
Coa4	cytochrome c oxidase assembly factor 4	E230029	RIKEN cDNA E230029C05
Heatr5a	HEAT repeat containing 5A	C05Rik	gene
Olfml1	olfactomedin-like 1	Hrasls	HRAS-like suppressor
4632427E13Rik	RIKEN cDNA 4632427E13 gene	Gdpgp1	GDP-D-glucose phosphorylase 1
Banp	BTG3 associated nuclear protein	Gm765	predicted gene 765
Sdf2l1	stromal cell-derived factor 2-like 1	Sytl2	synaptotagmin-like 2
Crem	cAMP responsive element modulator	Mrpl48	mitochondrial ribosomal protein L48
Slc5a3	solute carrier family 5 (inositol transporters), member 3	Tmc7	transmembrane channel-like gene family 7
Pdia4	protein disulfide isomerase associated 4	Cirbp	cold inducible RNA binding protein
Sik2	salt inducible kinase 2	Catsperd	cation channel sperm associated auxiliary subunit delta
Egr3	early growth response 3	A430105I19Rik	RIKEN cDNA A430105I19 gene
		Ucp3	uncoupling protein 3 (mitochondrial, proton carrier)

**Table 10: List of the 50 most differently expressed genes of all 987 DEGs in  $GNE^{+/-}C3^{-/-}$  vs. wildtype**

<b>Top 25 downregulated genes:</b>		<b>Top 25 upregulated genes:</b>	
<b>Symbol</b>	<b>Gene</b>	<b>Symbol</b>	<b>Gene</b>
C3	complement component 3	Pla2g4e	phospholipase A2, group IVE
Rps3a3	ribosomal protein S3A3	Rec8	REC8 meiotic recombination protein
Dio2	deiodinase, iodothyronine, type II	Btg2	B cell translocation gene 2, anti-proliferative
Folh1	folate hydrolase 1	Pot1b	protection of telomeres 1B
Nptx2	neuronal pentraxin 2	Pkd211	polycystic kidney disease 2-like 1
Hddc3	HD domain containing 3	Gm9866	predicted gene 9866
Sdf211	stromal cell-derived factor 2-like 1	Zc3h6	zinc finger CCCH type containing 6
Xbp1	X-box binding protein 1	Dusp1	dual specificity phosphatase 1
Homer1	homer scaffolding protein 1	Ier2	immediate early response 2
Ppp1r3g	protein phosphatase 1, regulatory (inhibitor) subunit 3G	Gstm6	glutathione S-transferase, mu 6
Iqgap1	IQ motif containing GTPase activating protein 1	Wnt9a	wingless-type MMTV integration site family, member 9A
Gm6969	cytochrome c oxidase subunit VIIa polypeptide 2-like pseudogene	Syt2	synaptotagmin-like 2
Pdia4	protein disulfide isomerase associated 4	Chaf1a	chromatin assembly factor 1, subunit A (p150)
Dusp4	dual specificity phosphatase 4	4732491K	RIKEN cDNA 4732491K20 gene
Gm15506	predicted gene 15506	20Rik	
Pcsk1	proprotein convertase subtilisin/kexin type 1	Ighm	immunoglobulin heavy constant mu
Hspa5	heat shock protein 5	2700046G	RIKEN cDNA 2700046G09 gene
Slc25a41	solute carrier family 25, member 41	09Rik	
Manf	mesencephalic astrocyte-derived neurotrophic factor	Mybpc3	myosin binding protein C, cardiac
Sik2	salt inducible kinase 2	Bche	butyrylcholinesterase
Tinagl1	tubulointerstitial nephritis antigen-like 1	Heyl	hairy/enhancer-of-split related with YRPW motif-like
Irs2	insulin receptor substrate 2	Gucyl1a3	guanylate cyclase 1, soluble, alpha 3
Fbln2	fibulin 2	Khsrp	KH-type splicing regulatory protein
Creld2	cysteine-rich with EGF-like domains 2	Zkscan2	zinc finger with KRAB and SCAN domains 2
Banp	BTG3 associated nuclear protein	Lmo2	LIM domain only 2
		Rnf169	ring finger protein 169
		Nxpe4	neurexophilin and PC-esterase domain family, member 4

## 7 Acknowledgements

First of all, I would like to dedicate my gratefulness to my doctorate supervisor Prof. Dr. Harald Neumann for giving me the opportunity to continue this very interesting project I have started in my Master's thesis. I very much appreciate that he was always willing to take his time to discuss the project or any other scientific ideas with me. He encouraged me in my work and he was supporting me to attend national and international conferences to present my work in the scientific community. I would also like to thank Prof. Walter Witke for taking over the position as second supervisor.

A special thank-you I would like to address to my direct project supervisor Dr. Bettina Linnartz-Gerlach. It has always been a pleasure to work with her, to learn new techniques from her and to share discussions about the project or other scientific questions with her. Her knowledge and advice was always very helpful. I really appreciate that she took the time for my questions and concerns and that for her it was beyond question to proof-read my thesis or any other scientific text I had to write during my Ph.D. time.

Furthermore, I would like to thank the group of Prof. Rüdiger Horstkorte for providing the engineered GNE<sup>+/</sup> mice. I would also like to thank my collaboration partners from the Epigenetics Team in Luxembourg. It was the first time for me to analyze RNA sequencing data and especially the excellent communication with Dr. Lasse Sinkkonen was very helpful and motivating. In addition, I have to mention all my colleagues and former colleagues from the Neural Regeneration Group in the Institute of Reconstructive Neurobiology for their help and support. I have really enjoyed being in the lab and without them it would not have been such a great time.

Last but not least, I would like to thank my family and my friends who supported me, whenever I needed their help. I would like to thank my native-speakers, Mona, Diahn and Steven, for proof-reading parts of my thesis. Finally, I would like to thank my partner Christian for accompanying me throughout this time and for his entire patient. It is also really important for me to specifically say 'thank you' to my mother Barbara and my father Wilhelm. Without their unlimited support I would not have reached where I am now. I am proud to have such wonderful and lovely parents. Thank you!